Ultrasound Elastography for the Characterisation of Cartilage

Alexandra Jane McCredie, B.Eng. (Hons)

UCL

Thesis submitted for the degree of Doctor of Philosophy

2010

I, Alexandra McCredie confirm that the work presented in this thesis is my own. Where information has been derived from other sources, I confirm that this has been indicated in the thesis.

This thesis is dedicated to everyone who has made me a cup of tea in the past four years.

Abstract

Articular cartilage is a layered porous fibril-reinforced biological composite which performs essential load bearing and shock absorption in mammalian joints; however it is unable to satisfactorily self-repair and is therefore of interest to tissue engineers. Engineering functional tissue requires full mechanical characterisation of the target tissue. 'Elastography' is an ultrasonic method which can be used to find depth-dependent strains in a material following the application of a global strain. In this thesis, ultrasonic elastography are applied to determine the importance of the specialised structure of articular cartilage. Existing ultrasonic elastography techniques are adapted in terms of experimental accuracy, protocol variation and signal-processing to allow experimental comparisons to be made with native articular cartilage, a native non-layered cartilage and engineered tissue constructs at different stages of tissue development. A one-dimensional axisymmetric phenomenological model is constructed, allowing extraction of further material properties from articular cartilage experimental data. The results of these novel comparisons demonstrate the importance of the structure of the tissue in determining the global and depth-dependent elastic properties of the tissue. The global elastic modulus of articular cartilage is dependent on the strain applied, which was not the case for the non-layered sample. Depth-dependent moduli of articular cartilage samples match those previously reported, whereas the cartilage with the non-layered structure has an approximately homogeneous modulus. The changes occurring in the engineered tissue with respect to culture time are small but quantifiable. The suitability of this elastography technique for application to engineered tissue is examined and discussed. The implications of the results demonstrating the importance of the depth-dependent structure for tissue engineering are also addressed and further work suggested.

Acknowledgements

Firstly, I would like to thank my supervisor, Dr. Nader Saffari, for the advice, support and friendship during these last few years. I am also so very grateful to Dr. Eleanor Stride for all the early morning technical advice over cups of tea and for the kind loan of many items of lab equipment. I owe many people thanks for their help on the experimental side: Rank's Green Farm for the time and effort to supply me with the necessary noses and knees, and my team who helped me with the sample preparation; Histology expertise provided by Mrs Nicky Mordan, Biomaterials and Tissue Engineering, UCL; and Mr. Kaveh Memarzadeh and Mr. Adam Bohr, for providing engineered tissue as part of their MSc projects. In terms of developing the foundations for the phenomenological model, Dr. Ian Eames was very helpful. Final bugs were ironed out of the elastography code partly by the work and the discussions generated by Mr. Fahad Ashraf's third year project. My studies would not have been possible without the departmental studentship I received, funded by the EPSRC. For their love and support, and always being on hand to assist, particularly with the less savoury aspects of the experiments, I would like to thank my parents and my husband, Mike. For celebrating the good days and brightening the lower days, thank you to the rest of the 5^{th} floor ultrasonics lab inmates. Finally, my friends and family, many of whom agreed to do proof reading at extremely short notice: Thank you for your patience and always believing in me.

Contents

Nomenclature

(units omitted where values dimensionless)

a	time-shift due to applied strain (s)
A	indenter radius (m)
b	virtual height of the fluid content of cartilage specimen (m)
$\dot{b}_i(t)$	time- and depth-dependent rate of fluid flow (ms^{-1})
B_0	applied magnetic field (T)
B_w	local dipole magnetic field (T)
c	speed of sound in a medium (ms^{-1})
c_p	speed of sound in Perspex (ms^{-1})
c_w	speed of sound in water (ms^{-1})
$cc_{s_1 s_2}$	correlation coefficient between pre- and post-compression signals
cov(x,y)	covariance between x and y
cov(x,x)	covariance between x and y
d	approximate pore size (m)
$d_B(-6dB)$	-6dB beam diameter (m)
D	transducer element diameter (m)
e	void fraction
e_0	initial void fraction
e_i	initial depth-dependent void fraction
E	Young's modulus (N)
E_{Mi}	depth-dependent matrix moduli (N)
f	frequency (Hz)
F	critical ANOVA value

$F(t)$	time-dependent force (N)
F_p	focal distance in Perspex (m)
F_w	focal distance in water (m)
F_z	length of focal zone (m)
g	void ratio
$\hat{g}$	uniform void ratio
G_x	random Gaussian noise amplitude (V)
h_{i0}	initial height of tissue slice (m)
H	full sample cylinder thickness (m)
H_o	initial cylinder height (m)
H_A	cartilage aggregate modulus (Pa)
H_D	'dipolar spin Hamiltonian', magnetic dipolar interaction level
i	window number
k_i	depth-dependent permeability coefficient (m^2)
k_μ	depth-dependent permeability divided by viscosity ($m^2Pa^{-1}s^{-1}$)
L_{DL}	thickness of delay-line (m)
L_w	water path length of beam (m)
m	number of repeat readings
M	dimensionless constant for permeability
n	number of windows
N	number of points in the signal
∇p	pressure gradient (Pa)
p_f	internal sample pressure (Pa)
p_0	pressure of the surrounding fluid (Pa)
P	load (kg)

q	velocity of fluid flow through a porous media (ms^{-1})
Q	near field distance (m)
r_1	pre-compressional complete signal amplitudes (V)
r_2	post-compressional complete signal amplitudes (V)
r	radius of dipolar field (m)
R	radius (m)
Re	Reynold's number
R_{fit}^2	value of the closeness of fit of the data points from the mean
s_1	pre-compressional reflection signal amplitudes (V)
s_2	post-compressional reflection signal amplitudes (V)
s_{xP}	signal amplitude at a point in the signal (V)
S_F	normalised focal length
S_{TE}	relative magnetic signal amplitude at time TE
S_0	relative magnetic signal amplitude at time = 0
S_x	standard deviation of X
t	time (s)
T_2	T2 relaxation time (s)
T_{SSD}	sum-squared difference time shift (s)
$T_{student}$	students T-test statistic
v	fluid velocity (ms^{-1})
w	magnetic moment of proton in magnetic field
x	displacement (m)
$\overline{X}$	mean of circumstances to be compared
z	depth from surface compared to H (m)

α_E	coefficient of linear depth-dependent modulus
α_g	coefficient of linear depth-dependent void ratio
ε	applied strain
ε_G	global strain
$\varepsilon_i(t)$	time- and depth-dependent strain
ε_{wi}	depth-dependent window strain
θ	fibril angles (°)
κ	indentation scaling factor
μ	dynamic viscosity (cP or $kgs^{-1}m^{-1}$)
ρ	material density (kgm^{-3})
σ_G	global stress (Pa)
τ	time-shift increments (s)
υ	Poisson's ratio
ψ	coefficient of depth-dependent permeability

List of Figures

List of Tables

Publications and Presentations

Publications

McCredie A.J., Stride E. and Saffari N. 2009. Quasi-static elastography comparison of hyaline cartilage structures. *Journal of Physics: Conference Series* **195**: 012004. doi: 10.1088/1742-6596/195/1/012004 (peer reviewed)

McCredie A.J., Stride E. and Saffari N. 2009. Ultrasound elastography to determine the layered mechanical properties of articular cartilage and the importance of such structural characteristics under load. *Conference Proceedings: Annual International Conference of the IEEE Engineering in Medicine and Biology Society 2009*: 4262-4265 (peer reviewed)

Conference Presentations

Quasi-static and dynamic elastography of depth-dependent cartilage behaviour. Anglo-French Physical Acoustics Conference 2009, Archachon, France. 8-10 December 2008.

Ultrasound elastography to determine the layered mechanical properties of articular cartilage and the importance of such structural characteristics under load. Annual International Conference of the IEEE Engineering in Medicine and Biology Society 2009, Minneapolis, USA. 3-6 September 2009.

Ultrasound elastography to determine the layered mechanical properties of articular cartilage and the importance of such structural characteristics under load. 22nd European Conference on Biomaterials, Lausanne, Switzerland. 7-11 September 2009.

Poster Presentations

Using ultrasound to investigate the layered mechanical properties of cartilages. Review of Progress in Quantitative Nondestructive Evaluation, Kingston, USA. 26-31 July 2009

1 Introduction

1.1 Overview

This chapter introduces articular cartilage in terms of its highly organised structure and complex mechanical properties. The motivation for mechanical characterisation is found in the need for tissue engineers to design functional replacement joint cartilage. However, the depth-dependent structure of articular cartilage causes global mechanical information to be insufficient for material characterisation. The precise problem this thesis will address, and the subsequent objectives of the study, are presented. The objectives cover how the original contributions of this work are made. This chapter concludes with an outline of this thesis.

1.2 Background and Motivations

1.2.1 Cartilage and tissue engineering

Articular cartilage is found covering the surfaces of bone in most mammalian joints (Mow and Guo 2002, Mow et al. 1991). It is a specialised form of hyaline cartilage (Mow et al. 1991) which allows joints to function correctly by providing a low friction, shock absorbing surface (Mow and Guo 2002). Hyaline cartilage is so named due to its glassy appearance (Fung 1993). Other types of hyaline cartilage include nasal, costal and tracheo-bronchial cartilages (Fung 1993). Articular cartilage tissue is prone to damage but unable to satisfactorily self-repair large defects. Impaired tissue function leads to pain in patients (Buckwalter and Mankin 1997). Tissue engineers seek to provide replacements for damaged tissue. Mechanical characterisation of structural tissue is essential to provide design parameters for engineered tissue (Guilak et al. 2003).

Figure 1-1 shows the location of articular cartilage in the joint with respect to the other key structural elements. The joint cavity is filled with synovial fluid.

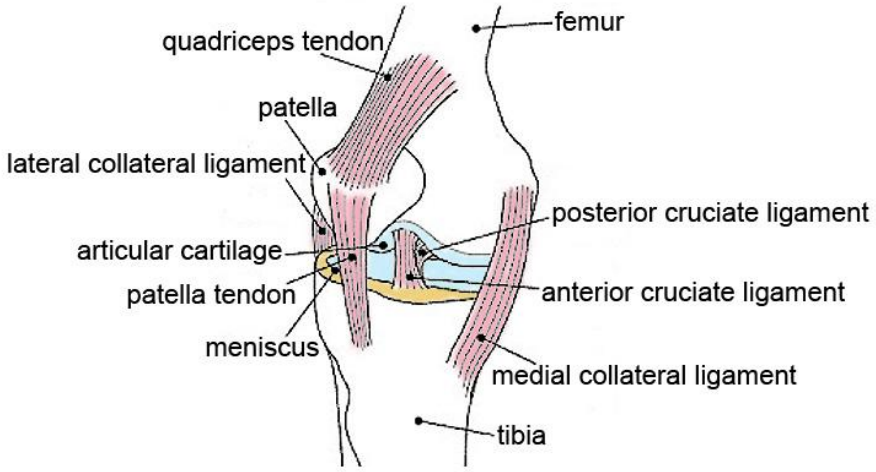

Figure 1-1: A schematic diagram of the key structural features in a human knee joint. The articular cartilage is shown in light blue. It also covers the hidden back surface of the patella bone. The meniscus is also made of cartilage, but not hyaline cartilage. It performs a different function to the hyaline articular cartilage and can self-repair more satisfactorily.

Articular cartilage is composed of a fluid filled, porous and collagen fibril reinforced composite matrix (comprised of proteoglycans and chondrocyte cells)

(Lu and Mow 2008). It is specialised for shock absorbency through both its poroelastic material properties and its structure (Mow and Guo 2002).

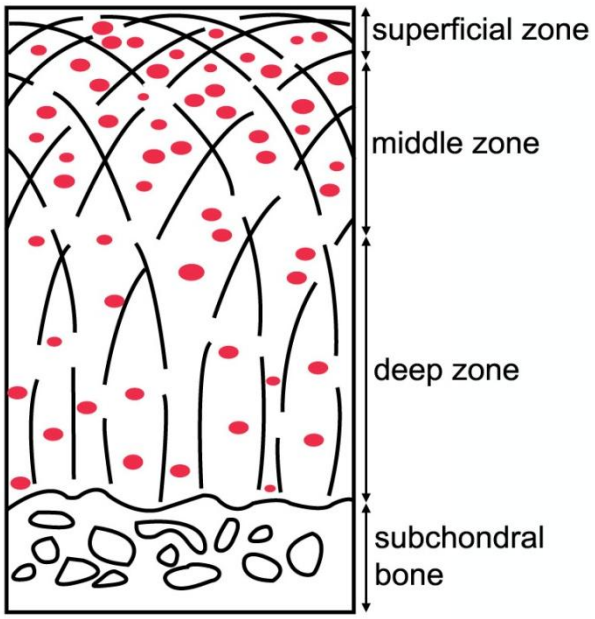

Figure 1-2: Schematic representation of the cross-section of articular cartilage. The approximate positions of the superficial, middle and deep zones and the subchondral bone are shown. The black broken lines are indicative of the collagen network orientation and the red dots represent the chondrocytes and the relative density with respect to depth. It can be seen that the zonal thicknesses are roughly determined by the fibril orientations

Articular cartilage has a depth-dependent matrix structure owing to the distribution of the chondrocytes and the collagen fibril architecture in the matrix (Mow et al. 1991) as shown in Figure 1-2. As a result of this structure it is an anisotropic material. In the superficial zone, the fibrils are aligned mainly parallel to the articular surface, and in the deep zone, the fibrils are perpendicular to the surface and the subchondral bone. The middle zone is a transitional region where the fibrils gradually change their orientation (Mow et al. 1991, Benninghoff 1925).

1.2.1.1Basic articular cartilage mechanics

The cartilage matrix (which can be considered elastic) filled with interstitial fluid acts as a poroelastic material (Lu and Mow 2008). When a strain is applied suddenly, a large initial 'composite' elastic modulus for the material is observed. This is termed the composite modulus as it is caused primarily by the pressurisation of the matrix fluid (Nguyen and Oloyede 2001, Wilson et al. 2007, Broom and Oloyede 1998, Olsen et al. 2004). The material then undergoes stress-relaxation as

the fluid moves through the pores, therefore depressurising (Lu and Mow 2008, Wu and Herzog 2002, Fung 1993). The true matrix modulus is considered to be found after the stress-relaxation curve has levelled, when no further net fluid movement occurs (Li et al. 2000). Similarly due to poroelasticity, articular cartilage 'creeps' under the application of a constant stress (Li et al. 2008). Graphical representations of these poroelastic material behaviours are shown in Figure 1-3.

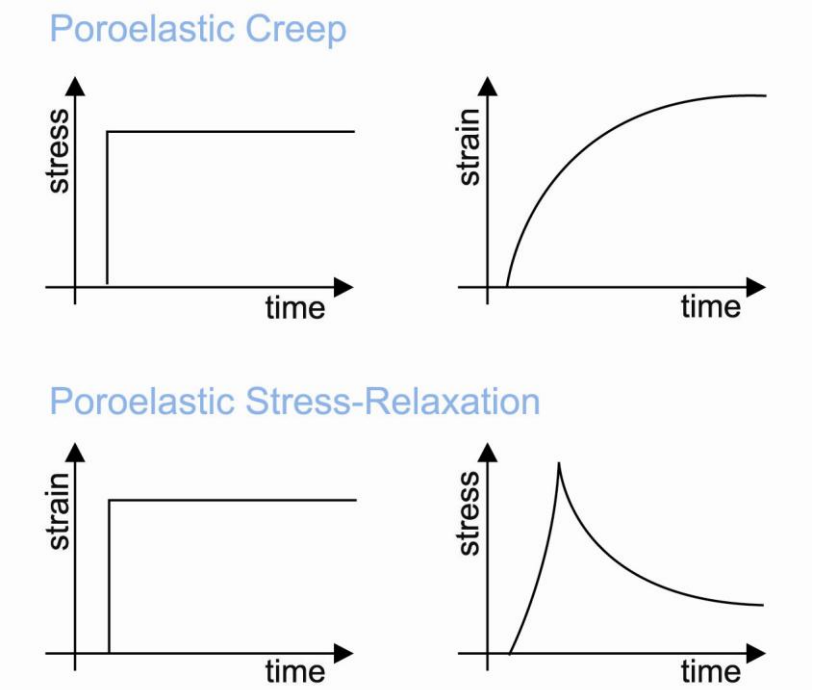

Figure 1-3: Graphical representation of poroelastic material behaviours with respect to constant applied stress and constant applied strain. Poroelastic materials creep under a constant applied stress and under-go stress-relaxation under a constant applied strain.

The proteoglycans, which are a major matrix constituent, are charged molecules, which attract water molecules into the matrix (Maroudas 1979). This allows tissue recovery after a load cycle has finished. Cartilage therefore exists in a highly hydrated state: the interstitial fluid in the cartilage comprises approximately 70% of the total cartilage volume (Mow and Guo 2002, Maroudas 1979). Fluid movement plays an important role in cartilage mechanics, determining the difference between initial tissue stiffness and equilibrium tissue stiffness (Akizuki et al. 1986). If fluid movement is excessive for the applied load the tissue is unable to resist applied strain; too little leads to the inability to absorb shock loads which can lead to fracture. Permeability (the ease of fluid movement) is expressed as a coefficient, *k*, which is defined as the constant of proportionality between the velocity of the fluid

flow and the pressure difference across the thickness of the tissue. It has been found to increase as compressive strain increases (Mansour and Mow 1976, Basalo et al. 2004), to decrease as the frequency of the applied load increases (Buschmann et al. 1998) and to decrease with depth from the surface (9.2×10^{-17} m^2 at the surface to 1.0×10^{-17} m^2 in the deep zones recorded under a 10% strain at room temperature) (Chen et al. 2001).

Mechanical models of cartilage behaviour are varied. Most commonly used is the biphasic (poroelastic) model (Li et al. 2005, Donzelli et al. 1999, Fortin et al. 2000, Ateshian et al. 1997, Setton et al. 1993, Haider and Schugart 2006, Soulhat et al. 1999, DiSilvestro and Suh 2002, DiSilvestro et al. 2001b, DiSilvestro et al. 2001a, Garcia and Cortes 2007, Garcia and Cortes 2006, Ehlers and Markert 2001, Huang et al. 2001, Huang et al. 2003, Ateshian et al. 2004, Suh et al. 1995, Herberhold et al. 1999) as this form of behaviour is most prevalent under large loads (Wilson et al. 2007, Herberhold et al. 1999). However, models also exist which take into consideration the charges of the proteoglycan acting against fluid movement (Wilson et al. 2007, Sun et al. 2004a, Nguyen and Oloyede 2001, Chen et al. 2006, Ateshian et al. 2004, Broom and Oloyede 1998). Models also vary in terms of whether they include considerations of the stiffness (Li et al. 2000, Li et al. 2002b, Li et al. 2003b, Li et al. 2008, Julkunen et al. 2007) and alignment (Julkunen et al. 2007, Julkunen et al. 2008a, Wilson et al. 2006, Wilson et al. 2007, Wilson et al. 2004, Nguyen and Oloyede 2001) of the reinforcing fibrils in the calculations.

1.2.1.2 Cartilage tissue engineering

Due to the inability of self-repair, knee joint articular cartilage is a particular target for regenerative medicine. Guilak et al. (2003) state that among the primary goals of tissue engineering are 'determining *in vivo* and *in vitro* responses of native tissue to identify functional requirements and develop design parameters' and the 'assessment of repair function'. Many different attempts of engineering cartilage tissue have been made (Klein et al. 2007, Duda et al. 2000, Risbud and Sittinger 2002, Morita et al. 2003, Ando et al. 2007, Obradovic et al. 2001, Ma et al. 1995, Hunziker 1999, Memarzadeh 2009). However, to enable the production of a functional tissue replacement, it is important to assess the effect of the depth-

dependent mechanical properties of this complex material and to provide design requirements for functional engineered tissue.

1.3 Aims and Objectives

1.3.1 Statement of the problem

Comprehensive mechanical characterisation of the depth-dependent elastic moduli of articular cartilage is required, under both quasi-static and dynamic loading protocols, to provide tissue engineers with the design information to produce functional tissue constructs.

1.3.2 Objectives

The objectives of this thesis can broadly be split into the following areas:

- Development of an 'elastography' method suitable for obtaining accurate depth-dependent strain information from different types of hyaline cartilage. Experiments should be performed in physiologically relevant conditions, such as at a temperature of 37°C. Application of automated and precise strains is required to allow continuity between repeat readings and accurate testing of very thin engineered samples.

- Obtaining depth-dependent strains and global composite moduli from cartilage samples during a range of global strain application protocols: quasi-static and cyclic.

- Establishing whether cartilage 'elastography' is capable of differentiating between different hyaline cartilage structures.

- Developing and utilising a phenomenological model to extract depth-dependent matrix elastic constants from the 'elastography' strain results.

1.3.3 Thesis outline

Chapter 2 reviews the relevant reported work regarding the characterisation of the mechanical properties of articular cartilage and, where applicable, tissue engineered cartilage. Details of the specimens to be tested are given in Chapter 3; including how the engineered cartilage tissue was made. Two different types of native hyaline

cartilage were selected for comparison to ascertain the importance of the depth-dependent structure for the mechanical behaviour of articular cartilage. The development of elastography method to be used, in terms of equipment selection and control, signal-processing method and data analysis, is presented in Chapter 4. Chapter 5 details the development of a phenomenological mechanical model of the depth-dependent behaviour of cartilage. The model is used to extract depth-dependent moduli from the strain information obtained from the elastographic data in Chapter 6. The experimental results are split into the global mechanical measurements and the depth-dependent strain measurements and these are presented and discussed in Chapters 6, 7 and 8. The results from the quasi-static protocols in both native tissues are found in Chapter 6. In Chapter 7, quasi-static step strain applications to native and engineered cartilage samples are presented. Chapter 8 presents the results of varying the frequency and magnitude of cyclically applied dynamic strains. In Chapter 9 the conclusions for the work undertaken are given and further work suggested for the potential development of an *in vivo* characterisation method.

2 Literature Review: Characterisation of the mechanical properties of cartilage

2.1 Overview

Characterisation of the structure and mechanical behaviour of articular cartilage tissue is an established area of investigation in the context of joint damage and disease. Healthy articular cartilage has been shown to have a layered structure, which affects its mechanical properties. This chapter is aimed at reviewing existing characterisation techniques in order to identify a suitable method to compare different hyaline cartilage structures. First the direct mechanical tests of confined and unconfined compression, indentation and tension are detailed in terms of methodology and results obtained from key studies. These direct mechanical tests are used to investigate mechanical behaviour throughout the whole cartilage thickness. Indirect mechanical characterisation methods using histology, magnetic resonance imaging (MRI) and ultrasound are also presented. These studies are relevant due to the strong dependence of the mechanical properties on the tissue composition. Finally, techniques which combine depth-dependent structural information during a global displacement application are reviewed. These techniques combine a form of tissue imaging such as microscopy, MRI or ultrasound with a 'global' mechanical test. The direction of this thesis is identified from areas requiring further research found in this review.

2.2 Introduction

The mechanical properties of hyaline cartilage, in particular articular cartilage, have been studied extensively. Articular cartilage has a specialised composition and structural organisation designed to withstand a vast range of loading cycles *in vivo* (Mow and Guo 2002); the response of the tissue is markedly different for compressive, tensile and shear stress conditions.

Compressive loading of cartilage causes the tissue volume to reduce as the interstitial fluid flows from the deformed region (Lu and Mow 2008, Wu and Herzog 2002, Fung 1993). This gives rise to time-dependent poroelastic behaviours (similar to viscoelastic behaviours) such as stress-relaxation under constant strain conditions and creep under constant stress conditions. *In vivo,* the most likely loading mode is compression. Tensile loading of cartilage is unlikely *in vivo*, however *in vitro* it can be used to determine the collagen network modulus (Charlebois et al. 2004) and viscoelasticity (Li et al. 2005). In tensile conditions these fibrils are the primary load support (Mow and Guo 2002). Shear conditions result both from indentation tests (Duda et al. 2000, Toyras et al. 1999, Arokoski et al. 1999) and from specifically applied shear tests (Spirt et al. 1989). Shear is not a common naturally occurring load condition for articular cartilage *in vivo,* but has been used in a protocol attempting to uncouple the intrinsic matrix viscoelasticity from the poroelasticity of the whole tissue as the fluid component is unable to resist shear forces (Spirt et al. 1989).

Owing to the physiological relevance of compressive testing, it is the most commonly employed direct method to measure the global (total thickness) mechanical properties *in vitro*. Compressive tests have been performed in radially confined (Ateshian et al. 1997, Jurvelin et al. 2003, Buschmann et al. 1998, Setton et al. 1993, Chen et al. 2001, Ma et al. 1995, Schinagl et al. 1997) and unconfined (Li et al. 2003a, Li et al. 2008, Julkunen et al. 2007, Fortin et al. 2000, Kiviranta et al. 2006, Langelier and Buschmann 2003, Morita et al. 2003, Park et al. 2008, Park and Ateshian 2006, Adams et al. 1999) configurations under quasi-static and dynamic (cyclic) applied loads. Boundary conditions are used to control the specific values obtained from the experiments, for example Young's modulus is obtained in unconfined compression (Langelier and Buschmann 2003, Kiviranta et al. 2006),

whereas the solid matrix (aggregate) modulus is obtained during confined compression (Mow and Guo 2002). Alternative direct mechanical tests include tensile (Li et al. 2005, Gratz et al. 2006, Elliott et al. 2002, Charlebois et al. 2004, Grellmann et al. 2006), permeability (Mansour and Mow 1976, Basalo et al. 2004, Wan and Li 2007), indentation (Duda et al. 2000, Toyras et al. 1999, Arokoski et al. 1999, Adams et al. 1999) and shear (Spirt et al. 1989). These methods are also used to determine specific parameters from the cartilage such as the fibril network modulus (Li et al. 2005, Charlebois et al. 2004). Indirect mechanical tests are where the material mechanical properties are estimated from measurements of the material composition using histology (Huckle et al. 2003, Lindahl et al. 2003, Pavesio et al. 2003, Toyras et al. 1999, Ma et al. 1995, Kiviranta et al. 2006, Arokoski et al. 1996, Julkunen et al. 2007), or estimates of the composition using ultrasound (Hattori et al. 2004, Laasanen et al. 2005, Pellaumail et al. 1998, Pellaumail et al. 1999, Wang et al. 2008) and magnetic resonance imaging (MRI) (Mlynarik et al. 2004, Eckstein et al. 1999, Lopez et al. 2008, Neu and Walton 2008, Suan et al. 2005) techniques. The composition of articular cartilage has been determined to vary with respect to depth from the articular surface. Three zones have been identified as the surface or superficial, middle or transitional and deep zones (Mow et al. 1991). This layered structure of articular cartilage leads to depth-dependent mechanical properties. In order to find the localised tissue strains, techniques have been developed to combine methods of locating markers within the tissue before and after the application of a quantified global strain. These local strains can be used to then determine the local elastic moduli.

In order to determine the effects of disease and injury on cartilage tissue samples, the composition can be altered using enzymes to deliberately remove different constituents. These include collagenase to remove collagen fibres (Toyras et al. 1999, Basalo et al. 2004) and trypsin to remove the proteins from the proteoglycan matrix (Qin et al. 2002, Zheng et al. 2001, DiSilvestro and Suh 2002). It is important to have methods to test healthy native cartilage that can also be applied to test engineered cartilage, as the mechanical properties of healthy native tissue are viewed as the ‘standard’ to which engineered tissue is to be compared (Lee et al. 2003).

2.3 Direct Mechanical Tests

2.3.1 Unconfined Compression

Unconfined compression is a commonly used global mechanical test configuration. It is an *in vitro* technique where cartilage sample discs are placed between smooth plates in a compression test machine. A schematic of this test configuration is shown in Figure 2-1.

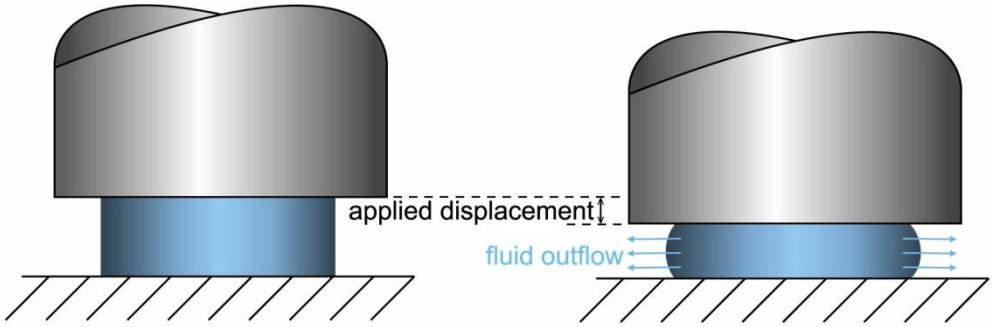

Figure 2-1: Schematic of unconfined compression test configuration. The cartilage sample is shown in blue. Neither the rigid surface at the base nor the compressors are usually permeable. The displacement is shown. The cartilage sample is free to expand radially, causing tension in the collagen fibrils, and fluid can flow out of the sample from the unconfined surface.

Loading protocols can either use a fixed applied strain to monitor material stress-relaxation (Li et al. 2008, Julkunen et al. 2007, Fortin et al. 2000, Kiviranta et al. 2006, Langelier and Buschmann 2003) or a fixed applied stress to provide creep conditions (Li et al. 2008, Adams et al. 1999). In both protocols Poisson's ratio can be found (Kiviranta et al. 2006). Because the radial edge of the cartilage specimen in this test configuration is a free surface for the interstitial fluid to escape during loading, the pressure decrease due to fluid dissipation is faster than in *in vivo* conditions (Wong and Carter 2003).

In stress-relaxation tests the initial modulus (at the instant of strain application) (Ling et al. 2007, Fortin et al. 2000, Kiviranta et al. 2006, Langelier and Buschmann 2003) and the equilibrium modulus (after the changes in stress can be deemed negligible) (Ling et al. 2007, Fortin et al. 2000, Kiviranta et al. 2006, Langelier and Buschmann 2003) can be found. In creep tests a similar equilibrium level is reached, but over a longer time period than stress-relaxation equilibrium because of differences in pressure profiles (Li et al. 2008). The initial and equilibrium moduli are both dependent on the amplitude and rate of the applied

strain (Fortin et al. 2000, Langelier and Buschmann 2003); this is thought to be due to the dependence of material permeability and the collagen network stiffness on the strain conditions (Kiviranta et al. 2006, Julkunen et al. 2007, Li et al. 2003a, Li et al. 2008).

The effect of the applied strain magnitude on the initial and equilibrium moduli in stress-relaxation tests was studied by Ling et al. (2007). Samples of 6.4 mm diameter were tested at room temperature with applied strains in 2.5% increments up to 20%. The authors noted that the 15 min allowed for stress-relaxation equilibrium to occur was insufficient for applied strain levels over approximately 10%. The initial and equilibrium moduli measured are shown in Table 2-1.

	% strain applied to articular cartilage							
	2.5	**5**	**7.5**	**10**	**12.5**	**15**	**17.5**	**20**
Initial modulus (MPa)								
Mean	0.21	0.39	0.62	0.9	1.11	1.6	2.42	2.86
Standard deviation	0.28	0.53	0.86	1.05	1.1	1.5	1.92	2.64
Modulus after 15 min stress-relaxation (MPa)								
Mean	0.05	0.13	0.19	0.28	0.37	0.54	0.7	0.87
Standard deviation	0.06	0.08	0.16	0.21	0.29	0.37	0.51	0.81

Table 2-1: Table of the averaged values of the initial and equilibrium moduli found for 20 articular cartilage samples in unconfined compression (Ling et al. 2007).

In a study conducted by Li et al. (2003a), the effect of rate of strain application on the initial stiffness was examined through the application of a poroelastic finite element cartilage model. With the applied strain rate as $0.5\%s^{-1}$, the initial modulus was found to be 0.36 MPa, increasing to 1.07 MPa at $5\%s^{-1}$ and 2.14 MPa at $50\%s^{-1}$. Langelier and Buschmann (2003) found the initial modulus to initially decrease for strains up to approximately 5% and then to increase for strains up to 30%; the greater the applied strain rate, the larger the initial modulus value. Using applied strain rates of $0.05\%s^{-1}$, the initial modulus was found between 1.2 and 2.8 MPa, increasing the applied strain rate to $5\%s^{-1}$ increased the measured initial modulus to between 4.3 to 5.7 MPa (Langelier and Buschmann 2003). Conversely, the equilibrium modulus was found in the same study to be inversely proportional to the strain rate: the lower strain rate yielding equilibrium moduli between 0.40 and 0.61 MPa while the higher rate producing results between 0.33 and 0.56 MPa. Values for the initial modulus range between 0.21 MPa (Ling et al. 2007) and 9.1

MPa (Julkunen et al. 2007). Stress-relaxation equilibrium has been determined to occur between the times of 300 and 600 s in 0.15 M phosphate buffered saline (PBS) at room temperature (Kiviranta et al. 2006, Julkunen et al. 2007, Langelier and Buschmann 2003), with equilibrium modulus values measured in the region of 0.05 MPa (Ling et al. 2007) to 0.48 ± 0.32 MPa (Kiviranta et al. 2006). The equilibrium modulus following creep loading was determined after 2 hours with a volumetric decrease of 34% in a study by Adams et al. (1999). The equilibrium moduli fall within a much smaller range of values indicating the dependence of the composite tissue moduli to be a result of the material poroelasticity rather than the intrinsic matrix behaviour.

The relationship between tissue composition and the mechanical parameters revealed Young's modulus to be strongly dependent on tissue proteoglycan content and collagen fibril stiffness, (Kiviranta et al. 2006, Julkunen et al. 2007, Li et al. 2003a) and inversely related to Poisson's ratio (Kiviranta et al. 2006). As the site-specific collagen content increased the global Young's modulus and Poisson's ratio changed from 0.77 ± 0.33 MPa and 0.15 ± 0.04 to 0.17 ± 0.06 MPa and 0.30 ± 0.07, respectively. Enzymatic removal of proteoglycans was found to drastically decrease the initial peak elastic modulus (2 MPa pre-treatment down to 0.5 MPa post-treatment (Murakami et al. 2004)).

Unconfined compression has also been applied with a sinusoidal displacement (Morita et al. 2003, Park et al. 2008, Park and Ateshian 2006) known as dynamic testing. This is representative of a more physiologically relevant loading protocol (Park et al. 2008) which can be used to find the dynamic modulus (Park et al. 2008, Park and Ateshian 2006), and the effects of loading frequency on the fluid flow-dependent viscoelasticity (Morita et al. 2003). It has been found that amplitudes of dynamic compressive strains decrease, and hence local elastic moduli increase, with respect to the frequency of applied stresses: compressive strains due to 40N applied load decreased from 22 ± 6% at 0.1 Hz to 9.6 ± 3.3% at 40 Hz (Park and Ateshian 2006). In the same study collagenase-digested cartilage was tested and it was found that the dynamic compressive strains were larger for the same loading amplitudes and frequencies: 26 ± 8% at 0.1 Hz and 13.5 ± 3.2% at 40 Hz (Park and Ateshian 2006).

In vitro tests on engineered samples in quasi-static unconfined compression found that as the proteoglycan matrix was produced by the chondrocytes in the scaffold, there was an increase in the measured elastic modulus (from ~1 kPa to ~30 kPa following 26 days culture) (Lee et al. 2003). When dynamic unconfined compression was applied to an engineered cartilage tissue, the dynamic modulus was found to increase after 7 days of cultivation (Morita et al. 2003).

Author	Cartilage	Strain / Stress	Rate of Strain / Stress App.	Time to Eq.	Inst. Young's Mod. (MPa)	Eq. Mod. (MPa)
Li et al. (2003a)	bovine articular 3mm discs (0.9-1.2mm thick)	1 to 20%	$0.5\%s^{-1}$ $5\%s^{-1}$ $50\%s^{-1}$	Instant loading only	0.36 1.07 2.14	-
Langelier and Buschmann (2003)	bovine tibial & femoral 3mm discs (1.5mm thick)	5 to 30%	$0.5\mu ms^{-1}$ $50\mu ms^{-1}$	< 600s, decreasing for lower strains	1.2-2.8 4.3-5.7	0.4-0.61 0.33-0.56
Julkunen et al. (2007)	bovine femur, tibia, patella & humerus 3.7mm discs (1.04-1.63mm thick)	2 steps of 5%	$1\mu ms^{-1}$	patella 600s a step tibia 500s a step	patella 1.12 tibia 0.2-0.23	patella 0.14-0.21 tibia 0.08-0.07
Kiviranta et al. (2006)	bovine patella, femur, tibia & humerus 4mm discs (1.19-1.72mm thick)	4 steps of 5%	$1\mu ms^{-1}$	250s	not reported	patella 0.58 femur 0.33 tibia 0.17 humerus 0.77
Basalo et al. (2004)	bovine femoral chondro. digested 6mm discs (1.55mm thick)	10%	$0.2\%s^{-1}$	50s (not full eq.)	~ 8 fresh and digested	-
Murakami et al. (2004)	porcine femur, fresh & chondro. digested semi-cylindrical 3mm discs (0.5mm thick)	13%	$13\%s^{-1}$	600s	2.3 fresh, 1.2 1hr digested, 0.69 3hr digested	0.38 fresh, 0.15 1hr digested, 0.08 3hr digested
Park and Ateshian (2006)	bovine humerus 4mm discs (1.98mm thick)	40N max cycled between 0.001Hz & 10Hz	dependent on the frequency cycle	N/A	3.0 at 0.001Hz 16.2 at 10Hz	-

Table 2-2: Summary table of the important results from the application of unconfined compression mechanical tests to articular cartilage samples. 'Eq.' is equilibrium, 'mod.' is modulus and 'inst.' is initial, 'chondro.' is chondroitinase ABC. All tests were performed at 'room' temperature.

A summary of a selection of important results from unconfined compression are presented in Table 2-2. Both dynamic and quasi-static unconfined compression techniques are limited to *in vitro* application and there is no access to the depth-dependent mechanical information.

2.3.2 Confined compression

Confined compression is similar to unconfined compression in that it may be performed in stress-relaxation (Ateshian et al. 1997, Buschmann et al. 1998,

Jurvelin et al. 2003, Ma et al. 1995), creep (Setton et al. 1993) or dynamic protocols (Chen et al. 2001, Ateshian et al. 1997). Samples are placed into a smooth impervious chamber to prevent lateral expansion during load application and compressed with a porous indenter (Ateshian et al. 1997, Jurvelin et al. 2003, Buschmann et al. 1998, Ma et al. 1995, Setton et al. 1993, Chen et al. 2001) to allow fluid exudation. The test configuration is shown in the schematic in Figure 2-2.

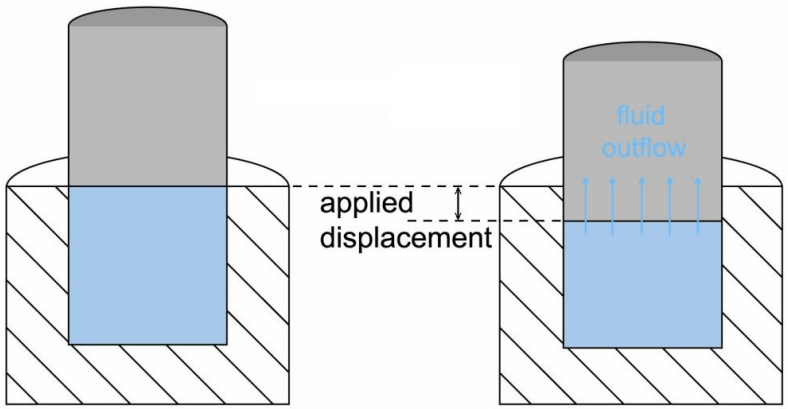

Figure 2-2: Cross-sectional schematic of the confined compression experimental configuration. The cartilage is shown in blue. The confining edges are impermeable. The indenter is permeable and the displacement is shown

The purpose of the radial confinement is to allow measurements of matrix stiffness, also known as the aggregate modulus, H_A, excluding the contribution of the fibril stiffness resisting radial expansion (Li et al. 2000). The aggregate modulus is therefore representative of the modulus of the PG component of the cartilage tissue. The use of the porous compression plates leads to a disturbance of the cartilage surface, which creeps into the pores (Buschmann et al. 1998). This effect causes disruptions to the matrix which may affect the accuracy of the results.

Compressional strains in the region of 15% to 20% (Buschmann et al. 1998, Ma et al. 1995, Schinagl et al. 1997) have been applied to the samples. The confined compression test configuration is more similar to *in vivo* conditions than unconfined compression: the radial confinement prevents fluid flow from the sides. This is representative of the conditions when the surrounding articular cartilage is highly pressurised due to the osmotically drawn in water molecules causing material saturation (Wong and Carter 2003).

Typical values of the time taken to reach equilibrium in confined compression have been found between 1,640 and 10,000 s in stress-relaxation (Ateshian et al. 1997, Setton et al. 1993) and 1,500 to 14,400 s in creep (Ateshian et al. 1997, Langeland et al. 2003); these are considerably longer relaxation times than those recorded for unconfined compression. The permeability of the sample may also be determined (Jurvelin et al. 2003, Ateshian et al. 1997, Buschmann et al. 1998): measured in quasi-static confined compression $k = 5.4 \pm 3 \times 10^{-17}$ m^2 (Ateshian et al. 1997) and in dynamic confined compression $k = 3.2 \times 10^{-17}$ m^2 (Buschmann et al. 1998). ('Quasi-static' is a term used to describe a process which is occurring extremely slowly, allowing changes to be addressed as negligible). This demonstrates a significant decrease of permeability under cycles of repetitive load. Initial matrix stiffness has been found to be anisotropic: $H_A = 1.237 \pm 0.486$ MPa when measured parallel to the surface and $H_A = 0.845 \pm 0.383$ MPa when measured perpendicular to the surface (Jurvelin et al. 2003). The aggregate modulus in equilibrium was found to be 0.40 ± 0.14 MPa (Ateshian et al. 1997) (in room temperature PBS), which is in the same range as the unconfined equilibrium modulus. It was also found to be strain amplitude and strain rate dependent (Buschmann et al. 1998) with values between 5.0 MPa and 12.3 MPa over an increasing range of 0.01 to 1 Hz.

In one study, confined compression tests were performed on engineered cartilage tissue over a 12-week culture period with reported results of the aggregate modulus of the engineered tissue reaching the same order of magnitude as native cartilage by week 9 of the culture (Ma et al. 1995). In another study (Vunjak-Novakovic 2003), the equilibrium aggregate modulus found from static confined compression tests performed on engineered cartilage tissue constructs (bovine calf chondrocytes on fibrous polyglycolic acid scaffolds) at 3 days, 6 weeks and 7 months of culture time was used in conjunction with histology tests to assess the tissue development. The results were compared to those from bovine foetal and mature articular cartilage samples. The collagen and PG production in the constructs was assessed histologically. The PGs reached the same levels as those found in both the foetal and the mature cartilage at 6 weeks. The collagen content of the constructs was found to match foetal at 6 weeks, but did not reach the levels found in mature cartilage even after 7 months of culture. The moduli of the constructs, assessed using confined compression, was found to be considerably lower than that of foetal

cartilage at 3 days of culture time, but after 6 weeks it had reached the same moduli as foetal. After 7 months the modulus of the constructs resembled that of the deep zones measured in the mature cartilage.

Author	Cartilage	Stress / Strain Applied	Rate of Strain / Stress App.	Time to Eq.	Aggregate Mod. (MPa)	Eq. Mod. (MPa)
Buschmann et al. (1998)	bovine humeral 3.6mm discs	15% initial strain & cyclic disp. 5, 10&15µm	1µms^{-1} initial strain cyclic strain 0.001 to 1Hz	30-100s for each step	0.56	-
Ma et al. (1995)	12 wk eng. & fresh bovine femur 10mm discs	20%	10 µms^{-1}	3,600s	0.45 fresh 0.064 12 wk eng.	-
Schinagl et al. (1997)	bovine femur (0.78×2.5×5 mm wafers)	8 to 32%	0.02 %s^{-1}	5,400s	-	0.38 full 0.079 top 1.14 middle 2.1 deep
Ateshian et al. (1997)	bovine femur 6.35mm (1.41mm thick)	5 steps of 10% & 0.19MPa stress	0.25 µms^{-1} strain (N/A C.)	1640s (SR.) 1500s (C.)	0.4 (0.14st.dev.)	0.29
Setton et al. (1993)	bovine femur 6.35mm discs	constant stress 0.01-0.07MPa	-	10,000s	0.54 (0.25 st.dev.)	-
Jurvelin et al. (2003)	human femur 1.7mm discs (1mm thick)	10µm steps up to 20% total strain	1µms^{-1}	~100s each step	0.845 (0.383 st.dev.)	0.4 (0.14 st.dev.)
Vunjak-Novakovic (2003)	bovine patella &3 day&6 wk eng. (sizes not stated)	10 - 40% strain	not stated	-	-	5 fresh, 2.0 6wks eng., 0.2 3days eng.

Table 2-3: A summary table of important selected results from studies of the application of confined compression to articular cartilage specimens at room temperature. 'SR.' is stress-relaxation, 'C.' is creep, and 'eng.' is engineered.

It is important when analysing confined compression test results that consideration is made for the measured properties' high dependency on the permeability of the compressing surface. The greater the porosity, the faster the fluid moves from the tissue and therefore increasing the rate of the viscoelastic like mechanical properties. A summary of the results from a selection of confined compression studies of articular cartilage is shown in Table 2-3. While the measurements of aggregate modulus are important for tissue modelling, they are not as physiologically relevant to cartilage behaviour as unconfined compression moduli, which take into account the action of the collagen fibrils in the load support.

2.3.3 Tensile tests

Tensile properties are impossible to measure *in vivo* and are less physiologically relevant to cartilage mechanics than compression properties, however the

information obtained from this method regarding the behaviour of the collagen fibrils is useful for tissue modelling. Tensile tests require the sample to be gripped between 2 points and moved apart either under a strain application which is then held constant (stress-relaxation) (Li et al. 2005, Gratz et al. 2006), a constant applied stress (creep) (Elliott et al. 2002, Charlebois et al. 2004) or a dynamically applied displacement (Park and Ateshian 2006). The samples can be strips of cartilage between grips (Elliott et al. 2002) or disc samples adhesively bonded between smooth compression plates (Li et al. 2005, Gratz et al. 2006, Elliott et al. 2002) (which may also be used to compress the samples). Tensile tests are mainly required to determine the behaviour of cartilage constituents for input into mechanical models (Charlebois et al. 2004, Elliott et al. 2002, Gratz et al. 2006, Li et al. 2005). The viscoelastic natures of the collagen fibrils (Li et al. 2005), collagen network modulus (Charlebois et al. 2004), tensile Poisson's ratio (Elliott et al. 2002) and tensile shear modulus (Elliott et al. 2002) have been determined.

The collagen network modulus was measured to be 1.7 ± 1.0 MPa per percentage applied strain which is within the range of self-assembled collagen fibres (Charlebois et al. 2004). The global tensile modulus for cartilage was found to be 5.2 MPa for native tissue (Gratz et al. 2006) which is considerably higher than the compressive modulus and is attributed to the collagen fibril network. The depth-dependence of the shear modulus was found (Elliott et al. 2002), with larger values at the surface (3.46 ± 1.80 MPa) than the deeper zones (1.10 ± 0.78 MPa). Equilibrium under stress-relaxation was reported to occur after a period between 900 s (Gratz et al. 2006) and 30 min (Elliott et al. 2002, Li et al. 2005). The variation in the collagen fibril arrangement of articular cartilage, with respect to depth, could account for the depth-dependency of the tensile moduli.

Tensile tests were applied to repaired cartilage tissue in a study by Gratz et al. (2006); the tensile modulus was found to average at 0.65 MPa, causing much greater strains to develop in regions of repaired tissue compared to regions of purely native tissue. Nasal cartilage, which is an alternative form of hyaline cartilage, was found to have a tensile modulus of 7.2 ± 3.4 MPa (Grellmann et al. 2006). The tensile modulus for nasal cartilage is higher than that of articular

cartilage, which could be indicative of the difference in the collagen fibril arrangements.

2.3.4 Indentation tests

Indentation tests may be performed *in vitro* (Duda et al. 2000, Toyras et al. 1999, Khaled et al. 2006, Rieppo et al. 2003, Barker and Seedhom 2001) or *in vivo* (Lindahl et al. 2003) using a porous (Basalo et al. 2004, Toyras et al. 1999, Rieppo et al. 2003) or impervious (Arokoski et al. 1999, Duda et al. 2000, Barker and Seedhom 2001) indenter. The test configuration for indentation tests is shown in Figure 2-3. The indenter diameter is required to be considerably smaller than the sample diameter.

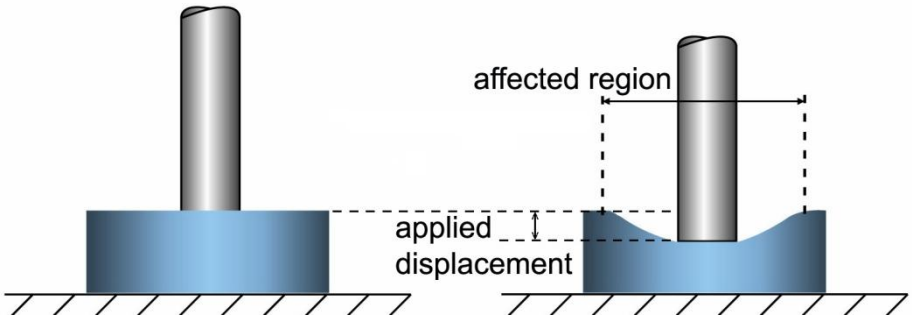

Figure 2-3: Schematic of the experimental configuration for indentation tests. The cartilage is represented in blue. The compressing surface may either be permeable or impervious. The applied displacement directly under the indenter and the subsequent surrounding surface displacements are shown

Measurements can be made of the initial elastic modulus, or the equilibrium modulus and the time taken to reach properties independent of fluid flow under both stress-relaxation and creep conditions. It is designed as a technique which causes 'minimal disruption of cartilage microanatomy' (Mow and Guo 2002) while measuring the composite Young's modulus of cartilage. The Young's modulus is calculated from the test conditions using a model of indentation (Basalo et al. 2004, Rieppo et al. 2003). This model requires values for the material's Poisson's ratio, applied load, deformation, indenter radius and a scaling factor (Hayes et al. 1972). Despite the increased complications in calculating the material mechanical properties as a result of the boundary conditions, this technique has been pursued due to its applicability *in vivo*. It is the only direct mechanical test which can be used in this manner. Compared with confined or unconfined compression lower loads are required to produce large stresses, as the area of the indenter is designed

to be small. To calculate the Young's modulus (E) from the measurements of the load (P) and the displacement (x), equation 2.1 is used.

$$E = \frac{P\left(1-\upsilon^2\right)}{2Ax\kappa} \qquad \textbf{[2.1]}$$

Where υ is the Poisson's ratio of the material, A is the indenter radius and κ is a scaling factor, which is solved numerically (Toyras et al. 1999). The scaling factor is used to take into account the boundary conditions of the sample.

Indentation strains up to 20% were used in a study by Toyras et al. (1999), where independent histological and ultrasonic measurements were made to quantify changes in tissue mechanical properties due to collagen and proteoglycan removal. Instant modulus measurements in bovine samples were found to range from 0.74 ± 0.13 MPa to 1.95 ± 0.51 MPa (Arokoski et al. 1999) and equilibrium modulus from 0.38 ± 0.006 MPa to 0.65 ± 0.15 MPa (Arokoski et al. 1999) depending on the sample extraction site. The time required for the tissue to reach equilibrium was recorded as 450 s (Toyras et al. 1999, Rieppo et al. 2003). The technique was also applied to inspect Young's modulus of engineered and enzymatically digested tissue (Duda et al. 2000, Arokoski et al. 1999). The Young's modulus for engineered tissue cultured for 12 weeks was found by Duda et al. (2000) to have only reached 25 – 30% of the measured value for healthy native cartilage. At 12 weeks the hyaline-like cartilage structure cultured *in vivo* was observed to be similar to nasal septal cartilage.

In a study by Barker and Seedhom (2001) cyclic loading was performed using indentation on cartilage samples from canine femoral chondyles and tibial plateaus at 37°C. A 3 mm diameter impervious indenter was used to apply 1.4 MPa of force in 1 s cycles with the loading portion of the cycle being half the length of the unloaded recovery portion (330 ms loading followed by 670 ms recovery). Important parameters of the cyclic load duty cycle were noted to include the frequency of load application, the amplitude of the applied stress, the loading rate, the ratio of the loading period to the recovery period and the number of loading cycles. Two characteristic phases were found in the cartilage behaviour when the 1 Hz cyclic loading was applied for 1 hour. The first phase occurred during the first 1,000 cycles (although was most pronounced during the first 200) where the data shows that the cartilage surface did not fully recover from the deformation part of

the cycle. The second phase is as the cartilage behaviour converged to a steady state, where the cartilage fully recovered the deformation sustained in each cycle.

Author	Cartilage	Stress / Strain Applied	Indenter Diameter (mm)	Rate of Strain / Stress	Eq. Time (s)	Young's Mod. (MPa)	Eq. Mod. (MPa)
Toyras et al. (1999)	bovine patella 6mm discs fresh, coll. & chon.	20% total in steps of 40µm	1.04 (porous)	1µms^{-1}	450	1.04 fresh 0.61 coll. 0.38 chon.	0.28 fresh 0.14 coll. 0.04 chon.
Rieppo et al. (2003)	bovine patella 6mm discs fresh, coll. & chon.	10% total in steps of 40µm	1.04 (porous)	1µms^{-1}	450	1.04 fresh 0.61 coll. 0.38 chon.	0.28 fresh 0.14 coll. 0.04 chon.
Arokoski et al. (1999)	canine femur & tibia	0.39MPa, 120µm disp.	0.4	creep test 2,500s	2,500	1.95 femur 0.92 tibia	0.65 femur 0.45 tibia
Duda et al. (2000)	12 wk eng.& human nasal septal	displaced 5mm (min^{-1})	4.0	5 mm (min^{-1})	-	Eng.& nasal 25-30% bovine articular (~4.0)	-
Barker and Seedhom (2001)	Canine femoral chondyles & tibial plateaus 12mm discs	max stress of 1.4 MPa applied at 1Hz	3.0	330ms on 670ms off	-	femur 19.5 max, 4.2 min. tibia 19.5 max 0.7 min	-

Table 2-4: Summary table of the results from a selection of cartilage mechanical tests using the indentation technique. 'chon.' is chondroitinase ABC, 'coll.' is collagenase, and 'disp.' is displacement. All tests at 'room' temperature except for Barker and Seedhom (2001), at 37°C.

A summary of a selection of results from cartilage indentation tests is shown in Table 2-4. The technique's main advantage is the ability for application *in vivo* under arthroscopy; however it is limited to global property measurements and has complicated boundary conditions for processing the data.

2.3.5 Shear tests and other specialist studies

Direct specialist tests of cartilage mechanics include shear in stress-relaxation conditions (Spirt et al. 1989). Application of shear strains ranging from 3% to 16% provided an experimental value for the cartilage shear modulus of 0.37 ± 0.14 MPa, which is considerably lower than all the depth-dependent shear moduli calculated through measurements of Poisson's ratio (Elliott et al. 2002). The behaviour of cartilage in stress-relaxation due to the shear strains was similar to that of compressive strains, with an initial peak value which subsequently decreased to the equilibrium value. Through application of loading in shear, the effects caused by the fluid-matrix interaction (poroelasticity) were removed due to the inability of the fluid to support the shear stress (Spirt et al. 1989). This intrinsic matrix viscoelastic

behaviour was determined to be strain-dependent. Cartilage is not naturally loaded in shear *in vivo*. Although this technique is useful for providing evidence about the intrinsic matrix behaviour, the anisotropy of the structure of articular cartilage coupled with the loading geometry may cause misleading results for the depth-dependent matrix properties.

Another specialist mechanical test is the push-out adhesion test for assessing the strength of engineered samples bonding with native tissue (Moretti et al. 2005). Samples are prepared with an outer ring of healthy native cartilage closely surrounding an inner disc of an engineered cartilage tissue replacement. After a culture period the inner disc engineered cartilage inserts begin to bond with the native cartilage. The bonded samples are then tested using a mechanical plunger of the same dimensions as the inner disc to push out the inner disc. The force required to break the adhesive bond is recorded. This technique does not assess the elastic properties of the engineered or native tissues. The adhesion may be found to be strong between the engineered cartilage and the native cartilage, but if a poor match exists in the elastic behaviour, the repaired joint surface will be rough during loading. This could lead to bone damage and therefore pain in the joint. It is therefore not a satisfactory test of the suitability of the engineered tissue.

2.4 Indirect Mechanical Tests

2.4.1 Histology

As the mechanical properties of cartilage are intrinsically related to the structure and composition, it is possible to conduct indirect assessments of cartilage mechanics by examining the tissue structure and constituent volumes histologically. In particular the collagen network architecture and the proteoglycan concentration can be used to provide a rough measure of the elastic properties (Huckle et al. 2003, Lindahl et al. 2003, Pavesio et al. 2003). Developing engineered cartilage tissue has been assessed for cell distribution using the haematoxylin and eosin (H&E) stain and cell viability through the use of live-dead stain assay, respectively. Healthy and osteoarthritic human cartilage was analysed for cell distribution with respect to tissue depth (Brocklehurst et al. 1984). Mechanical models (Julkunen et al. 2007) have been combined with histological methods of proteoglycan (PG) content (Huckle et al. 2003, Lindahl et al. 2003, Rieppo et al. 2003, Toyras et al. 1999, Ma

et al. 1995, Kiviranta et al. 2006) and collagen fibril density and orientation (Kiviranta et al. 2006, Arokoski et al. 1996, Rieppo et al. 2003, Toyras et al. 1999, Julkunen et al. 2007, Langsjo et al. 2002, Benninghoff 1925). The relative volume of PG in a sample can be determined by staining the tissue for PG content using Safarin O and then analysing the results with digital densitometry (Huckle et al. 2003, Lindahl et al. 2003, Rieppo et al. 2003, Toyras et al. 1999, Ma et al. 1995, Kiviranta et al. 2006). Collagen fibril density and orientation information can be extracted using polarised light microscopy (Kiviranta et al. 2006, Arokoski et al. 1996, Rieppo et al. 2003, Toyras et al. 1999, Julkunen et al. 2007, Langsjo et al. 2002, Benninghoff 1925). The collagen architecture of articular cartilage is of particular interest to researchers due to its effects on the material behaviour under load (Aspden and Hukins 1981, Clark 1985). Cartilage damaged by injury or disease can be assessed (Lu and Mow 2008). In order to perform histology the tissue needs to be excised from the joint. Despite the inability of the cartilage tissue to heal, biopsies are performed on living patients (Lindahl et al. 2003, Huckle et al. 2003, Pavesio et al. 2003). Biopsies have also been performed on regenerated cartilage tissue (Lindahl et al. 2003, Pavesio et al. 2003). The reliability of the diagnosis of disease from histology results following biopsy was assessed in a series of trials and found to be fairly unreliable (Ostergaard et al. 1997).

2.4.2 Magnetic Resonance Imaging

Magnetic resonance imaging (MRI) is a technique which can be applied both *in vivo* (Eckstein et al. 1999, Suan et al. 2005, O'Byrne et al. 2003) and *in vitro* (Mlynarik et al. 2004, Lopez et al. 2008, Neu and Walton 2008). It is a non-destructive method which maps tissue structure in terms of reactions of tissue constituents (normally protons in the water molecules) to applied magnetic fields (O'Byrne et al. 2003, Mlynarik et al. 2004, Eckstein et al. 1999, Lopez et al. 2008, Neu and Walton 2008, Suan et al. 2005).

For *in vitro* investigations of cartilage, magnetic resonance imaging offers extremely high resolution of structural characteristics (Julkunen et al. 2008a). The ability to only perform indirect mechanical measurements, the high financial cost of the measurements and the unsuitable nature of magnetic techniques for application on anyone with metal implants (for example if the patients other knee was already

an artificial replacement) are limiting factors for the magnetic resonance techniques. Detailed magnetic resonance images require a long acquisition time (Turgay et al. 2006), which can result in involuntary patient movements lowering the quality of the results.

In an investigation by Julkunen et al. (2008a), information was combined from relaxation times measured using T_1 (related to proteoglycan specific mechanical properties) and T_2 (related to collagen specific mechanical properties), with mechanical data obtained using two steps of 5% strain applied in unconfined compression. Experiments were performed at 25°C using a 9.4 Tesla vertical magnet. Using information from the T_2 relaxation, orientations of collagen fibrils have been found and shown to be consistent with polarised light microscopy measurements (Nieminen et al. 2001, Nissi et al. 2006). The collagen architecture found in the Julkunen investigation was used in their poroviscoelastic finite element model of cartilage. They concluded that, for functional cartilage imaging using MRI, T_1 information could be used to estimate the properties of the non-fibrillar matrix (mainly proteoglycan characteristics) and T_2 to find the collagen architecture, however T_2 was unreliable in determining the tissue elasticity.

MRI has also been used to perform elastography techniques as the positions and movement of internal structures can be mapped under dynamic high frequency excitations (Lopez et al. 2008), this is known as magnetic resonance elastography (MRE). It has been applied to approximate fluid flow from the tissue *in vivo* under deformation caused by patients performing knee bends: after 50 knee bends were performed the deformation sustained ranged from 2.4% to 8.6% and after the performance of 100 bends the range was 2.4% to 8.4% (Eckstein et al. 1999). These results allowed the calculation of a fluid flow range from 1.1 to 3.5 $mm^3(min^{-1})$.

2.4.3 Ultrasound

Ultrasound is a non-destructive, non-ionising method of material characterisation. It provides structural information from within tissues through analysis of the characteristics of the received signals (Wells 1977). The propagating wave will interact with structural discontinuities, causing portions of the sound wave to be reflected. Some of this sound energy will pass back to the receiver. Higher

frequency sound waves have smaller wavelengths and therefore have greater resolution within the material due to a greater number of reflections occurring; however these waves also have a lower material penetration as they are readily absorbed.

Ultrasound has been used to indirectly assess the mechanical properties of cartilage tissue *in vivo* (under arthroscopy) and *in vitro*. The sound speed (Patil and Zheng 2004, Toyras et al. 2003, Pellaumail et al. 1999), backscatter (Toyras et al. 1999, Laasanen et al. 2005, Pellaumail et al. 1999, Pellaumail et al. 1998) and attenuation characteristics (Toyras et al. 1999, Laasanen et al. 2005, Pellaumail et al. 1999, Pellaumail et al. 1998) of cartilage samples all depend on the tissue mechanical properties.

In vivo ultrasonic reflections from the tissue, recorded using a 10 MHz central frequency planar transducer, were processed via a wavelet transform series to provide information regarding the approximate Young's modulus (Hattori et al. 2004) and the structural integrity of the cartilage (Hattori et al. 2003). A correlation was found to exist between magnitude of the wavelet map of the Young's modulus (a three-dimensional representation of time, frequency and magnitude) and the aggregate modulus (modulus determined by the PGs) of cartilage (Hattori et al. 2003). A reduction in magnitude and an increase in duration of the echoes on the wavelet map were found to indicate cartilage degeneration consistent with the Outerbridge scale (Outerbridge 1961) indications of cartilage quality (Hattori et al. 2003).

Elevated roughness of the cartilage surface is an indication of damage, shown ultrasonically as a decrease in echo amplitude from the surface, and can be used to detect areas of osteoarthritis within the joint (Wang et al. 2008, Laasanen et al. 2006, Pellaumail et al. 1998). Cartilage surface roughness can be assessed ultrasonically (Laasanen et al. 2005) as a reduction in amplitude of surface reflections. The surface roughness of the cartilage was found to vary depending on the site of extraction from the articular joint using a 20 MHz central frequency (6 to 28 MHz -6 dB bandwidth) focussed (200 μm focal diameter, 15 mm focal length, 3mm focal zone) transducer (Laasanen et al. 2005). Laasanen et al. (2006) conducted a study on the *in vivo* spontaneous repair tissue in deliberately created

lesions in a porcine model. Using ultrasonic reflections from the cartilage surface produced using a 20 MHz transducer, the difference between the magnitude of reflections from the repair tissue were found to be significantly lower than those from intact tissue. This corresponded with a higher level of surface roughness for the repair tissue (44.0 ± 26.0 μm) than the healthy tissue (7.5 ± 2.3 μm) (Laasanen et al. 2006).

The effect of enzymatic digestion of the cartilage collagen was assessed with a 22 MHz centre frequency transducer (3 to 35 MHz -3 dB bandwidth) and found to cause a 96.4% decrease in the reflection coefficient and at 6.2% reduction in ultrasonic velocity (Toyras et al. 1999). In a separate study, the effects of progressive trypsin digestion on the ultrasonic reflections measured with a 50 MHz centre frequency focussed transducer (6.35 mm element diameter, -6 dB beam width 0.1 mm, -6 dB focal zone depth 0.95 mm) were reported. Attenuation and backscatter data from the ultrasonic signal are linked to the approximate tissue composition (Toyras et al. 1999, Laasanen et al. 2005, Pellaumail et al. 1999, Pellaumail et al. 1998), as reflections and absorption are due to the presence of the collagen fibrils and the proteoglycan macromolecules. Using a 55 MHz centre frequency focussed ultrasonic transducer (axial resolution 20 μm, lateral resolution 65 μm) it was confirmed that changes in the backscatter correlated with tissue digestion of proteoglycan or collagen, and furthermore the backscattered patterns could be used to distinguish between the digested constituents (Pellaumail et al. 1998). Combining planar ultrasonic data at 22 MHz (3 – 35 MHz -3 dB bandwidth), at room temperature in PBS containing digestive enzymes, with indentation, mechanical testing provided greater diagnostic accuracy of collagen and proteoglycan depletion (Toyras et al. 1999). Using a 55 MHz centre frequency focussed transducer (28 – 70 MHz bandwidth, 3 mm diameter, 7.5 mm focal length, axial resolution 25 μm, lateral resolution 65 μm), Pellaumail et al. (1999) found the attenuation coefficient to increase from 0.25 ± 0.03 $dBmmMHz^{-1}$ to 0.41 ± 0.12 $dBmmMHz^{-1}$ in immature and mature cartilage specimens respectively. Table 2-5 presents a summary of the ultrasonic findings from a selection of studies on articular cartilage.

Author	Ultrasonic Frequency (MHz)	Focussing Details	Processing	Detected
Hattori et al. (2004)	22	not focussed	Wavelet transform	Approximate Young's modulus
Hattori et al. (2003)	22	not focussed	Wavelet transform	Approximate Young's modulus and aggregate modulus. Cartilage integrity
Laasanen et al. (2005)	20	D: 200µm F: 15mm Z: 3mm	reflection coefficients	Surface roughness
Laasanen et al. (2006)	20	not focussed	reflection coefficients	Decrease in reflection magnitude from healthy and repair tissue
Toyras et al. (1999)	22	not focussed	Velocity and reflection coefficient	6.2% reduction in velocity, 96.4% reduction in reflection coefficient in surface damaged samples
Pellaumail et al. (1998)	55	A: 20µm L: 65µm	Backscatter	Backscatter changes correlated with digestion of PG and collagen
Pellaumail et al. (1999)	55	A: 25µm L: 65µm	Attenuation	Attenuation increase between immature and mature specimens

Table 2-5: Summary of a selection of results from the application of ultrasound to articular cartilage samples to determine structural information. In this table: 'A' is axial resolution; 'L' is lateral resolution; 'D' beam diameter; 'F' is focal length; 'Z' is focal zone.

Although links between ultrasonic parameters and both the global and the surface mechanical properties of the tissue have been found, the measurements are insufficiently consistent to allow extraction of accurate elasticity data. The information provided through these ultrasonic methods is global in nature and limited, particularly at the higher frequencies (55 MHz) used, to application *in vitro* or under arthroscopy *in vivo* (White et al. 2007). As there are mechanical tests available to measure the global mechanical properties directly, the main strength of the ultrasonic techniques is determining surface roughness.

2.5 Hybrid Mechanical Tests

2.5.1 Microscopy techniques

To mechanically characterise cartilage behaviour fully, it is necessary to find the depth-dependent (local) elastic moduli and determine whether the strain amplitude and strain rate dependence of the global moduli are related. Combining mechanical tests such as confined (Klein et al. 2007) or unconfined (Murakami et al. 2004, Wang et al. 2002) compression with methods to mark areas in the tissue samples, for tracking during the application of a global strain, have lead to data regarding the local moduli. Measurements of depth-dependent strains are used to calculate the local moduli. Regions of high elastic moduli are identified by low strain values. However, it is important to note that the protocols required to prepare samples for

these measurements may be damaging, so the values presented are intended as an indication of relative depth-dependence, as opposed to absolute values.

It is possible to directly stain the chondrocytes (Murakami et al. 2004, Klein et al. 2007, Wang et al. 2002) and optically monitor their positions within the tissue matrix as it deforms, allowing calculations of local strains. Klein et al. (2007) measured the depth-dependent moduli of bovine foetal, bovine immature and engineered articular cartilage samples after allowing a period of 30 min for stress-relaxation at 10%, 20% and 30% applied strains. The experiments were performed in confined compression conditions, so the aggregate moduli were recorded. The results demonstrated aggregate moduli of 89 ± 32 kPa in the foetal cartilage compared with 197 ± 21 kPa in immature cartilage. Strains in the 'top' (approximately 0.3 mm) of both of these sample types were significantly greater than the deeper layers. The moduli of the engineered tissue samples were not presented, but the investigators reported both the 'top' and 'bottom' (both approximately 0.2 mm) surfaces of the engineered samples straining significantly more than the centre of the constructs.

Erne et al. (2005) applied a laser based electronic speckle pattern interferometry (ESPI) technique which allowed access to strain maps from tissue regional displacements over the entire material cross-section. These hybrid methods, combining mechanical measurements with histology techniques, can be applied in stress-relaxation conditions to record the time-dependent behaviours of the local moduli. In confined compression the aggregate modulus was found to increase from the cartilage surface to the deeper tissue regions (0.27 MPa to 0.71 MPa, while the global modulus was measured as 0.47 MPa) (Erne et al. 2005).

Using microscopy combined with unconfined compression the local composite elastic moduli were found to be lower at the surface and increasing with depth (Wang et al. 2002, Erne et al. 2005), similar to the depth-dependence of the aggregate moduli from confined compression as presented previously. The Poisson's ratio was measured to be lower at the surface than in deeper regions (Wang et al. 2002). The superficial zone of cartilage was therefore found to absorb the most strain, while the deep layers absorbed the least. This trend was found to be

consistent over a range of global strains tested (Erne et al. 2005), however, the effect became less pronounced at higher strain levels.

These techniques are limited to use *in vitro* where access to the sides of the samples during compression can be obtained. The cell staining techniques present further problems in that the staining may damage tissue, causing an alteration in the absolute local properties. The stained cells are required to be near to the cut surface of the samples to allow optical access, possibly leading to boundary conditions that alter the measurable properties from their true values. Although useful as an indication of the depth-dependent variation of elastic moduli with respect to time, none of these destructive techniques are suitable for transferral to *in vivo* measurements or testing engineered tissue *in vitro* prior to implantation.

2.5.2 Elastography techniques

Elastography is a technique combining the tracking of ultrasonic signals recorded from reflectors identified within a sample before and after it is subjected to a displacement (Ophir et al. 1991). It has been used extensively, at the frequencies of conventional medical ultrasound scanners (for example at 5.5 MHz for the prostate (Souchon et al. 2003)), as a method of cancer detection to supersede manual palpation (Konofagou 2004, Khaled et al. 2006). Similar to the hybrid microscopy techniques, regions of high elastic moduli are identified by lower strain values. The displacement of the signals in time is quantified depth-dependently by splitting the pre- and post-compressional signals into a series of windows and using cross-correlation algorithms to find the shift where the signals best match (Zheng et al. 2005, Zheng et al. 2002b, Zheng et al. 2001, Fortin et al. 2003, Zheng et al. 2004, Qin et al. 2002, Zheng et al. 2002a). The further a signal moves with respect to time, the greater the strain in the matrix region where the reflector is found (Ophir et al. 1991). The accuracy of this signal-processing can be improved using techniques suggested by Ophir et al. (1991), such as parabolic interpolation of the peak shift and logarithmic signal compression (Fortin et al. 2003).

Quasi-static ultrasound elastography tests have been performed in both confined (Zheng et al. 2001, Qin et al. 2002) and unconfined compression (Zheng et al. 2005, Zheng et al. 2002b, Fortin et al. 2003) on cartilage samples *in vitro*. Elastography was adapted for application to materials such as articular cartilage and

skin by increasing the frequency and hence the axial resolution (Zheng et al. 2004, Cohn et al. 2000, Cohn et al. 1997a, Cohn et al. 1997b). Reflections from the cartilage matrix are thought to arise mainly from chondrocyte groups and bundles of collagen fibrils (Zheng and Mak 1996, Pellaumail et al. 1998). The main problem with the application of higher frequency signals is the increase in attenuation of the signal, leading to a decrease in the depth of propagation.

For *in vitro* cartilage elastography experiments, cylindrical bovine articular samples are prepared and compressed either by compression plates (with ultrasound access either axially (Zheng et al. 2005, Zheng et al. 2004, Zheng et al. 2002a, Zheng et al. 2002b) or laterally (Fortin et al. 2003)), or with displacements applied using the ultrasonic transducer (Qin et al. 2002, Zheng et al. 2001). The diameter of the cylindrical sample varies between investigations (ranging between 1.65 mm (Fortin et al. 2003) to 8 mm (Qin et al. 2002, Zheng et al. 2001)). There is a trade-off between a large enough diameter for the ultrasound beam to travel through the sample without boundary condition interference from the radial perimeter and a small enough diameter to prevent the need for large loads to be required to strain the tissue. The experiments have been conducted in 0.15 M PBS or plain NaCl saline solution at room temperature (Zheng et al. 2005, Zheng et al. 2002b, Zheng et al. 2001, Fortin et al. 2003, Zheng et al. 2004, Qin et al. 2002, Zheng et al. 2002a).

Investigations have been performed with 50 MHz central frequency transducers (Zheng et al. 2005, Zheng et al. 2004, Zheng et al. 2002a, Zheng et al. 2002b, Qin et al. 2002, Zheng et al. 2001, Fortin et al. 2003) at a sampling rate of 500 MHz. Both planar (Qin et al. 2002, Zheng et al. 2001) and focussed beams have been used (0.08 mm focal diameter, 0.95 mm focal zone length (Zheng et al. 2005, Zheng et al. 2004, Zheng et al. 2002a, Zheng et al. 2002b) and 8 mm focal diameter (Fortin et al. 2003)). Focussed beams restrict the amount of reflectors being monitored and may therefore eliminate some of the boundary conditions caused by the sample edges (Zheng et al. 2004). The behaviour of the cartilage under initial loading conditions (Zheng et al. 2005, Fortin et al. 2003) and subsequent stress-relaxation (Zheng et al. 2005) is monitored by tracking the positions of reflectors in the matrix using their position in the ultrasonic signal. Some of the published elastographic

investigations of cartilage lack automated strain application. The range of loading protocols for the global mechanical tests has revealed a large dependence of the behaviour of complete articular cartilage on the rate of strain application, magnitude of the strain applied and history of any previously applied strains. Characterisation of the local effects of these conditions is important for the development of functional tissue replacements.

The lateral application used in the investigation by Fortin et al. (2003) monitored the lateral expansion of the tissue ultrasonically. This was to determine the depth- and strain rate-dependence of the Poisson's ratio of bovine articular cartilage samples. Displacements of 15 μm amplitude were applied to the articular surface of the samples using ramp loadings at different rates. The Poisson's ratio measured immediately after the ramp displacement application was between 0.18 (displacement applied in 2 s) and 0.4 (displacement applied in 5 s). At both these ramp rates the lateral displacement was observed to be lower in the superficial zone and near to the subchondral bone. However, it is possible that the greater lateral expansion in the middle zones were caused by frictional boundary conditions between the articular surface and the compression plates. The global Poisson's ratio measured ultrasonically at equilibrium was approximately 0.12, which is consistent with the optical measurements (Fortin et al. 2003). These measurements are limited to *in vitro* application, both by the requirement of access to the cut sides of the tissue and by the high 50 MHz frequency of the ultrasound, which would be excessively attenuated *in vivo*. However, the results are useful for increasing the overall understanding of articular cartilage mechanics.

Zheng et al. (2002b) applied two steps (400 s of stress-relaxation allowed in between steps) of 0.1 mm displacement to samples averaging approximately 1.5 mm thickness to monitor the resulting depth-dependent strains (Zheng et al. 2002b). The strains in the superficial layers (0.35 ± 0.09) were found to be significantly higher than the middle (0.05 ± 0.07) and deep (0.01 ± 0.02) layers. During the stress-relaxation period the time-dependent cartilage behaviour was monitored, revealing that the positions of internal reflectors continued to change after the initial displacement in the stress-relaxation phase of the tissue. This result suggests the matrix constituents undergo a continued rearrangement in such conditions. No

depth-dependent differences were detected in the amounts of internal reorganisation, suggesting that the layered architecture of articular cartilage does not directly affect this procedure. The total strain in this experiment is quite high (~6% per step), but applied very slowly (~0.1%s^{-1}). Due to the dependence of global cartilage behaviour on strain application rate, it is possible that the depth-dependent strains measured are not representative of the behaviour from physiological displacements.

The results from elastographic monitoring of enzymatically induced cartilage degradation (using trypsin to remove the protein from the matrix proteoglycans) demonstrate the ability of the technique to determine approximate moduli from digested and undigested tissue portions. The digested and undigested cartilage had respective moduli of 58 ± 24 kPa and 470 ± 31 kPa compared to the global modulus of the untreated cartilage samples of 660 ± 230 kPa (Zheng et al. 2001). The moduli were determined by assuming a constant sound speed throughout so it is possible that the results post-digestion of the two portions are inaccurate. The sound speed is likely to have changed considerably as a result of the enzyme digestion. This technique was applied again in a later study in real time (Qin et al. 2002) to monitor the digestion boundary. The results from these studies demonstrate the sensitivity of these methods to detect depth-dependent changes in the elastic properties of articular cartilage in terms of measured strains.

Table 2-6 shows a summary of the published experiments where ultrasound elastography has been applied to articular cartilage. All experiments reported were conducted at room temperature rather than physiological body temperature (37°C).

Author	Cartilage	Strain / Stress applied	Ultrasonic Frequency & Focussing	Processing	Results
Zheng et al. (2001)	Bovine femur 7.9mm discs fresh & trypsin digested	Confined compression 4 automated steps 0.01mm (0.1mm(min^{-1})). 1,700s S-R	50MHz contact transducer (axial)	XCOR for time shifts. Moduli calculations assume CSS	Equilibrium moduli: fresh 0.66MPa 1hr trypsin 0.06MPa 2hr trypsin 0.04MPa
Qin et al. (2002)	Bovine femur 8mm discs fresh & trypsin digested	Confined compression 4 automated steps 0.01mm (0.1mm(min^{-1})). 1,700s S-R	50MHz contact transducer (axial)	XCOR for time shifts. Moduli calculations assume CSS	Equilibrium moduli: fresh 0.66MPa 1hr trypsin 0.06MPa 2hr trypsin 0.04MPa
Zheng et al. (2002a)	Bovine patella 6.35mm discs	Unconfined compression 2 manual steps 0.1mm (0.2mm(min^{-1})). 400s of S-R	50MHz focussed transducer (0.08mm diameter & 0.95mm length focus) (axial)	XCOR for time shifts	Displacement significantly greater in superficial zone (35% of total applied)
Zheng et al. (2002b)	Bovine patella 6.35mm discs	Unconfined compression 2 manual steps 0.1mm (0.2mm(min^{-1})). 400s of S-R	50MHz focussed transducer (0.08mm diameter & 0.95mm length focus) (axial)	XCOR for time shifts	Displacement significantly greater in superficial zone (35% of total applied)
Fortin et al. (2003)	Bovine humeral 1.7mm discs (~1.0mm thick)	Unconfined compression 11 automated steps of 15µm (0.18 mm(min^{-1})). 600s S-R	50MHz focussed transducer (0.07mm diameter & 0.95mm length focus) (lateral)	XCOR for time shifts.	Time- & depth-dependent solid radial displacement profiles. Greatest expansion in the centre
Zheng et al. (2004)	Bovine patella 6.35mm discs (1.5mm thick)	Unconfined compression 9.2kPa applied in creep for 900s	50MHz focussed transducer (0.08mm diameter & 0.95mm length focus) (axial)	XCOR for time shifts.	Depth-dependent strains observed to be greater in superficial zone and very small in deep zone
Zheng et al. (2005)	Bovine patella 6.32mm discs (1.54mm thick)	Unconfined compression 2 manual steps 0.05mm (0.1 mm(min^{-1})). 1,800s S-R	50MHz focussed transducer (0.08mm diameter & 0.95mm length focus) (axial)	XCOR for time shifts.	Strain redistribution observed throughout stress-relaxation. No significant depth-dependent differences of redistribution

Table 2-6: Summary table of the experimental application of ultrasound elastography to articular cartilage for the extraction of mechanical information. All tests performed at ~20°C. 'CSS' is constant sound speed, 'XCOR' is cross-correlation; 'S-R' is stress-relaxation.

2.6 Summary

The findings in this literature review have shown that the nature of the structure of articular cartilage, in particular the poroelasticity of the matrix, low permeability and depth-dependent fibril architecture, greatly affect the mechanical behaviour of the tissue. The reported properties were dependent on the test configurations, the magnitude and the rate of the applied deformations and the loading history.

Global mechanical tests have been extensively conducted. The test configurations providing the most physiologically relevant data were determined as those providing a compressive deformation: unconfined compression, confined compression and indentation. Results for the initial Young's modulus and aggregate modulus have been seen to vary considerably depending on test geometry and the magnitude and rate of strain applications. The time required to reach equilibrium also varied considerably, however the values for the equilibrium modulus were much closer between tests. Although the pressurisation and other fluid effects are less severe in unconfined compression than *in vivo*, unconfined compression has been determined as a suitable global mechanical test protocol owing to the access to the Young's modulus and the practical ease of implementation. The global mechanical tests however, are unable to provide the necessary depth-dependent information required to fully characterise articular cartilage tissue.

Methods to determine structural properties of articular cartilage and link them to mechanical characteristics were reviewed. Although all were able to predict some elements of cartilage mechanics effectively, all proved to be ultimately unable to return more than indication of the existence of depth-dependent cartilage elastic properties. Techniques combining structural information with mechanical testing in real time were determined as the most suitable method for the mechanical characterisation of articular cartilage owing to the access to the depth-dependent deformation information. Ultrasound elastography was identified as the most suitable method, as measurements could be conducted in normal unconfined mechanical test protocols with very little modification. Results can be obtained from the centre of the specimens, unlike the histology based methods, reducing the effects of the specimen edges in the analysis.

The present mechanical tests have applied a wide range of loading protocols to articular cartilage samples; however these tests lack access to the depth-dependent information necessary for full characterisation. Elastography investigations of cartilage so far have used only basic signal-processing strategies, which would be detrimental to the accuracy and resolution (Konofagou et al. 1999, Varghese and Ophir 1997b, Varghese and Ophir 1996, Varghese and Ophir 1997a, Viola and Walker 2003, de Korte et al. 1997) of the results. To this point no ultrasound

elastography cartilage investigation has combined the elastographic data with a mechanical model to provide depth-dependent moduli for the cartilage tissue, nor have the protocols been extended into dynamic cyclic loading. Systematic loading at physiologically relevant magnitudes and rates, in a test environment of 37°C, is required to fully characterise the depth-dependent mechanical properties of articular cartilage and to establish the importance of these properties with respect to the design parameters of engineered cartilage.

3 The Nature of Cartilage

3.1 Overview

The composition of all hyaline cartilages are similar, however the arrangement of the internal structures can vary considerably. This chapter details the composition of hyaline cartilages and the nature of the two differing structures (nasal and articular). The layered structure of native articular cartilage samples will be compared with the homogeneous structure of native hyaline nasal cartilage. The specimens used in this study are examined using histological techniques in order to verify the articular sample structure against literature and to investigate the structure of nasal cartilage. The manufacture and structure of engineered cartilage tissue specimens for this investigation are then detailed. Histological techniques were used to qualitatively assess the chondrocyte production of collagen and proteoglycan after 1, 5, 10 and 15 days of culture in the collagen scaffold.

3.2 Introduction

The composition and structure of hyaline cartilages, in particular articular cartilage, have been extensively studied. Found in all hyaline cartilages are proteoglycans (PGs), type II collagen fibrils, chondrocytes and interstitial fluid which is comprised mainly of water. The quantity and arrangement of these constituents varies between hyaline cartilage types, for example between articular and nasal cartilage. Alternative sources of hyaline cartilage are costal (supporting the ribs) and tracheo-bronchial (respiratory tracts). Nasal cartilage was selected as the comparison material due to the ease of extraction of suitable samples. All hyaline cartilages can be considered as highly hydrated porous fibril-reinforced composites.

Replication of the layered structure of articular cartilage poses a difficult challenge for tissue engineers (Ateshian and Hung 2004). In terms of identifying mechanical requirements and design parameters for functional engineered cartilage tissue it is important to gauge the necessity of this replication by comparing the articular structure with a homogeneous hyaline cartilage structure.

The details of the engineered cartilage produced for this investigation are given in section 3.6.2; however it is important to note that there are several different methods for engineering this tissue. The tissues created were tested at different developmental stages (1, 5, 10 and 15 days of culture time) to determine the matrix formation by the chondrocytes and the resulting changes in the mechanical properties.

3.3 Composite parts

The pericellular space (the chondrocytes and the matrix) are collectively known as the chondron. The main constituents of the chondron are the chondrocytes, the collagen fibrils and the proteoglycans.

3.3.1 Chondrocytes

Chondrocytes are responsible for the production of the matrix constituents (PGs and collagen) (Lohmander 2003). This matrix then protects the cells from external forces (Bachrach et al. 1995). The compressive stiffness of chondrocytes is of the order of 1 kPa (Jones et al. 1999); considerably lower than that of the surrounding

matrix. Chondrocytes are typically 3 – 5 μm in diameter (Clark 1985) and are found throughout the matrix, often grouped together in lacunae approximately 10 – 15 μm in diameter. Compared to the distribution of cells in many other tissues, chondrocytes are sparsely spread, accounting for only 2 – 5% of the total volume of articular cartilage (Miyata et al. 2005).

3.3.2 Collagen

Collagen is a structural protein forming around 75% of the drained matrix mass of hyaline cartilage (Lu and Mow 2008). The predominant collagen fibre type in healthy hyaline cartilage is type II, comprising 90 – 95% of the total collagen volume (Langsjo et al. 1999). Type II collagen molecules are made of three identical protein chains, which are similar to the α1 chain of type I collagen (Volpi and Katz 1991). The type II chains are approximately 35 – 50 nm in diameter (Langsjo et al. 1999) and vary in length from 251 ± 29 nm (Rammohan and Eppell 2002) to approximately 295 nm (Sun et al. 2004b). Individual collagen fibres group together, forming long bundles known as fibrils (Clark 1985). Collagen chains have high tensile strength (Zhu et al. 1996, Wu and Herzog 2002, Hiroshi et al. 1999) and are responsible for constraining excessive swelling of the cartilage tissue.

3.3.3 Proteoglycans

Proteoglycans (PGs) are the other major matrix constituent. The total proteoglycan content is 20 – 30% mass of the drained matrix (Lu and Mow 2008). They are found entangled in the collagen network and are thought to provide lubrication to the collagen fibrils (Zhu et al. 1996). PGs are protein-carbohydrate macromolecules consisting of an extended protein core to which many glycosaminoglycan (GAG) chains (up to 150) are attached (Zhu et al. 1996, Hardingham et al. 1987). These GAG side chains are negatively charged so naturally attract water molecules. The PGs are therefore responsible for maintaining the tissue hydration. The attraction of water molecules to PGs increases the compressive strength of cartilage at equilibrium (Maroudas 1979). This is because a balance is made between the external load which acts to force the water out and the PGs which act to draw the water in. Tissue permeability has been found to decrease due to the presence of PGs (Maroudas 1979, Gu et al. 1993).

3.3.4 Interstitial fluid

The interstitial fluid saturates the porous matrix. Around 65 – 85% of the weight of hyaline cartilage is fluid (Lu and Mow 2008). The average pore size is 6 nm (Lu and Mow 2008). The permeability of hyaline cartilage is low; typically of the order of 10^{-17} m^2 (Chen et al. 2001), meaning fluid motion is restricted. The fluid dynamics are responsible for the poroelastic behaviour of the cartilage (for further details please see Chapter 5).

3.4 Articular cartilage

3.4.1 Structure

Chondrocyte size and distribution vary depth-dependently from the surface to the deep zones of articular cartilage. There are up to three times as many chondrocytes in the superficial layer as there are in the deep layers (Wong et al. 1997, Brocklehurst et al. 1984). In the superficial zone, the cells appear flattened where they are trapped by the dense collagen network; in the middle zone they appear much more spherical; in the deep zone the cells are much the same shape as in the middle zone, but appear 'stacked' into small vertically arranged groups which lie parallel with the collagen fibrils (Wu and Herzog 2002).

The arrangement of collagen fibrils changes dramatically with depth from the articular surface (Benninghoff 1925, Mow et al. 1991). As shown in Figure 3-1, the fibrils are densely packed and parallel to the articular surface in the superficial zone whereas in the middle zone the fibrils are more randomly orientated as the bundles tend to change their angle to be perpendicular to the subchondral bone. These arrangements have been proposed to confer specific functions to the articular cartilage. The depth-dependent variations in the structure cause it to be an anisotropic material (Aspden and Hukins 1981). The parallel fibrils at the surface restrict the Poisson's ratio under large compressive strains, preventing damage from excessive shear strains. The deep zone fibrils are firmly anchored into the subchondral bone. In addition to the changing fibril architecture with depth, the fibrils have been found to increase in diameter from the superficial to the deeper zones (Langsjo et al. 1999).

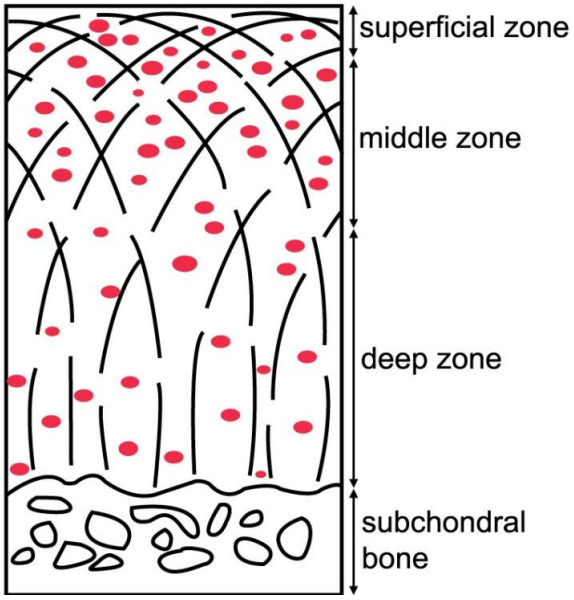

Figure 3-1: Schematic representation of the cross-section of articular cartilage. The approximate positions of the superficial, middle and deep zones and the subchondral bone are shown. The black broken lines are indicative of the collagen network orientation and the red dots represent the positions of the chondrocytes. The 'surface' of the sample is the superficial zone and the 'base' is where the deep zone meets the subchondral bone.

The volume of PG in articular cartilage has been found to be dependent on the depth from the articular surface (Chen et al. 2001, Maroudas 1979). The superficial zone has a low concentration of PGs (about 10% drained weight of the drained matrix). The concentration then increases to approximately 25% in the middle zone before decreasing again in the deepest zone (Maroudas 1979).

Articular cartilage permeability is also depth-dependent due to the nature of the porous network which changes as the fractional composition of the matrix changes. The permeability decreases with respect to distance from the articular surface from approximately 9.2×10^{-17} to 1.0×10^{-17} m^2 (Chen et al. 2001).

3.4.2 Samples

For this investigation, bovine articular samples were harvested from the patella of animals approximately 6 h after slaughter. A total of 14 patellae, each from different animals, were used over the various experiments. In each set of experimental repeats 2.36 ± 0.66 (average ± standard deviation) different patellae were represented. Figure 3-2 shows the harvest site of the samples.

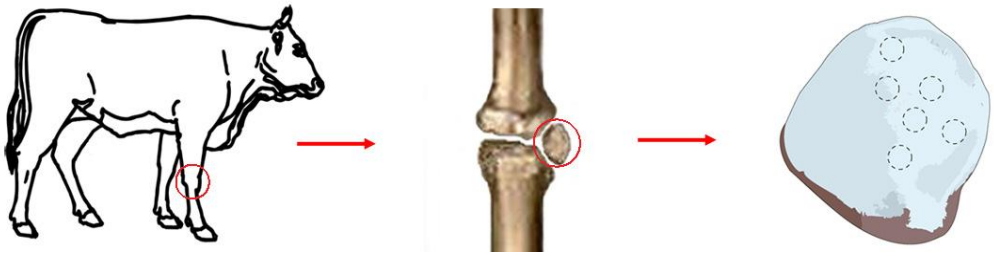

Figure 3-2: Figure to show the harvest site and the approximate relative size of the samples collected. The dotted circles in the third stage a representative of the biopsied samples in relation to the size of the patellae. Bovine patellae were excised following animal slaughter and cylindrical articular cartilage specimens prepared using 8 mm biopsy punches and scalpels.

Typical histological cross-sections are shown in Figure 3-3. The histology sections were stained with Haematoxylin & Eosin (H&E) to show the chondrocyte morphology and location in the tissue.

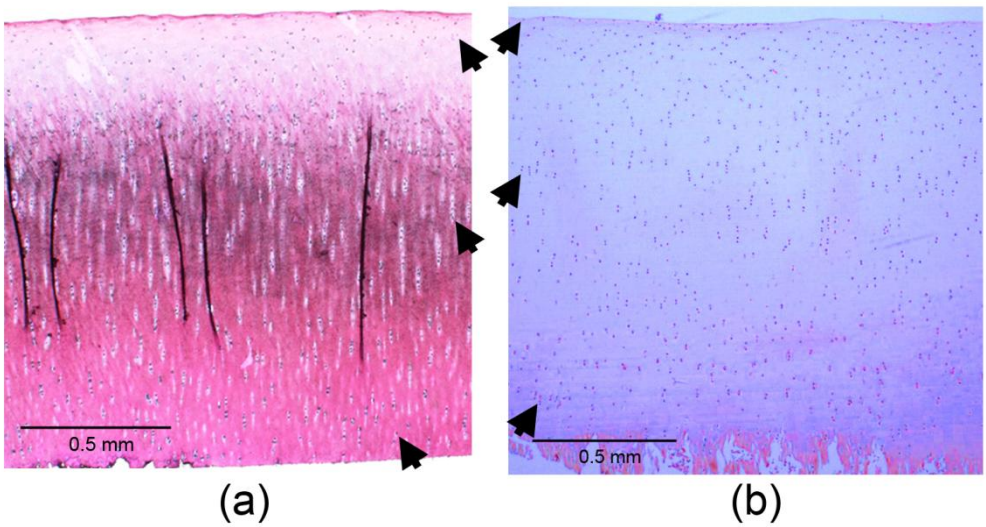

Figure 3-3: Histological cross-sections of articular cartilage stained to show presence of chondrocytes, a selection of these cells are indicated with the arrow heads. The sections are taken from two separate samples and the scale bars are shown. The subchondral bone interface has been removed more cleanly from the base of (a), which is why there are two clean edges shown on this specimen.

In order to establish the structural similarities of the articular cartilage samples with those previously published, cell counts were made via optical microscopy using 0.5 mm square windows at 0.1 mm intervals through the full thickness depth. These were performed at two positions in both histology sections (a) and (b) shown in Figure 3-3. These counts revealed cell distributions with respect to depth (normalised to the average thickness of the samples in this experiment of 1.61 ± 0.38 mm) as shown in Figure 3-4.

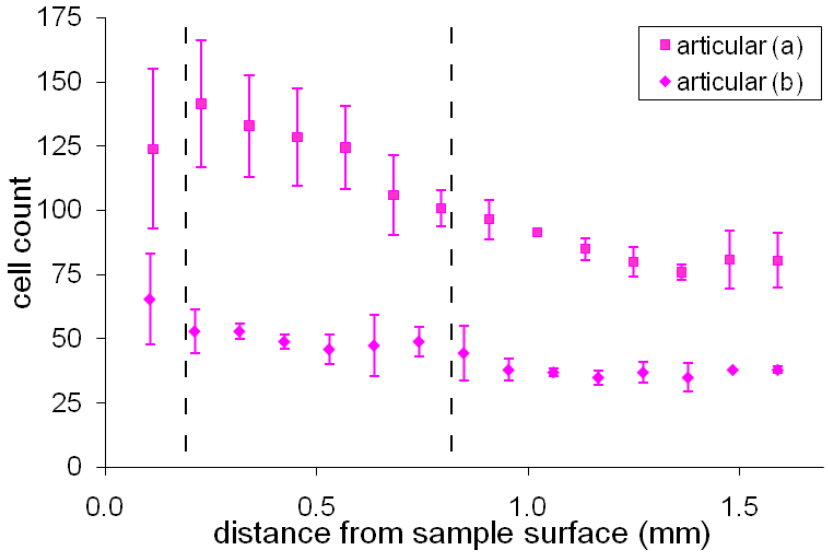

Figure 3-4: Cell count results from the surface to the base of the sample from the articular cartilage histology sections shown in Figure 3-3 (a) and (b). Cells were counted in overlapping 0.5 mm by 0.5 mm windows at varying depths from the sample surfaces. Although the counts made from cross-section (b) were considerably lower, a similar shape is represented with the greatest cell density being at the cartilage surface.

These findings are consistent with previous investigations (Wong et al. 1997, Brocklehurst et al. 1984): Wong et al. (1997) reported an increase of chondrocytes from the deep zone to the surface by a factor of three, and Brocklehurst et al. (1984) reported approximately 60% more chondrocytes in the superficial region, rapidly decreasing through the transitional zone and stabilising with respect to depth through the deep zone. The cell counts provided means for estimating the zonal thicknesses using regions of similar gradients. The approximate zonal thicknesses were found from the cell densities as 7% superficial, 36% middle and 57% for the deep zone from Figure 3-4.

In addition to the variation in chondrocyte population density with respect to depth, the chondrocyte morphology also changes slightly (Hunziker et al. 2002). The superficial zone contains chondrocytes which have been aligned and flattened. Figure 3-5 (a) to (d) demonstrates examples of chondrocytes in the superficial zone of the histological sections in Figure 3-3. Figure 3-5 (e) shows the shape found by Hunziker et al. (2002) for this region.

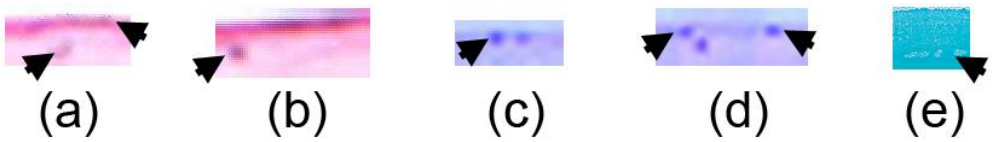

Figure 3-5: (a) to (d) show histological findings from specimens used in this investigation. (a) and (b) are from Figure 3-3(a). (c) and (d) are from Figure 3-3(b). The cells in the superficial zone are marked with arrows. For comparison, a cell from the same zone from Hunziker et al. (2002) is shown in (e).

The middle zone contains randomly distributed chondrocytes which are close to spherical. The collagen fibrils have a tendency to influence the position of the cells. Figure 3-6 (a) to (d) show examples of middle zone chondrocytes and (e) shows the morphology found in that region by Hunziker et al. (2002).

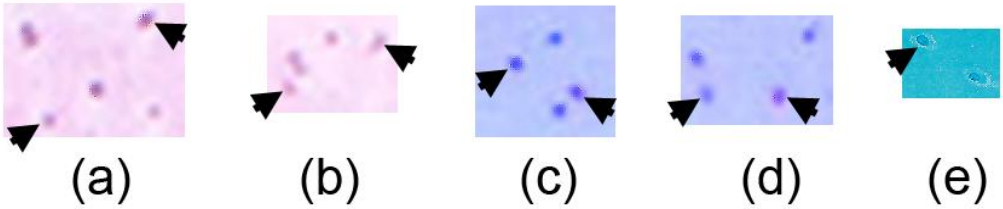

Figure 3-6: (a) to (d) show typical middle zone chondrocytes found in the histology slices in Figure 3-3. (a) and (b) are from Figure 3-3(a). (c) and (d) are from Figure 3-3(b). Cells from the same zone from Hunziker et al. (2002) are shown in (e).

The deep zone contains columns of chondrocytes aligned by the fibril directions. The chondrocytes in this region are of a similar shape as the ones in the transitional zone, but aligned into columns parallel to the collagen fibrils (as shown by Hunziker et al. (2002) and demonstrated in Figure 3-7 (e)). Examples of chondrocytes from this region are shown in Figure 3-7 (a) to (d).

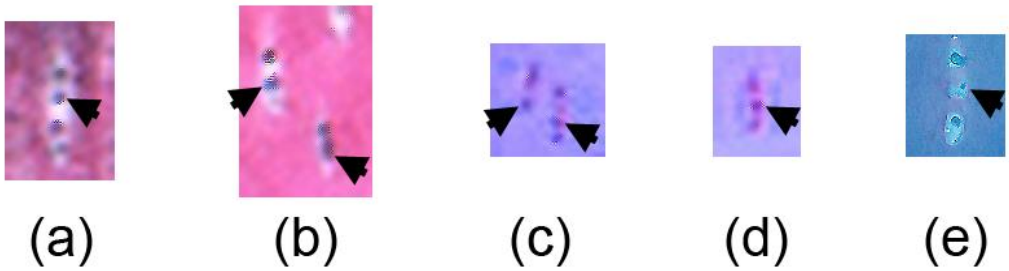

Figure 3-7: Chondrocytes from the deep zone of articular cartilage. The chondrocytes can be seen to be stacked into columns in lacunae. (a) and (b) are from Figure 3-3(a), (c) and (d) are from Figure 3-3(b). Cells from the same zone from Hunziker et al. (2002) are shown in (e).

The differences in the cell morphology can be used to approximate the zone thicknesses from the histological sections. There is a small amount of variation between the sections. Figure 3-3 (a) has approximate zone thicknesses of 3%, 32% and 65% for the superficial, middle and deep zones respectively. Figure 3-3 (b) has approximate superficial, middle and deep zone thicknesses of 4%, 38% and 58%. These results correlate reasonably well with the cell count and morphology results reported by Hunziker et al. (2002).

Magnetic resonance imaging can be performed on cartilage samples to obtain information regarding specific parameters, for example the orientation of the collagen fibrils in the matrix. This technique was used to further confirm the structure of the articular samples. The time constant which describes the decay of the transverse magnetisation of the sample is known as the transverse relaxation time (T_2). T_2 times are sensitive to collagen fibril alignment (Nieminen et al. 2001, Nissi et al. 2006, Xia et al. 2002, Dunn et al. 2004). Each collagen fibril has protons associated with it. Each proton has a magnetic moment (w), when placed in a magnetic field (B_0), and will generate its own small, local, dipolar magnetic field (B_w), as shown in Figure 3-8(a).

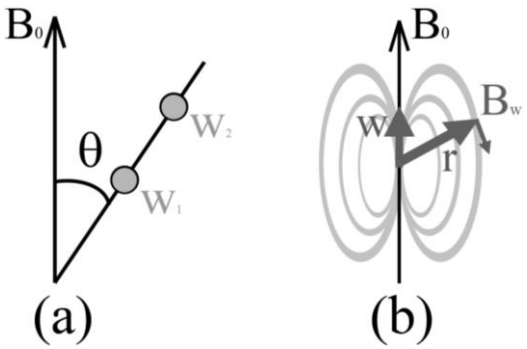

Figure 3-8: Representation of (a) two adjacent protons on a collagen fibril orientated at angle (θ) to the applied magnetic field (B_0). (b) The magnetic dipole and the associated local field. Every proton in the matrix experiences small magnetic forces from each of the neighbouring protons. Hyaline cartilage is proton rich, so there are many contributions to each field.

The initial coherency of the proton net magnetisation, resulting from the application of the MR excitation, quickly de-phases, due to the slight variations in the individual proton dipole fields. The time scale of the de-phasing is the T_2 time, and can be described using equation 3.1 (Dunn et al. 2004).

$$S_{TE} = S_0 e^{\frac{-TE}{T_2}} \qquad \textbf{[3.1]}$$

Where S_{TE} is the signal intensity at time *TE* (representing the time in milliseconds between the application of the 90° pulse and the peak of the echo signal in spin echo and inversion recovery pulse sequences) and S_0 is the initial signal intensity (intensity at t=0), which is determined by the density of the protons in the tissue. The duration of these local dipolar interactions have been observed to be determined by the relative angles of the fibrils (θ) to the direction of the magnetic field (B_0) (shown in Figure 3-8(b)). The protons are relatively fixed in the collagen network. This causes the net dipolar interactions, described by the 'dipolar spin Hamiltonian', (H_D), to not be averaged to zero, as they would be in a fluid. The angle of the proton dipole interactions relative to the applied magnetic field direction determine the relaxation time, summarised by the relationship shown in equation 3.2.

$$H_D = 3\cos^2\theta - 1 \qquad \textbf{[3.2]}$$

The higher the levels of dipolar interaction (H_D) the faster the T_2 relaxation occurs. Equation 3.2 yields the highest values for fibrils parallel to B_0, as would be found in the deep zone. The levels of interaction are also found to be high when the fibrils are perpendicular to B_0, as the fibrils are in the superficial zone. Equation 3.2 reduces to zero at approximately θ = 54°. In the middle zone the fibrils are randomly aligned. As a result the contribution from dipolar interaction is lower and therefore the T_2 relaxation time is longer.

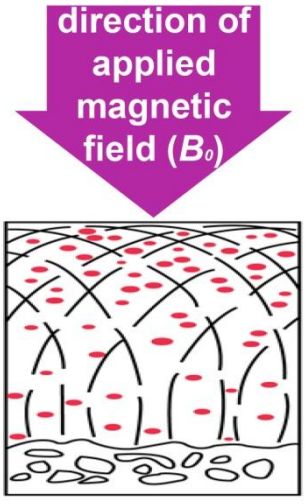

Figure 3-9: The direction of the applied magnetic field (B_0) with respect to the approximate fibril alignment in the articular cartilage sample tested.

In the experimental set up performed by collaborator Mr Peter Del Manso (Medical Physics, UCL) the cartilage is placed relative to the magnetic field as shown in Figure 3-9.

The images and depth-dependent relaxation time results from an MR T_2 test performed on a bovine articular sample as part of a collaborative study are shown in Figure 3-10. The imaging was performed using a multi-slice spin-echo (sems) sequence with; 6.4×12.8 mm field of view, 64×128 matrix, 0.5 mm slice thickness, 0.5 mm gap, 2s pulse sequence repetition time, 4.5, 5, 6, 7, 8, 10, 14, 20, 30 ms echo time (*TE*), 10 sample averages, 42 min acquisition time for one complete image.

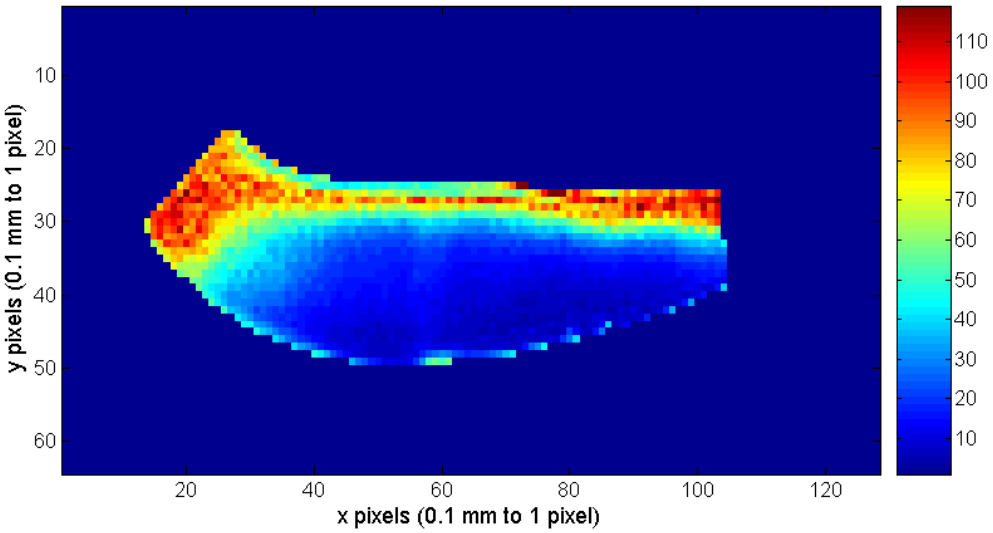

Figure 3-10: Generated T_2 map from articular cartilage. Colour bar shows T_2 times (ms).

The T_2 map generated from the procedure is shown in Figure 3-10, where the darker colours represent lower values of T_2 (ms). The results were relative to the angle of the sample to the magnetic field, so these were calculated and used to interpret the relaxation times in relation to the zone positions. The initial angle-corrected results were compared to model predicted relaxation times from expected fibril orientations and the differences between the two results minimised to obtain the zonal thicknesses (currently unpublished, Del Manso). These are shown in Figure 3-11.

The model resulted in calculations of relative thicknesses of the superficial, middle and deep zones as 6.8%, 15.6% and 77.6%. The middle zone was found to be considerably smaller than the results published by Hunziker et al. (2002), but the

superficial zone thicknesses were more consistent. The MR results serve to confirm the articular structure of the samples in the same manner as the cell counts.

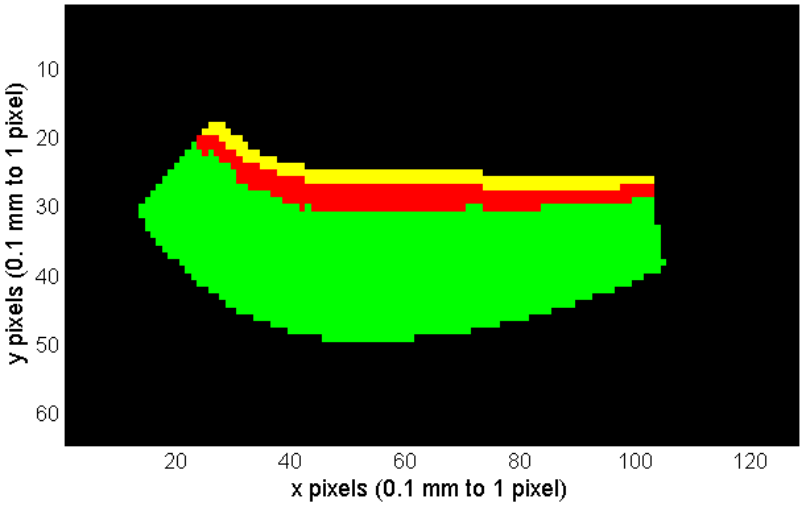

Figure 3-11: Zones calculated from the T_2 results and the model fitting. The zones are shown, from top to bottom, as the superficial, middle and deep zones.

3.5 Nasal cartilage

3.5.1 Structure

Nasal septal cartilage is a hyaline cartilage, but has a fairly homogeneous structure through its depth, closely resembling the middle zone of articular cartilage (Anderson and Sajdera 1971).

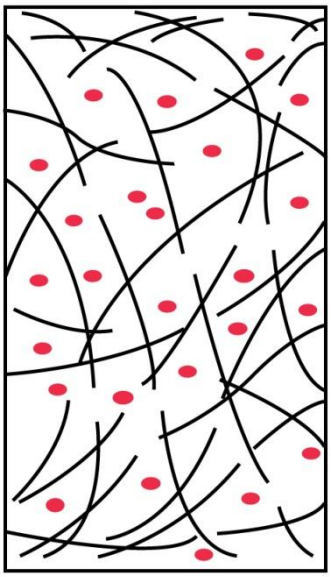

Figure 3-12: Representation of the cross-section through nasal cartilage. An approximation of the fibril network orientation (in black broken lines) and the chondrocyte positions (in red) are shown. The sample has no specific 'top' or 'base', but these are defined when the sample is placed on the rigid surface.

Collagen fibrils in nasal cartilage have been found to vary considerably in width; from 16 – 290 nm (Anderson and Sajdera 1971). A schematic representation of the cross section of nasal cartilage is shown in Figure 3-12. The samples are not attached to any subchondral bone, but *in vivo* have a membrane with a rich blood supply covering both free surfaces.

There have been few studies reported in the literature regarding the precise composition and structure of nasal cartilage. Owing to the structural function which nasal cartilage performs in animals (as opposed to the load-bearing function of articular cartilage), there is little requirement for nasal hyaline cartilage to have the same level of complexity in its organisation.

3.5.2 Samples

For this investigation, porcine nasal septal samples were harvested from the noses of animals approximately 6 h after slaughter. Porcine nasal samples were selected rather than bovine, as the tissue was easier to extract and handle. A total of 12 noses were used during all the experiments. Within each set of experimental repeats, 2.04 ± 0.57 (average ± standard deviation) noses were represented. Figure 3-13 shows the harvest site of the samples.

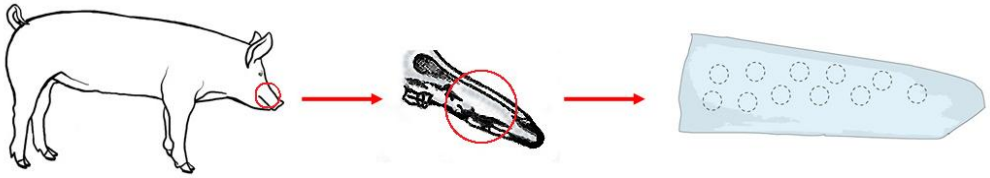

Figure 3-13: The harvest site and the approximate relative size of the samples collected. Porcine nasal septums were excised following animal slaughter and cylindrical nasal cartilage specimens prepared using 8 mm biopsy punches.

Nasal cartilage specimens were considerably thicker than articular cartilage, with the average measured thickness being 4.22 ± 0.56 mm (± standard deviation). Typical histological cross-sections of nasal cartilage are shown in Figure 3-14.

The remainder of part of the protective membrane can be observed on the base of specimen (a) in the figure. The protective membrane has been completely removed from the top surface of specimen (a) and both surfaces of specimen (b).

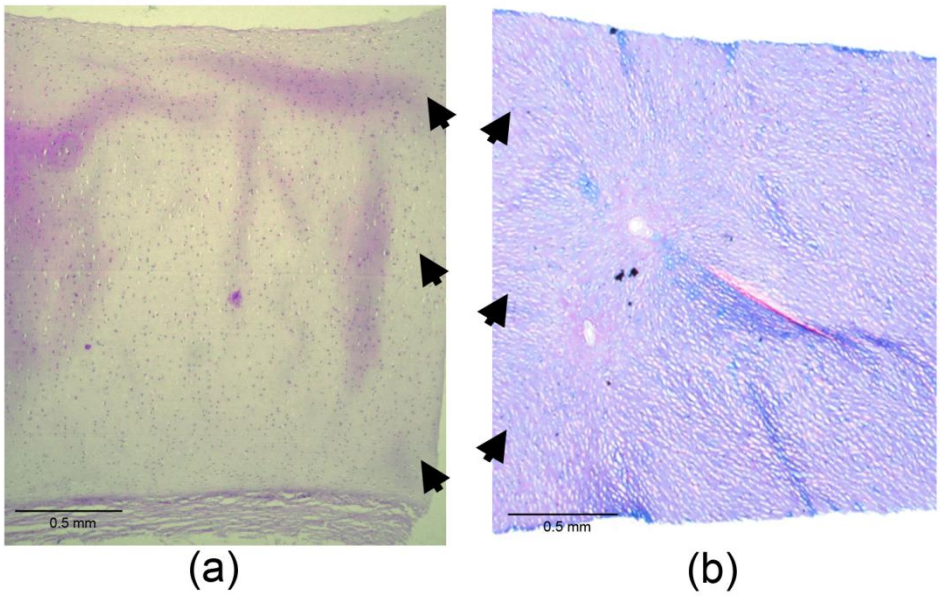

Figure 3-14: Histological cross-sections from two porcine nasal cartilage samples. In (a) part of the protective membrane remains on the base of the sample, so it looks different to (b). Cells were counted in overlapping 0.5 mm by 0.5 mm windows at varying depths from the sample surfaces. The chondrocytes can be seen spread throughout the matrix in lacunae which are likely to be aligned with the local collagen fibrils

Cell counts were performed in the same manner as described in section 3.4.2, with a window size of 0.5 mm^2 and placed every 0.1 mm along the cross-section. The results are shown in Figure 3-15.

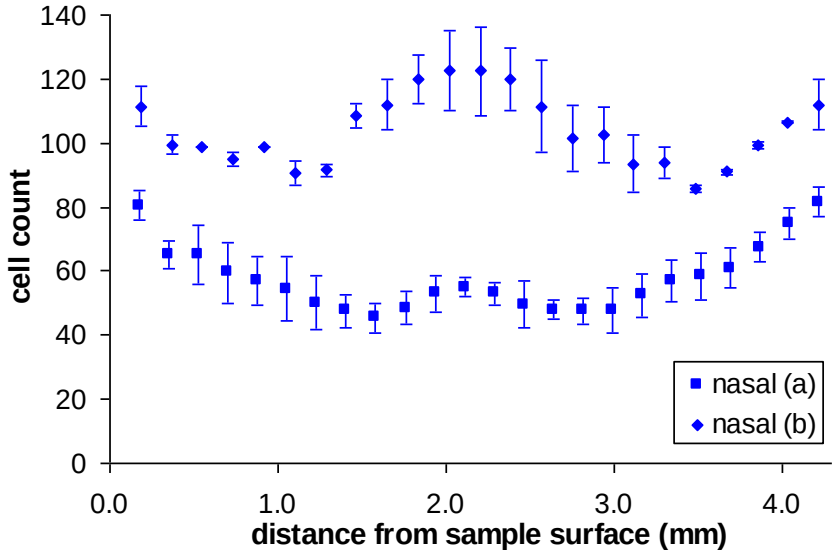

Figure 3-15: Cell count results through the thickness of porcine nasal cartilage samples. Similar to the results in Figure 3-4, one of the samples' cell count is significantly lower than the other but proportionally a similar cell distribution is demonstrated.

A clear difference can be observed between the cell count profiles in articular cartilage and the nasal cartilage cross-sections. The cell distribution in nasal cartilage is most concentrated in the centre and at the edges of the samples, unlike the articular cartilage which increases from the base to the surface. Nasal cartilage appears to have a higher density of chondrocytes than articular cartilage. This is expected as nasal cartilage has a rich blood supply to provide nutrients to the cells. Nasal cartilage is not subjected to the same magnitude of loading as articular cartilage. The shape of the lacunae visible in Figure 3-14 (b) demonstrates the random variation of the collagen fibril alignment.

Analysis of the chondrocyte morphology was performed in the same manner as for the articular cartilage samples. Groups of cells from different depths (top, middle and base of the nasal samples as shown in Figure 3-14) were selected and analysed. These are shown in (a) to (d) of Figure 3-16, Figure 3-17 and Figure 3-18.

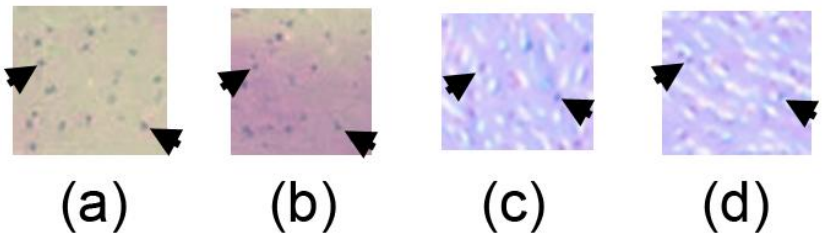

Figure 3-16: Cells taken from the 'top' edge of the nasal cartilage histology sections shown in Figure 3-14. (a) and (b) shown in this figure were taken from Figure 3-14(a). (c) and (d) were taken from Figure 3-14(b).

The chondrocyte morphology in all regions was expected to be similar to the middle zone of articular cartilage.

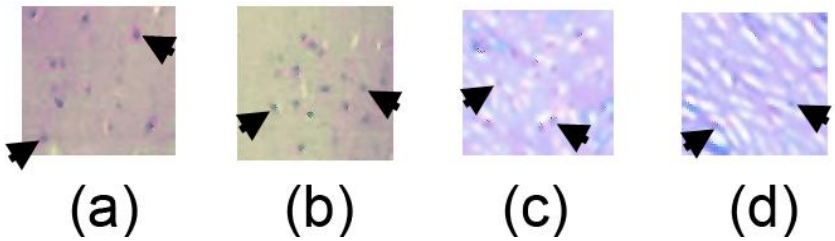

Figure 3-17: Cells taken from the centre of the nasal cartilage histology sections shown in Figure 3-14. (a) and (b) shown in this figure were taken from Figure 3-14(a). (c) and (d) were taken from Figure 3-14(b).

This result can be seen comparing the cells shown in Figure 3-6 with the cells shown in Figure 3-16, Figure 3-17 and Figure 3-18. The chondrocytes were more evenly spread across the nasal cartilage samples. These examples of cell morphology were taken from areas of denser chondrocyte populations as found in

the cell counts (Figure 3-15). The cells in the less dense regions are the same shape as the ones shown and also fairly evenly spread across the sample.

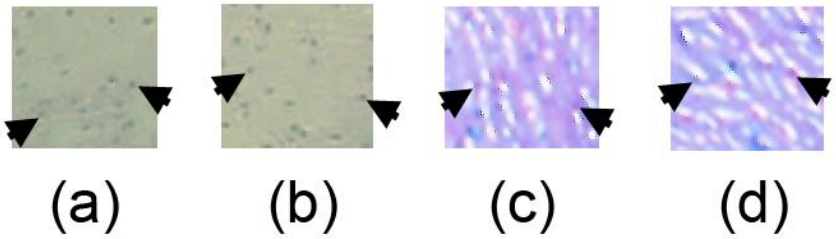

Figure 3-18: Cells taken from the 'bottom' edge of the nasal cartilage histology shown in Figure 3-14. (a) and (b) shown in this figure were taken from Figure 3-14(a). (c) and (d) were taken from Figure 3-14(b).

The chondrocytes in all the regions examined were round in shape and were evenly spread. At most three chondrocytes were seen in the same lacunae, but the majority were single. No deep zone was found to be present in nasal cartilage tissue.

3.6 Engineered cartilage

3.6.1 Cartilage engineering

In line with the primary goals of functional tissue engineering, stated in Chapter 1, engineered cartilage tissue is required to have similar or better mechanical properties than native tissue. The method used to engineer the cartilage tissue in this investigation is one of many existing methods. Engineered tissue constructs can be made from many different materials and in many different geometries. The basic requirement is to confine either chondrocytes or stem cells to the site requiring repair (Lohmander 2003). The cells can be contained in either a biological, synthetic or engineered matrix known as a scaffold. The purpose of a scaffold is to provide a template for cell attachment and subsequent tissue development (Vunjak-Novakovic 2003). Scaffolds can vary with respect to matrix material chemistry (e.g. collagen, synthetic polymers or agarose), structure (e.g. porosity and the orientation and connectivity of the pore network in gels, porous sponges or fibrous meshes), mechanical properties (e.g. compressive stiffness) and whether or not they will be dissolved in the body (Vunjak-Novakovic 2003).

3.6.2 Engineered tissue samples

Engineered cartilage tissue was made at the Division of Biomaterials and Tissue Engineering at the Eastman Dental Institute, UCL, by Mr. Kaveh Memarzadeh. The engineered cartilage tissue used in this study was created from chondro-progenitor

cells (cell line ATDC5) seeded into self-assembling collagen hydrogels. Approximately 10^5 cells were added to each individual gel (Memarzadeh 2009). The excess fluid was then removed from the gel though a process known as plastic compression in order to improve the mechanical properties of the construct (Brown et al. 2005). Single hydrated gel constructs were subjected to 50g weight applied to the 4.29 mm^2 surface area for exactly 5 min. The precise details of the construct manufacture can be found in Brown et al. (2005). Where the fluid leaves the construct at the base and edges, collagen fibrils have been observed to condense into layers ranging in thickness between 1 and 5 μm (Hadjipanayi et al. 2010). An individual, plastically compressed sheet is only approximately 100 μm thick. In order to increase the thickness of the constructs to a more functional level, five plastically compressed sheets were layered together.

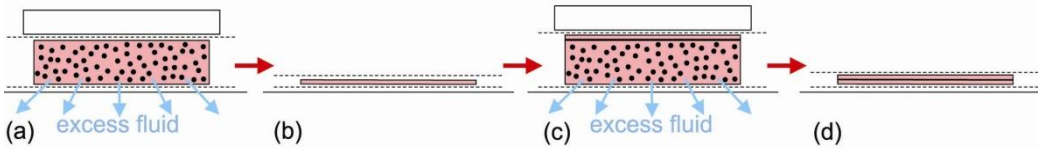

Figure 3-19: Construction of engineered cartilage samples: (a) Initial plastic compression of hyper-hydrated cell seeded collagen construct. White block represents load applied to specimen. Excess fluid drains into absorbent layer below. Construct contained between two gauze layers, represented by broken lines. (b) Single layer plastically compressed construct between gauze. (c) Single compressed layer placed on top of next hyper-hydrated construct. Load forces excess fluid out. (d) Two plastically compressed layers together. Repeated until five plastically compressed layers are made.

Multi-layering of the constructs was achieved by plastically compressing each seeded gel sequentially after carefully placing the stacked previously compressed layers of the construct on the surface (see Figure 3-19). The previously compressed sheet adheres to the newly compressed sheet. The five layered constructs were mechanically stable and approximately 0.5 mm thick.

In order to quantify the increase of construct mass as a result of the chondrocytes producing the matrix materials (collagen and PGs) over the culture periods, the thickness of the samples was measured using optical microscopy. The results are shown in Figure 3-20.

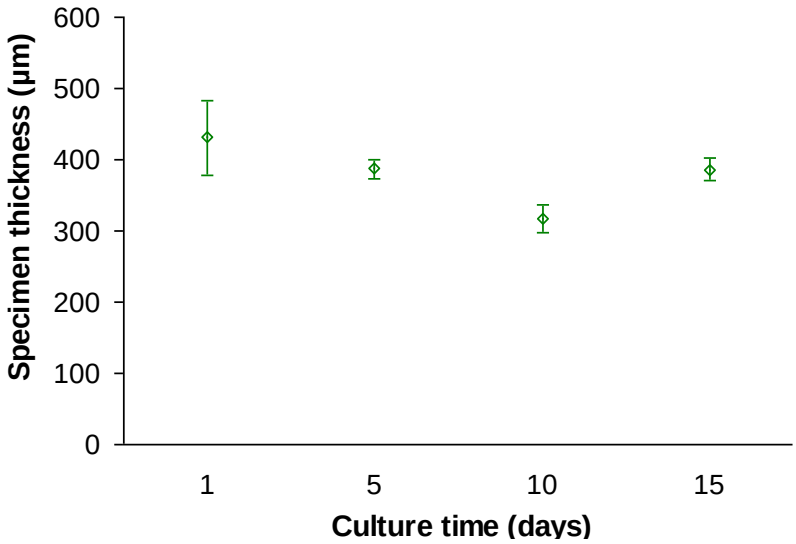

Figure 3-20: Graph showing the change of measured engineered cartilage thickness with respect to culture time. Error bars display the standard deviation of the (three averaged) measurements.

From 1 to 10 days there is a decrease in the measured sample thickness. By 15 days the samples have decreased 26% from the 1 day thickness. The exact causes of the decrease are unclear, but could be a result of initial cell death or the initial cell matrix secretions causing a contractile effect, drawing the layers closer together. Although PGs would have been excreted by the cells, no significant uptake of water appears to have occurred before 10 days. A 10% increase can be seen between 10 and 15 days. This increase is most likely to be caused partially by the cell matrix excretions, but also the subsequent uptake of water due to the presence of the charged PGs. The osmotic swelling of the tissue would be more likely to cause a measurable thickness increase than the cell matrix production alone. The statistical significances of the measured changes were determined using the student's T-test between individual days and 1-way analysis of variance (ANOVA) between all the sample means together. As seen in Figure 3-20, the standard deviations of the results from 5, 10 and 15 days are low, contributing to the statistical significance of the findings. ANOVA determined the differences between all of the means to be highly significant (>99.9%). However, using the student's T-test, thickness changes from 1 to 5, 5 to 15 and 1 to 15 days were not statistically significant at 90% confidence. By 15 days the engineered specimens have returned to the same thickness as 5 days. It is likely that the increase in thickness would continue with increasing culture time due to the excretion of more PGs into the matrix.

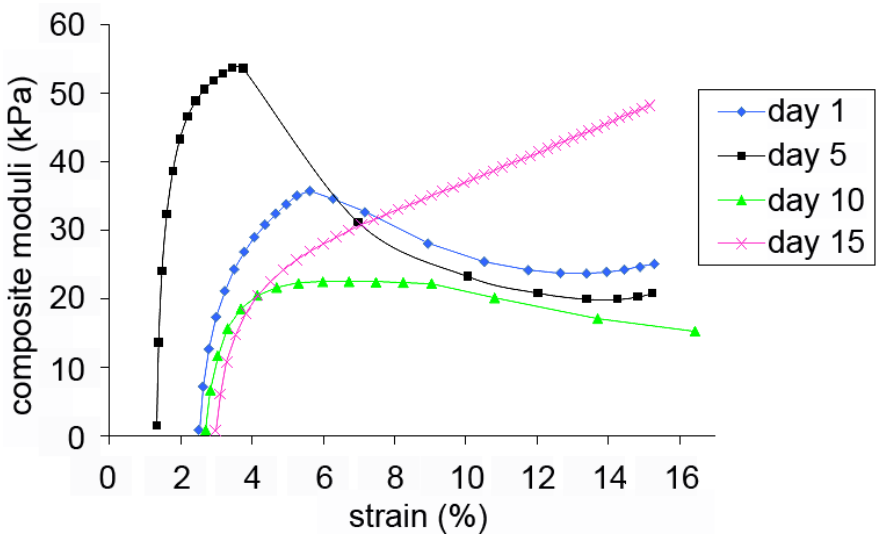

Figure 3-21: Graph from the results of mechanical testing of collagen scaffold based engineered cartilage samples at 1, 5, 10 and 15 days of culture time (Memarzadeh 2009) (average for three samples at each culture time. Standard deviation not available).

Compressive moduli were measured for the samples (Memarzadeh 2009) at 1, 5, 10 and 15 days using an unconfined compression method. The results are shown in Figure 3-21. The initial decrease in the measured compressive modulus was thought to be caused by the increase in water content of the tissue caused by the production of matrix PGs, but with lack of sufficient collagen remodelling to restrain excessive deformation (Memarzadeh 2009). The approximate composite modulus of articular cartilage in unconfined compression at 10% applied strain is 2 MPa (Langelier and Buschmann 2003)..

Histological analysis with H&E staining was performed to determine the number and positions of the chondrocytes throughout the collagen scaffold at each culture time investigated. It was found that the density of the cell populations decreased with respect to culture time, but this was not unexpected as chondrocytes are sparse in native cartilage tissue. The amount of PG was assumed to increase between days 10 and 15 due to the increase of the construct thickness and water uptake. The collagen matrix of the engineered samples was seen to have been extensively remodelled by the cells by day 15. These results indicated that the changes in the measurable mechanical properties of the constructs were directly attributable to cellular production of matrix constituents.

The production of PGs and collagens by the chondrocytes during cell culture correlates with the increase in the measured compressive moduli and a decrease in the permeability. As the PGs are produced by the chondrocytes, water molecules are attracted to the charged GAG side chains and so cause the tissue to swell. PGs have been found to reduce tissue permeability (Maroudas 1979, Gu et al. 1993). The type I collagen in the scaffold and the collagen also produced by the cells acts to restrain excessive swelling and movement of the PG molecules, thus increasing the compressive moduli. This is consistent with reports of the function of the constituent parts of cartilage (Maroudas 1979, Lai et al. 1991, Wu and Herzog 2002, Soulhat et al. 1999, Rieppo et al. 2003, Mow et al. 1991).

From Figure 3-21, it can be seen that the global moduli of the constructs are considerably smaller than those expected from native tissue. However, it is important to be able to quantify the properties of the engineered tissue in order to enable better understanding of the culture process and possible final properties. Over the culture period it is likely that developmental changes will not occur uniformly with respect to depth. The developmental changes will cause changes to the mechanical properties of the samples. The depth-dependence will be investigated with the elastography system as well as the global elastic properties.

3.7 Summary

This chapter described the similarities and differences between the three different types of cartilage specimen which were investigated in terms of the constituent parts and their structure. The preparation and handling details were provided for the native samples. The manufacture details of the engineered tissue were outlined alongside important data from our collaborators' study.

4 Development of the elastography method

4.1 Overview

As highlighted in the literature review, existing unconfined compression elastography methods are limited to quasi-static loading protocols performed at room temperature. The results found were also only processed with the most basic elastography signal-processing methods. In this chapter existing elastography techniques are adapted for application to various hyaline cartilage structures. The equipment selection and assembly are presented in order to demonstrate the improvements proposed by this work. The selection of a suitable signal-processing method is made to enable fast and reliable extraction of strain data from the signals collected. Different loading protocols are designed in order to test the dependence of the global and depth-dependent elastic properties on: the magnitude of the strain and the rate in which it is applied; the history of the strain applied to the specimens; and the frequency and magnitude of a cyclic strain. These protocols, detailed in this chapter, are termed ‘quasi-static strain’, ‘quasi-static strain steps’ and ‘dynamic strain’.

4.2 Introduction

The technique of elastography was selected for investigations into the depth-dependent structure of cartilage and the localised elastic response under different loading conditions.

4.2.1 Improvements

Similar previous investigations into cartilage mechanics were reviewed in Chapter 2. The elastography procedure is to be improved in the following ways:

- Allowing a greater range of loading protocols in the unconfined compression geometry.
- Performing measurements at body temperature (37°C) in a liquid isotonic to synovial fluid (~0.15 M (Patil and Zheng 2004)).
- Real time compensation for the effect of the load cell deflection on the magnitude of the strain actually applied to the cartilage sample.
- Lowering the ultrasound interrogation frequency to allow a reduction in attenuation and to allow measurements in the thicker nasal cartilage specimens.
- Improving signal-processing methods to obtain robust, repeatable depth-dependent strain measurements.

This chapter first addresses the changes made to the hardware of the ultrasound elastography system and secondly discusses the necessary experimental protocols. The selection and details of the signal-processing method and suitable statistical analysis techniques are then described.

4.2.2 Method outline

The method can be approximately split into three sections: experimental measurements of the mechanical and ultrasonic test response of cartilage samples as a result of global strain; suitable processing of ultrasonic signals to extract depth-dependent strains; and application of appropriate statistical methods to determine the significance of the results.

4.2.2.1 Experimental measurements

Global mechanical measurements of the force required to cause a pre-determined strain in the samples are used to establish the global composite moduli. The composite moduli represent a combination of both the solid matrix moduli and the pressurised interstitial fluid. Ultrasonic signals from inside the cartilage samples are recorded before and during the application of the strains.

4.2.2.2 Signal-processing

The change in arrival times of signals from reflectors inside the specimens as a result of the global strain application can be found. These time-shifts are used to determine localised material displacements and can be converted into depth-dependent strains. The depth-dependent strains found when the material has reached global mechanical equilibrium can be used to determine the local moduli.

4.2.2.3 Statistical methods

For each experiment, a number of repeat measurements will be performed. The spread of the data between the specimens will be taken into consideration when determining the significance of the findings. The results between the different specimen types and the different strain protocols will be compared.

4.3 Method development – equipment

4.3.1 Variable loading patterns

A programmable actuator with a movement range of 10 mm, capable of providing a force of up to 40 N (according to manufacturer) was selected (M-227-10 DC mike linear actuator, Physik Instrumente (PI) GmbH & Co. KG). The 40 N force capability of the device was determined to be sufficient. Although extremely high compressive moduli of articular cartilage have been found (19.5 MPa (Barker and Seedhom 2001)), a more typical value for the global modulus of cartilage at 10% applied strain is 2 MPa (Langelier and Buschmann 2003). For a sample diameter of 8 mm, this would require approximately 10 N of force. The velocity and displacement of axial motion were controlled using purpose written software in LabVIEW (National Instruments Corporation, Austin, Texas, USA). In calibration experiments (Appendix Ai), the repeatability of the actuator movements was tested and shown to be within 0.7% of the programmed input.

4.3.2 Global mechanical measurements

A load cell is required within the system, arranged in series with the specimen and the actuator, to record the force required to displace the surface of the specimens. The measurements made by the load cell can then be used in conjunction with the known cross-sectional area of the sample and the applied strain to calculate the composite moduli. The selected load cell (Interface, SM-50N, Crowthorne, Berkshire, UK) had a measurement range of 0 to 50 N, which was suitable in series with the selected actuator. The accuracy of the load cell, found from calibration experiments (Appendix Aii) was 0.057 $N\%^{-1}$ deviation from the true load.

The load cell undergoes small deflections (76.2 μm over its entire operating range, or 1.6 μmN^{-1}) in order to measure the force in the system. Although the deflections are small, they are of an order of magnitude which is significant compared with the cartilage strains. During the poroelastic stress-relaxation of the cartilage, changes in the load cell deflection with respect to time cause an underestimation of the actual strain applied to the cartilage. This would lead to errors in the modulus calculations. Rather than estimating the error as in previous publications (Zheng et al. 2005, Zheng et al. 2004, Zheng et al. 2002b), a linear variable differential transformer (LVDT) with a measurement range of 2 mm was selected (Omega, GP911-0.5-S, Omega Engineering Ltd, Manchester, UK) and fixed parallel to the load cell in order to measure the small deflections. This is shown in Figure 4-1. The accuracy of the measurements from this device was found to be 99.1% respectively (Appendix Aiii). The strain measured across the load cell was subtracted from the global applied strain before using the strain value to calculate the sample modulus.

4.3.3 Temperature and test environment stabilisation

The fluid medium for conducting the experiments was selected as 0.15 M phosphate buffered saline solution (PBS). In a study conducted by Patil and Zheng (2004) the effect of varying the molarity and the temperature of the fluid surrounding cartilage samples was tested. A significant increase in the sound speeds in the cartilage tissue were found when the saline concentration was varied from 0 to 2.5 M (1681 ± 50 to 1816 ± 53 ms^{-1} respectively) and when the temperature was raised from 15 to 40°C (1430 ± 39 to 1667 ± 50 ms^{-1} respectively). Maintenance of a constant temperature environment in the PBS for the duration of the experiments

was thus essential to ensure a constant sound speed in PBS and the samples. These conditions also allowed for the global and depth-dependent mechanical properties to be tested closer to the conditions *in vivo*.

A cylindrical 100W fish tank heater was selected due to its compatibility with salt water environments (as caused by the presence of the PBS in this investigation). It was placed in an adjacent tank and PBS was cycled at a flow rate of 1 mls^{-1} using a peristaltic pump from the test tank into the heating tank before flowing back into the test tank, as shown in Figure 4-2. Thermostatic control of the system was established (Temperature Controller HC, AB Aqua Medic GmbH, Bissendorf, Germany) with a measurement accuracy of ± 0.05°C. This heating system allowed fast adjustments of the heater response to prevent temperature fluctuations larger than 3°C during a single test.

The temperature of the water in the experimental tank throughout the duration of the experiments was independently measured using a thermocouple temperature data logger with ± 0.5°C accuracy (OM-PLT2, Omega Engineering Limited, Manchester, UK). The temperature results can be found in the Appendix C. The temperature varied cyclically around an average of 37.1°C with a standard deviation of 1.23°C. Each individual cycle took approximately 20 min. Based on the findings of Patil and Zheng (2004), it is unlikely that this temperature change (average temperature to maximum) will affect the speed of sound in PBS by more than 2.5%, or 1.5% in cartilage. It is also unlikely that such a small change in temperature would cause a significant effect on the elastic properties of the cartilage tissues.

4.3.4 Simultaneous ultrasonic and mechanical test measurements

4.3.4.1 Apparatus layout

The load cell, actuator and sample were required to be in series to allow the displacements and forces to be measured. The sample needed to be submerged in the PBS for environment stabilisation and ultrasonic coupling. The body of the actuator and the load cell were not water resistant, so were therefore required to be placed above the sample. The displacing tip of the actuator was submerged and in contact with the sample. The LVDT was positioned in parallel with the load cell to

allow measurements of load cell deflection. The arrangement of the load cell, LVDT and actuator are shown in Figure 4-1.

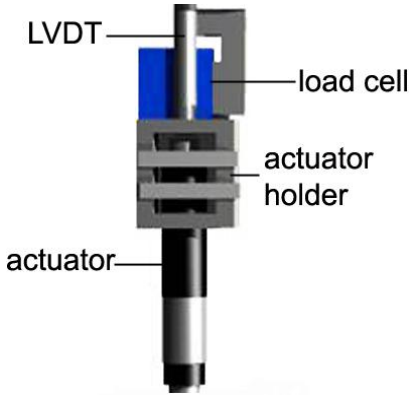

Figure 4-1: Actuator shown in the holder which connects in series with the load cell and the LVDT. The load cell and LVDT are in parallel with one another.

The ultrasound was applied from underneath the sample to allow the ultrasonic and mechanical measurements to be conducted at the same time. The complete rig and tank layout is shown in Figure 4-2.

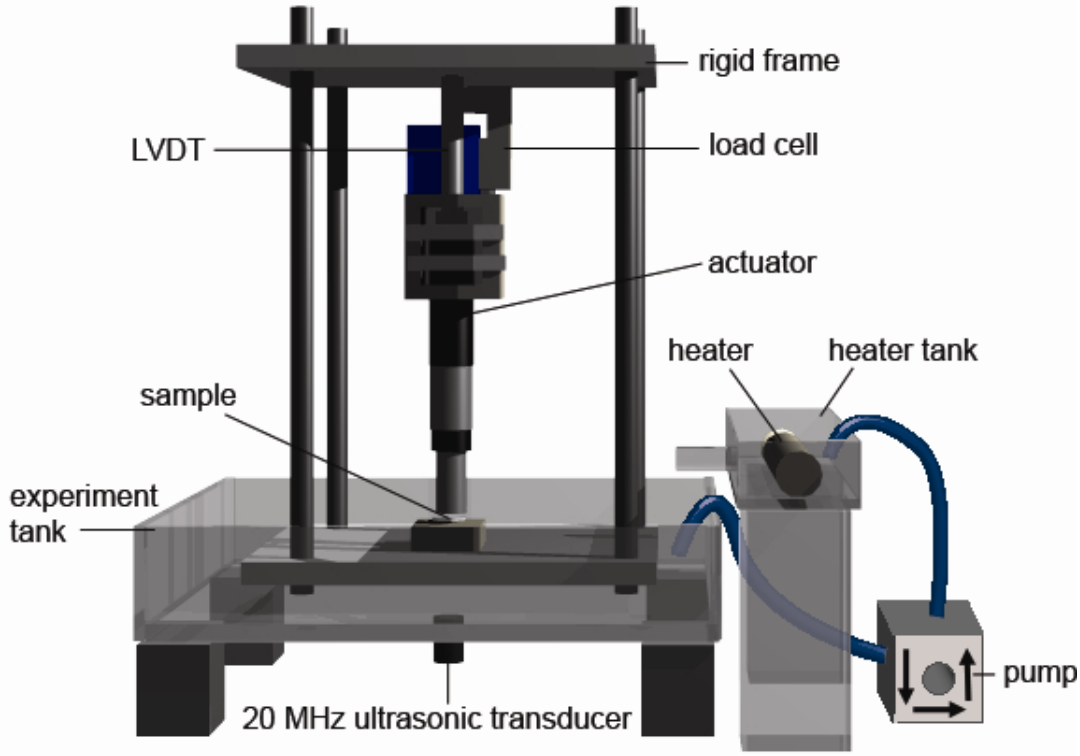

Figure 4-2: Diagram of the relative positions of the test tank (containing the transducer and the rig), the heating tank and the pump.

A rigid surface was required for the sample to rest on. Owing to the application of the ultrasound through the base of the tank, this rigid surface would also act as a delay-line for ultrasound pulses. It was therefore important to select a non-crystalline material to reduce internal scattering from grains of sufficient thickness

to avoid reverberations occurring during the cartilage reflections. Perspex was selected as the material due to the absence of grain boundaries. The higher levels of attenuation of the ultrasonic beam due to absorption were acknowledged, but were found to be acceptable, as the amplitude of the signals transmitted through the Perspex were found to be suitable in preliminary tests.

4.3.4.2Transducer beam profiling

A Panametrics model V317 20 MHz nominal centre frequency transducer (element diameter 6.35 mm, focal distance 19.05 mm) was selected for capturing the ultrasonic data to be used in the elastography measurements. The actual centre frequency of the transducer used is 21.33 MHz (-6dB bandwidth 16.0 – 26.7 MHz). The axial resolution of compressional ultrasound is determined by the pulse length. From the calibration sheet, the -20 dB pulse duration for this transducer model was 147 ns. The corresponding spatial pulse length was 243 μm in cartilage (assuming a sound speed of 1650 ms^{-1}). The axial resolution is defined as half the spatial pulse length, so therefore the axial resolution was found as 122 μm. This is suitable for use in the experiments as the smallest sample thickness will be the engineered tissue, which will be of minimum thickness 200 μm.

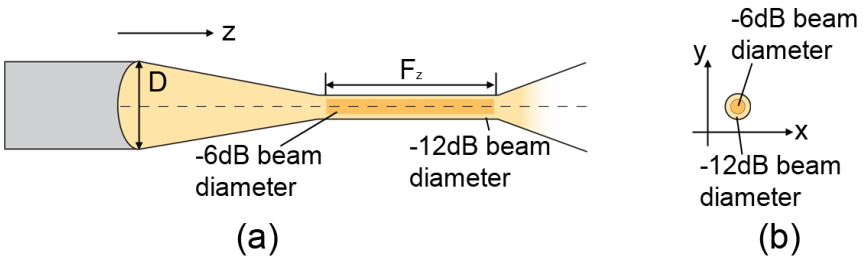

Figure 4-3: (a) The length of the focal zone (F_z) and the focussed beam diameters at -6dB and -12dB of the maximum signal intensity resulting from an element diameter D. (b) Cross-sectional view of the -6dB and -12dB maximum signal intensity in the focal zone.

The -6 dB beam diameter ($d_B(-6dB)$), shown in Figure 4-3, can be calculated using equation 4.1 (Olympus NDT 2006).

$$d_B(-6dB) = 1.02\frac{F_w c_w}{fD} \qquad \textbf{[4.1]}$$

F_w is the focal distance in water, given for the transducer as 19.05 mm, c_w is the sound speed in water, taken to be 1480 ms^{-1} and D is the transducer element diameter, which is 6.35 mm. The beam diameter is calculated as 256 μm. The

samples are prepared to 8 mm diameter, which is approximately 32 times larger than the beam diameter in the material.

The length of the focal zone (F_Z), also shown in Figure 4-3, is calculated using equation 4.2.

$$F_Z = Q * S_F^2 \left[\frac{2}{(1 + 0.5 S_F)} \right] \quad \textbf{[4.2]}$$

Where Q is the near field distance, calculated from equation 4.3.

$$Q = \frac{D^2 f}{4c} \quad \textbf{[4.3]}$$

c is the speed of sound in the medium (this is c_w if measured in water). S_F is the normalised focal length calculated using equation 4.4.

$$S_F = \frac{F_w}{Q} \quad \textbf{[4.4]}$$

The near field distance in water was calculated as 0.145 m, leading to a focal zone in water (F_Z) of 5.15 mm. In cartilage tissue samples, assuming the speed of sound of 1650 ms^{-1}, the near field distance is 0.130 m and the length of the focal zone is 4.99 mm. This is suitable for the experiments as very few of the nasal cartilage samples (<1%) were larger than this value.

As shown in Figure 4-4, the focal distance of the transducer in water (F_w) is changed due to the presence of the Perspex delay-line (F_{new}).

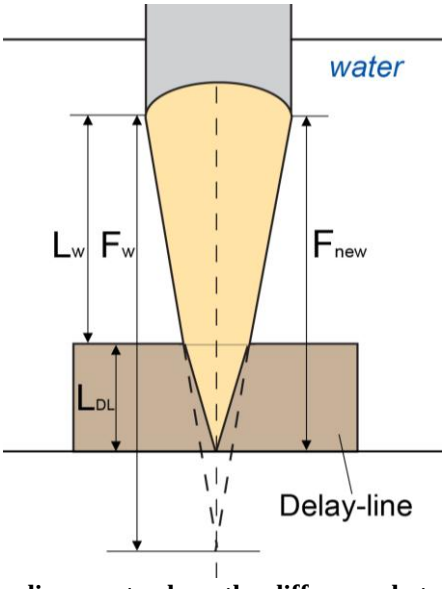

Figure 4-4: Schematic diagram to show the difference between the focal lengths of a focussed ultrasound transducer in water (F_w) and due to the presence of a delay-line (F_{new}).

Perspex has a higher sound speed than water (c_p = 2860 ms^{-1}) and as a result the ultrasound beam passing in to the Perspex from the water refracts according to Snell's law. In order to allow the system to be set-up correctly, the water path length, L_w, required calculation (equation 4.5).

$$L_w = F_w - L_{DL}\left(\frac{c_p}{c_w}\right) \qquad \textbf{[4.5]}$$

The thickness of the delay-line in the experimental system (L_{DL}) is 7 mm, which lead to L_w being calculated as 6.5 mm. The delay-line thickness was selected to be as slim as possible to reduce absorption whilst being sufficiently large that the reverberation echoes from the internal reflections did not interfere with the reflections from the cartilage tissue.

Ultrasound was produced using a voltage spike generated by the Panametrics pulser-receiver 5072PR (-3 dB bandwidth 35 MHz) with the gain set to 55 dB and the high-pass filter (1 MHz cut-off) applied to the received signal.

4.3.5 Speed of sound considerations

The velocity of the propagation of sound through a material is dependent on the modulus and density of the material. Wells (1977) quotes the approximate 'starting values for investigations' of some typical biological tissues as 1540 ms^{-1} for soft tissue, 1450 ms^{-1} for fatty tissue and 1650 ms^{-1} for muscle. Due to the changing structure through the thickness of articular cartilage there are local variations in density (fluid filled void fraction varying from 0.65 (Li et al. 2000) in the superficial zones to 0.88 (Wilson et al. 2005a) in the deep zones). The sound speed in cartilage would therefore be expected to vary over a range of values through the material as a result of these structural differences. Straining the material would also affect the density, therefore could also affect the sound speed. Due to physiological variations between cartilage tissue, dependent on species, age and trauma history of the joint, the sound speed measured in articular cartilage specimens varies over a wide range (1581 ms^{-1} (Ling et al. 2007) to 1735 ms^{-1} (Suh et al. 2001)). A summary of measured cartilage sound speeds found in literature is shown in Table 4-1.

The maximum speeds recorded in bovine patellae cartilage were 1735 ms^{-1} (Suh et al. 2001), measured at 'room' temperature with 10 MHz central frequency

ultrasound and 1720 ms^{-1} (Agemura et al. 1990), also measured at room temperature, but with 100 MHz central frequency ultrasound. The lowest bovine patellae speeds were recorded as 1581 ms^{-1} (Ling et al. 2007) and 1590 ms^{-1} (Zheng et al. 2004). These were both measured at 'room' temperature (for the 1590 ms^{-1} result, 'room' temperature was stated as 19.5 ± 1°C), using central frequency ultrasound of 5 and 35 MHz respectively. The global sound speed through articular cartilage can therefore be seen to vary over a wide range.

Study	Specimen	US frequency (MHz)	Test temp. (°C)	Sound speed (ms^{-1})
Agemura et al. (1990)	Bovine patella	100	Room	1617 ~ 1720
Jurvelin et al. (1995)	Canine & bovine femoral & tibial chondyles	10	Room (22.5)	1760
Pellaumail et al. (1999)	Rat patella	55	Room	1690 ± 10
Toyras et al. (1999)	Bovine patella	22	37	1654 ± 82
Suh et al. (2001)	Bovine patella & femoral chondyles	10	Room	1735 ± 35
Toyras et al. (2003)	Bovine patella, femoral chondyles, patello femoral groove & talus joint	10.3	Room (20)	1627 (1532 ~ 1754)
Patil et al. (2004)	Bovine patella	50	Room (19.5 ± 1)	1626 ± 25
Zheng et al. (2004)	Bovine patella	35	Room (19.5 ± 1)	1589.8 ± 7.8
Patil and Zheng (2004)	Bovine patella	50	37	1675
Nieminen et al. (2004)	Bovine patella	10.3	Room	1603 ± 27
Ling et al. (2007)	Bovine patella	5	Room	1581 ± 36

Table 4-1: A summary of a selection of sound speeds measured in articular cartilage samples in various animals and parts of the knee joint, recorded at different ultrasonic frequencies and different temperatures.

The zonal variation of sound velocity has been investigated by Patil et al. (2004) and Agemura et al. (1990) using methods which required the full thickness articular cartilage to be sliced into thinner sections to separate the zones. Comparing multiple positions in two different samples, Agemura et al. found the sound speeds to be 1671 ± 61 and 1635 ± 27 ms^{-1} in the superficial zones, 1647 ± 76 and 1617 ± 41 ms^{-1} in the middle zones and 1715 ± 25 and 1720 ± 99 ms^{-1} in the deep zones.

The speeds through the full thickness were not reported. The measurements were conducted with a 100 MHz scanning laser acoustic microscopy (SLAM) system at room temperature. The percentage difference between the superficial and deep zone sound speeds are 4.1% and 6.4% and both were statistically significant. Patil et al. found the sound speed to vary from 1574 ± 29 ms^{-1} in the superficial to 1621 ± 34 ms^{-1} in the middle and 1701 ± 36 ms^{-1} in the deep zone. The sound speed measured in full thickness samples was 1626 ± 25 ms^{-1}. The zonal differences in their investigation represent an 8.1% statistically significant change between the superficial and deep speeds. These measurements were conducted at 50 MHz at 19.5 ± 1°C, using the sound speed measurement technique of comparing the arrival times from a reflector in saline with and without the presence of the sample. The differences in the measurements between the two studies are likely to be caused by the way that the samples were sectioned into the 'zones' for testing.

As the elastic modulus of articular cartilage has been found to be dependent on the applied strain, the strain levels would be expected to impact the measured sound speed. Ling et al. (2007) studied this effect between 2.5% and 20% applied strain. The sound speed was measured by applying a known strain to the specimen between a pair of transmitting and receiving transducers (5 MHz) at room temperature. The values from their study are shown in Table 4-2. Their results demonstrated that the sound speed was dependent on the applied strain with an approximate quadratic relationship: the effect increasing with respect to the magnitude of the applied strain.

	% articular cartilage compression (*n* = 20)								
	0	2.5	5	7.5	10	12.5	15	17.5	20
US speed (ms^{-1}) (mean ± standard deviation)	1581 ± 36	1585 ± 43	1593 ± 46	1605 ± 42	1616 ± 44	1626 ± 44	1641 ± 47	1659 ± 49	1671 ± 56

Table 4-2: Table of sound speeds measured in articular cartilage after the application of different strains taken from Ling et al. (2007).

The variation of modulus up to 7.5% applied strain was found by Ling et al. (2007) to be only +1.5%; this change also fell outside the 80% significance level, so was concluded as being insignificant. At 10% applied strain the change in the sound speed increased by 2.2% (this change was statistically significant). Within the range

of strains proposed in this thesis, the effect of strain on the global sound speed can be assumed insignificant.

Depth-dependent variations in propagation velocity is unlikely to have a direct effect on the results of this study, as only the relative pre- and post-compressional positions of the scatterers are required. The absolute positions of the scatterers within the cartilage are less important when calculating the strain over a smaller 'windowed' region. The speed of sound is not used when calculating the strain in the window, only the difference in scatterer position on the trace, divided by the window length. If an average sound speed assumption was required, it would result in overestimates of strains in the deeper regions and underestimates in the superficial zone. A strain gradient will be produced across the samples, but the effect of strain on the sound speed has already been found to be insignificant for this experiment.

4.4 Method development – protocol design

The objectives of this thesis state that a range of global strain application protocols are required. The behaviour of hyaline cartilage specifically due to its structure needs to be found in different conditions to increase the understanding of potential design parameters to create mechanically functional engineered tissue. A strain protocol suitable for mechanical characterisation of engineered tissue samples is also required.

From the global mechanical tests and the elastography tests presented in the literature review, the following strain application protocols were identified for investigation:

- Single strain step applications and the corresponding stress-relaxation periods. These tests will increase the scope of existing studies by being conducted in physiologically relevant conditions and by comparing two different hyaline cartilage structures. To increase the data available for processing, 10 repeats at each strain level for each tissue are required.

- Multiple strain step applications and the corresponding stress-relaxation behaviours following each step. This will allow investigation of the

mechanisms responsible for the behaviour relating to cumulative strain applications to be found. These tests will compare the native structures in physiologically relevant conditions. Repeats are required to increase the information available, but these are limited to 5 for each native tissue, due to the large amount of time required to perform each repeat, and 4 for each engineered tissue, due to the limited availability of specimens.

- Cyclic strain applications and changes in mechanical tissue behaviour between the initial response to the transient and as the system approaches steady-state conditions. The frequency and magnitude of the strains applied are varied to dynamically characterise the mechanical behaviour of both native hyaline tissue structures. 10 repeats for each tested frequency and magnitude are performed for each native tissue.

For investigating the engineered tissue specimens, the stepped strain protocol was selected. This was preferable to the single step applications as it allowed information to be obtained regarding cumulative strain effects. Step tests were preferable to the cyclic strain applications, as preliminary studies showed the cyclic tests to be the least reliable, and the number of engineered specimens available was limited.

In all the tests, good contact between the samples and the compressing surfaces (rigid base and actuator) are required. From preliminary investigations, pre-loads of 5 N were selected for application to every sample for 5 min prior to any experiment. The application of the pre-load was additionally used to measure the thickness of the samples. The actuator was lowered in small incremental steps until a load of 5 N was measured. The position of the actuator relative to the rigid base was known, allowing the sample thickness to be extracted.

The following sections (4.4.1 to 4.4.4) outline the selection and justification of the range of strain magnitudes and test periods in order to extract the necessary global and depth-dependent information from the tissue.

4.4.1 Quasi-static tests with single step applications of varying strain magnitudes

Based on evidence in literature, physiologically relevant strain levels are up to approximately 20% compressional strain (Eckstein et al. 1999). Experimentally, the magnitude of the strain applied quasi-statically was limited by the correlation requirements of elastography (Konofagou et al. 1999) and the sound speed increases (Ling et al. 2007). For time-domain elastography methods, the decorrelation of the pre- and post-compressional signals becomes significant after approximately 10% applied strain (Konofagou et al. 1999). When the correlation between the signals is insufficient, the extraction of the correct time shift becomes unlikely. Strains of 10% were also the maximum limit for ensuring the sound speed increases were relatively small (Ling et al. 2007).

Global applied strain levels of 2%, 4%, 6% and 8% were selected for comparison. These represented a reasonable coverage of the physiological range and were within the limits of the constant ultrasound speed and elastography processing. The strains were equally spaced within this region for straight forward evaluation of the effect of strain magnitude on the stress-relaxation behaviour.

Selection of an appropriate stress-relaxation period was reliant on published values and a preliminary investigation conducted. A large variation of reported times for articular cartilage equilibration were found for unconfined compression configurations (approximately 4 min (Kiviranta et al. 2006) to 10 min (Langelier and Buschmann 2003, Julkunen et al. 2007, Murakami et al. 2004)). From preliminary experiments conducted, it was discovered that 20 min was a more suitable equilibration period. The programmed strains were applied to the specimen surface at the maximum travel rate the actuator would allow (0.75 mms^{-1}). This rapid application of strain allowed for measurements of the initial modulus by the mechanical tests. The quasi-static strain application protocol with respect to time is summarised in Figure 4-5(a).

Ultrasonic A-line RF data were gathered and digitised with a LeCroy 9310M (LeCroy, New York, USA) oscilloscope (300 MHz bandwidth, 100 mega-samples per second digitisation rate, 50 kilo-points per channel (maximum)) and stored in real time on a PC using custom built software written in LabVIEW. Mechanical test

data from the load cell and LVDT were digitised with a data logger (ADC-11 Pico Technology, ST Neots, UK) and at 1 s intervals on a PC. The temperature data were stored on a separate device at 2 s intervals during each test.

Elastography data were compared immediately following the initial strain application and after the 20 min stress-relaxation period.

4.4.2 Quasi-static tests with strain applied in multiple steps of fixed magnitude

From available evidence regarding the mechanical behaviour of cartilage it was apparent that the strain history would affect the global properties (Li et al. 2003a, Lu and Mow 2008). Obtaining depth-dependent information, regarding the local tissue behaviour following stepped strain application, would allow better understanding of the tissue mechanics.

Four steps of 2% strain were selected for this protocol. The summed strain at each step (2%, 4%, 6% and 8%) allowed a direct comparison with the instant strain applications of the same magnitudes from the tests described in section 4.4.1. Elastographic and mechanical test data were compared immediately following the application of each step and after the 20 min equilibrium period for each step (immediately prior to the application of the next step). The nasal and the articular data were compared to investigate the differences between the mechanical behaviour of the two structures. This protocol was also applied to the engineered tissue specimens at the different culture periods (1, 5, 10 and 15 days) to determine if the same mechanisms operated in these samples.

As with the previously described quasi-static tests, the maximum rate of actuator travel was used. The 20 min stress-relaxation time between each step was applied to allow tissue equilibrium at the point of each subsequent strain step. The strain application with respect to time is shown in Figure 4-5(b). Data collection was performed in the same manner as for the variable magnitude strain tests.

4.4.3 Dynamic tests with varying cyclic frequencies

Park et al. (2004) reported that increasing the cyclic frequency of strain applied to articular cartilage samples caused a measurable increase in the global moduli. It has also been reported that varying the applied strain frequency from 0.001 Hz to 10 Hz

caused the measured global moduli to increase by five times the lower value (Park and Ateshian 2006).

In order to establish how the frequency of the strain applied affected both the depth-dependent and the global elastic properties of the two hyaline cartilages, a range of suitable test frequencies were required.

The maximum frequency for the tests was determined by several mechanical and ultrasonic test factors. At 8% maximum strain in the thicker nasal cartilage samples, the fastest the actuator was found to be able to move through one complete cycle was 0.8 s, corresponding to a frequency of 1.25 Hz. Ultrasonically, the cyclic strain frequency was limited by the number of A-lines the oscilloscope was able to record per second. An oscilloscope with a faster digitisation rate than the one used for the quasi-static tests was selected. The LeCroy WaveRunner 62Xi, (New York, USA) oscilloscope (600 MHz bandwidth, 10 giga-samples per second digitisation, 4 mega-points memory) captured four ultrasonic A-lines per second and stored the results on the internal processor for later processing. From these limits it was determined that the maximum frequency investigated should be 1 Hz (one complete strain cycle per second). Physiologically, this is equivalent to a slow walking pace.

To investigate the effect of varying the straining frequency on the cartilage behaviour, a range of cyclic frequencies were required. With 1 Hz as the maximum frequency, 0.25, 0.5 and 0.75 Hz were selected for comparison. The strain at the peak compression of each cycle was required to be held constant across the frequencies and was selected as 4%.

In literature, cycles were applied for less than 20 s in order to determine the effect on the global mechanical properties (Park et al. 2004). In order to increase the time allowed for the system to approach steady-state following the transient, it was determined the strain cycles should be applied for 1 min.

The global and depth-dependent elastic behaviour from the first and final complete cycles in that minute were compared so as to assess any changes which occurred. The strain application, with respect to time, is shown in Figure 4-5(c).

Faster capture was required for the mechanical test data compared to the quasi-static tests, and were obtained from the data logger at 50 ms intervals for the full minute test. The temperature of the PBS was recorded at 2 s intervals as before.

4.4.4 Dynamic tests with varying strain magnitudes

Due to the physiological relevance, 1 Hz cyclic strain was selected as the frequency to be maintained whilst testing varying strain magnitudes. Magnitudes of 2%, 4% and 8% were selected as these represented a doubling and halving of the peak strain used for the varying frequency tests.

Tests were also conducted for 1 min and data were recorded and analysed in the same manner as the variable frequency tests.

4.4.5 Protocol summary

- Quasi-static varying initial strain experiments, with strains of 2%, 4%, 6% and 8%, were applied to nasal and articular cartilage samples and held for 20 min to allow stress-relaxation (Figure 4-5(a)).
- Quasi-static step applied strain experiments applied four sets of 2% strain (from 2% up to 8% total) holding each strain constant for 20 min before the next strain was applied (Figure 4-5(b)).
- Dynamic cyclic strain application at varying frequency experiments were performed at 0.25, 0.5, 0.75 and 1 Hz with a maximum strain during the cycle of 4%. Strain cycles were applied for 1 min (Figure 4-5(c)). Minimum and maximum global moduli and depth-dependent strains were compared for the first and final strain cycles.
- Dynamic cyclic application of varying strain magnitude experiments were conducted with magnitudes of the maximum strain in the cycle of 2%, 4% and 8% applied at a repetition frequency of 1 Hz (Figure 4-5(d)). Minimum and maximum global moduli and depth-dependent strains were compared for the first and final strain cycles.
- All samples were subjected to a 5 N pre-load for 5 min before the experiments were conducted.

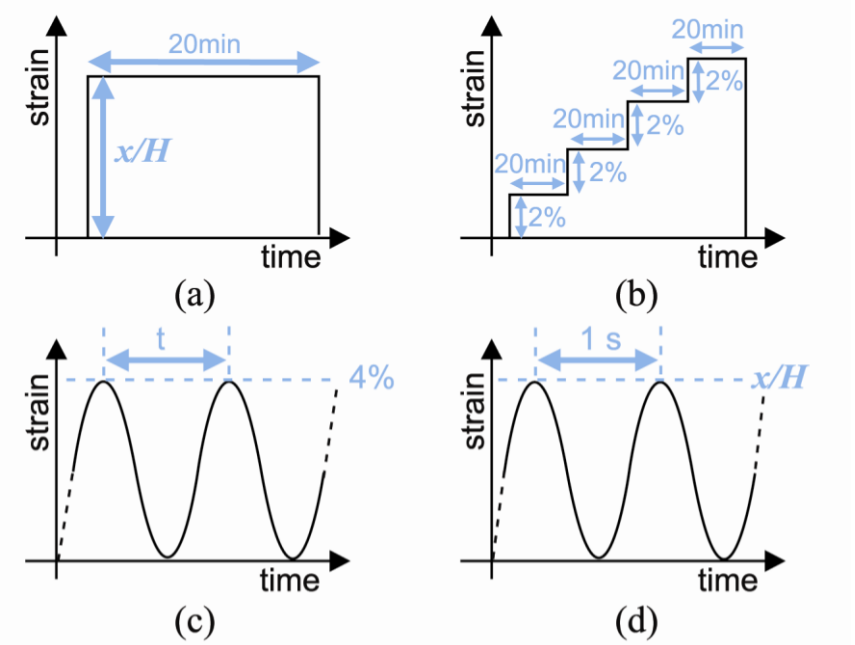

Figure 4-5: Representations of the strain loading protocols for the cartilage specimens. (a) Shows the variable magnitude single application strain protocol. *x* is set to 2%, 4%, 6% or 8% and the applied strain is held for 20 min. (b) shows the step test protocol. Each step adds 2% strain and is held for 20 min. (c) Shows the dynamic cyclic variable rate protocol. 4% maximum strain is cyclically applied over a 1 min period, with *T* set to 4 s (0.25 Hz), 2 s (0.5 Hz), 1.3 s (0.75 Hz) or 1 s (1 Hz). (d) Shows the varying dynamic amplitude protocol. Strains are applied cyclically at a rate of 1 Hz, with the maximum magnitude, *x*, varying between 2%, 4% and 8%.

- During quasi-static experiments, ultrasonic data were gathered at 4 s intervals through the LeCroy 9310M oscilloscope. The dynamic ultrasonic data were collected at a rate of four frames per second using the LeCroy WaveRunner 62Xi oscilloscope.

- Mechanical test data were recorded by the data logger (ADC-11 Pico Technology, St Neots, UK) every second during the quasi-static tests and at 5 ms intervals during the dynamic tests.

4.5 Signal-processing

Figure 4-6 shows a simplified example of the small shifts in the time signals which would result from the application of a strain to a sample under ultrasonic examination. In this example, the sample would be resting on a rigid surface, which is represented by the two superimposed signals on the left of the time trace.

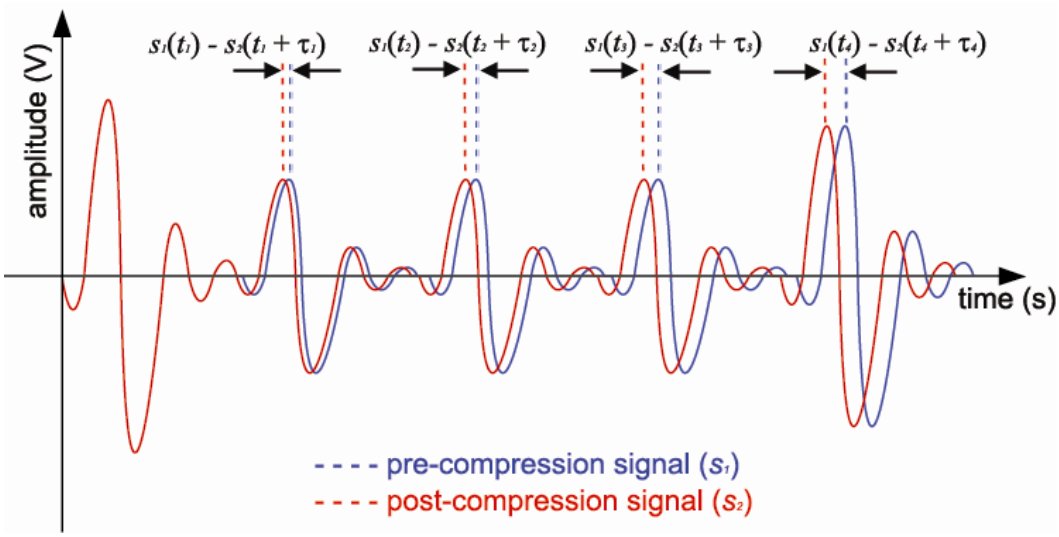

Figure 4-6: Simplified ultrasound signals from a sample pre- and post-compression. The strain is found by determining the value of each τ compared to the pre-compression signal time positions.

Time domain processing was selected to establish the magnitude of the time shifts occurring between the signals. Although it has been reported that signal decorrelation is higher in time domain techniques (loss of shift resolution in noise) than in frequency domain techniques (Konofagou et al. 1999, Konofagou et al. 2000, Varghese et al. 2000, Hoyt et al. 2006), processing in the time domain offers higher sensitivity to small changes in strain, which is favourable for this application (Konofagou et al. 2000, Ashraf 2010).

Alternative shift detection methods, for time domain processing, were reported and compared (de Korte et al. 1997, Viola and Walker 2003). For test conditions using a time shift of 10 ns produced by a physical transducer movement detected with 30 MHz centre frequency (20 – 40 MHz bandwidth) (de Korte et al. 1997) and also shifts of half a time period detected using 5 MHz (2.5 – 7.5 MHz bandwidth) (Viola and Walker 2003), the sum-squared difference technique was reported to perform better than other techniques. The results showed the shift detection and sizing accuracy was comparable to the cross-correlation technique, but the sum-squared difference technique was computationally faster. The sum-squared difference technique was selected.

Pre- and post-compressional signals, like the examples shown Figure 4-6, can be termed respectively r_1 and r_2 and described by equations 4.6 and 4.7.

$$r_1(t) = s_1(t) + G_1(t) \qquad \textbf{[4.6]}$$

$$r_2(t) = s_2(t+a) + G_2(t) \qquad \textbf{[4.7]}$$

a is the time shift due to the applied strain and G_1 and G_2 represent random Gaussian noise. In determining the time shift, due to the random nature of G_1 and G_2, only s_1 and s_2 are considered. To perform the sum-squared difference signal-processing, signal s_2 is moved across signal s_1 in increments of τ (determined by the separation of the digitised points in the trace, which is determined by the sampling rate of the oscilloscope), as shown in equation 4.8. When the value of T_{SSD} is found to be a minimum, the corresponding value of τ is the shift between the two signals.

$$T_{SSD}(\tau) = \int_{start\,of\,signal}^{end\,of\,signal} \left(s_1(t) - s_2(t+\tau)\right)^2 dt \qquad \textbf{[4.8]}$$

From Figure 4-6 it can also be seen that if the sum-squared difference equation were applied across the whole signals shown, information regarding some of the shifts would be lost and an 'averaged' value would be produced. It was therefore necessary to split the signal into smaller segments, or 'windows' for evaluation.

Windows were selected to be large compared to the ultrasonic pulse length (Bilgen and Insana 1997a). An example of a simple window applied to the pre- and post-compressional A-lines is shown in Figure 4-7.

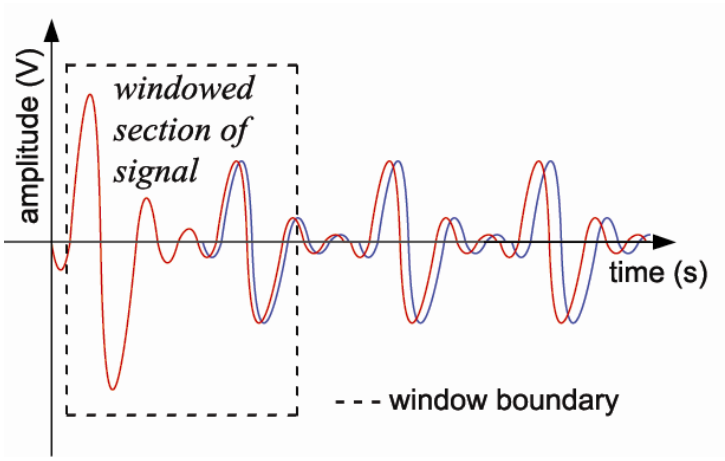

Figure 4-7: Example of a simple rectangular window applied to a part of the pre- and post-compressional A-lines.

In the literature, windows typically take a shape similar to a Gaussian distribution. Some windows use Gaussian sloped sides with a flat centre section equal to the maximum window height. Window overlap is determined after finding the minimum overlap; this is accepted as being the point at which the slopes from the edges of two adjacent signals cross at 2/3^{rds} of the window height. The overlap can then be increased to obtain a higher sampling rate of the data, therefore increasing

depth resolution. However, increasing the number of windows in this way increases the computational load and has also been seen to decrease the signal-to-noise ratio (Bilgen and Insana 1997b). The signals of pre- and post-compression are multiplied by the window function prior to the application of the displacement estimation algorithm.

The three types of cartilage investigated in this thesis represent three different approximate thicknesses: articular 1.60 ± 0.38 mm (mean ± standard deviation); nasal 4.22 ± 0.56 mm and engineered (across all the different culture times) 0.51 ± 0.43 mm. To select the optimum window size for each sample type, the correlation coefficients of captured pre- (s_1) and post-compressional (s_2) quasi-static test signals after the application of varying the window lengths were found. The correlation coefficient between the two signals ($cc_{s_1 s_2}$) was calculated from equation 4.9. (cov(*x*, *y*) is the covariance between signal *x* and signal *y* and cov(*x*, *x*) for the covariance between the same two signals).

$$cc_{s_1 s_2} = \frac{\mathrm{cov}(s_1, s_2)}{\sqrt{\mathrm{cov}(s_1, s_1)\,\mathrm{cov}(s_2 s_2)}} = \frac{\sum_{p=1}^{N} \left(s_{1p} - \bar{s}_1\right)\left(s_{2p} - \bar{s}_2\right)}{N\sqrt{\mathrm{cov}(s_1, s_1)\,\mathrm{cov}(s_2 s_2)}} \qquad \textbf{[4.9]}$$

Where *N* is the number of points (each point at *p*) describing the signal. The larger the value of $cc_{s_1 s_2}$, the greater the similarity between the two windowed signals. The tested window lengths represented 1/2 to 1/14th of the total pre-compressional signal length. The results for each window length were plotted with respect to the depth in the tissue, and window lengths producing the best correlations across all the test data for a particular cartilage type were selected. The window lengths were selected as 1/8th of the signal length for articular, 1/10th of the signal length for nasal and 1/3rd of the signal length for engineered.

The results from applying the sum-squared difference technique to the windowed data were compared using the correlation coefficient to test whether there was sufficient similarity of the two signals for the point to be used. The acceptable level was determined experimentally by observing the data and the output of the code and selecting the similarity level which provided the most accurate output. This level was selected as 55%, and was confirmed by Ashraf (2010), who determined the amount of useful window information lost from increasing the correlation from

0% to 100%. For both the middle zone of articular cartilage and the whole thickness of nasal cartilage, it was found that 50% to 60% correlation represented the highest threshold where 70% of the window strains were suitable for inclusion. This level still represents only moderate correlation between the corresponding pre- and post-compressional windows; this is due to signal decorrelation still being partially present even where particular signals can be easily tracked by eye. Higher threshold levels led to insufficient record of useful data points. Lower threshold levels led to greater levels of anomalous data.

No evidence of this correlation technique being used to check the validity of the sum-squared difference algorithm output was found in the literature. However, when used in our investigation, the reliability of the result output was increased. The resulting values of strain for each window were then averaged with the data gathered from corresponding windows from repeat samples. This allowed the average and standard deviation of the repeats to be determined.

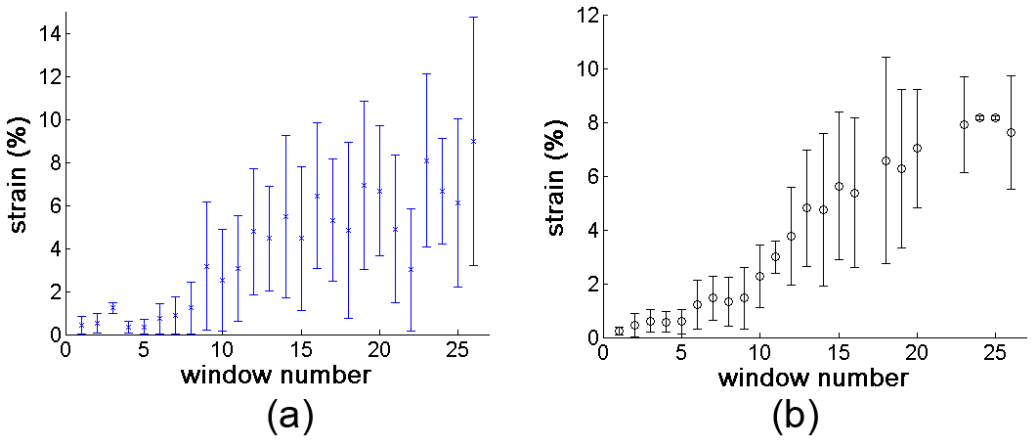

Figure 4-8: Two strain-maps obtained from 6% global strain applied to nasal cartilage demonstrating the difference between (a) no cross-correlation application and (b) 55% match correlation.

Examples of the same data with and without the cross-correlation application are shown in Figure 4-8. The larger error bars and greater scatter were typical for results where the cross-correlation processing was not used, particularly in the nasal sample data. The scatter of the results and the magnitude of the standard deviations across the specimens were seen to be reduced. The signal-processing is summarised in the flow chart shown in Figure 4-9. The code was implemented in Matlab and can be found in Appendix Dii.

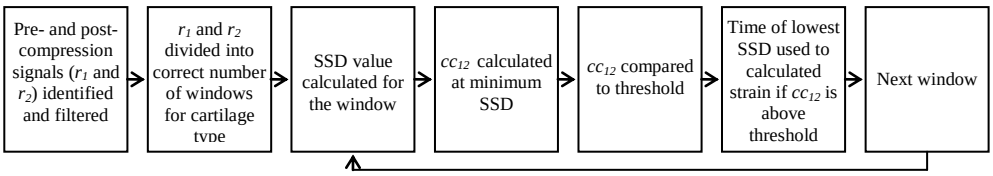

Figure 4-9: Flow chart showing an overview of the elastography signal-processing used to extract depth-dependent strain data from the comparison of pre- and post-compressional signals.

4.5.1 Normalisation of the experimental elastography values

Due to the rigid fixed surface at the base of the sample, which is the cause of the stationary first echo of the ultrasound, the depth-dependent measured displacements, and therefore the calculated strains and moduli, depend both on the distance from the rigid surface and the material properties. It is necessary to separate the two effects to be able to assess the depth-dependent material elasticity. Considering a material with a uniform modulus, as shown in Figure 4-10(a), the plot for the moduli calculated from the measured displacements with respect to distance from the rigid surface, would appear as shown in Figure 4-10(b).

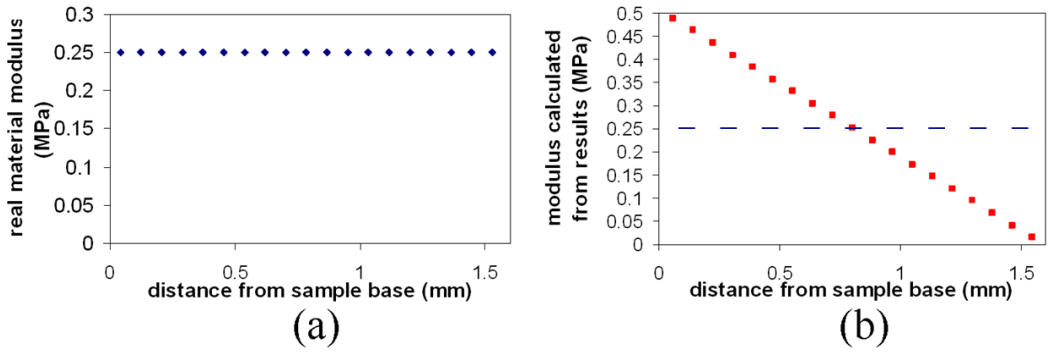

Figure 4-10: Demonstration of how a completely uniform real material modulus (a) is shown in the elastography experimental results (b) due to the presence of the rigid boundary at the base of the sample (dashed line shows true modulus). The area under the points in both (a) and (b) are equal.

As the stress applied is global, the smaller displacements measured near to the fixed base cause an apparently lower strain and therefore higher moduli to result if no correction is made for the slope of the strain data. The converse applies at the top of the samples. As the results are plotted in terms of strain, as opposed to composite moduli, the strains must be normalised so as to remove the effects of proximity to the rigid base. Using the example values shown in Figure 4-10 it is possible to develop the formula for this normalisation, shown in equation 4.10.

$$\varepsilon_i = \varepsilon_{wi}\left(\frac{0.5n}{i}\right) \quad \textbf{[4.10]}$$

ε_i is normalised strain, ε_{wi} is measured strain, *n* is the number of windows and *i* is the window number. Dividing the number of windows by two is to account for half the points being above and half below the true modulus line. Equation 4.10 is applied to all the strain data in order to produce results which more accurately represent the local moduli.

4.6 Analysis techniques

Raw data from the mechanical tests were converted into composite elastic moduli using calculations of engineering stress and strain. The strains used in the calculations were corrected for the load cell displacement, measured by the LVDT. Data of the composite global modulus were compared between the cartilage types and between the different applied strains or frequencies. The mean and standard deviation of the moduli were calculated for the repeat readings at known time intervals for each experiment. The intervals were 15 s for both the quasi-static tests and 0.01 s (depending on the number of points representing each signal) for both dynamic tests. Elastographic repeat readings were similarly used to find the mean and standard deviation values representing each window from the samples.

Statistical analysis was performed on both the mechanical and elastographic test results. The unpaired student's T-test was used to find whether the mean data from a particular reading, for example articular cartilage 2% strain at T0, is significantly different to another reading, for example, articular cartilage 4% strain at T0. The test statistic ($T_{student}$) describing the statistical difference between the two samples is calculated using equation 4.11.

$$T_{student} = \frac{\overline{X}_1 - \overline{X}_2}{S_{X_1X_2}\sqrt{\frac{2}{m}}} \quad \textbf{[4.11]}$$

Where $\overline{X}_1$ and $\overline{X}_2$ represent the means of the two circumstances to be compared, *m* is the number of repeat readings and $S_{X_1X_2}$ is defined in equation 4.12.

$$S_{X_1X_2} = \sqrt{\frac{S_{X_1}^2 - S_{X_2}^2}{2}} \quad \textbf{[4.12]}$$

Where S_{X_1} and S_{X_2} are the standard deviations corresponding to $\overline{X}_1$ and $\overline{X}_2$ respectively. The unpaired student's T-test assumes that all data are approximately normally distributed and independent. The lower the $T_{student}$ value the more significant the similarity between the two samples. Critical values of $T_{student}$, at different levels of significance (Appendix Bi), were used to determine whether the two means were equal. The number of degrees of freedom for the test was determined by the number of specimens for each test minus 1.

One-way analysis of value (ANOVA) tests were performed to compare data at 0, 5, 10, 15 and 20 min at the four applied strains to determine if significant differences existed between the means for the quasi-static variable magnitude tests. The same tests were applied to compare data at each peak and equilibrium point of the step-tests and at various points in the dynamic cycle at the beginning and end of the 1 min cycle application period. ANOVA is calculated by examining the ratio of variance and variation within the sample groups (repeat readings for one condition) compared to the variance and variation of the whole population of readings. The full equations and calculation process are given in Appendix Bii. The calculated values are compared to critical '*F*' values found in tables to determine whether differences between the four compared means were significant.

In addition to the statistical analysis of the differences of means, the elastographic signal-to-noise values were calculated for each experiment. This was used to test the validity and reliability of the ultrasonic data.

4.7 Summary

Equipment and protocols were selected in order to apply a range of strain conditions to cartilage specimens. From evidence of existing mechanical and elastography test techniques, four different test protocols were selected to investigate the effects of strain magnitude, stress-relaxation and strain history of quasi-static conditions and the frequency and magnitude of cyclically applied strains. The signal-processing method was adapted from the ones found in the literature to be better suited to the conditions and protocols used in this application. Suitable statistical analysis tools were identified to provide the means for testing the confidence in the obtained data.

5 Phenomenological Modelling of Articular Cartilage

5.1 Overview

Extraction of depth-dependent elastic constants from the elastographic investigation of articular cartilage tissue is essential for the mechanical characterisation. Due to the poroelastic nature of the cartilage tissue, consideration of the properties dependent on the pressurisation and flow of the interstitial fluid is required. This chapter first reviews mechanical models of articular cartilage which already consider the depth-dependent solid matrix properties, but which only use global strain information. An outline is provided of the important phenomenological parameters that affect the behaviour of the tissue under mechanical compression and initial input values for the model are established. The development of the fluid pressurisation and flow model is then demonstrated. Analysis of the model using 'ideal' rather than experimental inputs is given and the sensitivity of the model-derived elastic constants, to experimental error, is quantified.

5.2 Introduction

In the case of engineered tissue, insufficient matching of implant properties (for example matrix modulus or permeability) with those of the surrounding healthy native tissue could lead to shear stresses at the interface, which could be sufficiently large to cause damage. As outlined in previous chapters, the mechanical behaviour of hyaline cartilage is determined by the poroelastic nature of the tissue matrix. The poroelastic material properties of hyaline cartilage are the elastic modulus, the void fraction (volume of matrix occupied by water) and the permeability of the solid matrix and the dynamic viscosity of the interstitial fluid.

The depth-dependence of the poroelastic solid matrix properties have been documented (Murakami et al. 2004, Schinagl et al. 1997, Chen et al. 2001, Lipshitz et al. 1976, Brocklehurst et al. 1984). However many existing mechanical models do not consider any of these parameters as depth-varying (for example, Ateshian et al. 1997, Lai et al. 1991, DiSilvestro et al. 2001b, Ehlers and Markert 2001, Suh et al. 1995, Simon et al. 1984). Existing models which do consider depth-dependent matrix parameters do not utilise experimental inputs from the matrix strains obtained in elastography tests. This has limited the use of existing elastography techniques for the extraction of mechanical properties from cartilage tissue (Zheng et al. 2005, Zheng et al. 2002b, Qin et al. 2002, Zheng et al. 2001). A phenomenological model of cartilage behaviour relating to the mechanical interaction between the fluid and solid constituents was required. As a result of this model, the depth-dependent matrix modulus would be extracted from experimental results without the requirement of stress-relaxation equilibrium in the elastography tests.

In addition to the poroelastic mechanical properties of hyaline cartilage (see section 1.2.1.1), there are osmotic charges resulting from the proteoglycan content of the matrix. In articular cartilage these have also been reported as depth-varying (Broom and Oloyede 1998, Nguyen and Oloyede 2001, Oloyede and Broom 1993, Olsen et al. 2004). These effects however, are not included in the model developed in this chapter because the pressures resulting from osmotic charges are small (of the order of 10^{-5} Pa) (Tombs and Peacocke 1974, Muir 1979, Olsen and Oloyede 2002, Brocklehurst et al. 1984).

PGs are considered to be the main compressional load bearing element of cartilage (Li et al. 2005). In two- and three-dimensional models the matrix stiffness is considered as a combination of the fibril stiffness and the non-fibrillar stiffness. However, since the fibrils are only considered to be active in tension (Wilson et al. 2006, Wilson et al. 2005a, Wilson et al. 2004, Korhonen et al. 2008, Julkunen et al. 2007, Julkunen et al. 2008b), and this model is designed to determine the compressional moduli of the tissue, their contribution in the proposed model would be negligible.

The density of the matrix varies with depth from the articular surface (Silvast et al. 2009, Wilson et al. 2007, Julkunen et al. 2008b, Mow et al. 1991), which is reflected in a variation of void fraction (as presented in section 5.4.3.1). The matrix modulus has been measured at equilibrium to vary between 0.27 MPa in the superficial zone to 0.71 MPa in the deep zone (with 0.47 MPa measured as the global equilibrium modulus) (Chen et al. 2001).

In the model developed here, depth-dependent expressions of fluid flow have been established through the application of Darcy's law, with literature defined values of permeability, dynamic viscosity and void fraction, and experimentally derived values of global stress and depth-dependent strain. This model was designed to allow more rigorous mechanical characterisation of articular cartilage than any method previously reported.

5.3 Overview of existing mechanical models with depth-dependent material properties

Despite the depth-dependency of the composition and structure of cartilage being extensively documented (Mansour and Mow 1976, Mow et al. 1991, Zhu et al. 1996, Julkunen et al. 2008b, Miyata et al. 2005, Silvast et al. 2009, Aspden and Hukins 1981, Clark 1985, Kaab et al. 1998, Rieppo et al. 2003, Volpi et al. 1991, Qin et al. 2002, Schinagl et al. 1997, Murakami et al. 2004), few authors have modelled cartilage as having depth-dependent properties. A summary of the authors with depth-dependent considerations are shown in Table 5-1.

Author	permeability	pore pressure	osmotic pressure	void fraction	Poisson's ratio	matrix stiffness	fibril stiffness	fibril dist.
Li et al. (2000)	x	x		x	x	x	x	
Li et al. (2002a)	x	x		x	x	x	x	
Li et al. (2003b)	x	x		x	x	x	x	
Li et al. (2008)							x	
Julkunen et al. (2007)	x			x			x	x
Julkunen et al. (2008b)		x	x	x				x
Wilson et al. (2004)	x			x				x
Wilson et al. (2005a)		x	x	x				
Wilson et al. (2006)		x	x	x				x
Wilson et al. (2007)		x	x	x				x
Nguyen and Oloyede (2001)		x	x	x		x		
This model	x	x		x		x		

Table 5-1: Summary of the parameters of articular cartilage treated as depth-dependent in existing mechanical models. The parameters in the model developed in this chapter are shown.

5.4 Phenomenological model parameters

From the experimental data gathered and from values obtained from the literature, the matrix moduli can be extracted from the depth-dependent strains. The flow rates can then be used to determine the time-, depth- and strain-dependence of the void fraction.

Experimental inputs (where *i* indicates depth in terms of distance from the fixed sample base and *j* indicates time step):

- Global strain (ε_G).
- Time-dependent global stress ($\sigma_G(t)$).
- Time- and depth-dependent strains ($\varepsilon_i(t)$).

Literature inputs:

- Depth-dependent permeability coefficient (k_i).
- Initial depth-dependent void fraction (e_i).

Model outputs:

- Time- and depth-dependent rate of fluid flow ($\dot{b}_i(t)$).
- Depth-dependent matrix moduli (E_{Mi}).

5.4.1 Experimental inputs

The experimental measurements provide the global composite stress response of the tissue. The applied global strain is fixed for each test. Small adjustments to the global applied strain are measured and incorporated into this value (section 4.3.2). The depth-dependent strains were measured ultrasonically and these were used as inputs for each spatially discretised tissue layer in turn at each time-step. The depth-dependent strain information between strain application and equilibrium were used to determine the rate of the fluid flow from the structure. The depth-dependent equilibrium moduli found after 20 min equilibration (T20) were compared to the moduli found from the model at different time steps. The model calculated moduli were expected to remain constant with respect to time.

5.4.2 Existing values of solid matrix properties

In order to establish the expected range of values for the model derived depth-dependent matrix moduli, existing published properties were examined.

Explicit definitions of the depth-dependent solid matrix modulus are available from Li et al. (2002b), (2003b) and (2000), as shown in equation 5.1.

$$E_m = \hat{E}_m\left(1+\alpha_E\left(\tfrac{(H-z)}{H}\right)\right) \qquad \textbf{[5.1]}$$

Where *z* is the depth from the surface compared to the full sample thickness *H*, $\hat{E}_m$ the non-depth-dependent modulus was 0.226 MPa and α_E 3.2 (coefficient of linear depth-dependence) in Li et al. (2000). These values are comparable with the measured values of Chen et al. (2001). The moduli extracted from the model were compared to those given by Li et al. (2000).

5.4.3 Contribution of the fluid component

5.4.3.1Void fraction

Globally hyaline cartilage is considered to have an approximate fluid fraction of 65 – 80% (Mow and Guo 2002). This water content is not distributed evenly through the thickness. The fluid fraction of the superficial zone of articular cartilage

accounts for up to 85% of the total tissue mass decreasing down to approximately 65 – 70% in the deep zone (Lipshitz et al. 1976, Brocklehurst et al. 1984, Mow and Guo 2002). As cartilage is assumed to be saturated, the volume of voids in the structure is assumed equal to the water volume (Li et al. 2003b, Li et al. 2000).

In published values, both the 'void ratio' (*g*) and 'fluid fraction' (*e*) are used to express the same material property. The relationship between these two values is shown in equation 5.2.

$$e = \frac{g}{(g+1)} \qquad \textbf{[5.2]}$$

The variation of void ratio, *g*, with depth is expressed as shown in equation 5.3.

$$g = \hat{g}\left(1 - \alpha_g\left(\frac{(H-z)}{H}\right)\right) \qquad \textbf{[5.3]}$$

Where $\hat{g}$, the uniform void ratio, was 3.6 and α_g, the coefficient of depth-dependence of void ratio, was 0.2 (as used by Li et al. (2000)). The void ratio calculation of Li et al. (2003b) and (2000) leads to a ratio of 3.59:1 water to solid (volume fraction (*e*) of 0.78) in the superficial zone ($1/10^{th}$ depth) and 3.4:1 water to solid (*e* = 0.74) in the deep zone (if (*H* - *z*) / *H* = 1); the void fraction was alternatively expressed as in equation 5.4.

$$e_0 = 0.85 - 0.15\left(\frac{(H-z)}{H}\right) \qquad \textbf{[5.4]}$$

The subscript '0' denotes 'equilibrium' properties, referring to cartilage in an unstrained state (Wilson et al. 2005a, Wilson et al. 2006, Wilson et al. 2007). This equation leads to a water volume fraction of 0.84 in the superficial zone and 0.7 in the deep zone, which is a larger variation than the values used by Li et al. (2000), but closer to the published work of Lipshitz et al. (1976). Lipshitz et al. (1976) studied the fluid content at equilibrium of bovine articular cartilage samples by examining the swelling ratio (the volume of fully hydrated tissue divided by the volume of the dried matrix) of cut sections (either 50 or 100 μm thick) taken from different depths. Through this experiment, the water volume fraction was found to be approximately 0.86 in the superficial zone smoothly decreasing down to 0.74 in the deep zone (Lipshitz et al. 1976). The variation of alternative published values for equivalent void ratios and void fractions are shown in Table 5-2.

Author	Void fraction (*e*) in superficial zone	Void fraction (*e*) in deep zone	Void ratio ($\hat{g}$)	Coefficient of depth-dependence (α_g)
Li et al. (2000)	0.78	0.74	3.6	0.2
Li et al. (2003b)	0.78	0.74	3.6	0.2
Wilson et al. (2005a)	0.88	0.7	7.88	0.7
Wilson et al. (2006)	0.84	0.7	5.67	0.59
Wilson et al. (2005b)	0.88	0.7	7.88	0.7
Lipshitz et al. (1976)	0.86	0.74	6.48	0.56

Table 5-2: A comparison of some of the values found in literature for the initial depth-dependent void fraction of articular cartilage. Values are given for the superficial and deep zones of the cartilage to demonstrate the full range of values. The variation is considered as linear between these points.

Figure 5-1 demonstrates the difference between Li et al. (2000) (and Li et al. (2003b)) void fraction and the void fraction used by Wilson et al. (2006).

Due to the influence of the void fraction on the permeability, the void fraction will therefore also have a significant effect on the magnitude of the initial pressurisation and the subsequent stress-relaxation rate (poroelastic behaviour described in section 1.2.1.1). The depth-dependent void fraction found for articular cartilage, using the model developed in this chapter, was compared to the range of values used in the literature (see Chapter 6).

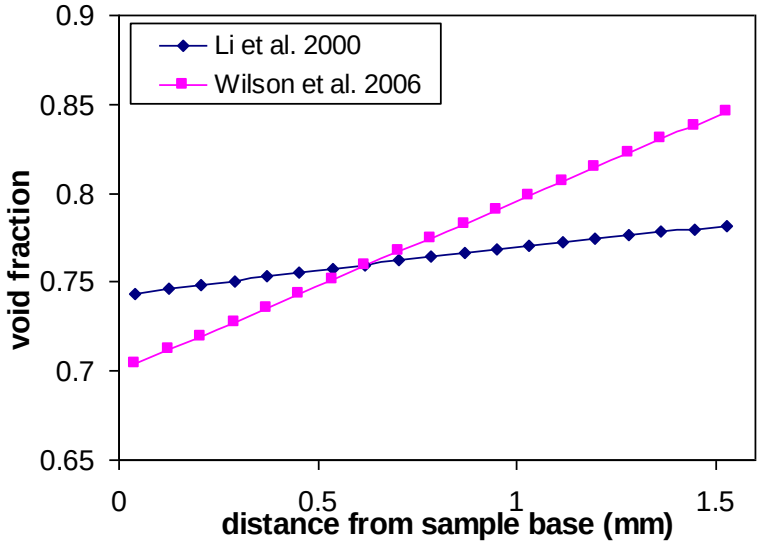

Figure 5-1: Plot demonstrating the difference between the void fractions used in the models of two different authors.

5.4.3.2Rate of fluid flow

If it is assumed that the voids are saturated and that any deformation applied to the cartilage leads to pressurisation of the fluid in the pores and subsequent outflow of fluid, Darcy's law is used to describe the rate of fluid flow. Darcy demonstrated experimentally (Darcy 1856) that the velocity of fluid flow through porous media (q) was directly related to the pressure gradient (∇p) causing the flow. This is shown in equation 5.5.

$$q = \frac{-k}{\mu} \nabla p \qquad \textbf{[5.5]}$$

The dynamic viscosity (μ) of the fluid in the cartilage (synovial fluid) will be assumed as 20 cP = 0.02 $kgs^{-1}m^{-1}$ (Rybicki et al. 1979). The greater the strain applied, the greater the fluid pressure developed in the samples and therefore the greater the fluid velocity. For Darcy's law to maintain validity, the following conditions are required (Satter et al. 2007):

- Fluid is incompressible.
- Flow is steady state and laminar (Reynold's number smaller than 1).
- Fluid flow occurs perpendicular to the direction of the applied compression.
- Only 1 fluid is present in the system, occupying the entire pore space.
- There is no chemical reaction between the matrix and fluid.

The assumption of laminar flow (Re < 1) through the media can be tested using the approximate pore size (d) of 5 nm (in the superficial zone) for cartilage (Langworthy et al. 2004). ρ is the density of the fluid in kgm^{-3}. Reynolds number (Re) is then calculated using equation 5.6.

$$\mathrm{Re} = \frac{\rho v d}{\mu} \qquad \textbf{[5.6]}$$

The Reynolds number can be seen to be many orders of magnitude lower than the maximum value permissible for the assumption of laminar flow for fluid velocities (v) up to 10^6 ms^{-1}. The assumption of laminar flow through cartilage is therefore valid.

5.4.3.3Permeability

Permeability, as defined from Darcy's law (equation 5.5), relates the fluid properties (dynamic viscosity ($kgs^{-1}m^{-1}$)) and the fluid flow rate (q (ms^{-1})) through a structure to the pressure gradient applied (Pa). Darcy permeability therefore has units of m^2. If the permeability of a structure is high, the structure offers low resistance to the flow of fluid through it.

Cartilage permeability has been found directly experimentally (Maroudas et al. 1968) and derived using other experimental methods (Chen et al. 2001). Published values have been assigned units of $m^4N^{-1}s^{-1}$ or, in an alternate form, $m^2Pa^{-1}s^{-1}$. This measure of permeability corresponds to Darcy permeability divided by the dynamic viscosity of the fluid, as shown in equation 5.7.

$$k_\mu = \frac{k}{\mu} = \frac{q}{\nabla p} \qquad \textbf{[5.7]}$$

As stated in 5.2, cartilage has a low permeability (of the order of 10^{-17} m^2 or 10^{-15} $m^4N^{-1}s^{-1}$ (Riches et al. 2002)). The articular surface membrane is comprised of densely packed collagen fibrils and has the lowest permeability value (Mow and Guo 2002). However, as the compressing surface used in this case experimentally is impervious, the boundary is to be considered as completely impermeable. The permeability in the superficial zone (below the membrane) is relatively high compared to the rest of the cartilage (found as 4.6×10^{-15} $m^4N^{-1}s^{-1}$ or 9.2×10^{-17} m^2 (Chen et al. 2001)). The permeability then decreases down into the deep zones (measured as 0.5×10^{-15} $m^4N^{-1}s^{-1}$ or 1.0×10^{-17} m^2 (Chen et al. 2001)). The bases of the samples are, like the top surface, considered as impermeable due to the experimental configuration.

As previously stated, the permeability is also dependent on void fraction. Due to the strain-dependence of the void fraction, permeability is also strain-dependent. The depth and strain-dependency of the permeability can be expressed as equations 5.8 and 5.9 respectively.

$$k_\mu = \hat{k}_\mu \psi(z,H)\exp(M\varepsilon) \qquad \textbf{[5.8]}$$

$$\text{Where } \psi = 1 + 4.3\left(\tfrac{(H-z)}{H}\right) - 7.8\left(\tfrac{(H-z)}{H}\right)^2 + 3.1\left(\tfrac{(H-z)}{H}\right)^3 \qquad \textbf{[5.9]}$$

(Lai and Mow 1980) where ε is the applied strain, M is a positive constant of approximate value 25 (Li et al. 2003b, Li et al. 2000, Li et al. 2002b) and $\hat{k}_\mu$ is approximately 2.0×10^{-15} $m^4N^{-1}s^{-1}$ (Li et al. 2000, Li et al. 2003b). Alternative values published for M and $\hat{k}_\mu$ for articular cartilage are shown in Table 5-3.

Author	$\hat{k}$ (10^{-15} $m^4N^{-1}s^{-1}$)	M (dimensionless)
Li et al. (2002b)	2	23
	3.2	30
	4	23
	3	23
	3	25
Li et al. (2003b)	3	10
	3	15
Li et al. (2000)	2	23
Nguyen and Oloyede (2001)		
(layer 1)	1.56	N/A
(layer 2)	0.45	N/A
(layer 3)	0.12	N/A
Average across tissue	1.45	N/A
Chen et al. (2001)		
(layer 1)	4.55	5.48
(layer 2)	1.46	5.49
(layer 3)	0.5	7.38
Average across tissue	7.3	8.41

Table 5-3: Table of published values for $\hat{k}_\mu$ and M from a selection of authors. Nguyen and Oloyede (2001) and Chen et al. (2001) found the values by dividing articular cartilage into three zones, mechanically testing and then fitting the experimental results.

The initial (zero-strain, ε = 0) depth-dependent permeability is therefore shown in equation 5.10.

$$k_\mu = \hat{k}_\mu\left(1+4.3\left(\frac{(H-z)}{H}\right)-7.8\left(\frac{(H-z)}{H}\right)^2+3.1\left(\frac{(H-z)}{H}\right)^3\right) \qquad \textbf{[5.10]}$$

The depth-dependent permeability profile of articular cartilage found when $\hat{k}_\mu$ of 2.0×10^{-15} $m^4N^{-1}s^{-1}$ is shown in Figure 5-2. These values approximately correspond with experimentally obtained depth-dependent permeability values of 2.9×10^{-15} $m^4N^{-1}s^{-1}$ (5.9×10^{-17} m^2) and 0.27×10^{-15} $m^4N^{-1}s^{-1}$ (0.55×10^{-17} m^2) in the superficial and deep zones respectively, found at 8% global strain (Chen et al. 2001). The equation therefore reflects a reasonable permeability profile of articular cartilage with higher permeabilities at the articular surface, but appears to underestimate the difference in permeability between the layers.

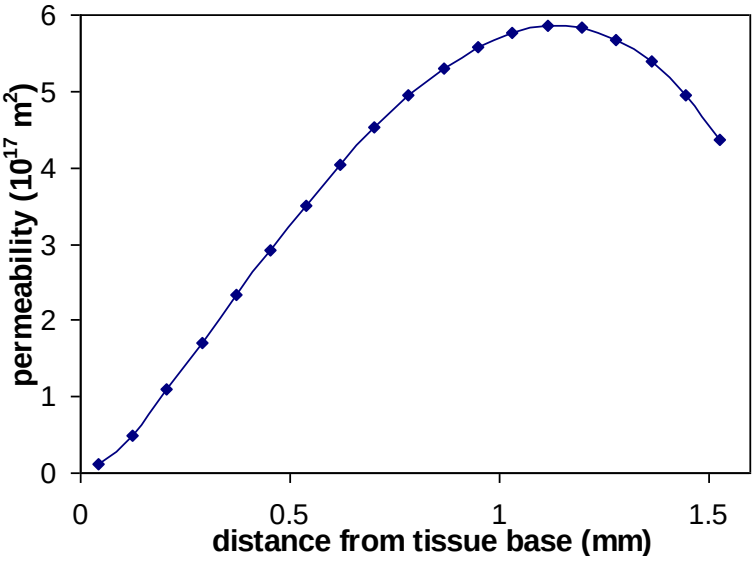

Figure 5-2: Plot of the depth-dependent permeability profile of articular cartilage using calculated from the published value of $\hat{k}_\mu$ of 2.0×10^{-15} m^{4}N^{-1}s^{-1}. The permeability is seen to steadily increase from the base and reach a peak during the middle zone before decreasing in the superficial zone.

As a simplifying assumption in this model, the strain-dependence of the permeability (determined by *M*) was assumed to be negligible. The strains used in this experiment are lower than those used by Chen et al. (2001) who experimentally determined the strain-dependency of the permeability with respect to depth. Additionally the values published for *M* vary between 5.48 and 30, as shown in Table 5-3. Without further experimental evidence it would not be possible to select an accurate value for this parameter. However, it is not possible to completely rule out the effects of the strain, and this is acknowledged as a potential weakness of the model.

5.4.4 Summary of initial values

Data of one-dimensional depth-dependent strains, global stress applied to the material and composite global moduli were obtained from the elastographic experiments between initial loading and equilibrium. These values were to be used in a one-dimensional axisymmetric depth-dependent poroelastic model.

The initial permeability will be assumed as equation 5.11, multiplied through by the dynamic viscosity, 0.02 kgs^{-1}m^{-1}, so as to be considered as Darcy permeability. *M* is assumed to be zero, so the exponential term in equation 5.8 is not used in this equation.

$$k_{i0} = 0.02\hat{k}_{\mu}\left(1 + 4.3\left(\frac{(H-z)}{H}\right) - 7.8\left(\frac{(H-z)}{H}\right)^2 + 3.1\left(\frac{(H-z)}{H}\right)^3\right) \quad \textbf{[5.11]}$$

5.5 Model development

To develop the one-dimensional axisymmetric poroelastic model from the available parameters, certain assumptions were required. These are explicitly listed in section 5.5.1. The discretisation process is then detailed, demonstrating the use of the experimental inputs in determining the construction of the model. Fluid pressurisation and flow effects are then described, leading to the solution via an iterative process.

The model was developed specifically for articular cartilage; however it would be applicable to nasal cartilage samples if the depth-dependent permeability and void fraction are known.

5.5.1 Assumptions

The following assumptions are required for model validity:

- Constant temperature – which is important for maintaining a constant ultrasonic sound speed as well as constant material elasticity.
- Each individual articular cartilage sample has a 'typical' structure, as this is how the initial conditions from literature are prescribed.
- The voids are saturated with incompressible fluid of a constant dynamic viscosity (0.02 $kgs^{-1}m^{-1}$).
- The voids are interconnected so that internal pressure is constant throughout each section of the material.
- The matrix is elastic and incompressible.
- The applied global strain (ε_G) is constant during the stress-relaxation process.
- The applied global stress is uniform across the contact surfaces (top and bottom) of the samples.

- The sample diameter ($2R$) remains unchanged as a result of the applied compression (i.e. all axial displacement occurs as a direct result of fluid flow).
- The speed of sound in cartilage is constant before and after compression.
- Fluid will only leave the structure through the outer cylinder walls (the top and bottom of the sample are rigid impermeable boundaries).
- Equilibrium exists when internal sample pressure (p_f) is equal to the pressure of the surrounding fluid (p_0).
- Following a compression, the fluid content will decrease until p_f returns to p_0.
- Darcy's law is valid to describe the fluid flow (section 5.4.3.2).
- The global measured stress is a consequence of the combination of solid matrix stress and fluid pressurisation ($\sigma_G = \sigma_M + p_f$) caused by the quasi-static application of strain.

5.5.2 Model discretisation

The complete sample was considered as a cylinder of height H and radius R. The global properties of this sample cylinder were found from the experimental strain applied and the measurements of the subsequent time-dependent stress. The applied global strain, ε_G, caused a displacement, dH, which acted on the initial cylinder height, H_0. These relationships are shown in equations 5.12 and 5.13.

$$dH = H_0 - H \qquad \textbf{[5.12]}$$

$$\varepsilon_G = \frac{dH}{H_0} \qquad \textbf{[5.13]}$$

From windowing the ultrasonic data, the depth-dependent displacements were found. These were converted into depth-dependent strains. The total cylinder height, H_0, was considered to be divided into a series of equal sections of tissue of height, h_0. These corresponded to the ultrasonic windows. Within each of the ultrasonic windows, which remained fixed before and after the strain application, the material displacement is measured as detailed in Chapter 4. This displacement

was used to determine the strain and the height of the tissue segment as a result of the global strain application as shown in equations 5.14 and 5.15 (where *i* denotes the window number in the tissue from the rigid fixed base).

$$dh_i = h_{i0} - h_i \quad \textbf{[5.14]}$$

$$\varepsilon_i = \frac{dh_i}{h_{i0}} \quad \textbf{[5.15]}$$

The pre-strained interstitial fluid pressure (p_f) was considered to be the same as the pressure of the fluid surrounding the sample, (p_f = p_0). Application of a strain would cause the interstitial fluid to pressurise. This is shown in Figure 5-3.

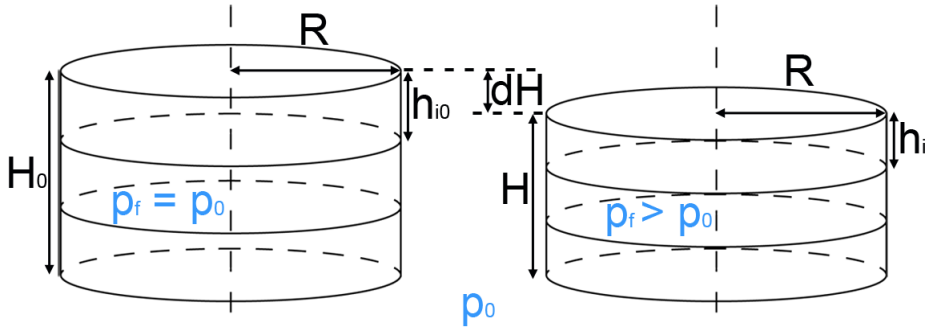

Figure 5-3: The discrete layers of a cylindrical specimen pre- and post-compression application. The corresponding fluid pressures are shown.

The maintenance of the applied quasi-static global strain in the sample required a time-dependent force *F(t)*. The global stress was therefore calculated from equation 5.16; it was assumed that *R* remained fixed with respect to time.

$$\sigma_G(t) = \frac{F(t)}{\pi R^2} \quad \textbf{[5.16]}$$

Due to the depth-varying articular cartilage properties of permeability, void fraction and matrix elastic modulus, each depth-dependent slice was considered independently. This is shown in Figure 5-4.

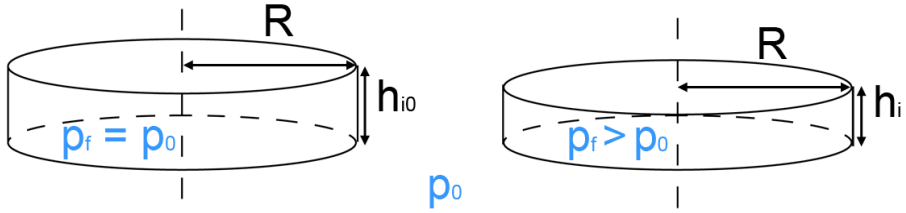

Figure 5-4: Change of height in an individual layer *i*, (h_{i0} to h_i) and the corresponding change of pressure as a result of the global applied strain. Each layer is considered to have its own set of discrete material properties. h_i is calculated using the elastography strain values.

5.5.3 Fluid flow model

In order to extract the depth-dependent matrix moduli before stress-relaxation equilibrium conditions were reached in compression, it was important to characterise the fluid pressurisation and outflow. It was therefore important to establish the volume of fluid in each layer undergoing pressurisation and the layer material properties which would affect the outflow.

The initial depth-dependent void fraction, e_{i0}, was used to determine the initial fluid volume in each slice. This liquid volume was visualised as a separate cylinder of radius *R*, like the complete slice, but of height *b*. The relationship between *b* and the height of the tissue, *h* is shown in equations 5.17 and 5.18.

$$e_{i0} = \frac{\pi R^2 b_{io}}{\pi R^2 h_{io}} \qquad \textbf{[5.17]}$$

$$\rightarrow \qquad b_{i0} = h_{i0} e_{i0} \qquad \textbf{[5.18]}$$

Under an applied strain, the pressure developed, causes the height of the fluid cylinder, *b*, to decrease due to fluid outflow. This rate was expressed as $\dot{b}$, a time-dependent value due to the time dependency of the applied pressure.

The outflow rate from the slice (*q*, units of ms^{-1}) was expressed as shown in equation 5.19.

$$q = \frac{\pi R^2 \dot{b}_i}{2\pi R h_i} = \frac{R\dot{b}_i}{2h_i} \qquad \textbf{[5.19]}$$

This was combined with Darcy's law to establish the pressure required to produce the flow rate *q* when k_i and μ were known values. This is shown in equations 5.20 and 5.21.

$$q = -\frac{k_i \nabla p}{\mu} = \frac{R\dot{b}_i}{2h_i} \qquad \textbf{[5.20]}$$

$$\nabla p = -\frac{R\dot{b}_i \mu}{2h_i k_i} \qquad \textbf{[5.21]}$$

The depth-dependent permeability was assumed to be radially constant and net flow of the fluid was considered to occur down the pressure gradient (from the centre of the slice out toward the edges). As defined in Darcy's law (equation 5.4), permeability acts at surface boundaries, so therefore equation 2.1 must be integrated with respect to the distance from the slice centre to the outer radius, *R*.

The sample slice was therefore considered as a series of concentric cylinders as shown in Figure 5-5.

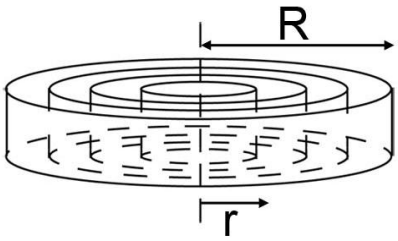

Figure 5-5: A simplification of splitting the main cylinder (radius = *R*) into a series of concentric cylinders, to allow calculations of the permeability field.

At the sample edge, $r = R$, the pressure was considered to be the same as the surrounding fluid ($p_{r=R} = p_0$). The integration across the slice is shown in equations 5.22 and 5.23.

$$\int_0^R \frac{\partial p}{\partial r} = \int_0^R \frac{-\dot{b}_i r \mu}{2k_i h_i} dr = p_0 - p_{f(r=0)} \qquad \textbf{[5.22]}$$

$$\rightarrow \qquad p_{f(r=0)} = \frac{\dot{b}_i \mu}{2k_i h_i} \cdot \frac{R^2}{2} + p_0 = -0 + \frac{R^2 \dot{b}_i \mu}{4k_i h_i} \qquad \textbf{[5.23]}$$

To find the average pressure across each layer, equation 5.24 was used.

$$p_f = \frac{p(r=0) - p(R)}{2} \qquad \textbf{[5.24]}$$

Within the layer, the global stress σ_G was considered to cause the depth-dependent strain ε_i. The stress was required to both force out the excess fluid and to overcome the solid matrix stiffness, E_{Mi}, as shown in equation 5.25 and 5.26. The matrix stiffness was considered as a fixed material parameter with respect to time.

$$\sigma_G(t) = E_{Mi}\varepsilon_i(t) + p_f(t) \qquad \textbf{[5.25]}$$

$$\rightarrow \qquad \sigma_G(t) = E_{Mi}\varepsilon_i(t) + \frac{R^2 \dot{b}_i(t)\mu}{8k_i h_i(t)} \qquad \textbf{[5.26]}$$

The sample radius (R), permeability (k_i) and dynamic fluid viscosity (μ) were assumed to be fixed with respect to time. $\sigma_G(t)$ and $\varepsilon_i(t)$ were taken from experimental measurements and h_i was found from $\varepsilon_i(t) = (h_0 - h_i(t))/h_0$ yielding $h_i(t) = h_0(1-\varepsilon_i(t))$. The flow rate was determined by the time-dependent void fraction (e_i) and slice height (h_i), as per equation 5.20.

$$E_{Mi} = \frac{\sigma_G(t) - \dfrac{R^2 \dot{b}_i(t)\mu}{8k_i h_0(1-\varepsilon_i(t))}}{\varepsilon_i(t)} \qquad \textbf{[5.27]}$$

Equation 5.27 was rearranged to express depth-dependent matrix modulus. It was therefore used to iteratively solve for depth-dependent modulus and flow rate, as within each slice the modulus was constant with respect to time. This is shown in equation 5.28.

$$E_{Mi} = \frac{\sigma_G(t_n) - \frac{R^2 \dot{b}_i(t_n)\mu}{8k_i h_0(1-\varepsilon_i(t_n))}}{\varepsilon_i(t_n)} = \frac{\sigma_G(t_{n+1}) - \frac{R^2 \dot{b}_i(t_{n+1})\mu}{8k_i h_0(1-\varepsilon_i(t_{n+1}))}}{\varepsilon_i(t_{n+1})} \qquad \textbf{[5.28]}$$

In equation 5.28, for each slice *i*, all the values were known from literature or are obtained experimentally except $\dot{b}_i(t)$ and E_{Mi}. $\dot{b}_i(t_n)$ and $\dot{b}_i(t_{n+1})$ values were varied in the iterative routine until the same value of E_{Mi} was obtained at two time steps. Values for E_{Mi} and $\dot{b}_i(t_n)$ were then recorded.

The model outline is shown in Figure 5-6, summarising the inputs, processes and outputs.

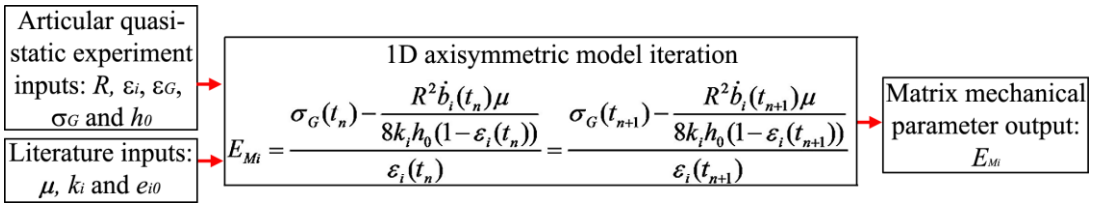

Figure 5-6: Outline of the one-dimensional axisymmetric model developed for the extraction of depth-dependent matrix moduli using quasi-static elastography results for articular cartilage specimens.

5.6 Analysis of the model

The model performance was evaluated using 'ideal' depth-dependent strains. These were produced using the linearly distributed moduli, $E_{i(ideal)}$ from equation 5.1, (using the same values as Li et al. (2000)) and the experimentally gathered global stress data, σ_G. These strains were then 'de-normalised' for input into the model, $\varepsilon_{wi(ideal)}$, by reversing the process shown in section 4.5.1.1. Equation 5.29 demonstrates the process of preparing the 'ideal' strain inputs.

$$\varepsilon_{wi(ideal)} = \frac{\sigma_G(t)}{E_i}\left(\frac{i}{0.5n}\right) \qquad \textbf{[5.29]}$$

The depth-dependent strain inputs for 2%, 4%, 6% and 8% globally applied strains are shown in Figure 5-7.

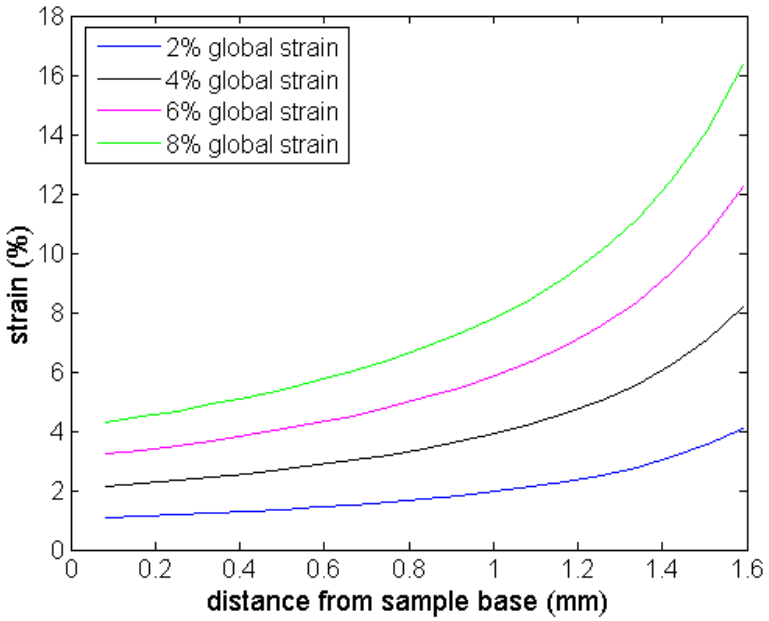

Figure 5-7: The 'ideal' strains produced from the linear modulus from Li et al. (2000) and the applied global strains.

The model outputs for moduli and void fraction at 2%, 4%, 6% and 8% global applied strains are presented and the limitations of the model discussed.

5.6.1 Moduli

The 'ideal' moduli outputs from the model are shown in Figure 5-8. The values generated for the matrix moduli were compared to those available from authors using alternative measurement techniques (see Chapter 2) in equilibrium conditions. Erne et al. (2005) recorded the moduli to vary from 0.27 MPa in the superficial zone to 0.71 MPa in the deep zone (where the global modulus was measured as 0.47 MPa). These values can be seen to be similar to those used by Li et al. (2000). Schinagl et al. (1997) found a greater variation between the moduli of the zones, recording 2.1 MPa, 1.14 MPa and 0.079 MPa for deep, middle and superficial zones, respectively.

None of the model determined moduli were linear. At 2% global applied strain, the output moduli were shown to be much larger in the deeper zone of the cartilage and smaller in the middle zones. The results for 4%, 6% and 8% applied global strain were lower than the linear modulus from Li et al. (2000). The strain inputs shown in Figure 5-7 were larger than would be expected in experimental practice for 4%, 6% and 8%, which would lead to these lower moduli outputs from the model.

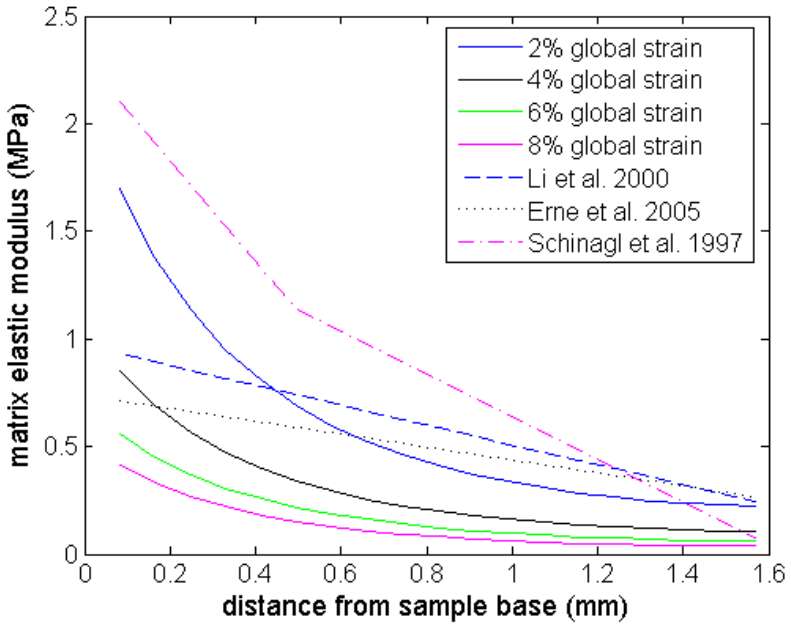

Figure 5-8: Demonstration of the 'ideal' depth-dependent moduli produced from the model when the 'ideal' strains shown in Figure 5-7 were used as the strain inputs. The original linear modulus is shown for reference.

The model output and the published matrix values are similar in terms of approximate magnitude and distribution with respect to depth. This is suitable evidence to suggest the model is producing the correct output.

5.6.2 Void fraction

In addition to matrix moduli, the model also allowed time- and depth-dependent void fractions to be extracted. The relationship between b_i and e_i was shown in equation 5.18. The changes in the fluid component of the tissue (Δb) were required. These values were obtained by integrating $\dot{b}_i$ with respect to time. The calculation is shown in equation 5.30.

$$\Delta b = \int_0^t \dot{b}_i(t) = \int_0^t \left(-\frac{8k_i h_0 (1-\varepsilon_i(t))(E_{Mi}\varepsilon_i(t) - \sigma_G(t))}{R^2 \mu} \right) \qquad \textbf{[5.30]}$$

Figure 5-9 demonstrates the time-, depth- and strain-dependence of the void fraction. The void fractions in the deepest part of the tissue, where the smallest strains were experienced due to the rigid base, remained constant with respect to strain and were similar to the unstrained values of b_0. The void fractions were smallest in the superficial zone, at every global strain. The superficial zone experienced the greatest deformations owing to the experimental set-up, so the large matrix deformations and high levels of fluid pressurisation were expected.

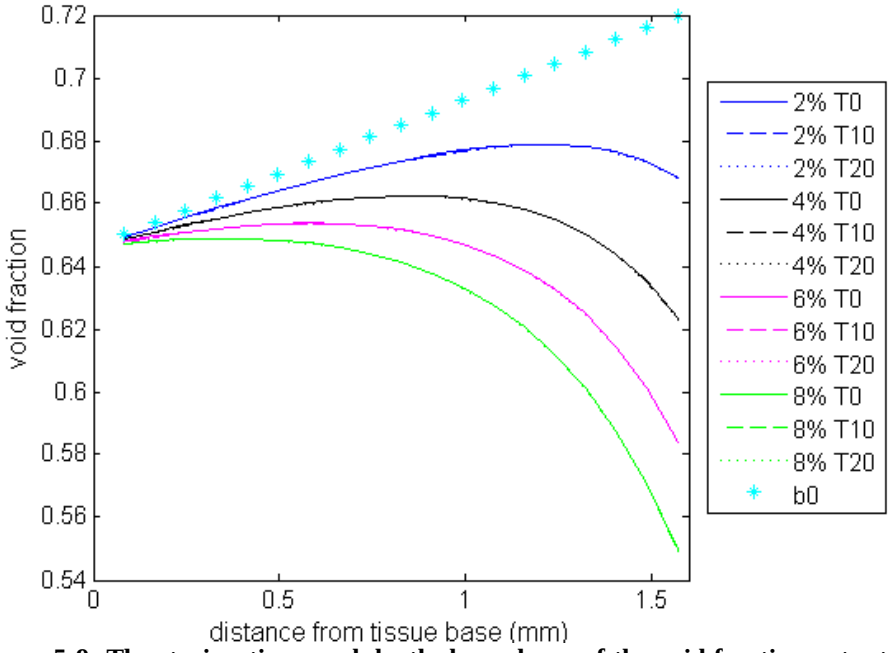

Figure 5-9: The strain-, time- and depth-dependence of the void fraction outputs of the model. For each strain, the results at after 0, 10 and 20 min (T0, T10 and T20) of stress-relaxation were so close in value they appear as a single line.

At every global strain applied, the void fraction remained constant during the 20 min stress-relaxation. This means that as the fluid pressure decreased, the pores remained a constant size, demonstrating the matrix material to be incompressible.

5.6.3 Boundary conditions

The model proposed in this chapter was developed for specific boundary conditions in terms of the pressure field. At the sample edges ($r = R$), the pressure is at equilibrium. Therefore the radial pressure gradient is established. In other compression configurations, such as confined compression or indentation, the pressure at the edges will be higher than the equilibrium pressure of the fluid surrounding a sample in unconfined compression, thus decreasing the gradient and reducing the rate of fluid flow.

By assuming an even distribution of the applied force, there is an implicit assumption that the compressing surface is larger than the sample. This implies an unconfined compression configuration. For cylindrical specimens tested *in vitro* there is no problem with this assumption. The model would however not be applicable to *in vivo* situations in its current form.

An indentation test would be used *in vivo* and the global mechanical modulus could be calculated using the appropriate equations. For both indentation and unconfined compression tests, the pressure maximum would be centred under the compressing surface and decrease radially in a linear fashion. However, the boundary conditions (as previously stated, at $r = R$) would be different. In the indentation situation there is no specific boundary where equilibrium pressure would occur in the same manner as at $r = R$ in the current model. The inability to define the pressure gradient, and the nature of the displacement field around the indenter edges, would need to be addressed if the model were to be developed for use *in vivo*.

5.7 Sensitivity of model to experimental errors in the input parameters

In order to assess the errors in the model mathematically, the equation for E_{Mi} (equation 5.29) was differentiated with respect to each input parameter in turn. The root-sum-square of the errors was then calculated (dE_{Mi}), as shown in equation 5.31. The partial derivatives used in the equation are presented in Appendix E.

$$dE_{Mi} = \pm \sqrt{\begin{aligned} &\left(\frac{\partial E_{Mi}}{\partial \sigma_G} d\sigma_G\right)^2 + \left(\frac{\partial E_{Mi}}{\partial R} dR\right)^2 + \left(\frac{\partial E_{Mi}}{\partial \dot{b}_i} d\dot{b}_i\right)^2 + \left(\frac{\partial E_{Mi}}{\partial \mu} d\mu\right)^2 \\ &+ \left(\frac{\partial E_{Mi}}{\partial k_i} dk_i\right)^2 + \left(\frac{\partial E_{Mi}}{\partial h_0} dh_0\right)^2 + \left(\frac{\partial E_{Mi}}{\partial \varepsilon_i} d\varepsilon_i\right)^2 \end{aligned}} \quad \textbf{[5.31]}$$

The errors in the experimental values of global stress and depth-dependent measured strains and the literature input of permeability, dynamic viscosity and void fraction were examined. The smallest iterative step in determining $\dot{b}$ was 10^{-9} times smaller than the resulting $\dot{b}$ values. Fractional errors are shown as fractional errors in Table 5-4.

strain (%)	Fractional errors (±)						
	k	ε_i	σ_G	μ	R	h_0	$\dot{b}$
2	0.53	0.4	0.13	0.1	0.03	0.02	10^{-9}
4	0.53	0.35	0.12	0.1	0.03	0.02	10^{-9}
6	0.53	0.3	0.15	0.1	0.03	0.02	10^{-9}
8	0.53	0.2	0.11	0.1	0.03	0.02	10^{-9}

Table 5-4: Fractional errors at 2%, 4%, 6% and 8% applied strain.

The magnitudes of each of the partial differentials calculated at all of the global applied strains are shown in Table 5-5.

strain (%)	$\frac{\partial E_M}{\partial \varepsilon_i} d\varepsilon_i$	$\frac{\partial E_M}{\partial \sigma_G} d\sigma_G$	$\frac{\partial E_M}{\partial k} dk$	$\frac{\partial E_M}{\partial h_0} dh_0$	$\frac{\partial E_M}{\partial R} dR$	$\frac{\partial E_M}{\partial \dot{b}_i} d\dot{b}_i$	$\frac{\partial E_M}{\partial \mu} d\mu$
2	2899	950	6.10	0.61	4.88E-4	6.10E-8	6.10E-8
4	3045	1048	3.11	0.31	2.49E-4	3.11E-8	3.11E-8
6	2988	1497	2.12	0.21	1.69E-4	2.12E-8	2.12E-8
8	2434	1340	1.62	0.16	1.30E-4	1.62E-8	1.62E-8

Table 5-5: Partial differential numerical values for error analysis of E_{Mi} in the order of numerical significance to the outcome.

It can be seen from the table that the model is most sensitive to errors in the strain and stress measurements. These are the experimental inputs and should be improved in order to increase the accuracy of the model outcome.

The maximum errors resulting from the error analysis were ±1.4%, ±1.3%, ±1.5% and ±1.2% for 2%, 4%, 6% and 8% applied strain, respectively. These are small errors.

5.8 Summary

A one-dimensional axisymmetric mechanical model of articular cartilage was developed using phenomenological observations from the behaviour of this material. The model can be used to find the depth-dependent matrix modulus from the calculated rate of fluid flow from an articular cartilage sample. Experimentally gathered information of the depth-dependent deformations and global mechanical values of stress and strain are required as input, as well as values of permeability and initial void fraction determined from literature. The model developed was tested and analysed using the 'ideal' strain values determined from literature, rather than experimental elastography values. The sensitivity of the model to errors in experimental inputs and processing was also quantified.

6 Results and Discussions: Quasi-Static Experiments

6.1 Overview

This chapter presents and discusses the global and local mechanical results, obtained during the stress-relaxation period of quasi-static compression, from nasal and articular cartilage samples. The global mechanical results of time- and strain-dependent elastic moduli are followed by the elastography strain maps. The theoretical mechanical model, described in Chapter 5, was then applied to the data from the articular cartilage quasi-static tests to determine the depth-dependent moduli and void fractions. Suggestions for the differences in behaviour between the two hyaline cartilage structures are given.

6.2 Mechanical test data from variable strain quasi-static tests

6.2.1 Nasal cartilage

The results in Figure 6-1 show the average composite global elastic modulus of nasal cartilage tissue following the application of a strain of 2%. The initial composite modulus at the instant of load application was 0.97 ± 0.18 MPa. The standard deviation of the results from the 10 samples is shown. The stress-relaxation rates, as seen in the shape of the curve, were fairly consistent. The criterion for equilibrium was determined to be when the change in the composite modulus was less than 10 kPa in 1 min. Equilibrium was reached at approximately 17 min.

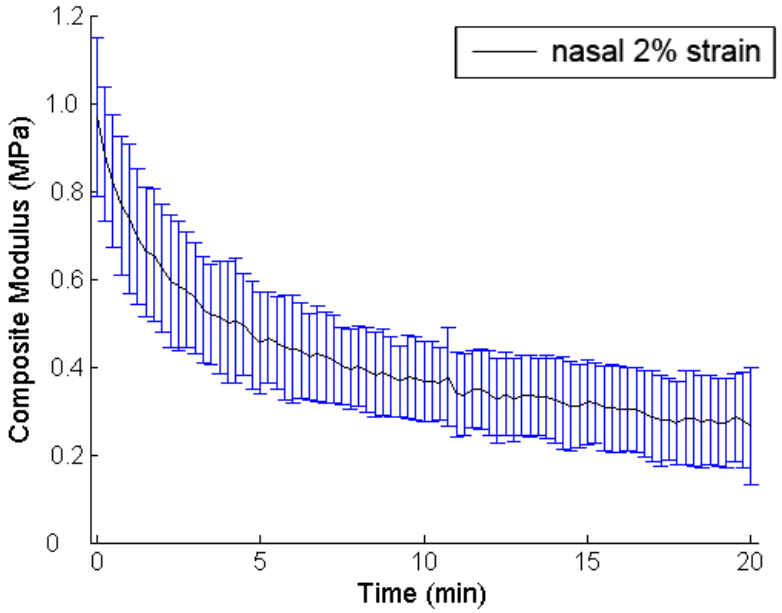

Figure 6-1: Graph to show the time-dependent composite Young's modulus over 20 min following the application of a quasi-static 2% strain to 10 nasal cartilage samples. The error bars show the standard deviation of the results.

Figure 6-2 shows the results for the composite global modulus from the application of a 4% strain to nasal cartilage tissue. The initial composite modulus was 0.97 ± 0.22 MPa. The equilibrium average modulus was 0.27 ± 0.03 MPa. The stress-relaxation rates were consistent, with equilibrium being reached after approximately 18 min.

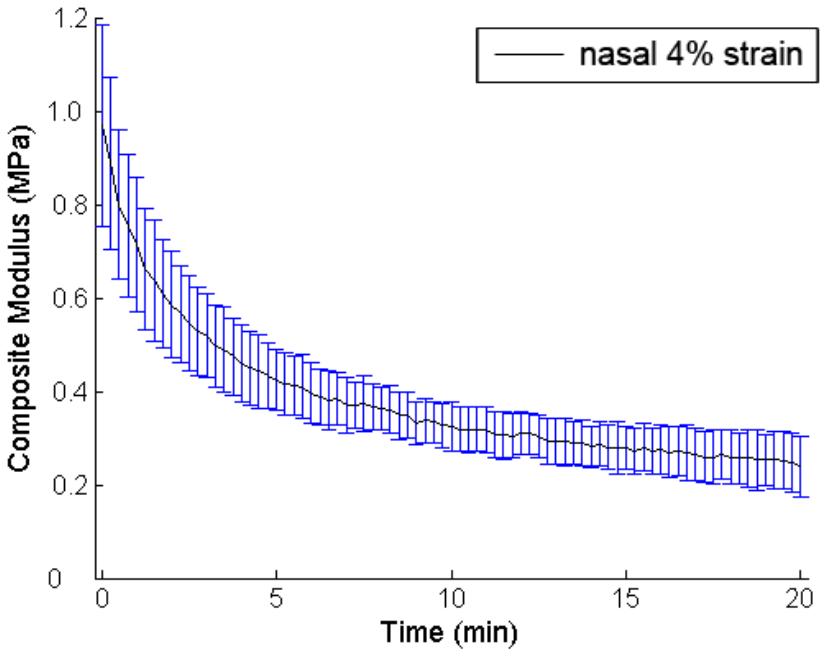

Figure 6-2: Graph of the composite elastic modulus measured throughout the 20 min period of the application of 4% quasi-static strain to 10 nasal cartilage specimens. Error bars show the standard deviation.

Results for the composite global modulus calculated with respect to time following the application of 6% strain to nasal cartilage tissue are shown in Figure 6-3. The initial composite modulus is 1.03 ± 0.20 MPa. The stress-relaxation rates were again seen to be consistent, with approximately 15 min being required to reach equilibrium. The global equilibrium modulus was 0.30 ± 0.04 MPa.

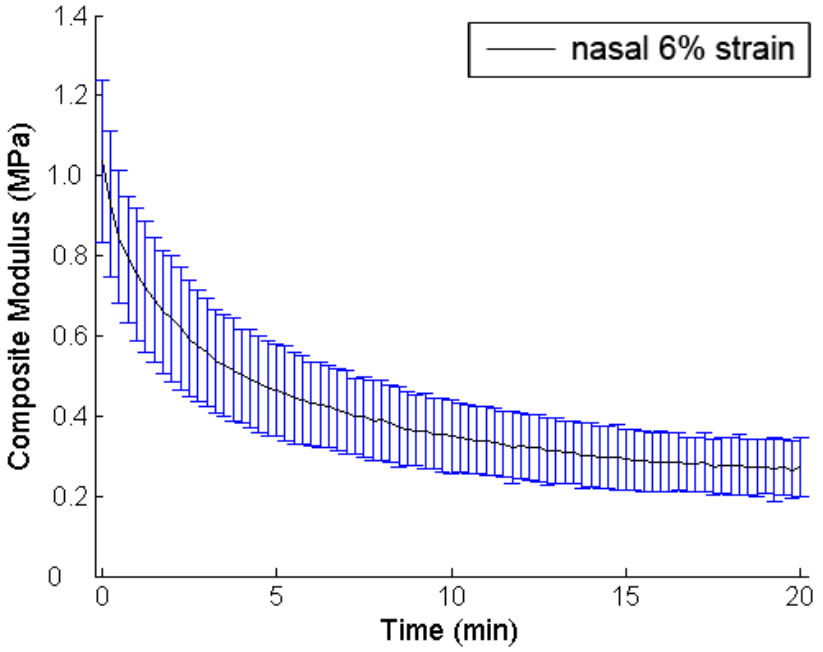

Figure 6-3: Graph of the composite moduli averaged for 10 specimens under a 6% quasi-static strain for 20 min stress-relaxation. Error bars show the standard deviation.

Figure 6-4 shows the results of the composite global modulus, averaged between the repeats, for an 8% strain applied to nasal cartilage samples.

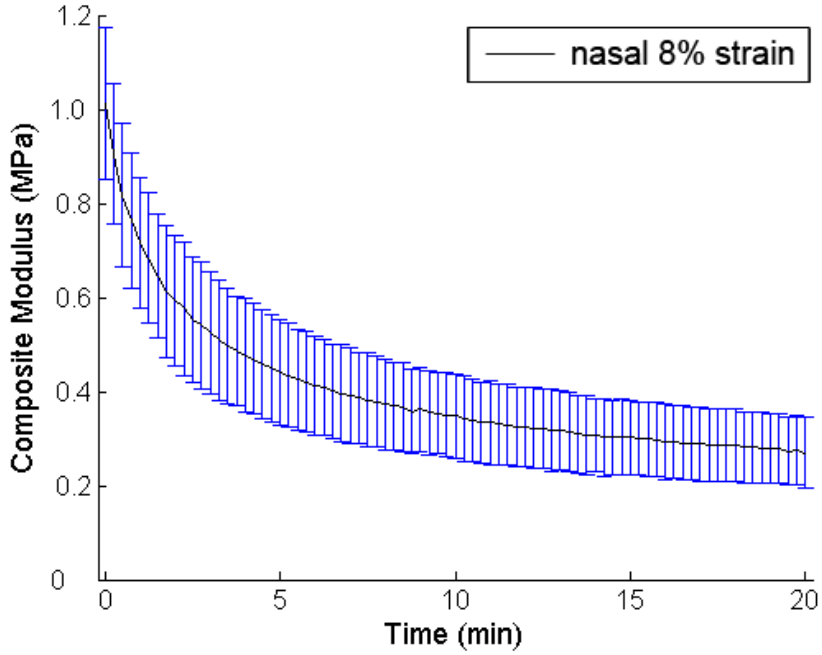

Figure 6-4: Graph of the resulting composite modulus over 20 min stress-relaxation period following the application of 8% quasi-static strain. Results were averaged over the 10 nasal samples and standard deviation is shown using the error bars.

The initial composite modulus was 1.01 ± 0.16 MPa. This was similar to the moduli measured at 2%, 4% and 6% applied strains; this result was found to be statistically significant with ANOVA (>90% confidence). Equilibrium at 0.32 ± 0.04 MPa was reached after approximately 13 min.

Figure 6-5 shows the results of all the levels of strain application on the nasal cartilage. The standard deviation error bars are omitted from this graph for clarity. The similarities between the moduli and stress-relaxation of all the applied strains can be seen.

The time-constants (time taken for the magnitude of the curve to fall to 1/e of the initial value) were calculated for each curve. The results are shown in Table 6-1.

strain (%)	time-constant (min)
2	2.00
4	2.00
6	2.25
8	2.00

Table 6-1: Time-constants in min calculated from the nasal cartilage mechanical test results.

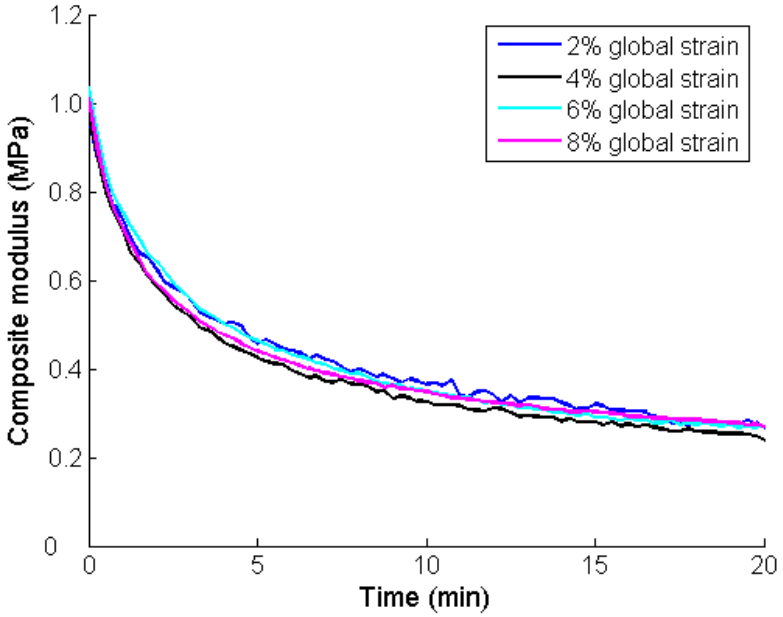

Figure 6-5: Graph showing the composite global moduli from nasal cartilage, over 20 min stress-relaxation, at each of the applied global strain levels. Error bars have been omitted for clarity.

The implication of these similarities between the shapes of the curves and the time-constants is that this non-layered hyaline cartilage does not undergo a strain-dependent change in global composite moduli.

6.2.2 Articular cartilage

The average composite global moduli results, following the application of 2% strain to articular cartilage samples, are shown in Figure 6-6. The initial composite modulus was 0.73 ± 0.18 MPa. 'Equilibrium' (as defined in section 6.2.1) was reached after 14 min with an average equilibrium modulus of 0.24 ± 0.03 MPa.

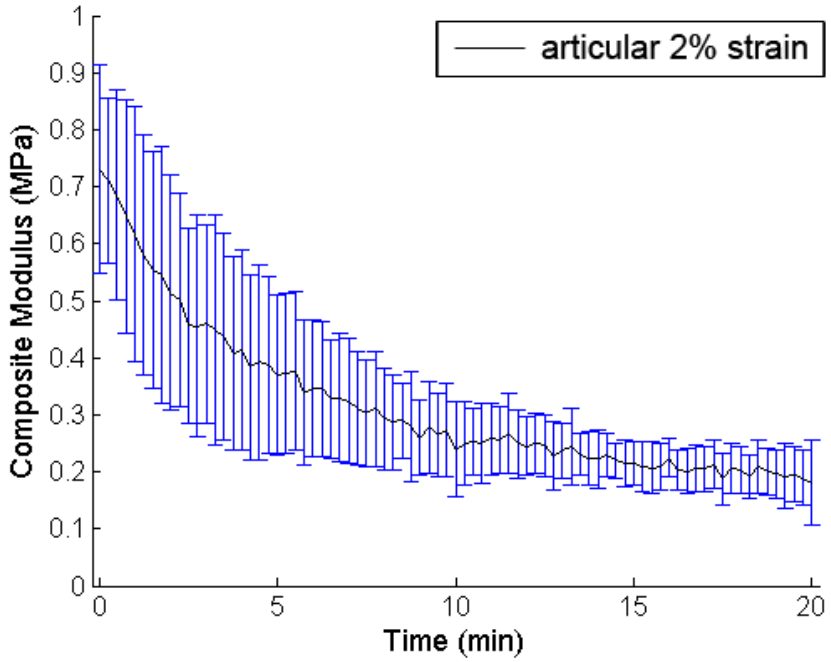

Figure 6-6: Graph of the composite moduli, during 20 min of stress-relaxation, in 10 articular cartilage samples, following the application of a 2% global strain. Error bars show the standard deviation.

Figure 6-7 shows the average composite global moduli throughout the 20 min period following the application of a 4% global strain to articular cartilage samples.

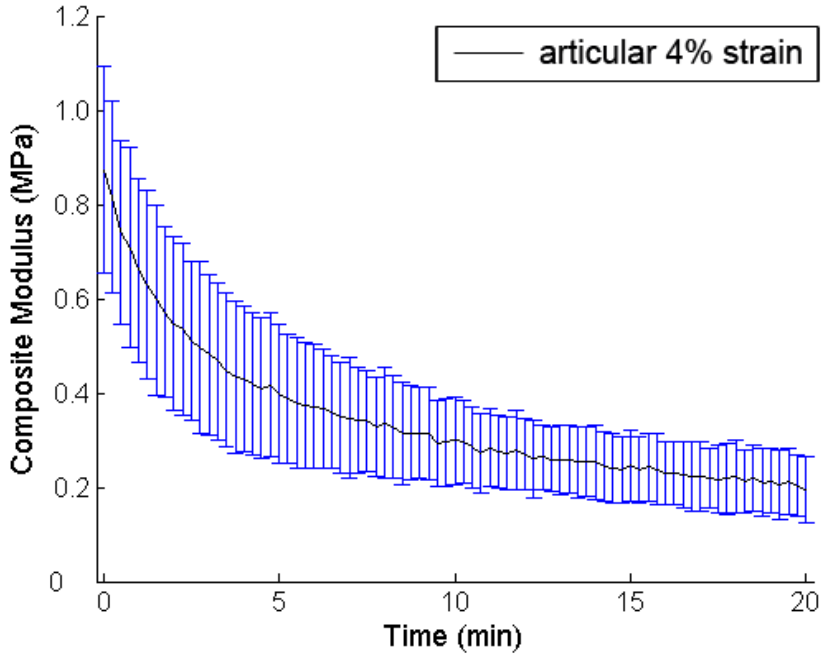

Figure 6-7: The composite elastic modulus application of 4% global strain to articular cartilage for 20 min. The error bars show the standard deviation across averaged results for the 10 specimens.

The initial composite modulus was 0.87 ± 0.22 MPa. This is not statistically different to the initial moduli from a 2% global strain application to articular

cartilage (>90% confidence). An average 'equilibrium' modulus of 0.24 ± 0.04 MPa was found after approximately 17 min. This was highly similar to the equilibrium modulus after 2% compression (>90% confidence).

Results of the composite global moduli for 20 min following the application of 6% strain to articular cartilage samples are shown in Figure 6-8. The average initial composite global modulus was 1.00 ± 0.27 MPa. This was determined to be statistically significantly larger than the instant moduli from 2% applied global strain (>90% confidence), but not the instant moduli from 4% global strain. The average equilibrium modulus reached after approximately 17 min was 0.24 ± 0.04 MPa. This was highly similar to the equilibrium moduli from 2% and 4% global applied strains (>90% confidence).

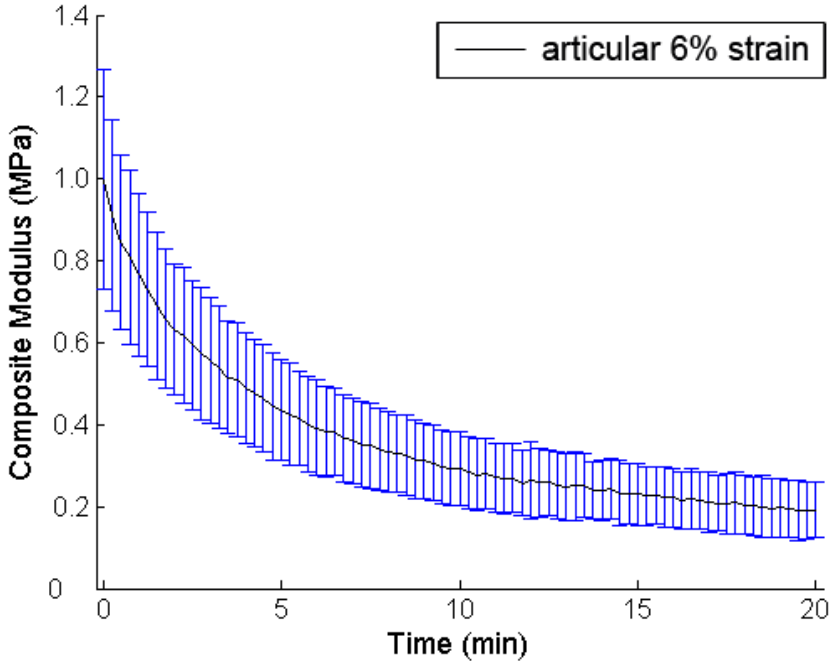

Figure 6-8: Graph showing the composite global moduli, for 20 min stress-relaxation, averaged for 10 samples following the quasi-static application of 6% strain to the surface. Error bars show the standard deviation.

Figure 6-9 shows the composite global moduli calculated for the 20 min following the application of 8% global strain to articular cartilage samples. The initial average modulus is 1.22 ± 0.35 MPa. This was statistically significantly larger than initial moduli at 2% and 4% global strain (100% confidence) and 6% global strain (>95% confidence). After an equilibrium period of 17 min, the 'equilibrium' modulus was found to be 0.24 ± 0.03 MPa, which was highly similar to the results from the equilibrium moduli of 2%, 4% and 6% global applied strains (>90% confidence).

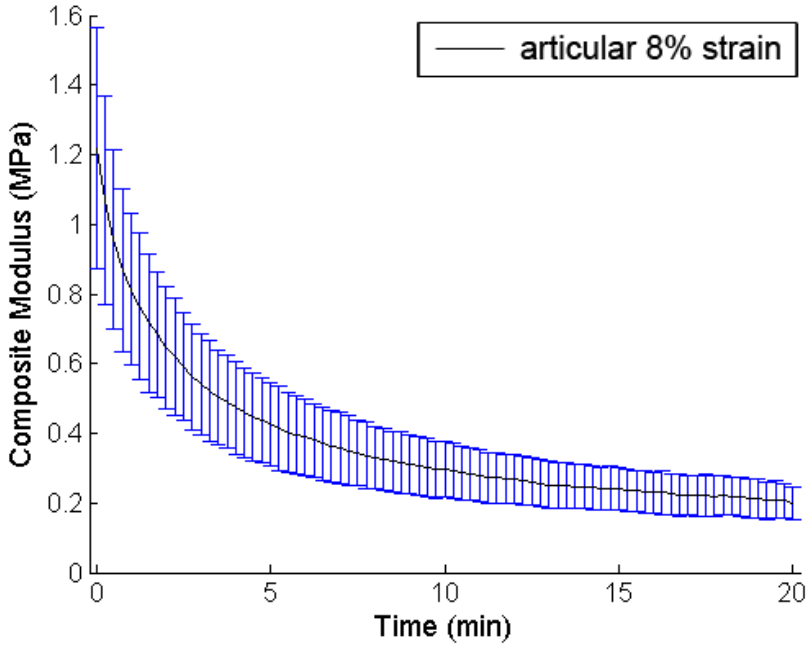

Figure 6-9: Averaged composite global moduli, with standard deviation error bars, from 10 articular cartilage specimens, during 20 min of stress-relaxation following the application of 8% quasi-static strain.

The results from all of the applied strain levels are plotted together in Figure 6-10. The variation of the average initial moduli, although not statistically significant is visible compared to the significant similarity of the average equilibrium moduli. As with Figure 6-5, the standard deviation error bars are omitted for clarity.

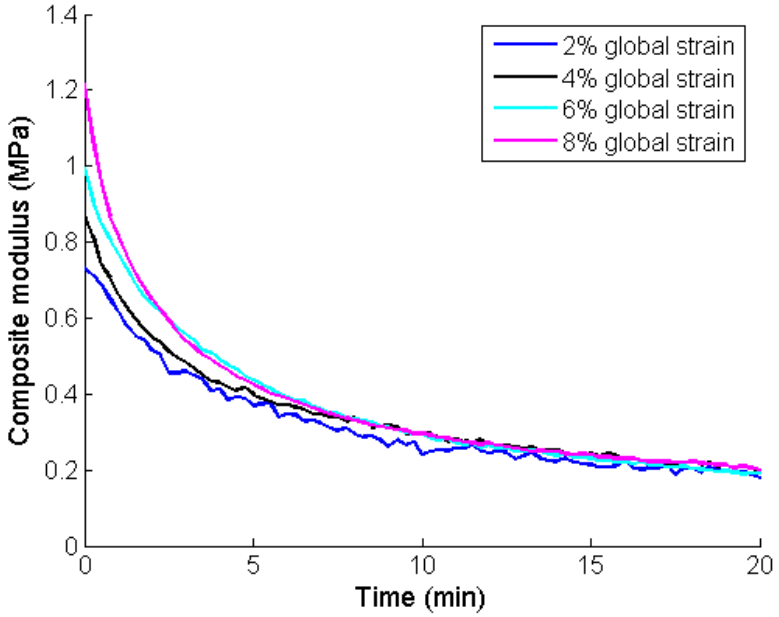

Figure 6-10: Comparison of the stress-relaxation curves of the composite moduli of articular cartilage samples, during 20 min of quasi-static strain, applied at 2%, 4%, 6% and 8%.

The time-constants, as described in section 6.2.1, were calculated. The results are shown in Table 6-2.

strain (%)	time-constant (min)
2	4.25
4	3.75
6	3.00
8	2.00

Table 6-2: Time-constants of the stress-relaxation rates of articular cartilage samples during mechanical tests.

The general trend appears to be that the stress-relaxation rates increase as the applied strain increases.

6.2.3 Comparison of the two native cartilage structures

The variation of averaged initial and equilibrium moduli with respect to the applied strain is shown in Figure 6-11. Both the articular and nasal instant composite moduli were observed to increase with respect to the applied strain; however the nasal increase was only very slight and statistically insignificant. The strain-dependence of articular cartilage was found to be statistically significant (100% confidence) between 2% and 8%. The strain-dependence of the articular cartilage initial modulus appeared to be exponential, so a trend-line was fitted. The relationship found from this line was $y = 0.68e^{0.1x}$. The fit of the line to the data was measured using the R_{fit}^2 value, which was 0.98, which is indicative of a close fit between the trend-line and the plotted data.

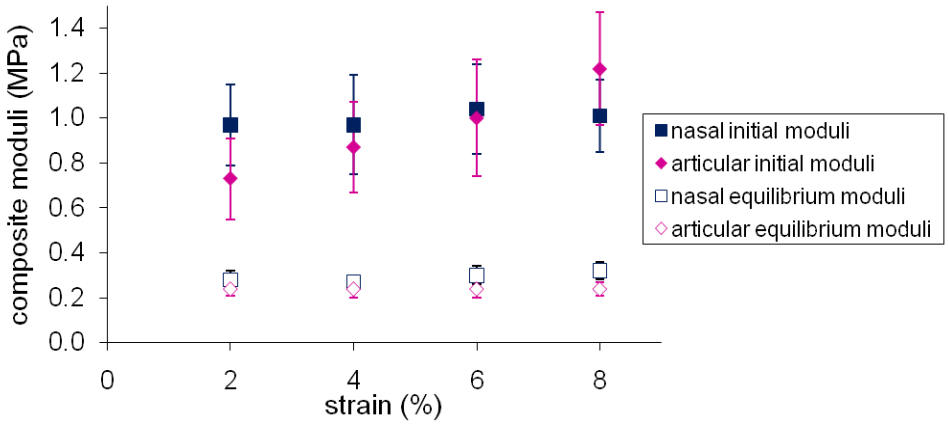

Figure 6-11: Comparison of the mean and standard deviation values for the composite moduli, measured at initial strain application and after 20 min of stress-relaxation ('equilibrium'), at the different strain levels applied, for both nasal and articular cartilage samples.

The results for the initial modulus of nasal cartilage were found to be independent of the applied strain (>70% confidence). The initial modulus from nasal cartilage was therefore determined as 0.99 ± 0.04 MPa. In articular cartilage the initial modulus was found to vary between 0.73 ± 0.18 MPa and 1.22 ± 0.35 MPa for 2% to 8% applied strain respectively (>70% confidence). The statistical differences between the other strains examined for articular cartilage were lower than this value, but despite this it appears that a trend does exist. It is therefore likely that the structure of articular cartilage affects the way that hyaline cartilage tissue behaves under initial load application. The increase of stiffness at higher strains would act to shield the chondrocytes in the matrix from damaging excessive shear strains. The stress-relaxation occurred faster with the higher elastic moduli. The equilibrium moduli of nasal and articular cartilage at all the applied strains were 0.29 ± 0.02 MPa and 0.24 ± 0.01 MPa respectively. The equilibrium moduli for both hyaline cartilages appeared to be independent of the strain applied. The similarities between the two native tissues at equilibrium suggest that collagen fibril architecture has little effect on the equilibrium moduli.

The main implication of the variation in the elastic result between the two hyaline cartilage structures is for tissue engineering. If a completely non-layered tissue such as nasal cartilage was used to replace damaged articular cartilage, neighbouring sections of healthy articular cartilage and replacement cartilage could strain differently under the applied load. At lower strains the nasal cartilage is stiffer, so would therefore strain less than the articular cartilage, causing shear strains between the materials. The best match between the nasal and articular cartilage was at 6% applied strain. At higher levels of strain the articular cartilage is stiffer than the nasal cartilage which would again cause unfavourable shear conditions in between the two materials.

6.2.4 General observations of the mechanical test results

The testing geometry and the sample sizes will have affected the mechanical test results in this study. *In vivo* articular cartilage is loaded regularly in both constant strain and constant stress. The unconfined stress-relaxation only addressed the behaviour under constant strain. To fully characterise the behaviour of human cartilage samples and the suitability of engineered samples for implantation it may

be necessary to design apparatus for further tests in creep. However, one of the objectives of this thesis was to determine if mechanical differences in the samples could be detected experimentally. This objective has been met as it has been shown that it is possible to determine mechanical differences between the two hyaline cartilages, with the behaviour of articular cartilage being determined as strain dependent. The articular samples investigated were from bovine patellae; engineered tissue will eventually be required to replicate human tissue, so the mechanical values cannot be taken here as absolute design parameters. The results function as indications of behaviour trends and proof of the ability of ultrasound elastography techniques to correctly distinguish these.

Differences between the stress-relaxation time reported in this investigation and those from the literature could be attributed to differences in sample diameters. The diameter of the samples during *in vitro* experiments will affect the rate of fluid flow from the sample due to the larger surface-to-volume ratio and the cut surfaces providing a significantly easier passage for the fluid to move through due to the large relative pressure differences. Continuous cartilage surfaces *in vivo* would not have such cut surface boundaries and so the pressure gradients would be smaller across the tissue. The permeability of the intact material *in vivo* would appear lower as the fluid would move slower. It is important therefore to acknowledge that the current experimental set-up should not be used to obtain absolute values for the sample mechanical behaviour such as the relaxation times. The values for the initial and equilibrium moduli should be fairly accurate representations of the continuous properties, as they do not rely on the pressure gradients. At the initial moduli it is assumed that the fluid has had insufficient time to flow, and at equilibrium it is assumed that all significant fluid flow has already occurred.

Frictional forces would have occurred between the bases and tops of the samples with the delay-line and actuator respectively. The friction force is proportional to the contact area between the surfaces, therefore also dependent on the sample diameter. These are potential explanations for differences found between the experimental data gathered in this study and those reported by other authors.

6.3 Elastography results

6.3.1 Strain-dependence of sound speed

Due to the differences in sound speed, reported by Ling et al. (2007), resulting from the application of strain to the samples, the sound speeds in the specimens used here were examined. These tests were performed on the A-lines collected for the quasi-static elastography tests, using time-of-flight analysis between the reflections from the top and bottom surfaces and the recorded thickness of each individual sample. In order to use elastography results to determine material properties, it is assumed that the speed of sound in a material is not affected by the applied global strains.

The average pre-compressional speeds of sound measured for nasal and articular cartilage in this thesis were 1671 ± 47 and 1693 ± 39 ms^{-1} respectively, with experiments conducted at 37 ± 1.1°C. The sound speeds measured at initial loading and after stress-relaxation periods of 20 min at 2%, 4%, 6% and 8% in both nasal and articular cartilage are shown in Table 6-3. The differences between these measured speeds were analysed for significance, using unpaired student's T-tests (described in Chapter 4). It was determined that the changes are not significant (>90% confidence).

Strain applied (%)	Sound speed in nasal cartilage (ms^{-1})		Sound speed in articular cartilage (ms^{-1})	
	At the instant of compression	Following 20min stress-relaxation	At the instant of compression	Following 20min stress-relaxation
2	1607 ± 36 (-3.8%)	1628 ± 40 (-1.0%)	1695 ± 32 (+1.0%)	1693 ± 48 (+0.0%)
4	1611 ± 49 (-1.0%)	1631 ± 37 (-1.0%)	1690 ± 55 (-1.0%)	1697 ± 54 (+1.0%)
6	1623 ± 41 (-1.0%)	1639 ± 64 (-1.0%)	1697 ± 46 (+1.0%)	1690 ± 38 (-1.0%)
8	1632 ± 58 (-1.0%)	1621 ± 78 (-1.0%)	1696 ± 73 (+1.0%)	1695 ± 31 (+1.0%)

Table 6-3: The measured time of flight sound speeds for the nasal and articular cartilage used in this investigation following application of 2%, 4%, 6% or 8% strains. Speeds calculated both at the instant of strain application and after the full 20 min stress-relaxation period are compared. The percentage differences compared to the unstrained tissue are shown in the parentheses.

6.3.2 Elastography data from variable strain quasi-static tests

The following sections present the results from nasal and articular cartilage specimens from the application of quasi-static strains of 2%, 4%, 6% and 8%. The

normalised strain maps show the strains calculated from the time shifts measured in each window, at 55% correlation. The strains are presented, opposed to calculated moduli, as the moduli results would be misleading. The moduli at equilibrium can be assumed to represent those of the matrix, but prior to that are composite moduli incorporating contributions from both the matrix and the fluid.

The results are presented at 0 and 20 min (T0 and T20, respectively) after the strain was applied. Figure 6-12 demonstrates the points at which the ultrasonic signals were extracted to produce the elastography results at T0 and T20.

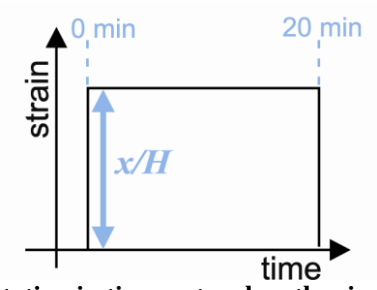

Figure 6-12: Representation in time as to when the signals were extracted for quasi-static elastography comparisons. *x/H* is the strain applied.

The sample 'tops' and 'bases' are as described in Chapter 3, Figure 3-1 and Figure 3-12. To enable 'zonal' comparisons between the magnitudes of normalised strains within and between the strain maps, numerical results from articular cartilage have been grouped approximately into deep, middle and superficial zones. Within each zone, the depth-dependent strain and standard deviation values resulting from the experimental repeats have been averaged, providing values for statistical comparisons. In Chapter 3 it was found that the thicknesses of the zones in articular cartilage corresponded to 4%, 38% and 58% (superficial, middle and deep, respectively) of the total tissue. The divisions used here were approximated to 10.6%, 36.8% and 52.6% due to the number and separation of the windows used in the signal processing, and are shown on the figures. These divisions are estimations, based on literature values and the findings in Chapter 3; they are not based on the findings of the individual samples shown. These divisions have not been applied to nasal cartilage, due to the evidence of a more homogeneous structure.

6.3.2.1Nasal cartilage

A comparison between the strain maps at the instant of strain application at all the investigated strain levels is shown in Figure 6-13. At all of the applied strain levels, the strain maps were indicative of a mostly homogeneous tissue structure of nasal cartilage.

At the instant of strain application, as shown in section 6.2.1, the global moduli were similar for every level of strain tested. For 2%, 4% and 6% global applied strains, the strain maps from the 1 mm of the tissue closest to the rigid delay-line base were found to be similar in magnitude. This similarity could either be attributed to experimental error or to the way in which the strains were distributed through the structure. However, due to the larger scatter observed in this first 1 mm, particularly following the application of 8% global strain, experimental error was determined to be the most likely cause. The large scatter in this region could be a result of the low signal-to-noise ratio of both the pre- and post-compressional signals causing difficulty for the elastography processing to reliably measure very small shifts from noisy signals. In the normalisation process, the strains in the lower half of the samples were multiplied, so any errors would have been proportionally increased.

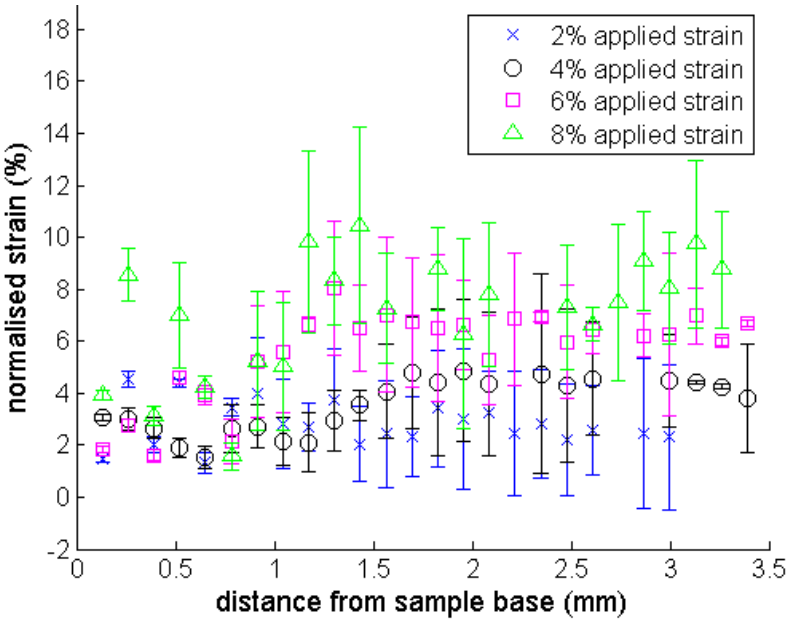

Figure 6-13: Normalised elastography strain maps comparing shape and magnitude of the response in nasal cartilage immediately following the application of varying strain levels.

Due to the similarity in shape of the 2% and 6% strain maps, it was concluded that the structural differences shown at 4% strain were also more likely attributable to

experimental error. It was observed from Figure 6-14 that at T20, the strain maps from all levels of applied global strains appeared more linear than at T0. However, the scatter had increased. Within the T20 results the scatter increased as a result of increasing the applied strain. The increase of strain in the lower 1 mm from T0 to T20 was observed. Again there could be different explanations. It is possible that during the 20 min of stress-relaxation, the distribution of the strains in the material changed and larger strains occurred in the lower regions of the tissue, but there is still very large scatter of the results in this area, indicative of the inability of the elastography processing to reliably detect correct shifts. The general increase in strain could therefore be a result of the signal shifts becoming easier to register in this region because of the stress-relaxation process. This would cause more correct strains to be calculated and therefore move the average to the expected level.

The evidence of the relative homogeneity of the nasal cartilage structure suggests that the tissue samples used have no real 'top' or 'base' like the articular samples, therefore there was no purely structural reason why the strains were lower in the region closest to the rigid delay-line.

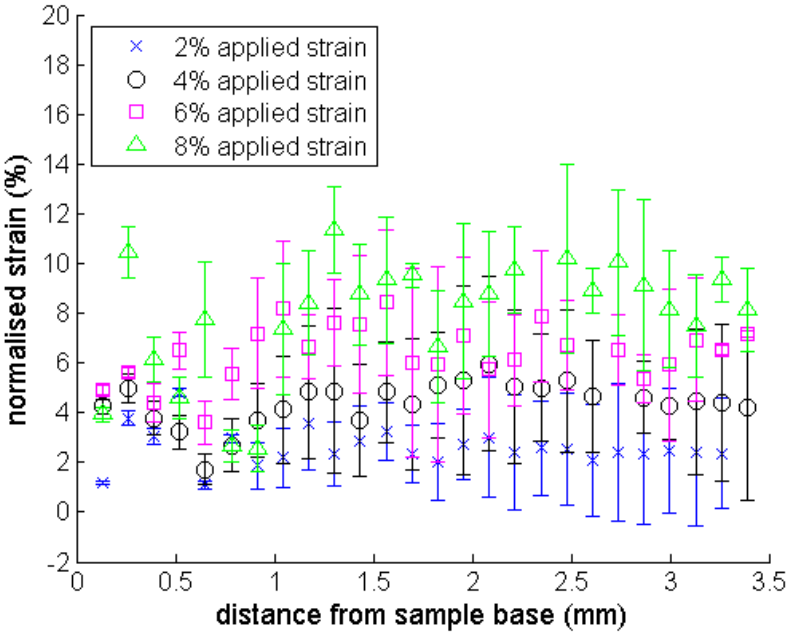

Figure 6-14: Normalised elastography strain maps from nasal samples following 20 min of application of varying strain.

The scatter of the results was considerably higher at 8% than the lower global applied strains for the times shown on both Figure 6-13 and Figure 6-14. A possible cause for this mis-registration of correct strains could be the low correlation between the pre- and post-compressional signals (due to the low signal-to-noise

ratio), combined with evidence in literature that time-domain techniques function less well at higher strains (Konofagou et al. 2000, Konofagou et al. 1999).

6.3.2.2 Articular cartilage

The normalised strain maps at the instant of strain application for all the strains applied are shown in Figure 6-15. The larger scatter and error bars from the results at 4% global applied strain were observed, as all the remaining maps were of a similar shape. The gradient in strain distributions between the superficial and middle zones appeared to be more pronounced at higher levels of applied strain. The scatter of the results also increased with strain (for 2%, 6% and 8% global applied strains). The strains in the deep and middle zones were fairly similar for 6% and 8% global applied strains. The deep zone strains were similar for 2%, 6% and 8% global applied strains. This implied that proportionally more strain was experienced in the deep zones at lower global strains. This may link directly to the measured global moduli, which were smaller for the lower global strains. The deep zones appeared to be strained more.

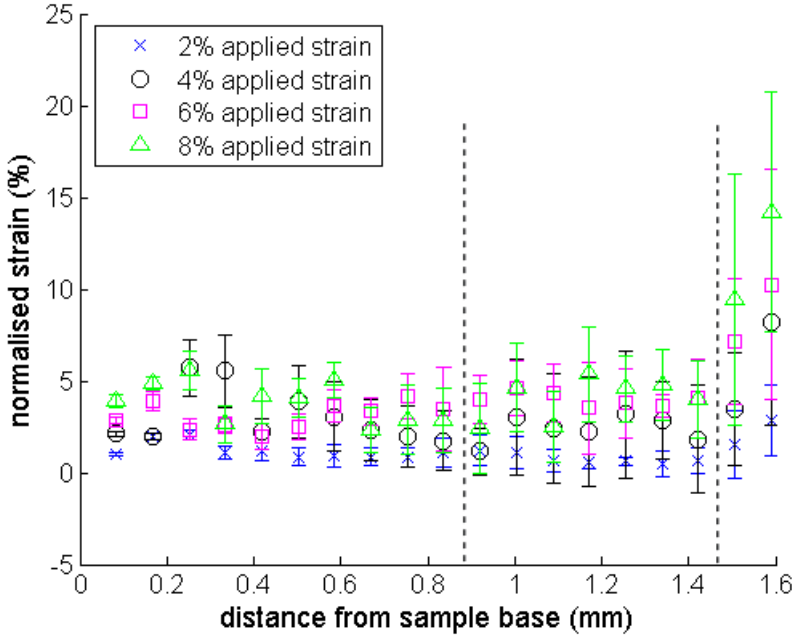

Figure 6-15: Normalised elastography strain maps shown to compare the shape and the magnitude of the depth-dependent articular cartilage tissue response, at initial application of the various global strains. The dashed lines represent the approximate positions of the zones: deep, middle and superficial from left to right.

The correlation between the pre- and post-compressional signals was higher for articular tissue than for nasal tissue. As a result there were always suitable shifts

detected in each window to allow the calculation of a strain. However, the error bars, indicative of the level of shift mis-registration, were still large and generally increased with respect to time. Similarly to the nasal results, the strains found in the tissue closest to the rigid base demonstrated a large degree of scatter. It was likely that the same problems in shift recognition were the cause.

Figure 6-16 shows the normalised strain maps obtained from articular cartilage samples 20 min after the application of a quasi-static global strain. The similarities between the strains in the deep zones at 2%, 6% and 8% applied strains were observed. The regional strains for 4% applied global strain were even more scattered at T20 that at T0 in this zone. Due to the same result being observed between the middle and superficial zones after 20 min of stress-relaxation at both 6% and 8% global applied strain, it was likely that the decrease in difference in strain distribution was attributable to the stress-relaxation process inside the samples over the equilibration period.

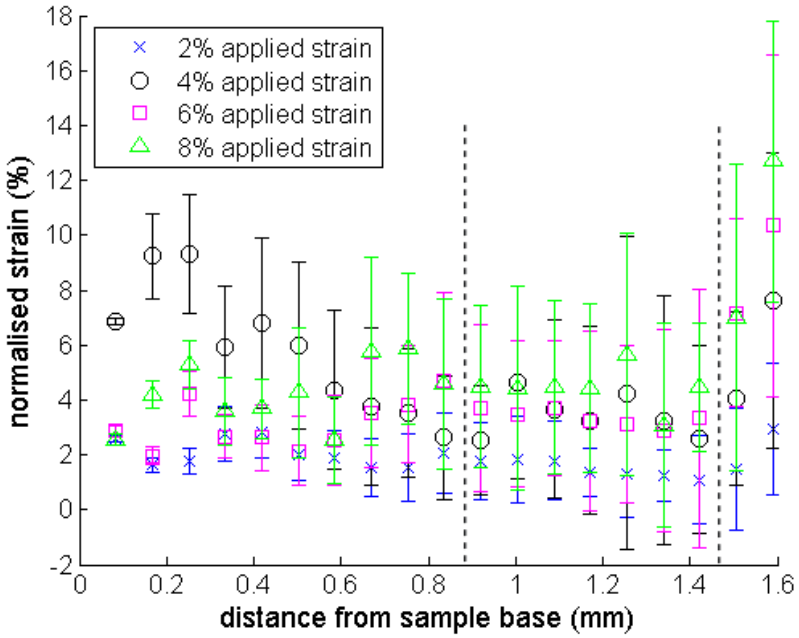

Figure 6-16: Normalised elastography strain maps from articular cartilage samples as a result of 20 min quasi-static application of the various global strains shown. The dashed lines are the same as in Figure 6-15.

The maximum strains in the superficial zone, appeared to be more regularly distributed than at T0, where the values at 4% and 6% were closer together. The regional strains for 4% to 8% global strains were similar in the middle zones, and were larger than the middle zone strains in Figure 6-15. In the same way as the results at T0, the deep zone strains were similar for 2%, 6% and 8% applied strain.

The error bars were generally larger for the T20 results than those at T0, which would suggest that either the error of the method increased with respect to stress-relaxation time, or that the mechanical response of the articular cartilage becomes more varied with respect to time. The error would only be likely to increase if the scatterers moved into positions where they were not readily detectable.

6.3.2.3Comparison of the two native cartilage structures

The differences in the strain profiles of the two native cartilages are most likely to be attributable to differences in both the fibril architecture and the local PG content. Whilst the nasal tissue behaved like a homogeneous structure, the articular tissue had clearer regional variations of measured strains, indicative of depth-varying elastic moduli.

From the appearance of the strain maps in Figure 6-13 to Figure 6-16 articular cartilage at 6% and 8% global applied strain underwent the most obvious stress-relaxation process involving strain redistributions. The strain distributions changed over the 20 min equilibration period. With respect to statistically significant changes, more occurred in the nasal cartilage samples; however, these were linked to the first 0.5 mm of tissue from the rigid base, where the scatter was largest. The nasal cartilage results were also inconsistent in terms of local strain measurements, so no conclusions regarding the time-dependent behaviour of the specimens could be drawn.

The error bars for measurements made in both native structures were comparable in magnitude throughout the test duration. Slightly smaller errors were observed for articular data at initial strain application than for both the nasal times; however, the error bars for articular cartilage after 20 min were larger than all the nasal errors. This suggests that during the stress-relaxation process a change occurred within the articular cartilage which made it harder for the elastography routine to measure the correct strain, or that the difference in the mechanical behaviour of individual samples increased with respect to time. Variation in behaviour could be caused by biological variations between matrix elastic constants, which were masked when the contribution of the pressurised fluid to the composite modulus was larger. However, it is more likely that the increase in the scatter of the results was caused

by difficulty in measuring the correct strain, particularly in the middle zone. This hypothesis is discussed further in the following section.

6.3.3 General elastography limitations

Throughout all of the elastography experiments, the signal-to-noise ratio of the reflections from inside the hyaline cartilage structures was low. The primary cause for this was most likely the low scatterer size inside the cartilage tissues. The acoustic impedance differences between the proteoglycan, collagen and chondrocytes, is likely to be high. Reported chondrocyte stiffnesses are approximately 10^{-3} that of the equilibrium stiffness of articular cartilage (Jones et al. 1999). Collagen fibrils have substantially larger stiffness (up to 10^{4} that of equilibrium cartilage matrix) (Sasaki and Odajima 1996). Bundles of chondrocytes in lacunae in the articular tissue are likely to have provided some reflections, as these have been shown to be surrounded by a dense network of secondary collagen fibrils (Clark 1985). However, both the chondrocyte and collagen fibril diameters are very small compared to the ultrasonic wavelength, therefore only yielding small reflections. This particularly appeared to cause problems in the middle zone of articular cartilage and throughout the thickness of the nasal cartilage tissue.

A structural feature common to both the middle zone of articular cartilage and the whole thickness of the nasal cartilage is the random collagen fibril alignments. As it is likely that the collagen fibrils contribute to the backscattered signal content, a link between lower signal-to-noise ratio and pre- and post-compressional signal correlation was proposed. In the superficial zone the fibrils are aligned primarily perpendicularly to the direction of beam propagation, this would cause better reflections and a higher signal-to-noise ratio. Although within this test set-up, the superficial zone reflections arrive in close proximity to the reflections of the actuator. In the middle zone, the random fibril orientation is more likely to cause scattering of the ultrasound away from the ultrasound beam axis, leading to lower received signal amplitudes from the region and therefore a lower signal-to-noise ratio. In the deep zone, the fibrils are mainly orientated parallel to the direction of ultrasound propagation. This would cause a lower signal-to-noise ratio for the region due to there being fewer surfaces to cause reflections. However, the low pre- and post-compression correlation was not necessarily only caused by low signal-to-

noise ratio, as the correlations in the deep zone were high. It is therefore most likely that the changes which cause signal decorrelation were caused by the alterations of fibril orientations as a result of the applied compression. Figure 6-17 demonstrates approximate changes in dominant fibril alignment, in the zones of articular cartilage, caused by the application of a strain.

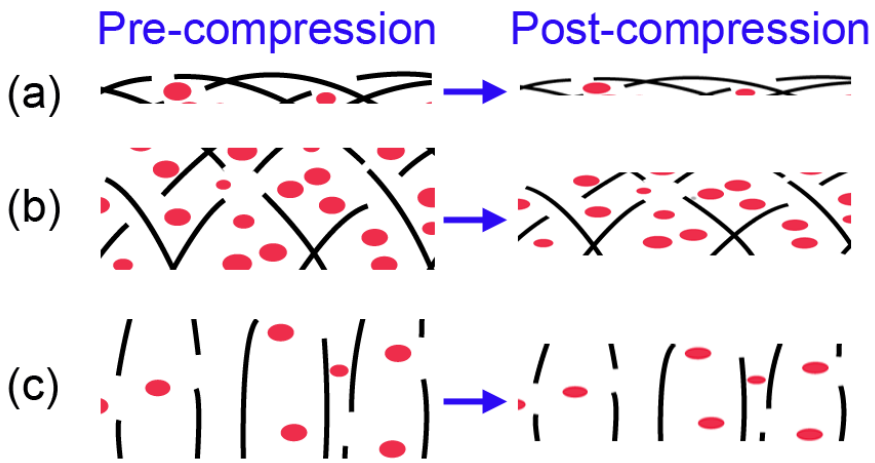

Figure 6-17: Approximations of what occurs in the (a) superficial, (b) middle and (c) deep zones during the application of a strain to the matrix.

It is proposed that in both the deep and superficial zones, that the fibril orientations remained fairly constant between pre- and post-compression. However, in the middle zone, the dominant angles of the fibrils changed. This would result in both the appearance of new reflections and the removal of some previously present reflections from this region. This would cause the decorrelation between the two signals. As the arrangement of collagen fibrils in nasal cartilage is similar to the middle zone of articular cartilage, this would explain why there was loss of signal correlation throughout the different depths of this structure. The resulting decorrelations of the middle zone of articular cartilage and throughout nasal cartilage were shown to be higher than the decorrelations in the superficial and deep zones in a supporting investigation (Ashraf 2010).

Far less is known about the nature of the collagen fibrils in the nasal cartilage. It is possible, as this tissue is not required to withstand forces of the same magnitude as articular tissue, that the fibrils were finer. This offers an additional explanation for the lower reflections from nasal tissue, as finer fibrils would be harder to detect ultrasonically, either before or after compression. This would also add to the problem of decorrelation, as pre- and post-compressional pairs of signals have

fewer common features. Additionally, the chondrocytes in nasal tissue do not appear to group in lacunae, so the secondary fibril network is less likely to provide strong reflections from around the cells.

The strains measured in the first 0.5 mm from the tissue base, in both the nasal and articular samples, had generally high levels of scatter. Due to the way the signals were normalised in order to present the strains, any small errors in those measurements were magnified. The converse effect occurred in the top half of the sample, whereby any small errors would have been diminished relative to the strain measured. It was likely that more errors were found in the sections of the tissues closest to the interface between the delay-line and the tissue, due to the presence of the large amplitude reflections from the interface ringing. This caused a 'dead' zone in the samples, which was determined by the pulse length of the transducer. The pulse length was found to be, at worst, 243 μm in cartilage tissue (see Chapter 4). The 'dead' zone was equal to half this length (122 μm) and caused difficulty in reliably determining the strains in the vicinity. In nasal cartilage tissue, this length was approximately equal to 4% of the total thickness, therefore only really affecting the first and sometimes second windows. In articular cartilage, this length was found to be approximately equal to 9% of the total tissue thickness, which would have affected the first and second windows, approximately 20% of the deep zone.

6.4 Modelling results for depth-dependent fluid movement to determine the local moduli

6.4.1 Depth-dependence

Figure 6-18 shows a comparison between the depth-dependent moduli defined by Li et al. (2000) and the moduli found using the equilibrium strain and global stress data for quasi-static elastography results at 2%, 4%, 6% and 8% global strains for articular cartilage. The equilibrium moduli in the deep zone were found to increase with respect to global strain applied. The middle zones were closer, and the superficial zone moduli were very similar to the predicted linear moduli. The implication of this result is that the deep zone of the articular cartilage specimens increased in stiffness due to increasing the global applied strains. Although 20 min had been assumed to be sufficient for equilibration of the sample it is possible that full stress-relaxation had not occurred in the deep zone at any of the applied strains.

This effect appeared to worsen as the applied strain increased. These values were used for comparison to the model results. However, it is also possible that the large moduli were a result of the strains being under-estimated in the elastography.

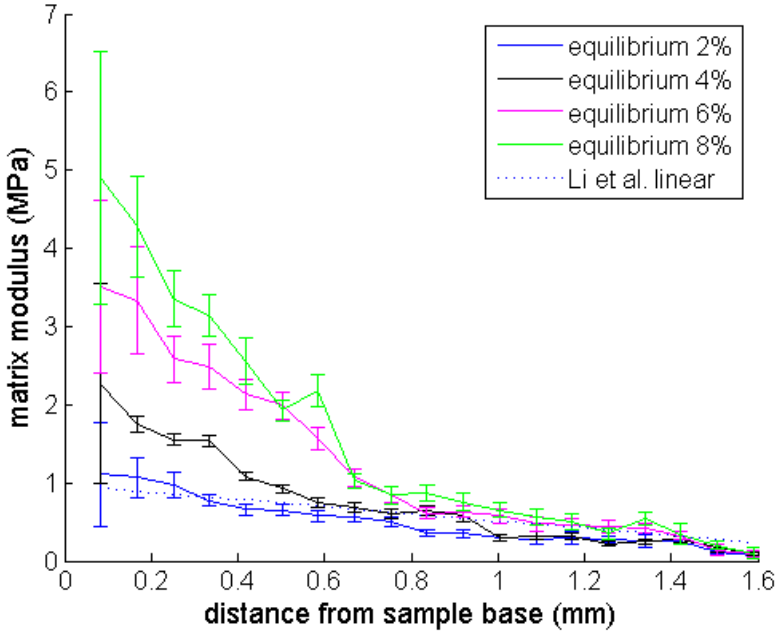

Figure 6-18: Depth-dependent moduli found from equilibrium elastography data compared to the 'ideal' linear moduli from Li et al. (2000) (see section 5.6).

The results from applying the model to the experimental data at each applied quasi-static strain are presented in Figure 6-19.

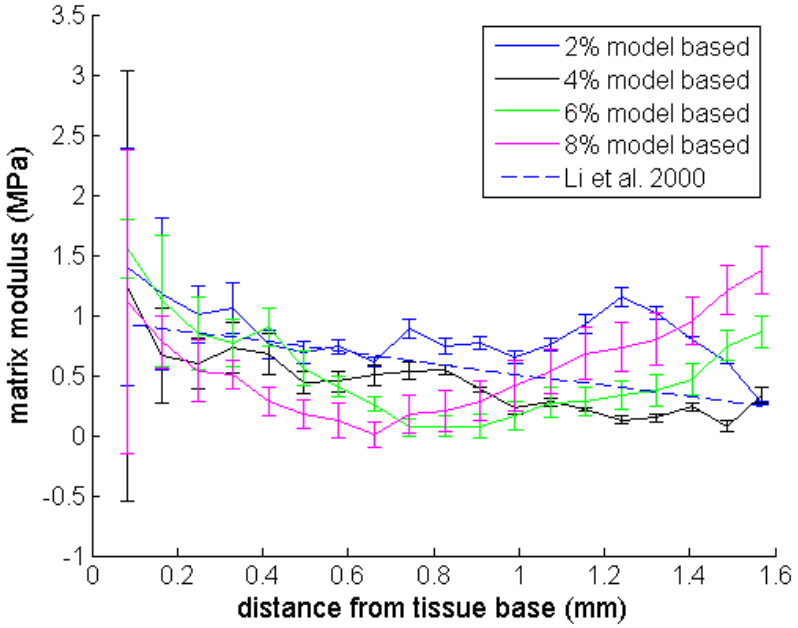

Figure 6-19: Comparison between the model-based calculation of moduli using experimental results at 2%, 4%, 6% and 8% strain applied to articular cartilage and the 'ideal' linear moduli.

For reference the linear 'ideal' depth-dependent moduli, used by Li et al. (2000), (as described in section 5.6) are also shown. The results at 2% global strain were significantly larger than the other strains in the deep and middle zones (100% confidence). It is unclear why the 2% results should be so much larger than the others, however, the same behaviour was observed in the 'ideal' model outputs (shown in Figure 5-8), when the 2% 'ideal' output was larger than the other global strains.

The results at 2% and 4% global strains most closely match the shape of the 'ideal' output. At 6% and 8% global strains, model results from the middle and superficial zones appear to increase in stiffness. These apparent increases are therefore likely to be attributable to an error in the calculation of the modulus. A possibility exists that this error was a result of assuming, in the model, that permeability was not dependent on strain. Low composite stiffness in the centre may be associated with the highest permeabilities in this region (as shown in Figure 5-2). Due to the experimental set-up, the larger strains were experienced in the middle and superficial zones. This means that if the permeability is dependent on the strain, the errors caused by assuming no dependence would be larger in these zones at higher strains.

Figure 6-20 shows a comparison between depth-dependent moduli (averaged from those obtained at equilibrium, for all the global strains) with the average of the model output. The linear 'ideal' modulus is also plotted for reference. The equilibrium moduli were observed to estimate larger moduli in the deep zone, similar moduli in the middle zone and smaller moduli in the superficial zone compared to the model output. However, only the superficial zone results were found to be significantly different (100% confidence). Although the deep zone strains were still large in the model results, they were smaller than those recorded from the equilibrium data. This supports the theory again that the experimental data obtained at 'equilibrium' represented incomplete stress-relaxation, as the deep zone results in the model represented fully relaxed matrix moduli.

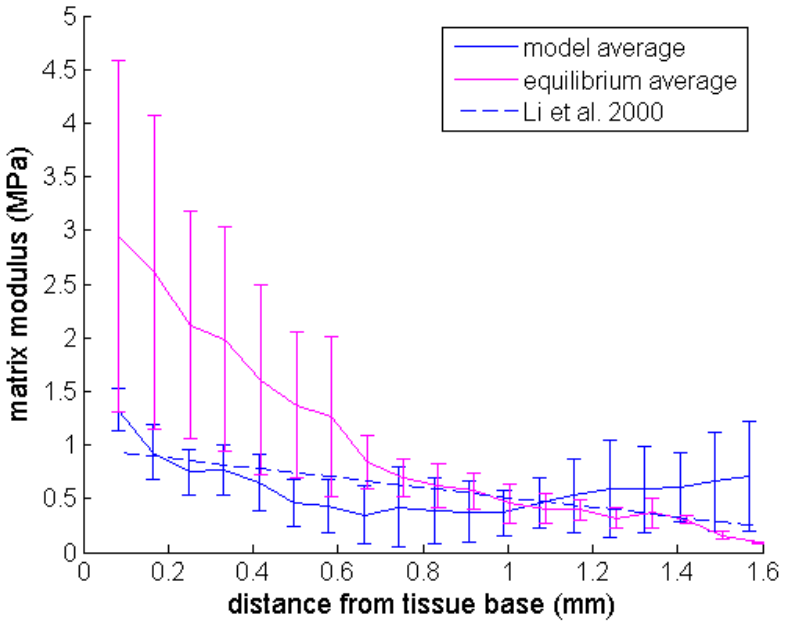

Figure 6-20: Averaged depth-dependent moduli across all the QS tests compared to Li et al. (2000).

The model was applied to find the depth-dependent void fractions. The results at different times in the quasi-static tests (0, 10 and 20 min following the application of the global strain) are presented in Figure 6-21, for each global applied strain.

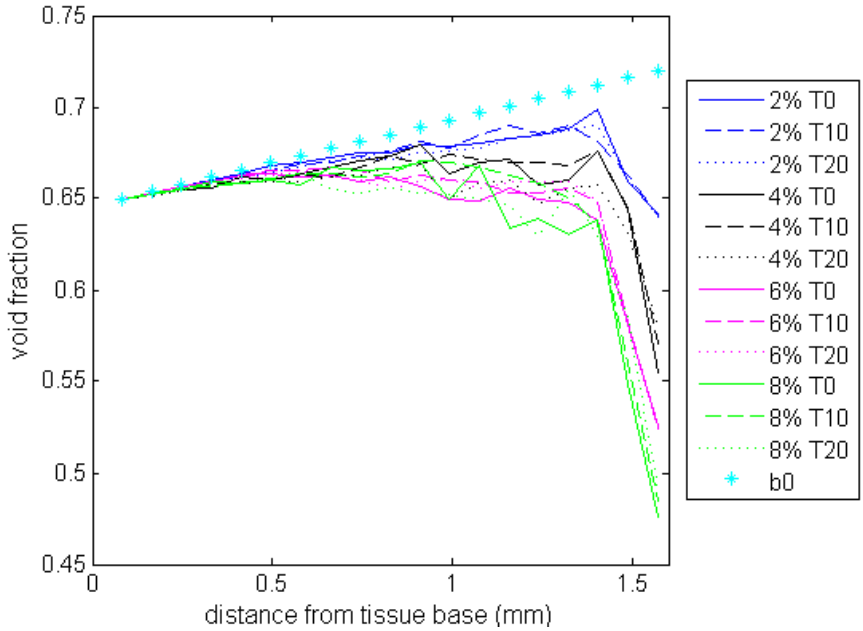

Figure 6-21: Comparison of the depth-dependent void fractions in the model. b0 was the void fraction input in the initial conditions for the model and was determined by literature values. The other results compare the strain- and time-dependent results of the model output.

These results were compared to the initial input of void fraction from literature values. It was observed that the post-compression void fraction distributions were strain-dependent, but relatively constant with respect to time. Similar to the results

shown in section 5.6.2, the base of the tissue maintained the initial void fraction value. At this position, the least strain occurred in the tissue. The deep zone void fractions were also similar. In the superficial zone, the greatest variation occurred between the strains applied. The superficial zone experienced the largest relative strains, and the void fractions therefore decreased under the initial strain application. The reasonable consistency of the void fraction, with respect to time, suggests that the stress-relaxation mechanism of pressure reduction in the tissue causes a deformation in the matrix which remains as long as the strain is applied.

6.4.2 General limitations of the model

An uncertainty analysis is given in section 5.7. These errors were found to be generally small at each of the global strains applied. With respect to the actual experimental results, it would appear that the greatest errors were caused by neglecting the strain-dependency of the permeability field and the large experimental variation of the stress and depth-dependent strain values. In terms of the assumptions made for the model, additional explanations for discrepancies were found. The water temperature was known to fluctuate by approximately ± 1.5°C during the tests. While the effect of this change on the sound speed was examined, it is unknown how greatly it would have affected the local permeability fields or elastic moduli of the matrix.

It was assumed that the structure of each articular cartilage specimen tested represented the 'typical' structure; however these were seen to vary slightly in section 3.4.2. The size of the transitional middle zone was the largest area of variation, and this would, in turn, affect the distribution of the matrix moduli from the top to the base of the samples. The matrix was assumed to be elastic, which despite evidence of it actually having small levels of viscoelasticity (Huang et al. 2003, Wilson et al. 2005a, Murakami et al. 2004, Huang et al. 2001), was still deemed as a valid assumption due to the small magnitude of the effects of this error in compression. The applied global strain was assumed constant over the duration of the stress-relaxation; however, it actually increased slightly due to the decrease in load cell deflection as the pressure in the tissue decreased. The maximum change in deflection would have been 8.7 μm (calculated from the maximum peak load to the minimum stress-relaxation load experience in articular cartilage at 8% globally

applied quasi-static strain), which represents a strain of 0.7% in a sample of 1.23 mm thickness. This increase may explain why the cartilage tissue had not undergone complete stress-relaxation in 6% and 8% global applied strains after 20 min. It would also be responsible for some errors in estimating the local moduli from the model. The cartilage tissue was assumed to undergo no lateral expansion during the tests, so that all axial deformation was attributable to fluid flow. There would, however, have been small amounts of lateral deformation in the tissue, which would have varied with respect to depth due to the variation of the Poisson's ratio (Elliott et al. 2002, Fortin et al. 2003). However, the increase from superficial to deep zones was not determined to be statistically significant. The lateral expansion would cause an error in estimating the fluid flow out of the structure. It would also physically increase the path distance for the fluid to travel, changing the fluid flow characteristics.

6.5 Summary

The mechanical and elastographic test results obtained from the application of quasi-static global strain to nasal and articular cartilage specimens were compared. For the mechanical test results, articular cartilage was found to show strain-dependence of composite elastic modulus at the instant of the strain application. This effect was not observed in nasal cartilage, leading to the conclusion that it is therefore a behaviour most likely determined by tissue structure. The equilibrium moduli were not strain-dependent for either of the cartilage structures examined. Elastographically, stress-relaxation reorganisations of internal strains were observed in articular cartilage, particularly at 6% and 8% global applied strains. The effects were less significant in nasal cartilage structures. In both types of cartilage, changes occurred within the structures, particularly within regions of randomly aligned fibrils, which decreased the pre- and post-compressional signal correlations. The theoretical mechanical model (from Chapter 5) was applied to the articular cartilage specimens and, for 4% global applied strain, predicted local moduli similar to those from Li et al. (2000). At higher applied strains, the moduli predicted in the superficial and middle zones appeared too large. Possible reasons for these errors were proposed. The depth-dependent void fraction was shown to be dependent on the strain applied.

7 Results and Discussions: Step-Test Experiments

7.1 Overview

This chapter presents the results and discussions obtained from the stepped application of quasi-static strain to cartilage samples. Mechanical test results from native cartilage samples are presented followed by those from engineered cartilage tissue at different culture periods. A comparison between the global composite moduli, with respect to time and the number of steps applied, is made. The corresponding depth-dependent strain behaviours from the elastography results are then presented, firstly for the native samples and then for the engineered samples. Elastography was performed on the ultrasound shifts, gathered at each instant a new step of strain was applied and again at the sample 'equilibrium', which was taken (as for the quasi-static strain experiments in Chapter 6) to be 20 min after the last step was applied. The limitations of the method and the implications of both the global and local results are discussed.

7.2 Mechanical test data from quasi-static step-tests

The strain protocols for the step-tests are shown in section 4.4.5, Figure 4-5(b).

7.2.1 Nasal cartilage

The results of the composite elastic moduli found for nasal cartilage samples following the application of four steps of 2% strain are shown in Figure 7-1. The peak initial modulus can be seen to increase with each additional application of 2% strain. The first two steps, which appear to be close, were found to be significantly different (>99.9% confidence). The third step of strain application raised the initial modulus to 1.54 ± 0.40 MPa, which is significantly larger (>90% confidence) than the 6% instant strain application results for nasal cartilage (1.28 ± 0.12 MPa). The fourth and final step of strain applied raised the initial composite modulus to 2.19 ± 0.37 MPa, which is also statistically larger than the 8% applied strain in section 6.2.1. The standard deviation of the averaged result increased as the number of applied steps increased.

The time-constants, shown in Table 7-1, increased with each step of applied strain. Nasal tissue therefore required more time to reach 'equilibrium' conditions with respect to the number of steps applied. Following the first step of strain application, equilibrium is reached in a similar manner to the 2% non-stepped applied strain as shown in section 6.2.1. The second step also appeared to reach equilibrium. This occurred after approximately 18 min of strain application. The equilibrium modulus increased to 0.39 ± 0.11 MPa, which is different to the results of the 4% instant strain applied in section 6.2.1 (0.27 ± 0.03 MPa at equilibrium). Following the third step strain application, the stress-relaxation curve suggested that equilibrium would approximately need an additional 5 min than the protocol allowed. The final step appeared to need a longer period than the previous step to reach equilibrium conditions. The differences between the 'composite' moduli immediately prior to the next strain application (or the end of the test for the final step) were examined statistically. The difference between the equilibrium moduli of the first and second steps were found to be significant (>90% confidence). Between both the second and third step, acknowledging that equilibrium had not yet occurred in the third step, the difference was found to be significant (>99% confidence). However, between the third and fourth final moduli the difference was not found to be statistically

significant. Despite the large difference in the means, the standard deviation in the fourth step was sufficiently large enough to reduce the significance of the increase.

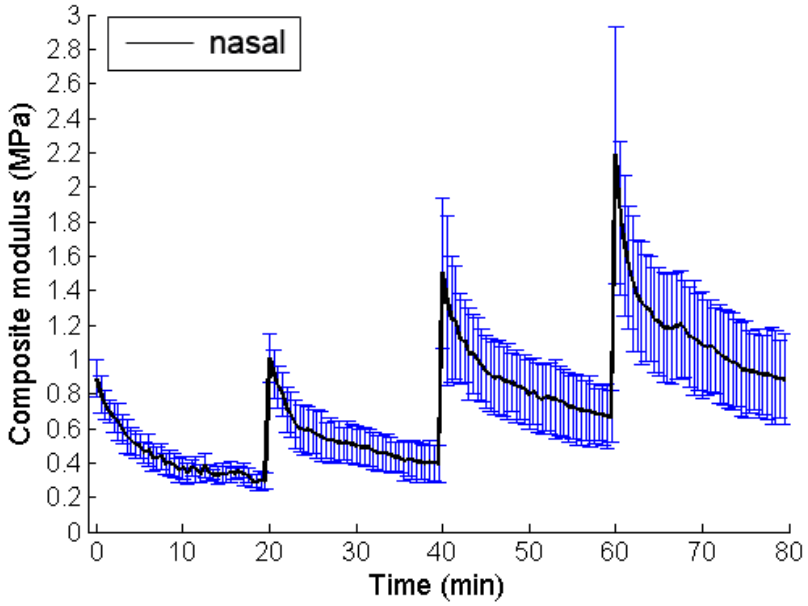

Figure 7-1: Composite elastic modulus of five nasal cartilage samples following the application of four steps of 2% allowing 20 min of stress-relaxation prior to the application of the following step. Error bars show the standard deviation.

The time-constants of the stress-relaxation occurring at each step were calculated (see section 6.2.1) and the results are shown in Table 7-1.

step	time-constant (min)
1	2.75
2	2.75
3	3.50
4	3.75

Table 7-1: Time-constants of stress-relaxation calculated for nasal cartilage samples at each step application of 2% strain.

These results confirm that the time required for stress-relaxation was increasing with respect to the number of steps applied to the nasal cartilage.

7.2.2 Articular cartilage

Figure 7-2 demonstrates the step-test results for articular cartilage. The peak initial moduli increase slightly between each subsequent step. None of the differences, including that between the first and the fourth peak, were found to be statistically significant at 90% confidence. The magnitude of the standard deviation of the results remained approximately constant, between 0.08 and 0.15 MPa, throughout the test duration. The first peak was determined to be similar to the peak of the 2% instant strain application, however, each of the subsequent stepped peaks were

significantly (>97% confidence) smaller than those from the instant strain applications.

The stress-relaxation time-constants, shown in Table 7-2, were similar for each step. The equilibrium moduli values increased with each step. Statistically this was found to be significant only between the first and fourth steps, (>95% confidence). To a certain degree, the results support the findings of other authors, for example Ling et al. (2007), Zheng et al. (2005), Zheng et al. (2002b), Zheng et al. (2001) and Li et al. (2008) who observe that articular cartilage undergoes a certain degree of 'hardening' with each applied strain. However, it would appear that this strain hardening is fairly minimal.

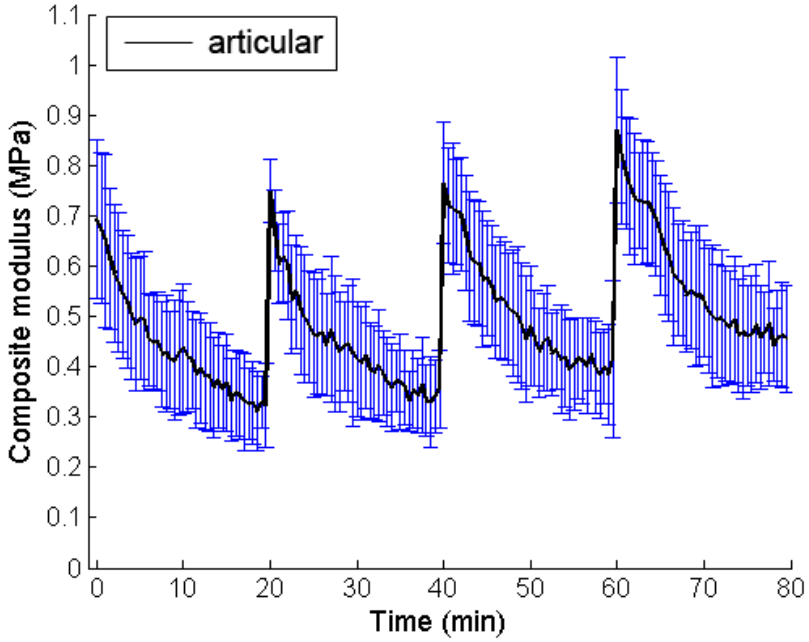

Figure 7-2: Initial and subsequent stress-relaxation composite moduli, averaged for five articular cartilage specimens, following the application of four steps of 2% strain and allowing 20 min of stress-relaxation between each step. The error bars show the standard deviations.

Stress-relaxation time-constants were calculated for each step of the strain application. The results are shown in Table 7-2.

step	time-constant (min)
1	4.75
2	4.25
3	4.75
4	4.50

Table 7-2: Stress-relaxation time-constants at each step of 2% strain applied to articular cartilage samples.

The results demonstrate the similarity of the stress-relaxation response at each step of strain application in articular cartilage.

7.2.3 Comparison of the two native cartilage structures

In Figure 7-3 it can be seen that although the two stress-relaxation curves of the native cartilage structures begin in a similar fashion for the first step application of 2% strain, the nasal moduli were higher for the subsequent stresses. Both the initial and the equilibrium moduli reached were higher for the nasal cartilage samples. These results suggest the 'strain hardening' effect observed by other authors (Ling et al. 2007, Zheng et al. 2005, Zheng et al. 2002b, Zheng et al. 2001, Li et al. 2008) to be more apparent in non-layered hyaline tissue structures than articular cartilage.

The standard deviation of the nasal cartilage results increased with each step, which was not the case for the articular results. This suggests that there is greater variation between the fluid-flow mechanisms present in the nasal cartilage samples.

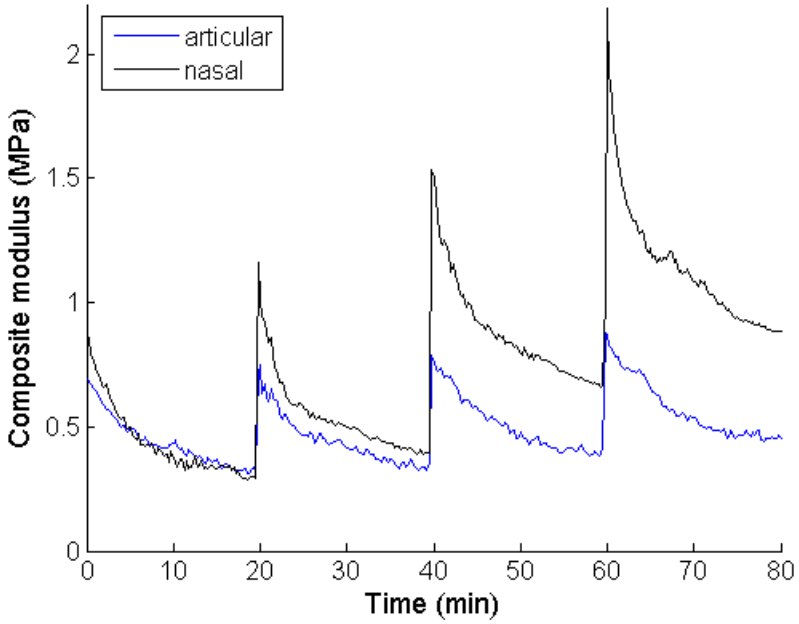

Figure 7-3: Comparison of the initial composite elastic moduli and subsequent stress-relaxation for four 2% applied strain steps in nasal and articular cartilage samples. The difference increased with respect to the number of applied steps. Error bars were omitted for clarity.

The time-constants calculated (Table 7-1 and Table 7-2) show that although the nasal cartilage specimens produced larger peak moduli with each subsequent strain application, the stress-relaxation times increased slightly. The nasal samples generally relaxed faster than the articular samples.

If the difference in structure of the hyaline cartilages tested here is directly responsible for the reported difference in global mechanical behaviour under the application of repetitive strain steps, then this result suggests that great care should be taken when designing engineered tissue so as not to generate harmful levels of shear stresses at the interface of the engineered and native tissues.

7.2.4 Engineered cartilage samples

The results for the thicknesses measured experimentally (and compared to the results of independent measures of thicknesses of the same culture times) are shown in Table 7-3. The numbers of samples measured varied between the two techniques. The optical method measured four samples at 5, 10 and 15 days of culture and three samples following 1 day of culture. In the mechanical tests the thicknesses of five samples at each culture time were recorded. The results from the two different measurement methods were not found to be significantly different for the thicknesses at 1, 10 or 15 days (>90% confidence). At 5 days the results were found to be significantly different (>99% confidence), but it is likely that this was due to an error in manufacturing, such as incomplete plastic compression of one of the layers.

Measurement technique	**Day 1 thickness (mm)**		**Day 5 thickness (mm)**		**Day 10 thickness (mm)**		**Day 15 thickness (mm)**	
	average	**st. dev.**	**average**	**st. dev.**	**average**	**st. dev.**	**average**	**st. dev.**
Mechanical system	0.4	0.018	0.91	0.268	0.34	0.063	0.39	0.143
Optical system	0.43	0.053	0.39	0.013	0.32	0.021	0.39	0.015

Table 7-3: Table showing the comparison between the sample thicknesses (average and standard deviation of the samples) measured mechanically and the results shown in Chapter 3 (Memarzadeh 2009) measured using an optical microscope.

As shown in Figure 7-4, the mechanical test results from four samples cultured for 1 day demonstrate minimal pressure developed to contribute to the composite moduli (0.22 ± 0.05, 0.31 ± 0.06, 0.13 ± 0.03 and 0.11 ± 0.02 MPa first to last peak respectively).

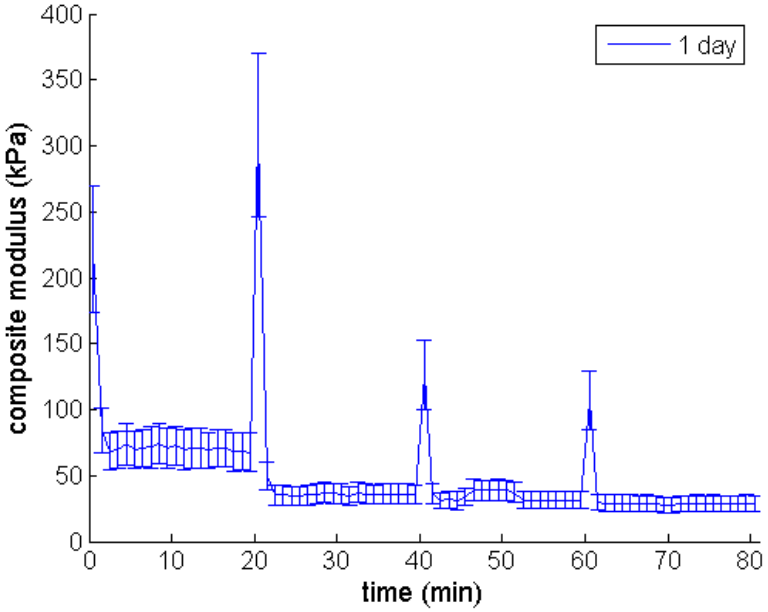

Figure 7-4: Time-dependent composite moduli measured in 4 engineered cartilage structures cultured for 1 day. The 2% global strain steps were applied at 0, 20, 40 and 60 min. Error bars show the standard deviation.

The time-dependent composite moduli from samples cultured for 5 days are shown in Figure 7-5. Although the first and second peak moduli are large (0.46 ± 0.1 and 0.22 ± 0.05 MPa respectively), the third and fourth peaks are considerably smaller (0.08 ± 0.01 and 0.06 ± 0.01 MPa respectively).

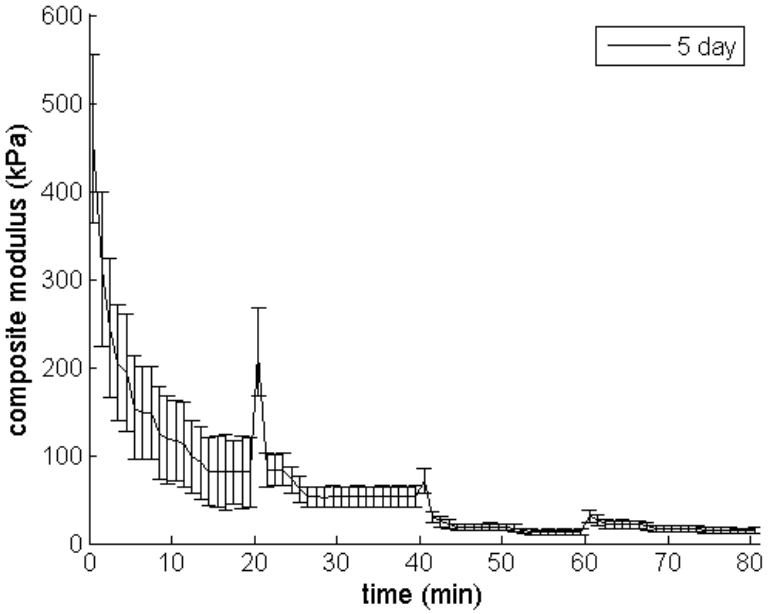

Figure 7-5: Time-dependent global composite moduli recorded from engineered cartilage tissue cultured for 5 days. Strains were applied in 2% steps at 0, 20, 40 and 60 min. Error bars show the standard deviation.

Results from the samples cultured for 10 days in Figure 7-6 show similar magnitude peaks than those recorded for the 1 day (0.21 ± 0.05, 0.26 ± 0.05, 0.22 ± 0.03 and 0.20 ± 0.03 MPa steps 1 to 4 respectively).

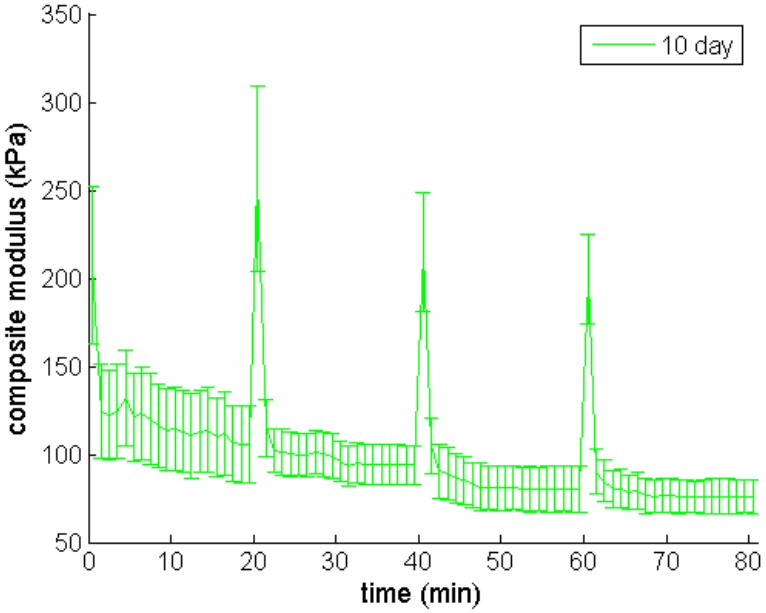

Figure 7-6: Composite moduli results from four steps of 2% global strain applications at 0, 20, 40 and 60 min applied to engineered cartilage tissue cultured for 10 days. Error bars show the standard deviation.

As shown in Figure 7-7 the peak step moduli of samples cultured for 15 days increased between each step (0.24 ± 0.05, 0.27 ± 0.06, 0.28 ± 0.04 and 0.29 ± 0.03 MPa from first to fourth step respectively).

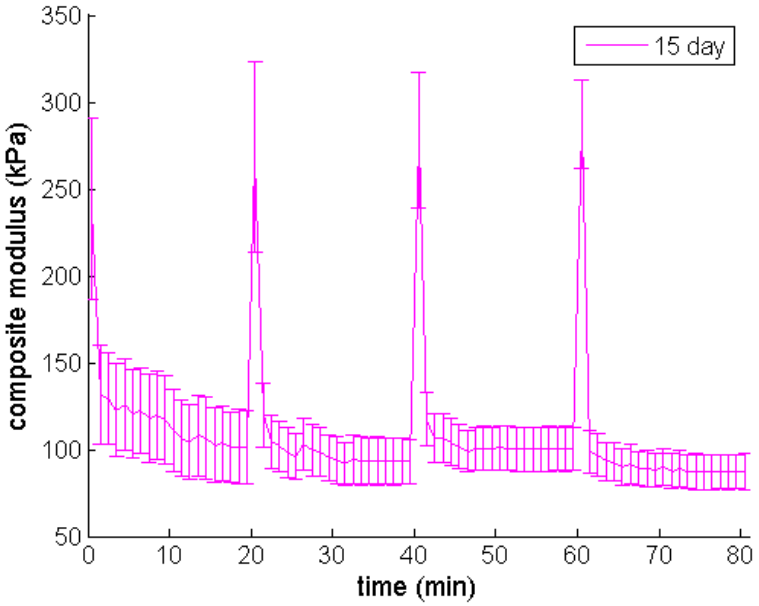

Figure 7-7: Time-dependent composite moduli in engineered cartilage cultured for 15 days following the application of 2% global strain steps at 0, 20, 40 and 60 min. The error bars show the standard deviation of the results.

The comparison of the global mechanical results for the engineered cartilage tissue tested at culture times of 1, 5, 10 and 15 days are shown in Figure 7-8.

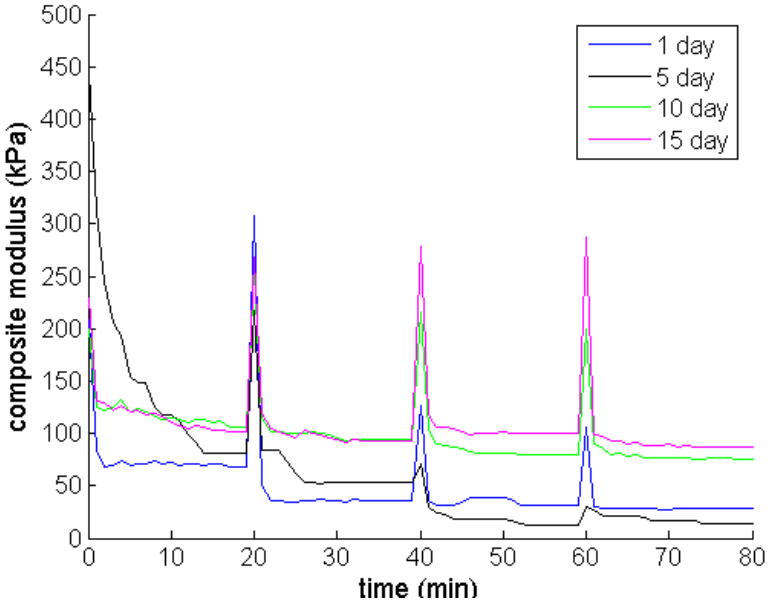

Figure 7-8: Quasi-static step-test stress-relaxation curves at culture times of 1, 5, 10 and 15 days of engineered cartilage constructs. The peaks in each line are a result of the application of the next strain step. It can be seen from how quickly the composite moduli decay that the constructs are not capable of supporting large amounts of applied strain. Error bars omitted for clarity.

The time-constants of stress-relaxation were calculated for each culture period at each step of strain application. The results are shown in Table 7-4. The time-constants of stress-relaxation were very similar with respect to the number of steps applied for the engineered tissue cultured for 1, 5, 10 and 15 days.

step	time-constant (min)			
	day 1	day 5	day 10	day 15
1	0.50	2.25	0.75	0.50
2	0.75	0.50	0.50	1.00
3	1.00	1.25	1.25	1.25
4	1.50	2.00	1.50	1.75

Table 7-4: Stress-relaxation time-constants calculated for each culture period of engineered cartilage tissue following every application of the 2% strain steps.

It can be immediately observed that the results for the day 5 samples tested appear to be anomalous. During the experiments, the day 5 samples were found to be far thicker than expected. Statistically, the only differences between consecutive peaks which were significant were the decreases from the first to the second, the second to the third and the third to the fourth peaks for 5 days of culture (>95%

confidence). This means that the mechanical test results demonstrate only very subtle changes, which are not statistically significant over the range of culture times tested.

The variation was found to be large following each step of strain application, but highest after the third and fourth steps. The lowest variation occurred immediately prior to the application of the second strain step. Higher standard deviations from the mean measured mechanical test behaviour are indicative of greater variations between structures. Following 10 and 15 days of culture time, the engineered cartilage constructs are likely to have higher amounts of variation due to differing rates of cell matrix production and construct internal structure remodelling due to the action of the chondrocytes. These changes to the internal structure would cause the permeability to decrease due to additional complexity of fluid flow paths. At day 5, large standard deviations were also attributable to large structural variations, although it is less likely that these were caused by cellular matrix production rather than manufacture error.

Cartilage tissue engineered using this production technique would have very low or negligible levels of PG to draw in water molecules into the pores, particularly at the earliest stages of development (for example 1 and 5 days of culture). As the volume of PGs increase, as a result of longer culture times, the equilibrium pressure in the pores also rises slightly. The equilibrium moduli of the samples increased with respect to the culture period; this was most obvious following the third and fourth steps. This is an encouraging result in terms of engineering cartilage tissue, as it indicates that although the equilibrium global modulus is still considerably lower than that of native tissue, it is increasing as the tissue is cultured.

7.2.5 Comparison between the mechanical test behaviours of native and engineered cartilage structures

The composite moduli and time-constants of stress-relaxation of all the engineered tissue constructs were found to be considerably lower than the moduli of the native tissue. At each step application, the initial composite moduli, as described in Chapter 5, are a direct result of the additional stress in the tissue due to the pressure developed in the porous matrix. A low initial modulus would therefore be indicative of fluid being less pressurised, for example in a situation where the

permeability of the material was very high and the pressure dissipating very quickly. This high permeability would also account for the lower time-constants of stress-relaxation; fluid can flow out of the structure more readily in the engineered constructs than from native tissues.

This demonstrates the importance of permeability as a design factor for the engineered tissues. It would be necessary for the time constants and initial moduli to be sufficiently matched so as not to produce shear stresses between native and engineered cartilage tissues. It is also important to protect the bone below the cartilage surface from experiencing damaging levels of stress transmitted through the engineered tissue.

7.2.6 General observations of the mechanical tests

The nasal, articular and engineered cartilage tissue demonstrated a large difference in relative behaviours during the mechanical step tests. The natural variations between the nasal cartilage samples became more significant with each step of strain applied. Because the tissue had not been able to recover in the 20 minutes, subsequent strain applications caused the moduli to increase dramatically. The articular cartilage composite moduli, both at the applications of the steps and at the subsequent equilibrium, increased slightly. Over the culture period investigated, the engineered tissue did not change significantly in terms of the initial composite moduli or the time-constants of stress-relaxation; however, the equilibrium moduli increased.

In the nasal cartilage, the magnitude of the error bars increased as more steps were applied. It may be that some of the differences between the nasal samples could be reduced by ensuring that all the sample sources were of the same breed of pig. The smaller error bars throughout the duration of the step tests applied to articular cartilage were indicative that there were less biological variations between the articular structures. The standard deviations were even smaller for the engineered sample tests, which could be attributed to the reasonably uniform nature of their construction.

7.3 Elastography data from quasi-static step-tests

The elastography data were produced from ultrasound signals extracted at the point each subsequent step was applied and at 'equilibrium', a few seconds prior to the application of the next step. These positions are shown on Figure 7-9.

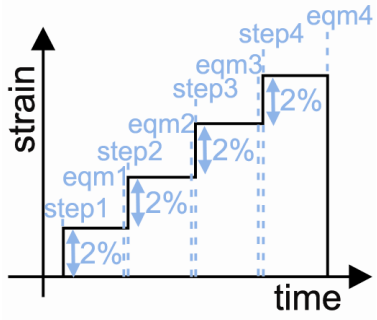

Figure 7-9: Representation of when the ultrasound signals were extracted to perform elastography for the step-tests.

7.3.1 Nasal cartilage

From Figure 7-10 it was observed that the strain maps recorded at the instant of application of each of the 2% global strains were approximately linear in the top halves of the tissues (furthest from the rigid bases), similar to the results described in section 6.3.2.1. The amount of scatter increased at each subsequent step.

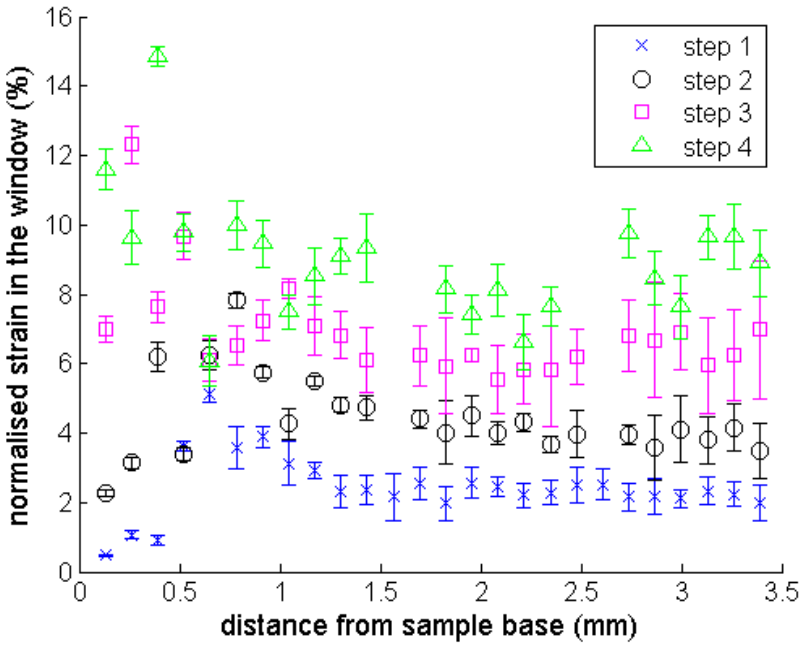

Figure 7-10: Normalised strain maps from the averaged elastography data comparing the initial strains found at each step application, in five nasal cartilage specimens. The error bars show the standard deviation.

The similarities between the strain maps from equivalent quasi-static strain magnitudes were examined. Between the first step and the results at 2% applied

global strain there were no significant differences, which was expected. Between the second, third and fourth steps, significant increases were shown in the strains in the bases of the samples (>99% confidence) compared to 4%, 6% and 8% instant applied strain, respectively.

Figure 7-11 shows the results at the 'equilibrium' of each applied strain step, recorded 20 min after the step was performed. The scatter was smaller than for the results at the instant of step application, but was still largest at the fourth step. No significant differences were found between the 'peak' and 'equilibrium' maps at any of the step numbers.

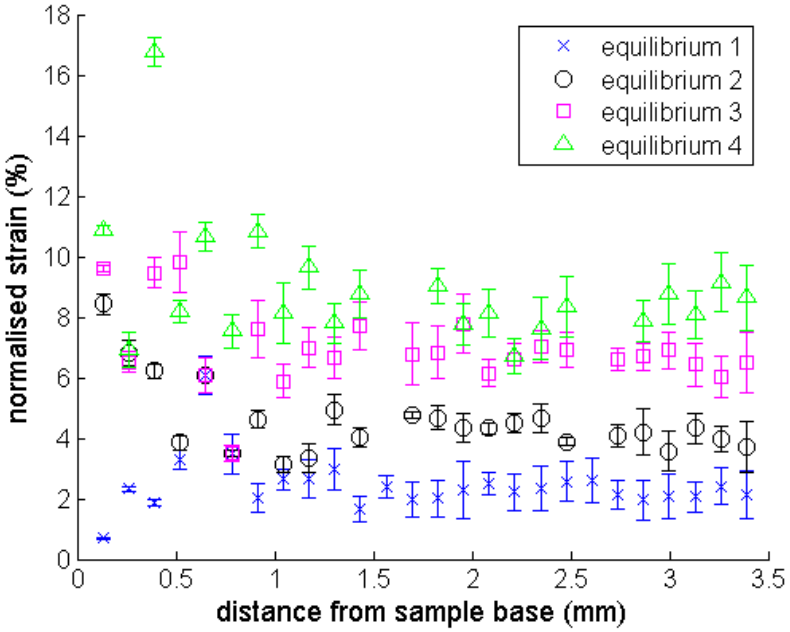

Figure 7-11: Normalised strain maps from elastography data obtained at each step's 'equilibrium', for five nasal cartilage specimens. The error bars show the standard deviation.

The linear nature of the values and the way in which they approximately represent the value of the strain applied is indicative of behaviour of a homogeneous material structure. The larger strains in the 1 mm of the samples closest to the rigid base compared to the results in section 6.3.2.1 indicate that repeated applications of strain caused the tissue to distribute more strain deeper in the tissue; however, due to the large scatter in the base 1 mm, it is also possible that anomalous shifts were being recorded.

7.3.2 Articular cartilage

Figure 7-12 demonstrates that the strain map shapes, recorded at steps 1 and 2, represent the expectation of low strains in the deep and middle zone and high strains in the superficial zone. The maps from steps 3 and 4 were far more scattered, with the strains generally high in the deep zones. The differences between the strains in the zones were analysed for statistical significance. Following the first step there were no significant differences. However, following steps 2, 3 and 4, significant increases occurred between both deep and superficial and middle and superficial zone strains. Compared to the results at T0 from section 6.3.2.2, no significant difference was found between 2% and 4% global strain and steps 1 and 2. No difference was expected between 2% strain and step 1. Between 6% and 8% global strain and steps 3 and 4, significant increases were seen in the strains in the deep zones (>99% confidence).

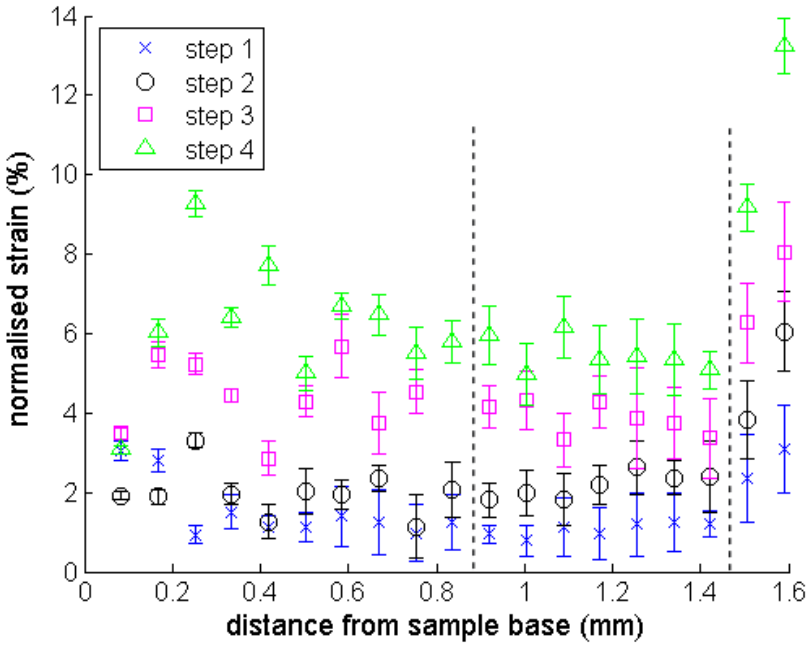

Figure 7-12: Normalised elastography strain maps from five articular cartilage samples at each initial step application. Error bars show the standard deviation. Dashed lines show the approximate positions of the zones.

The strain maps recorded from articular cartilage at each equilibrium are shown in Figure 7-13.

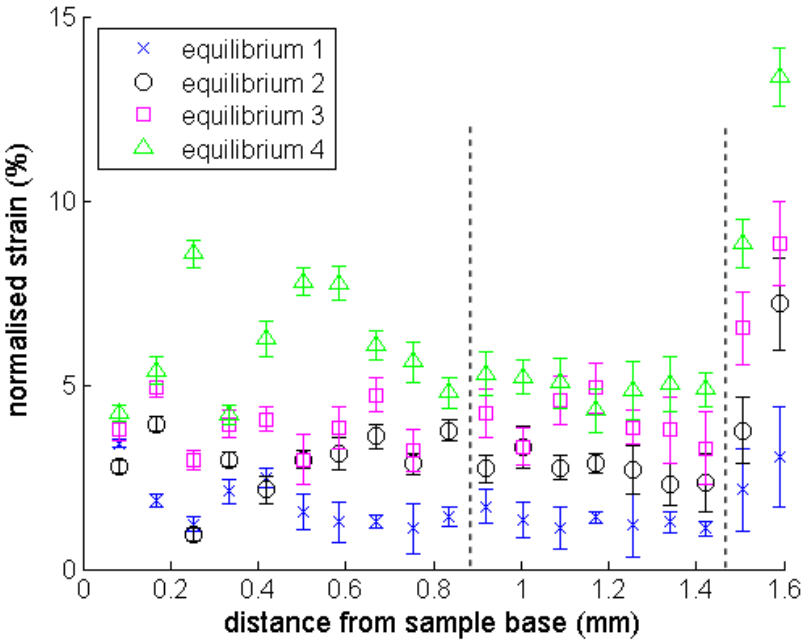

Figure 7-13: Articular cartilage normalised strain maps from 'equilibrium' data five articular cartilage specimens. The standard deviation of the results is shown in the error bars.

The error bars were smaller than for the step results. No significant differences were found between the zones of equilibrium 1. Equilibriums 2, 3 and 4 demonstrated significant increases (confidence >99%) between the superficial zone compared to both the deep and middle zones. Comparing the step and equilibrium values, there were no significant differences for the first, third or fourth. However, the strains in the deep zone significantly (>99% confidence) increased from step 2 to equilibrium 2.

7.3.3 Comparison of the depth-dependent mechanical behaviour of the two native cartilage structures

Results for both native structures reported an increase of strains in the deep zone with respect to the number of strains applied. It therefore appeared to be a common feature of the strain distribution mechanics of hyaline cartilage structures. With respect to the global composite moduli (sections 7.2.1 and 7.2.2), which demonstrate increases in both the initial and equilibrium moduli at each step, it is unlikely the deep tissues become less stiff with the number of steps applied. Both the global and local tissue behaviours appear to be different to when the same total magnitude of strain was applied instantly (Chapter 6).

Globally, nasal cartilage tissue stiffened the most significantly with respect to each step applied. It would therefore follow that the strain distribution would inversely represent the depth-dependent stiffness; rather than the tissue closest to the rigid base softening, the tissue further from the base (approximately from 1.5 mm from the rigid base to the top of the sample) stiffened. A possible cause for this localised stiffening could be the change in void fraction resulting from the compression. As shown for articular cartilage tissue (Chapters 5 and 6), the void fraction decreases as a result of an applied strain. This decrease then remains over the entire stress-relaxation period. The void fraction would decrease most significantly at the top of the sample, where the actuator is applying the strain. In nasal cartilage, as a result of the homogeneous structure, it is mostly likely that this decrease would follow a fairly linear distribution with respect to depth. The decrease in the void fraction, even after the most complete equilibrium conditions of the first step, would cause a decrease in the local permeability. When each subsequent step is applied, the fluid pressure would dissipate more slowly, and the local deformation would decrease. Closer to the tissue base, the fluid would still be able to dissipate as normal, so the local strains would be larger.

It is likely that a similar process was occurring in the articular tissue; however, the increases in stiffness were less pronounced than in the nasal tissue. Due to the non-homogeneous tissue structure, the superficial zone (the tissue region closest to the actuator) has a relatively larger initial void fraction and permeability with respect to the remaining tissue. Although the void fraction, and therefore permeability, in this region would decrease due to the application of the global strain, it would appear that flow is still able to occur at a rate which is reasonably comparable to that of the unstrained tissue. Physiologically, it is important that articular cartilage does not become too stiff; it is required to absorb the stresses applied *in vivo* to prevent damage to the underlying bone. It is therefore possible that this complicated pressure redistribution mechanism is a result of the specialised structure of articular cartilage.

The results in Chapter 6 demonstrated that the global mechanical response of nasal tissue, to the initial application of strains of varying magnitude, was independent of the strain applied. In the homogeneous structure of nasal cartilage, it is therefore

likely that the instantaneous large pressure rise associated with the larger initial strains either caused the void fraction change to be distributed differently across the tissue, or produced a sufficiently large pressure gradient as to allow flow to occur faster. In articular cartilage, the initial moduli in Chapter 6 were dependent on the strain applied, but the equilibrium moduli were not. Therefore the main difference in the articular cartilage behaviour between the two different tests was the increase in the equilibrium moduli caused by the cumulative strain application.

The magnitude of the error bars was fairly consistent throughout the steps in the articular cartilage; however, they generally increased, with respect to the number of steps applied to the nasal tissue. This would have been mainly due to the correlation in the nasal cartilage experiments decreasing with each applied step. The relatively high signal decorrelation could also possibly be linked to the global stiffening seen in the mechanical test results for the nasal tissue.

7.3.4 Engineered cartilage

The results from the application of the first strain step to engineered tissue samples cultured for 1 to 15 days are shown in Figure 7-14.

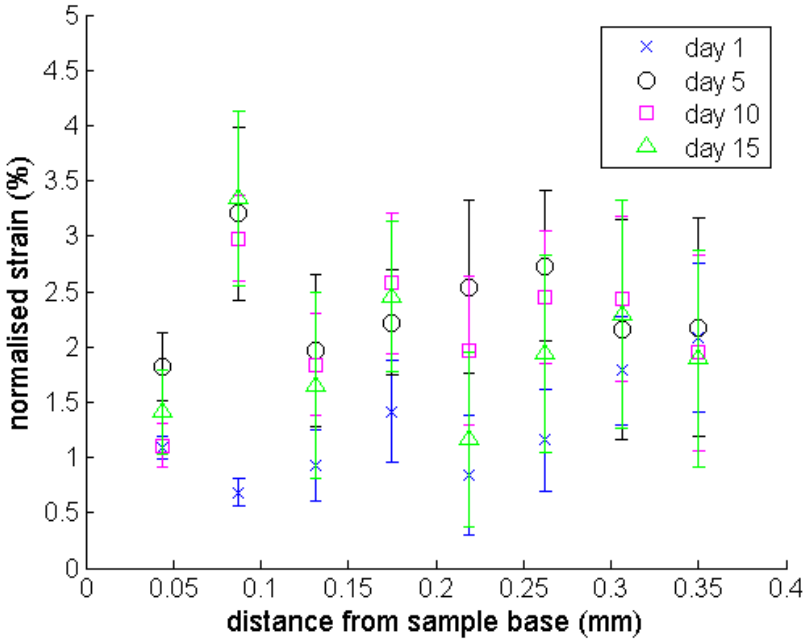

Figure 7-14: Normalised strain maps for elastography performed at initial application of the first strain step to three engineered cartilage tissue samples, at varying culture periods. The error bars show the standard deviation.

The strains at 0.04 and 0.35 mm from the sample base were similar with respect to culture time. However, the strains in the centre of the sample increased; meaning it

is likely that the top and base surfaces were stiffening. Globally, the composite modulus was greatest for the 5 day and least for 1 day cultured tissue.

The corresponding equilibrium strain maps following step 1 of applied strain are shown in Figure 7-15. Between 0.22 and 0.35 mm the strains were very similar with respect to culture period and fairly linear. The strains from 0.04 to 0.17 mm were more varied and did not appear to follow a particular pattern relating to the culture period.

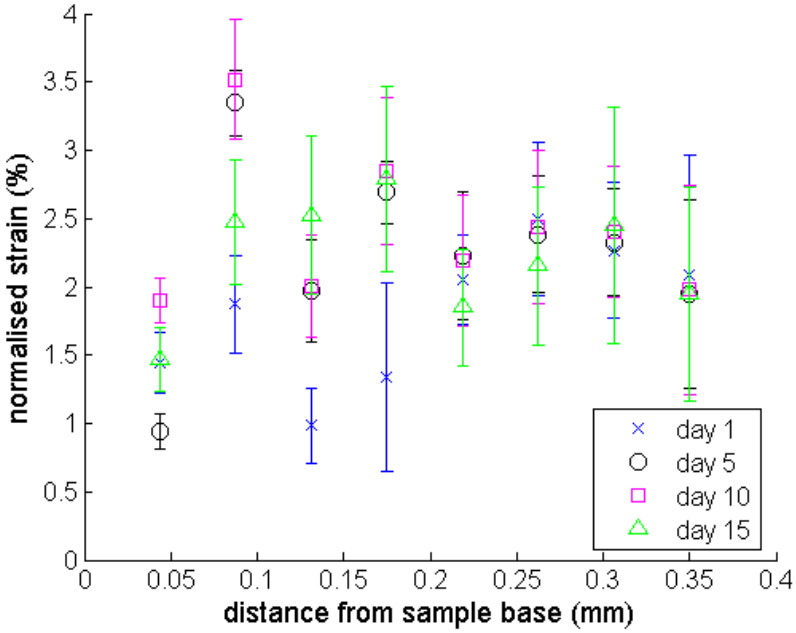

Figure 7-15: Normalised elastography strain maps showing the results at the first step equilibrium of engineered cartilage tissue at different culture times. The error bars show the standard deviation.

The elastography results from the initial application of the second strain step to engineered cartilage samples cultured for varying periods are shown in Figure 7-16. The strains for the tissue cultured for 1 day appeared to remain fairly linear with respect to distance from the sample base. As the tissue culture time increased, so did the strains measured in the centre of the samples. The strains at the base of the sample decreased after 15 days of tissue culture.

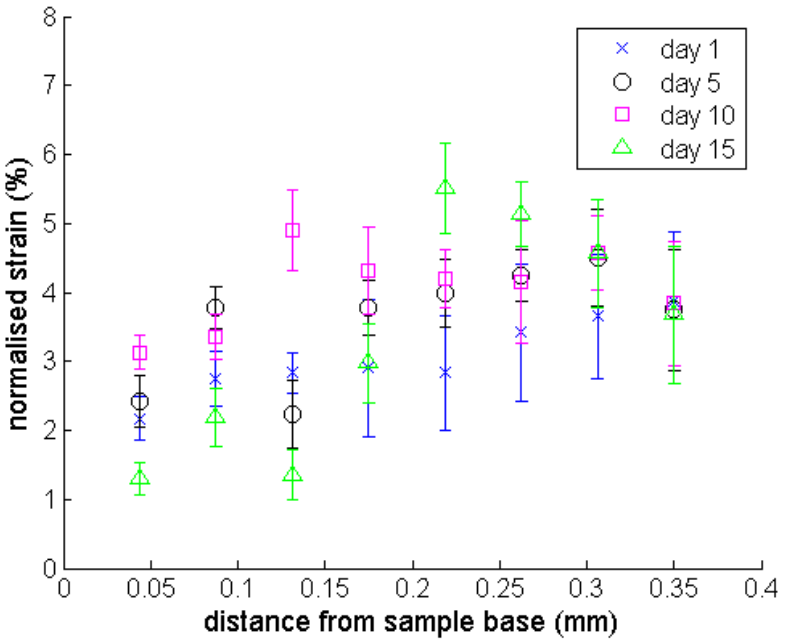

Figure 7-16: Strain maps of normalised elastography at the initial application of the second global strain step to samples of engineered cartilage tissue cultured for varying periods. The error bars show the standard deviation.

The depth-dependent strain results from the second step equilibrium, for engineered cartilage tissue cultured for varying culture periods are shown in Figure 7-17. The results represent a different strain pattern to those from the initial step application and are more similar with respect to length of culture time.

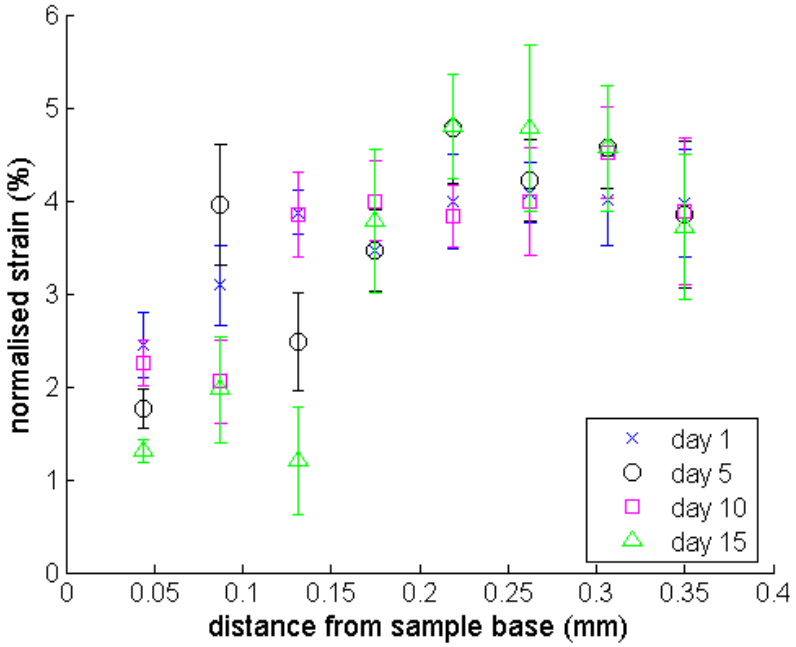

Figure 7-17: Normalised elastographic strain maps of the second equilibriums from engineered cartilage samples cultured for varying periods. Error bars show the standard deviation.

The results from the normalised elastography data recorded at the initial application of the third strain step to engineered cartilage tissue, cultured for varying periods, are shown in Figure 7-18. At the tops of the samples (0.35 mm from the sample base), the strains are very similar. In the middle of the tissue the strains are more varied with respect to culture period, but there is no clear pattern relating strain distribution to length of culture time.

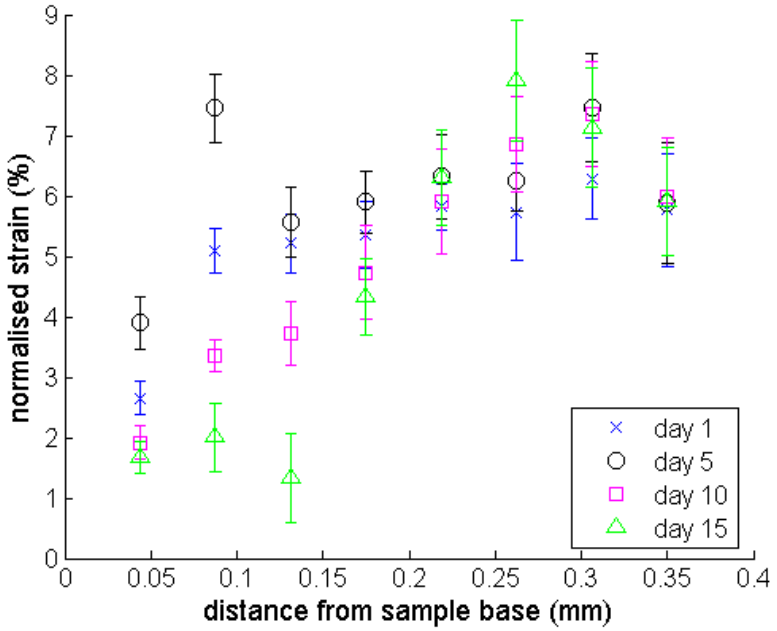

Figure 7-18: Strain maps of normalised elastography from specimens of engineered cartilage tissue cultured for varying culture periods at the initial application of the third strain step. The error bars show the standard deviation.

Figure 7-19 demonstrates the strain maps from the third strain step equilibrium. Similarly to the results following the second strain step application, the depth-dependent strain distributions are different at equilibrium compared to the initial strain application. The strains through the tissue cultured for 1 day are approximately linear. The strains between 0.04 and 0.13 mm from the sample base decreased with respect to culture time. The strains at 0.35 mm from the sample base are similar for all the culture periods. The global stiffnesses at the equilibrium of the third step increase with respect to increasing tissue culture time. The depth-dependent strain distributions change with respect to this increasing stiffness.

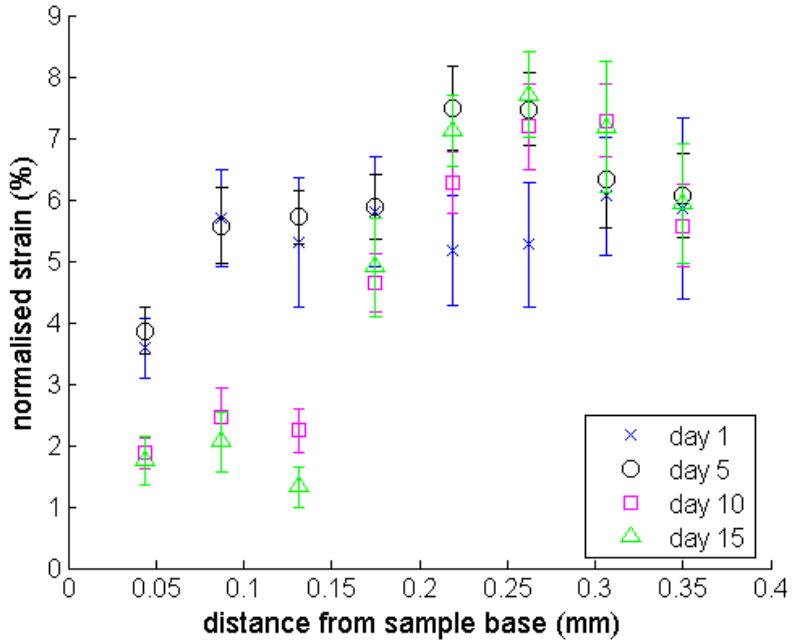

Figure 7-19: Normalised elastography strain maps from the equilibrium of the third step applied to engineered cartilage tissue specimens, cultured for varying periods. Error bars show standard deviation.

The normalised depth-dependent strain results from the elastography data at the initial application of the fourth strain step to engineered cartilage, cultured for varying periods, are shown in Figure 7-20.

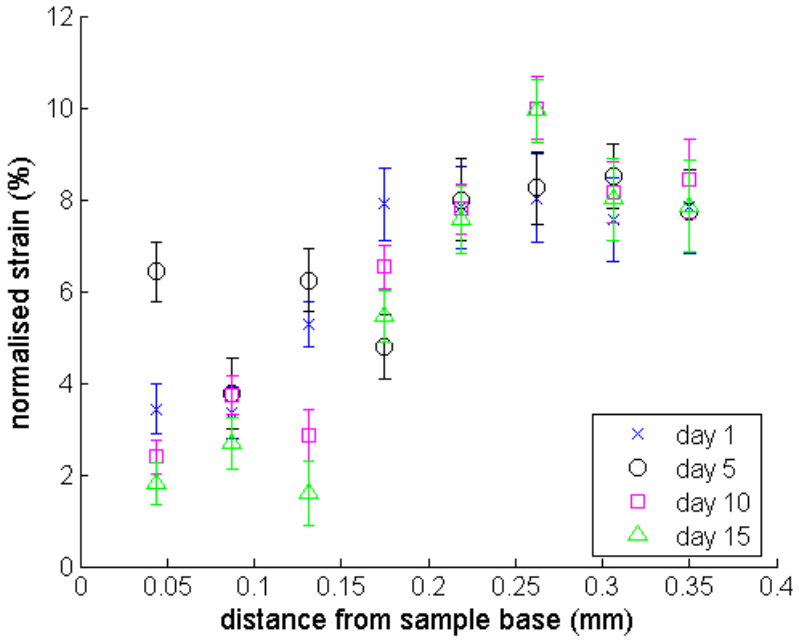

Figure 7-20: Normalised elastography strain maps from the initial application of the fourth step of global strain to engineered cartilage specimens cultured for varying periods. Error bars show the standard deviation.

The strains at the tops of the samples (0.31 and 0.35 mm from the tissue base) do not appear to be dependent on the culture period of the tissue. With the exception of

the results from the tissue cultured for 5 days, in the base of the tissue (between 0.04 and 0.13 mm from the sample base) the strains decrease as the culture time increases.

Figure 7-21 shows the normalised elastography strain maps from the corresponding equilibrium of the fourth applied strain step. Similar to the initial strain application results, the strains appear to decrease in the base of the tissue as the culture time increases. The strains in the remaining tissue appeared to be less dependent on the culture period. The global strain results at this equilibrium are the most distinct with respect to the tissue culture time: the global stiffness increasing as the culture time increases. Although the strain distributions shown in Figure 7-21 are fairly similar, the actual local stiffnesses are different.

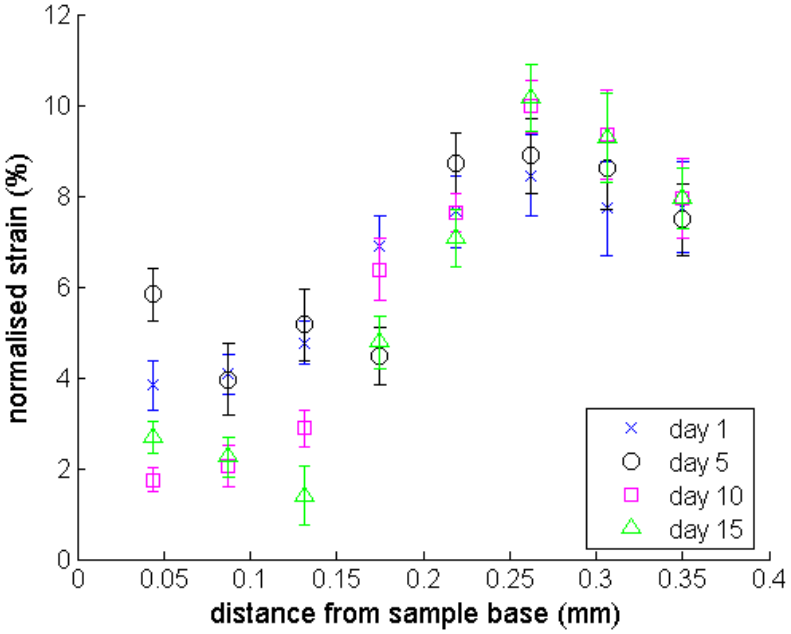

Figure 7-21: Normalised elastography strain maps from engineered cartilage tissue samples, cultured for varying periods, at the equilibrium of the fourth step. The error bars show the standard deviation.

Engineered samples following only 1 day of culture would be expected to be mechanically similar to pure collagen scaffold. Collagen scaffolds undergo rapid plastic deformations as a result of applying a strain (Brown et al. 2005). No significant difference would therefore have been expected in the depth-dependent strains. It is therefore possible that the low strains in the bases of the samples (approximately 0.04 to 0.13 mm) could be a result of experimental inaccuracies being multiplied in the normalisation process.

Comparing the step and equilibrium results revealed that no statistically significant differences existed between the stress-relaxation times for any of the steps applied. According to the findings published by Memarzadeh (2009), the engineered cartilage scaffolds were not considerably different to pure collagen scaffolds; but engineered tissue was slightly less stiff. These particular samples used for the elastography investigation were thicker than those reported in that thesis, therefore may have behaved differently.

From the strain maps alone it was not possible to determine whether within the samples the middle of the tissue was softening, or the edges were stiffening, as a result of increasing the culture time. The global mechanical test results in this study showed an increase from all the steps of 1 day and from steps 3 and 4 of the 5 day cultured specimens. This result would indicate an increase in the edge stiffness. However, the independent mechanical tests reported in Section 3.6.2 showed a decrease in the elastic moduli of tissue cultured for 10 days, which would suggest the centre of the samples were softening. By the tenth day of tissue culture, Memarzadeh (2009) reported the chondrocyte production of proteoglycans and matrix collagen remodelling. Although it has not been specifically investigated, it is likely that the chondrocytes near the layer interfaces had a better nutrient supply, so therefore may have been able to produce matrix materials more rapidly. This effect would have been most prominent at the tissue edges such as the top and base. The presence of proteoglycans is known to increase tissue stiffness (Maroudas 1979), so therefore it is most likely that the top and base surfaces were increasing in stiffness.

The engineered tissue samples provided a high level of pre- and post-compressional correlation at every step applied. However, due to the low thickness of these samples, the ‘dead’ zone in the tissue, as described in section 6.3.3 would have been more significant in comparison with the total tissue depth, affecting around 35% of the total tissue thickness. It could therefore be advisable to select an alternative ultrasonic transducer to produce a smaller dead zone in future *in vitro* elastography tests applied to engineered tissue.

7.3.5 Comparison between the depth-dependent mechanical behaviours of native and engineered cartilage structures

In the earlier culture periods (1 and 5 days), the strain maps were mostly approximately linear, and therefore similar to the results from the nasal cartilage tissue. However, the actual elastic moduli were considerably lower in the engineered tissue. As the culture time increased, a trend can be seen to emerge for the strains at the top of the samples to decrease. This was markedly different to the results for both the native tissues, and was likely to be caused by the way in which the chondrocytes were producing the cartilage matrix.

The error bars and scatter in engineered specimens were less significant than for the native samples, which was indicative of better correlation between the pre- and post-compressional signals. This was possibly a result of stronger reflections from the layers, although a single layer is too thin to be properly resolved with this particular transducer. The engineered constructs were made from predominantly type I collagen fibrils aligned perpendicularly to the ultrasound beam axis due to the manner of manufacture (Hadjipanayi et al. 2009, Brown et al. 2005). The superficial regions of articular cartilage had high levels of signal-to-noise ratio, and in this region the fibrils were also mainly perpendicular to the ultrasound beam axis. The results from the engineered samples should, however, be treated with caution as few repeats were performed due to a limited number of samples available. The small error bars were most likely a result of the manufacturing similarities of the engineered tissue samples.

The moduli were found to be considerably smaller in the engineered tissue than the native cartilages. Evidence was also found of the permeability being lower in the engineered cartilage compared to the native cartilage. This means that the engineered tissue in this form is not mechanically suitable to be used as a cartilage replacement. However, the ability to detect global and depth-dependent changes in the tissue moduli distributions is shown. This technique could therefore be a valuable tool in terms of monitoring the development of the tissue properties.

7.4 Summary

The structural differences between the two native hyaline cartilages were found to cause significant differences in the global and depth-dependent mechanical behaviours during step strain application. It was proposed that this is likely to be caused by changes in the depth-dependent void fractions of the samples. Applying the same test protocols to engineered cartilage samples provided information regarding the increasing equilibrium stiffness and peak stiffness with respect to increasing culture time. The difference became clearer with each step of strain applied. The elastography results from the engineered samples demonstrated good correlations between pre- and post-compressional signals. The depth-dependent strain results provided evidence of possible edge stiffening with respect to culture time. The moduli of the engineered samples were considerably lower than those of the native samples; after a culture period of 15 days the tissue would be unsuitable as a tissue replacement. The ability to test the tissue in this manner should provide greater understanding of the tissue development with respect to the depth-dependent stiffness increase resulting from increasing culture times.

8 Results and Discussions: Cyclic Strain Experiments

8.1 Overview

This chapter presents and discusses the results from cyclic strain applications to nasal and articular cartilage samples. The global mechanical data obtained from varying the frequency of the applied strain, but maintaining the same maximum amplitude of 4% are presented, followed by the corresponding depth-dependent strain behaviours obtained from elastography. The global mechanical behaviours resulting from varying the magnitude of the maximum strains while maintaining a constant frequency of 1 Hz are then presented. The corresponding elastography results then follow. The effects of varying the frequency and magnitude of the applied strain are investigated at the beginning of the transient response and one minute later. Both the global and depth-dependent tissue behaviour are examined while the minimum and maximum strains are applied during the first and final cycles of the one minute tests. The implications of the similarities and differences of behaviours of the two cartilage structures and the limitations of this experimental method are discussed.

8.2 Effect of varying the cyclic strain frequency

It is important to determine how the structure of hyaline cartilage is responsible for the mechanical response during cyclic loading. Varying the frequency and examining the behaviour at the beginning of the response and one minute later allows the relationship between the frequency and the tissue behaviour to be compared at different times during the transient response. At the times examined, data were collected at points corresponding to the minimum and maximum strain applications during the cycle, allowing both the loading and recovery behaviours to be examined.

8.2.1 Mechanical test data from variable frequency dynamic tests

The strain protocols for the cyclic tests are shown in section 4.4.5, Figure 4-5(c) and (d). Data were gathered for 1 min of repeated straining cycles at different frequencies. The data presented represent one full loading cycle at the start and another at the end of the minute test and therefore demonstrate material behaviour during the beginning of the transient and later, as the system approaches steady-state. The moduli and strains occurring in the tissue as a result of the minimum and maximum strain amplitudes in those cycles are compared allowing access to both the loading and recovery phases of tissue behaviour. The values gathered at 50 ms intervals were averaged for the 10 specimens for each tissue for each test.

8.2.1.1 Nasal cartilage

As shown in Figure 8-1, the calculated minimum and maximum composite moduli from the first and final cycles of applied strain increased with respect to the frequency of the strain applied. The increase between each subsequent frequency is significant (>99.5% confidence). Both the minimum and maximum composite moduli increased between the first and final strain cycles. The difference between the first and final composite moduli increased with respect to increasing the frequency of the applied strain. At 0.25 Hz the calculated moduli during the first and final cycles were statistically similar for both the minimum and maximum strains applied.

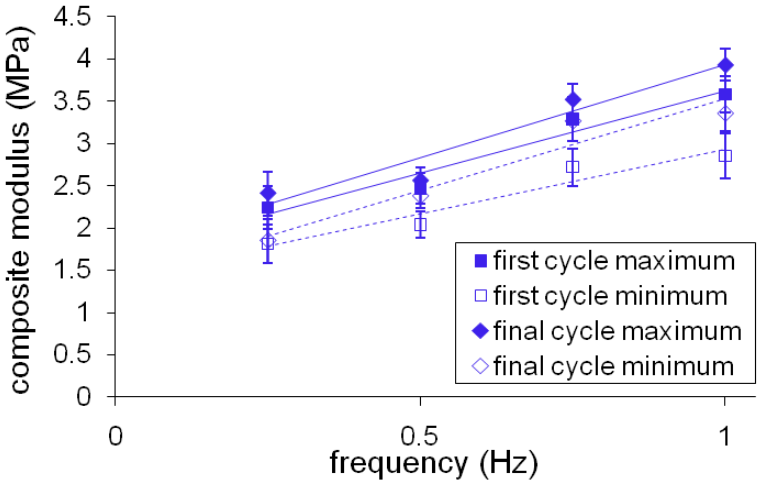

Figure 8-1: The relationship between increasing frequency of applied strain cycles and the minimum and maximum composite moduli found for the cycle for the first and final cycles applied to nasal cartilage. The maximum strain applied was 4%. Error bars show the standard deviation. Trend lines are shown.

The trend-lines fitted to these data had gradients and R_{fit}^2 values as shown in Table 8-1.

	first cycle		final cycle	
	maximum	**minimum**	**maximum**	**minimum**
gradient ($MPaHz^{-1}$)	1.94	1.52	2.21	2.17
R_{fit}^2	0.95	0.93	0.93	0.93

Table 8-1: Gradients and R_{fit}^2 values from the minimum and maximum composite moduli found for nasal cartilage samples during the first and final cycles in a minute resulting from the application of varying frequencies.

The difference in gradients can be seen clearly. As the system approached steady-state the tissue stiffens. This effect increases with respect to increasing the frequency of the strain cycles, and is more significant during recovery than loading. This behaviour can be likened to the shear-stiffening of some non-Newtonian fluids. The R_{fit}^2 values are suitably high to conclude that the trends, with respect to frequency for the moduli, measured under both maximum and minimum applied strains at the beginning and end of the minute were significant.

It is likely that the increase in moduli, resulting from both increasing the applied frequency and cycling the strain application for 1 min, was attributable to fluid flow characteristics. The matrix would still have undergone some elastic recovery during each strain removal, but this was shown to be incomplete by the moduli found during the application of the minimum strains being smaller than those during the

maximum. Some degree of stiffening, as seen in Chapter 7, is likely to be occurring.

8.2.1.2 Articular cartilage

As shown in Figure 8-2, increasing the applied frequency of strain cycles increased the minimum and maximum calculated composite moduli from articular cartilage samples for both the first and final cycles recorded in 1 min of repeated strain application. The differences between the first and final cycles were smaller at lower frequencies. The difference between moduli resulting from the minimum strain applications was fairly consistent respect to those resulting from the maximum strain applications at each frequency. This would indicate that the recovery is proportional to the maximum stress.

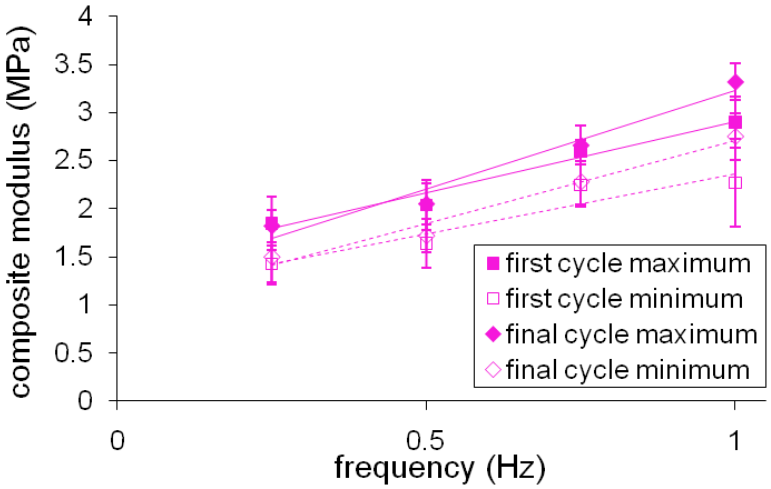

Figure 8-2: The relationship between the frequency of the applied strain cycle and the minimum and maximum composite moduli found for articular cartilage. Trends are shown for both the first and final complete cycles for 1 min of straining. The maximum strain applied was 4%. Error bars show for the standard deviation. Trend lines are shown.

The gradients and R_{fit}^2 values for the trend lines shown on Figure 8-2 are shown in Table 8-2.

	first cycle		final cycle	
	maximum	**minimum**	**maximum**	**minimum**
gradient ($MPaHz^{-1}$)	1.48	1.25	2.04	1.72
R_{fit}^2	0.97	0.89	0.96	0.97

Table 8-2: Gradients and R_{fit}^2 values obtained for the relationship between the frequency of the applied strain and the magnitude of the moduli during the first and final cycles applied over 1 minute to articular cartilage.

The increases in composite moduli with respect to the strain applied are larger during the final cycle than the first cycle. This appears to be a result of stiffening and cumulative loading over the minute test duration. The moduli resulting from the minimum strain applications are less sensitive to the applied strains than those resulting from the maximum strains. The R_{fit}^2 value is fairly low for the first cycle minimum results, so this gradient is less likely to be a true representation of the relationship between the strain frequency and the minimum composite modulus. The general trends appear to be that articular cartilage stiffens as the system approaches steady-state conditions. The stiffening effects increase with respect to increasing the applied frequency. The results imply that at frequencies lower than 0.25 Hz, the steady-state modulus of the tissue would be lower than the transient modulus. A change in the tissue behaviour with respect to the applied frequency, such as this, increases the likelihood that both the increases and decreases in tissue stiffness are due to the nature of the fluid movement. At lower frequencies, there is increased time available per strain cycle for fluid outflow to occur, therefore reducing the pressurisation effects at loading.

8.2.1.3 Comparison between the two native cartilage structures

For both the first and final cycles, the composite moduli of the hyaline cartilage samples increased with respect to frequency. The moduli resulting from both the minimum and maximum strain applications increased from the first cycle to the final cycles in the minute test duration, as the system approached steady-state. For the nasal tissue, this increase was fairly consistent with respect to the applied frequency. For articular cartilage, there was very little difference at the lower frequencies; when the frequency reached 1 Hz there was an increase between both the minimum and maximum moduli in the first cycle and the final cycle. This suggests that the stiffening effects demonstrated in Chapter 7 are more apparent in the nasal tissue. It is possible that the tissue structure is responsible for the difference observed. Articular cartilage appears to be structured in such a way so as to minimise cumulative pressure build up as a result of repetitive loading.

The two native hyaline cartilages appeared to respond in a similar manner to the minimum and maximum strains applied in the cycle. The moduli from the minimum strain were consistently between 0.5 to 1.0 MPa smaller than those from

the maximum strains. This result suggests that over the course of each individual strain cycle a similar amount of elastic recovery occurs in the two tissues. This is potentially of interest to tissue engineering, as it appears the structure of the cartilage does not significantly affect the elastic recovery of the tissue in an individual strain cycle.

8.2.1.4 General mechanical test observations

The general reliability of the dynamic results, particularly at the higher frequencies, was dependent on the sampling rate of the data logger. Whilst a suitable number of points could be recorded during each cycle to clearly show the trends in the materials response to the strain application, it is very likely the minima and maxima were not always captured. The results possibly represent an underestimation of the moduli resulting from the maximum strain and an overestimation of the moduli resulting from the minimum strain during the cycles.

Some difficulty was encountered in determining the lag times of the responses accurately. It was not possible to measure the lag times during the dynamic experiments, so these were determined in a separate set of experiments where strains of 4% were applied to nasal and articular cartilage specimens. The lag times were determined as approximately 20 ms for both the cartilage structures; these were applied to the dynamic data stress-response curves to allow moduli calculation from the stress and strain curves together.

The test duration was 1 minute. It would be possible to extend the experiments further by comparing the composite moduli from the minimum and maximum strains during cycles at 1 min intervals over a longer period, for example the full 20 min of stress-relaxation required for quasi-static equilibrium. This would allow more information to be obtained regarding the nature of the transient and steady-state responses under different frequency cyclic loading.

8.2.2 Elastography data from variable frequency dynamic tests

Figure 8-3 demonstrates the points in the cycle from which the minimum and maximum strains in the first and final cycles were obtained.

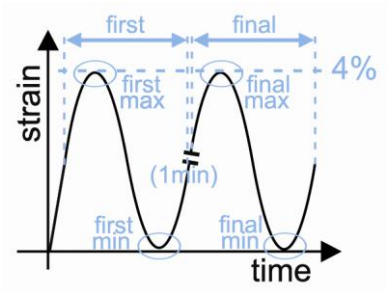

Figure 8-3: Representation of the positions in time from which the ultrasonic signals were extracted to perform elastography. In this figure, 'max' is maximum and 'min' is minimum.

8.2.2.1Nasal cartilage

A comparison between the strain maps during the maximum strain applications in the first cycles in nasal cartilage under different cyclic frequencies is shown in Figure 8-4. A material which had no dependency on the frequency of the strain applied would produce no significant difference between the strain maps obtained at different frequencies. In the top 1.5 mm of the samples the strains are very similar. The strains in the bases were highly scattered, which caused the observed differences between them to be statistically insignificant.

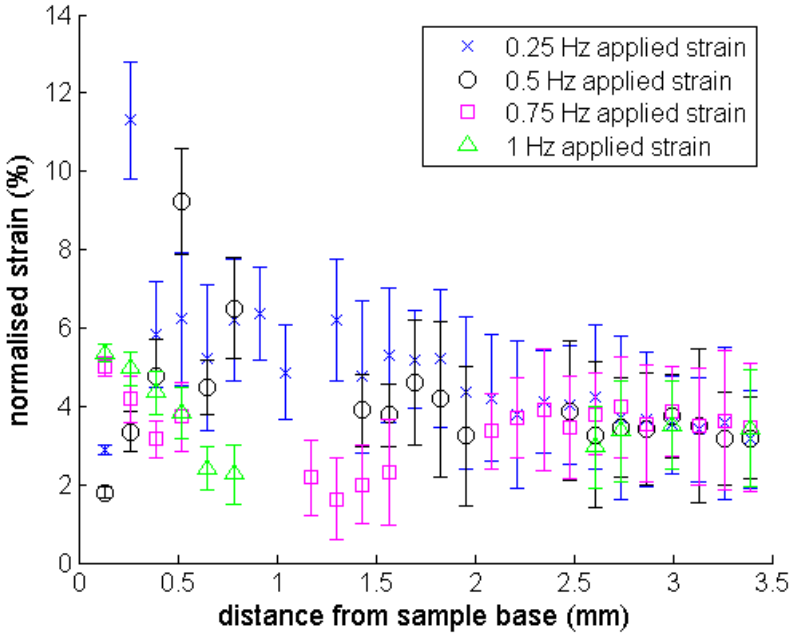

Figure 8-4: Comparison of the strain maps of the first cycle maximum strain magnitudes from the different frequencies of strains applied 10 nasal cartilage samples. Error bars show the standard deviations.

The strain maps from the final cycle maximum strains are compared in Figure 8-5. The similarities between the frequencies are large particularly in the regions of the tissue closest to the actuator surfaces. The signal decorrelation is consistently

highest in the middle of the samples, but the points which are available indicate that the strains in the centre decrease with respect to increasing the cyclic frequency (not statistically significant). Comparing the results in Figure 8-4 and Figure 8-5, the response to the maximum strain in the cycle appeared to become less dependent on the frequency applied over the course of a minute. This result implies that changes introduced during the transient application at different frequencies reduce as the tissue approaches steady-state. The nasal tissue behaved as a tissue with a homogeneous structure, equally straining across all the depths. The global moduli, during both the minimum and maximum strain applications in the first and final cycles, increased with respect to the frequency of the strain cycles. The depth-dependent results indicate that it is unlikely that this is due to anything occurring other than the strains expected for the homogeneous tissue structure.

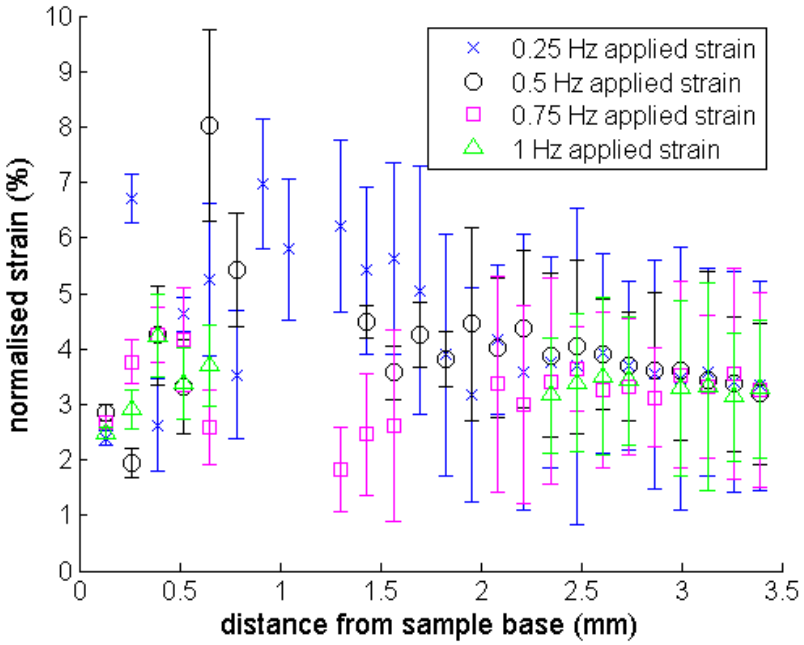

Figure 8-5: Strain maps from normalised elastography data from nasal cartilage, at the maximum magnitude of strain, during the final cycle. Error bars show the standard deviation of the 10 samples tested at each frequency.

Figure 8-6 compares the depth-dependent strains recorded during the minimum global strain application in the first cycle at varying frequencies. All of the strains are very similar in the top 2 mm of the samples, with the exception of those recorded at 0.75 Hz. This suggests that the result from 0.75 Hz may be slightly anomalous. The strains in the tissue closest to the rigid base (between 0 and 0.5 mm) are generally higher than those recorded from the remaining tissue. This result indicates that at all the frequencies applied, the first strain cycle causes residual

strains throughout the structure, however the tissue closest to the actuator is most able to elastically recover and therefore appears stiffer than the tissue closer to the fixed base.

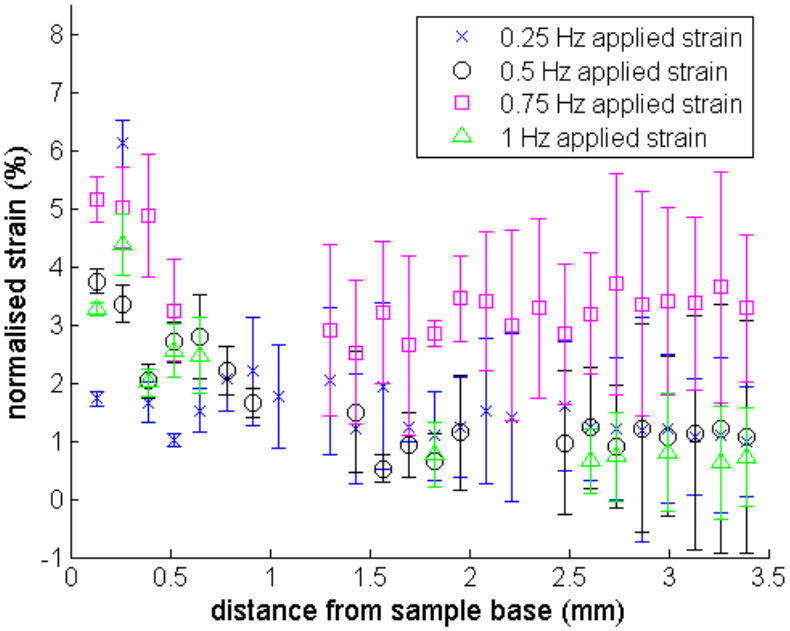

Figure 8-6: Comparison between the strain maps during the minimum applied strain magnitudes in the first cycles applied to 10 nasal cartilage samples at each frequency. Error bars show the standard deviation.

The local strains resulting from the minimum global strain applications in the final cycle are shown in Figure 8-7. The strains are high and have a large amount of scatter in the 0.75 mm of tissue closest to the sample base at all frequencies, with the exception of 1 Hz where the results available appear to be fairly linear with respect to depth. This result indicates that the tissue recovery has become more evenly distributed throughout the structure over the course of the minute cycle. Similar to the results under the maximum strains, it is likely that this is due to the strain gradients becoming more like those found for nasal tissue under quasi-static loading (section 6.3.2.1) as steady-state is approached. As a result of repeating the cycles over one minute, the strain behaviours became more similar at 0.25, 0.5 and 0.75 Hz. At the lower frequencies the tissue closest to the base is still less able to recover than the tissue closer to the actuator.

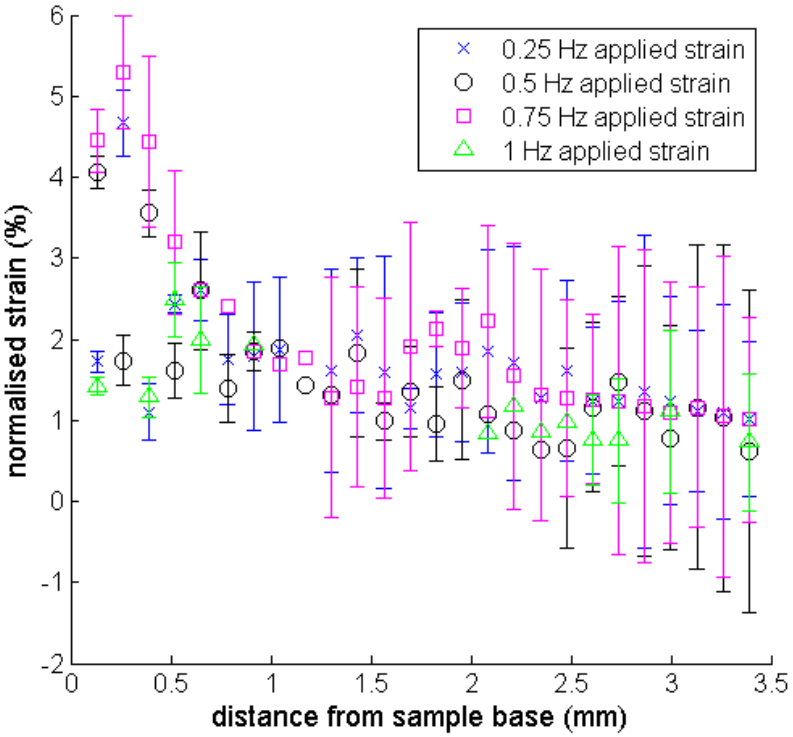

Figure 8-7: Results from normalised elastography strains recorded during the minimum strain magnitudes applied during the final cycles to nasal cartilage (10 samples at each frequency, error bars show the standard deviation).

The global moduli found during the minimum strain application in the final cycles were higher than those during the first cycle at all straining frequencies. The larger levels of depth-dependent recovery shown in Figure 8-7 are therefore expected.

8.2.2.2Articular cartilage

A comparison between the strain maps obtained during the maximum global strain applications in the first cycles at different frequencies is shown in Figure 8-8. The strains, in both the middle and superficial zones, remained the same irrespective of the frequency of the applied strain cycles. The scatter of the results increased with respect to frequency, but the magnitude of the error bars decreased. This was possibly caused by small fluctuations in the composite modulus at different depths, most likely attributable to fluid redistribution. The decrease in error bar magnitude is indicative that the changes occurring were more easily detectable and that the depth-dependent behaviours became more similar with increasing applied strain. This implies that at the beginning of the transient response the behaviours were similar with respect to applied frequency. As an increase in the global composite moduli was observed with respect to increasing the frequency, this suggests that the

stiffening of the tissue occurred evenly with respect to depth, otherwise the strain gradients would have changed.

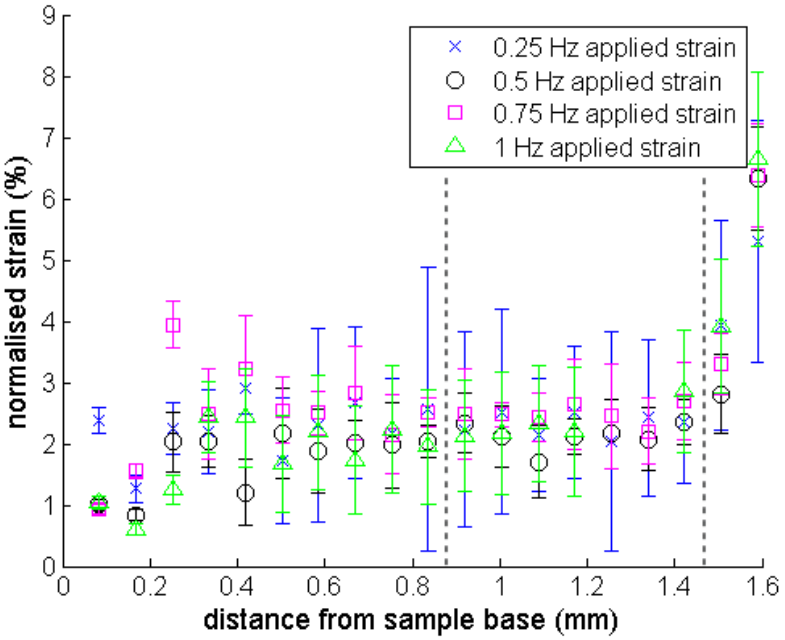

Figure 8-8: Comparison between the strain maps from the maximum strain applied to articular cartilage during the first cycles at varying frequencies. Error bars show the standard deviation of the 10 samples tested at each frequency. The dashed lines show the approximate positions of the zones: deep, middle and superficial (left to right).

Figure 8-9 shows a comparison between the elastography strain maps obtained during the application of the maximum strain during the final strain cycles. The results were not as similar as those seen for the first cycle maxima, with respect to the frequency of the applied strain. As the global moduli were found to be similar for each applied strain frequency, with the exception of 1 Hz, it was expected that the results in Figure 8-8 and Figure 8-9 would be very similar as the system approached steady-state; but this was not found to be the case. The results are less scattered and the error bars are generally smaller than the results shown in Figure 8-8. It is possible that the smaller middle zone strains at 0.25 Hz are physiologically significant. However, as the error bars are large in this region, it is also possible that the result is due to an underestimation of the local strains by the elastography routine. The statistical significance between the zones is smaller during cyclically applied strain, than quasi-static, at all the applied strains. This result implies that the strain gradients were reduced in the cartilage tissue as steady-state is approached. It is likely that this mechanism is designed to prevent chondrocyte damage from shear strains.

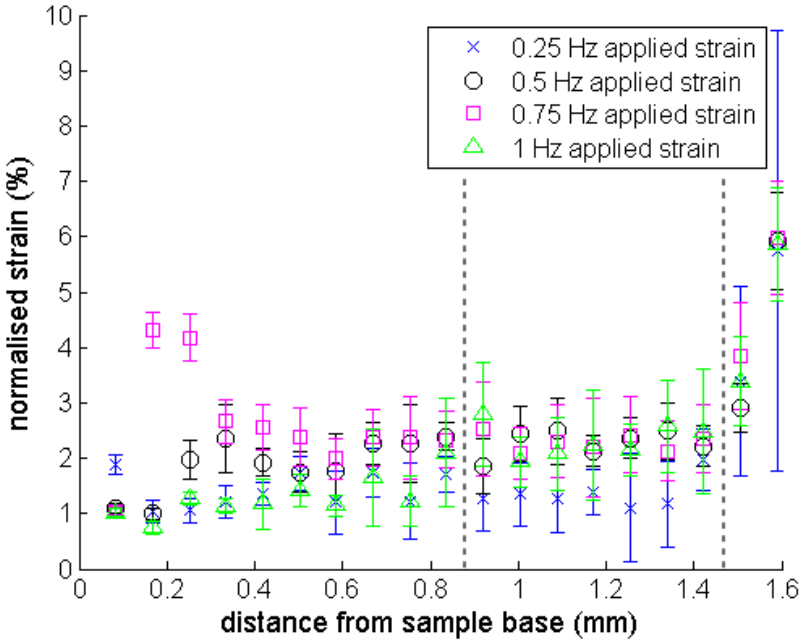

Figure 8-9: Results from the maximum strain magnitude applied during final cycles at different frequencies of strain applied to articular cartilage. Error bars show the standard deviation over the 10 samples tested at each frequency. The dashed lines show the approximate zones.

A comparison between the strain results found during the application of the minimum strains during the first cycles is shown in Figure 8-10, representing recovery behaviours during the transient part of the dynamic response. The middle zone strains were all seen to be fairly similar, but the residual deep zone strains were larger during 0.25 and 1 Hz cycles. This trend is unlikely, and is therefore more probably caused by small errors being multiplied during the normalisation process. The superficial zone strains were highest during 0.25 Hz cycles, indicating this region was softer and less able to recover from the strain application at this frequency. The strains in the deep zone were large for all the applied frequencies, indicating an accumulation of strain in a region of tissue unable to recover as quickly as the rest.

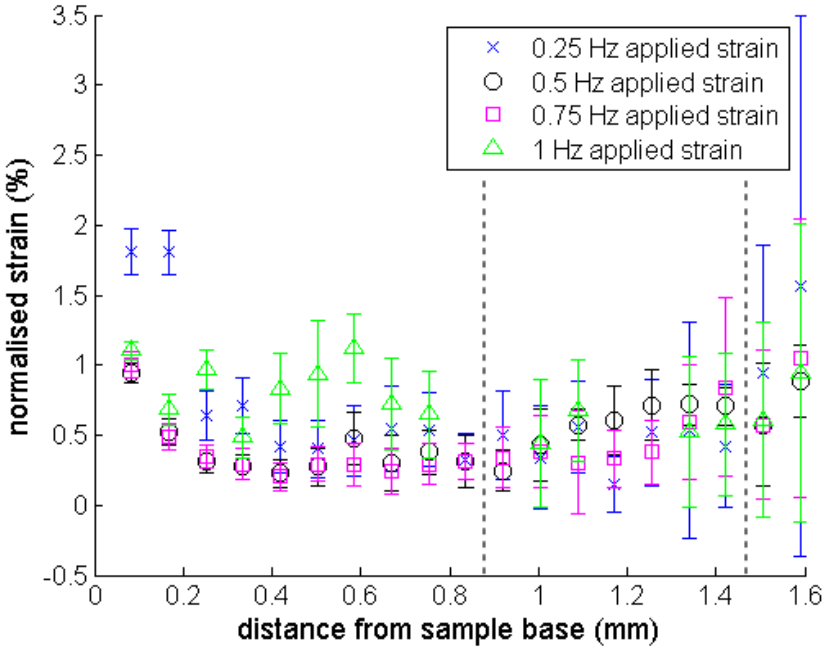

Figure 8-10: Normalised strain maps from the minimum strains applied in the first cycle to articular cartilage. Error bars show the standard deviation of the 10 samples tested at each frequency and dashed lines show the approximate zones.

Figure 8-11 shows the depth-dependent strain results during the minimum strain application of the final cycle of global strains repeated over one minute.

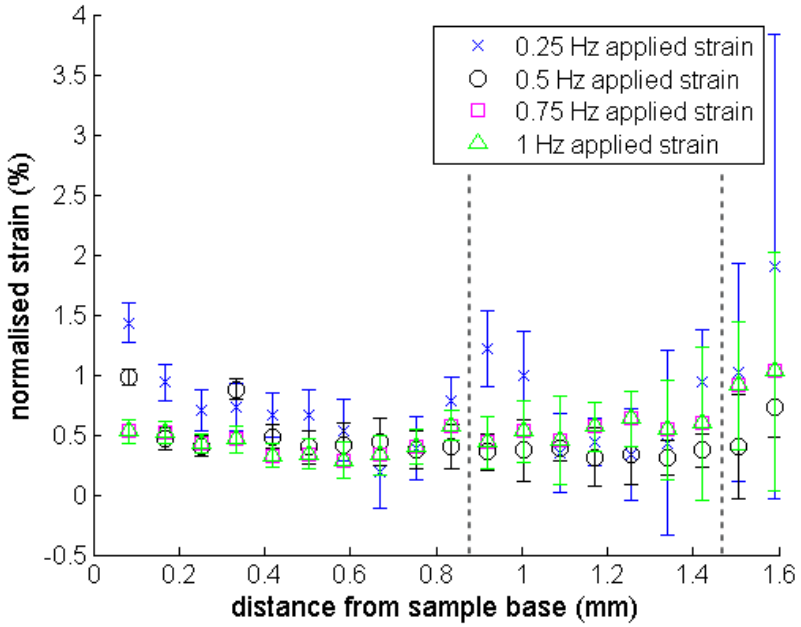

Figure 8-11: Results from normalised elastography data recorded during the minimum strains applied to articular cartilage during the final cycle. Error bars show the standard deviation across the 10 samples tested at each frequency and the dashed lines approximately show the zones.

The results at all frequencies are similar, with 0.25 Hz strain demonstrating the larger strains in both the deep and superficial zones. It is possible that over the 0.25 Hz strain cycle, more fluid was expelled than at higher frequencies, causing there to be less reaction force to allow recovery, thus causing strain accumulations. The similarities between the strain recoveries are greater after one minute than in the first cycles, which would be expected as the system approaches steady-state conditions.

8.2.2.3Comparison between the two native cartilage structures

For both hyaline cartilage types, at all frequencies tested, recovery was incomplete in the minimum cycles during both parts of the transient response examined. Calibration tests on the actuator cycles (Appendix Aii) demonstrate that this recovery is not due to the strain being only partially removed from the structures. This means therefore, that the hyaline cartilage structure in the deepest regions of the tissue is unable to elastically recover during the half-cycle time of 2 s for the 0.25 Hz cycle, which is the lowest frequency investigated here. From what is known of the fluid flow from the tissue, this is a reasonable result for both tissue types, as each loading cycle would cause some fluid to be expelled from the structure.

The nasal cartilage specimens, representing a uniform hyaline structure, appeared to accumulate higher levels of strains in the base of the tissue following the application of cyclic loads at all frequencies meaning that the tissue closer to the actuator surface stiffen more significantly. Increasing the applied frequency appeared to have the greatest effect on the middle of the nasal cartilage specimens, where the strains decreased with respect to frequency. For the depth-dependent behaviour of both nasal and articular cartilage, no statistically significant differences were found with respect to frequency at either the minimum or maximum strains during the first and final cycles. This result indicates that the global moduli increases with respect to increasing the frequency are most likely due to the fluid pressurisation and the rate at which it is compressed, rather than any changes in the depth-dependent strain distributions.

Although not statistically significant, it appeared that the strain recovery behaviours became more similar within the specimens with respect to applied frequency at the

end of the minute cycle compared to the beginning. This would imply that removing strain accumulations is likely to be of some physiological benefit in hyaline cartilage.

Both tissues demonstrated similar frequency dependent strain maps as steady-state approached. This suggests that the structure is not directly responsible for determining the steady-state behaviour.

Only two of the maximum strain maps in articular cartilage demonstrated a significant increase of strains between the deep and superficial zones of the tissue, meaning that, despite its structure, articular behaved more like a homogeneous tissue during the cyclic loading. This result should be encouraging for tissue engineering, as it means that the structural differences are less significant in determining recovery during dynamic loading conditions than during quasi-static straining. However, it is likely that the structure was responsible for producing different frequency dependent responses globally.

8.2.2.4General elastography observations

As with the quasi-static results, elastography results for the articular cartilage specimens benefited from better signal correlations between the pre- and post-compression signals. However, cyclic strain applications appeared to worsen the signal decorrelation problems in both the native tissues. This was a significant problem for the nasal cartilage experiments as large tissue regions sometimes produced no reliable strain measurements which could be compared. The error bars were generally large in magnitude, which caused difficulty in establishing statistical significance between regions where behaviour appeared to be quite different.

8.3 Effect of varying the cyclic strain magnitude during 1 Hz strain cycles

8.3.1 Mechanical test results

8.3.1.1Nasal cartilage

As shown in Figure 8-12, the relationship between increasing the magnitude of the cyclic strain applied to nasal cartilage and the increases in the resulting minimum and maximum composite moduli, is similar to that of the effect of increasing the frequency (section 8.2.1). The minimum moduli during the cycles also increased.

At each of the magnitudes investigated, the averaged composite moduli of the final cycles were found to be significantly larger than those of the first cycles (>95% confidence). This can be directly compared to the behaviour reported in section 8.2.1.1, where a similar stiffening effect occurred within the nasal cartilage over the minute of cycle repetitions.

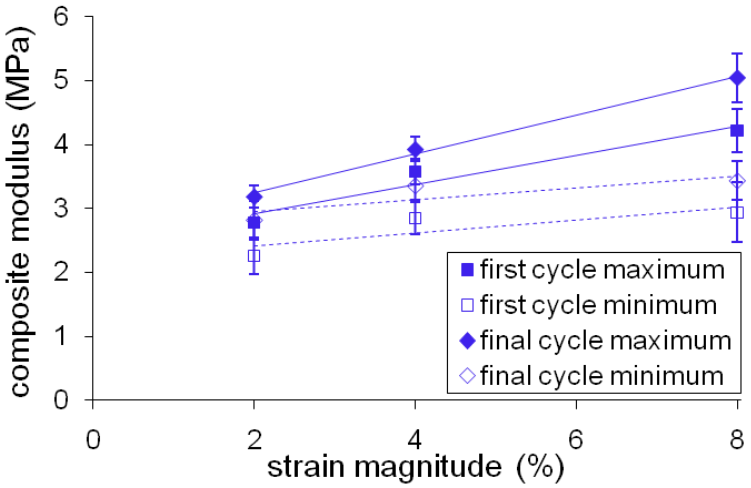

Figure 8-12: The relationship of the magnitude of maximum applied strain to the minimum and maximum composite moduli of nasal cartilage samples during the first and final cycles of strain applied at 1 Hz for 1 min. Error bars show the standard deviation of each averaged cycle. Trend lines are shown.

The differences between the first and final composite moduli are fairly consistent for the moduli found during both the minimum and maximum strain applications. The relationship between the maximum applied strain and the resulting composite moduli were determined using the trend lines. These are shown in Table 8-3.

	first cycle		final cycle	
	maximum	**minimum**	**maximum**	**minimum**
gradient (MPa%$^{-1}$)	0.23	0.1	0.31	0.091
R_{fit}^2	0.94	0.69	0.99	0.69

Table 8-3: Gradients and R_{fit}^2 values for the relationships between the magnitude of the maximum applied strain during 1 Hz strain cycles to the resulting composite moduli in nasal cartilage specimens.

The significance of the slope of the trend lines is low for both the minimum applied strain results. For the maximum applied strains, it can be seen that the resulting composite moduli are more sensitive to the magnitude of the strain applied during the final strain cycle in one minute than during the first. This result suggests that the effect of any changes occurring within the tissue becomes more significant as the

tissue is repetitively strained. The lower gradients of the moduli during the minimum applied strain would indicate that the tissue recovery is fairly constant and less reliant on the maximum strain magnitude.

8.3.1.2Articular cartilage

Figure 8-13 shows the minimum and maximum composite moduli recorded during the first and final cycles recorded from articular cartilage specimens at varying peak magnitudes. The differences between the moduli found during the maximum strain application were fairly consistent during the first and final cycles; this implies that the rate of approaching steady-state is not affected by the strain magnitude in articular cartilage. The global composite moduli found during the minimum strain applications did not follow a recognisable pattern between the first and final cycles.

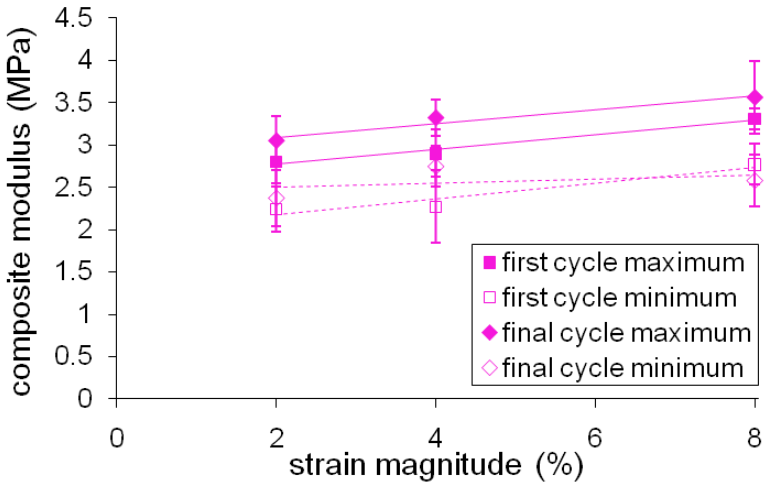

Figure 8-13: Relationship between the magnitude of the maximum strain applied in each cycle (2%, 4% or 8%) and the composite moduli for articular cartilage. Strain cycles were applied at 1 Hz for 1 min and the results from the minimum and maximum strain applications in the first and final cycles are shown. Error bars show the standard deviation across the 10 samples tested at each magnitude. Trend lines are shown.

The gradients and R_{fit}^2 values for the trend lines are shown in Table 8-4. The gradients were found to be small and the correlation of the results was generally good, except of the final cycle minima. The effect of increasing the magnitude of the applied strain was small, but fairly consistent for the composite moduli results obtained during both the minimum and maximum strain applications in the first cycle and the maximum strain application in the final cycle. The R_{fit}^2 value was not sufficiently high to allow any conclusions to be made for the final cycle minima.

	first cycle		final cycle	
	maximum	**minimum**	**maximum**	**minimum**
gradient (MPa%$^{-1}$)	0.088	0.094	0.081	0.024
R_{fit}^2	0.98	0.92	0.95	0.15

Table 8-4: Gradients and R_{fit}^2 values for the trend lines relating increasing the magnitude of the maximum strains applied to articular cartilage during 1 Hz cycles. The trends during the first and final cycles in 1 min are shown.

The results suggest that the composite moduli, during the initial transient response of the tissue to the cyclic strains and the subsequent approach to steady-state, increase proportionally in articular cartilage as a result of increasing the magnitude of the maximum applied strains.

8.3.1.3 Comparison between the two native cartilage structures

Both the nasal and articular cartilage demonstrated an increase in the composite moduli in both the first and final cycles resulting from an increase in the maximum applied strain. The composite moduli during the maximum strain application to nasal cartilage, was more sensitive to the changes in applied strain magnitude than the articular tissue. This was similar to the results for increasing the frequency of the strain (section 8.2.1.1). The trend line gradients were significantly larger for the nasal cartilage specimens.

The gradients of the trend lines representing the relationships of the composite moduli during the recovery phase of the cycle (when the minimum strains are being applied) are similar for both the hyaline structures. As the magnitude of the applied strain increases, the proportional magnitude of the tissue recovery decreases. This does not appear to affect the maximum moduli of articular cartilage tissue. However, it is possible that the relative inability for the tissue to recover during each cycle could be the cause of the larger moduli as the system approaches steady-state. The increases between the composite moduli during the initial part of the transient response and those found as the system approaches steady-state appear to be fairly proportional to the magnitude of the applied strain. The mechanisms of this increase could be similar to those proposed for the increase of composite moduli with respect to the cumulative strain applied (section 7.2.3): the deformed matrix causes the permeability to increase, and therefore the pressurisation increases.

8.3.2 Elastography data from varying the magnitude of cyclically applied strain

The points in the strain application cycle where the ultrasound signals were obtained to produce the elastography data are shown in Figure 8-14.

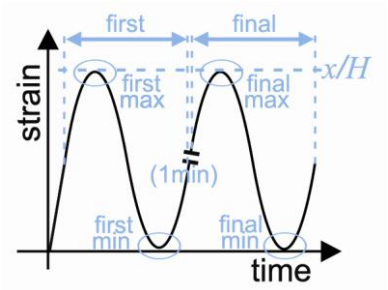

Figure 8-14: Representation of the points in the cyclic strain application where the ultrasonic signals used for the elastography were extracted.

8.3.2.1Nasal cartilage

Figure 8-15 compares the local strain behaviour at the maxima for the first cycles of global strain applied to nasal cartilage at different magnitudes.

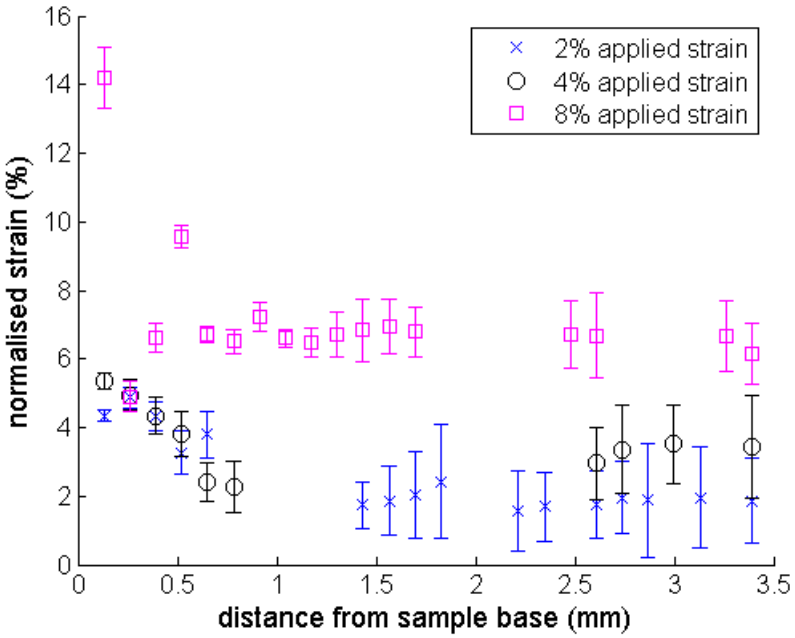

Figure 8-15: Comparison between the normalised strain maps from the maximum strain applications in the first 1 Hz cycles applied to nasal cartilage.

It was observed that strains closest to the rigid base appear larger than those in the rest of the tissue, where strains followed approximately linear patterns close to the magnitude of the strain applied. This was expected in the results from nasal cartilage due to the homogeneous hyaline cartilage structure. The lower strains in the tissue 1 to 3.5 mm distance from the tissue base are likely to represent tissue stiffening, as proposed in section 7.3.3. The signal decorrelation between pre- and

post-compression was observed to be very high for all of the strain magnitudes, but particularly at 4% maximum strain. This caused problems in interpreting the data as effectively as it should be, as some comparisons were unable to be made because no information was available for the centre of the samples at 4% global maximum strain.

A comparison of the depth-dependent strain results, obtained from the maximum applied global strains in the final cycles, as the system approached steady-state, is shown in Figure 8-16.

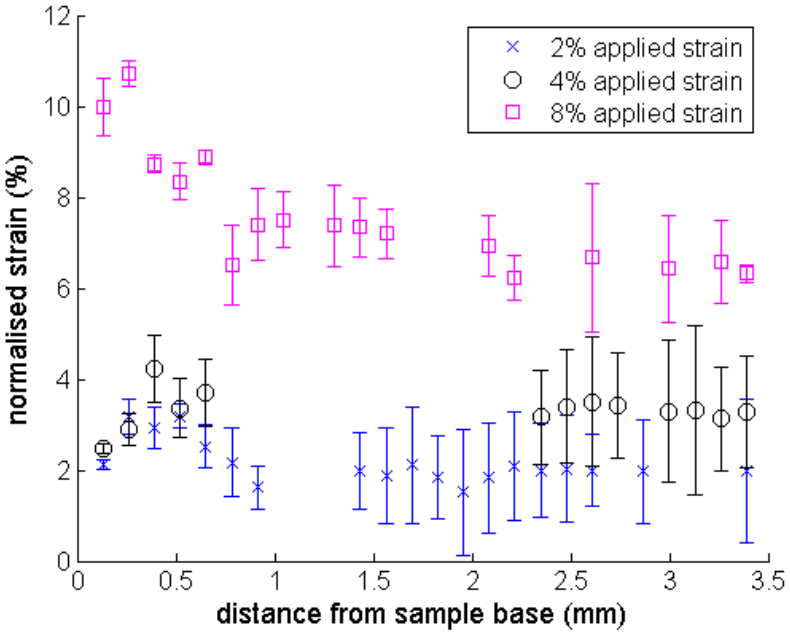

Figure 8-16: Results comparing the magnitude of the depth-dependent nasal cartilage strain maps (10 specimens) resulting from the application of the varying maximum strains in the final 1 Hz cycle. Error bars show the standard deviation.

The signal correlation was shown to be approximately similar to that of the maximum magnitude first cycles. The results were still scattered, the error bars were large and many of the windows did not have any reliable strains to plot. The strain results were more linear during the final cycle than the first. This indicated a reduction in the uneven distribution of the stiffening effects which were seen in Figure 8-15.This was expected as the tissue response changed, as it approached steady-state conditions. The global moduli increased between the first and final cycles, so it is likely that the whole tissue was stiffening with respect to depth.

Figure 8-17 shows the depth-dependent strains during the minimum global strain application in the first strain cycles. All the results were quite scattered, but were similar in magnitude and apparently unaffected by the maximum global strain applied. The strains closest to the rigid base were larger than the other regions, indicating that during the first cycle at 1 Hz, regardless of the applied strain magnitude (between 2% and 8%), the recovery characteristics were the same for the nasal cartilage specimens.

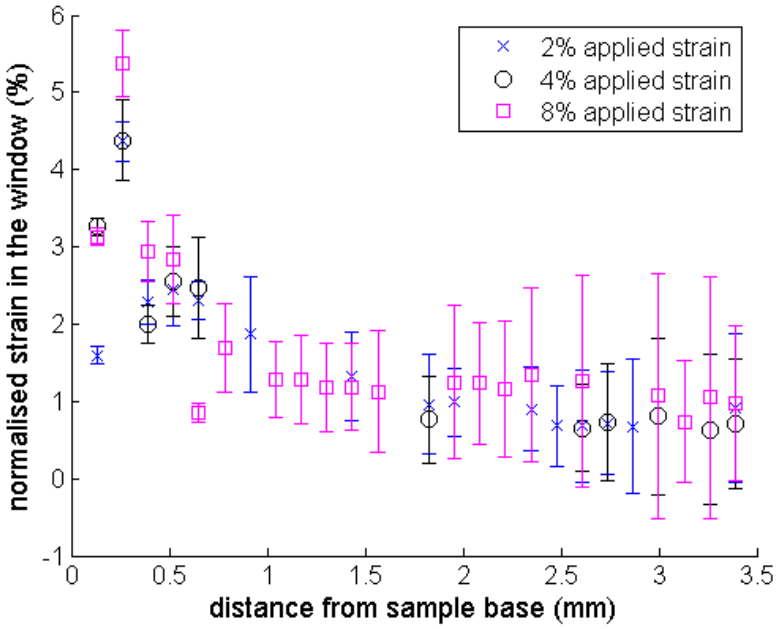

Figure 8-17: Normalised strains resulting from the application of minimum strains to 10 nasal cartilage specimens during the first 1 Hz cycle. Error bars show the standard deviation.

The results from the final cycle minimum applied strains, shown in Figure 8-18 (compared to Figure 8-17) demonstrate the similarities of the first and final cycle strains. The recovery behaviour of nasal cartilage at the beginning and the end of the one minute test are therefore the same. There was most scatter closest to the rigid base, but the remaining strains were of similar magnitude, with similar error bars, at every applied global maximum strain, to the results in the first cycle. This shows that after one minute of cyclic strain, as the system approaches steady-state, the magnitude of the maximum global strain did not significantly affect the recovery characteristics of nasal cartilage tissue. The strains were generally linear, as expected from the knowledge of nasal cartilage structure.

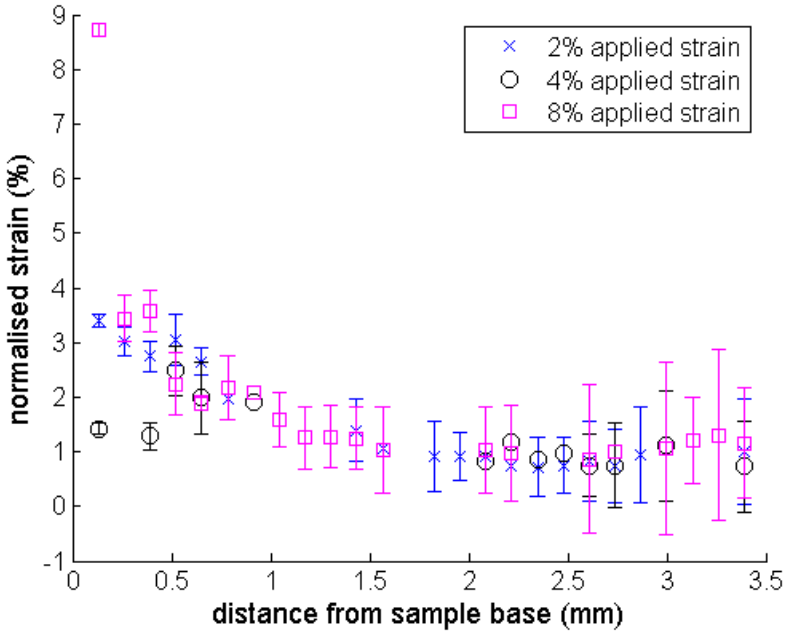

Figure 8-18: Comparison between the normalised depth-dependent strains resulting from the minimum strain application at 1 Hz in the final cycles. 10 nasal samples at each magnitude, error bars show the standard deviation.

8.3.2.2 Articular cartilage

A comparison between the depth-dependent articular cartilage strains found during the initial part of the transient response is shown in Figure 8-19. This comparison revealed how large the deep zone strains were. It is unclear whether this result is physiologically significant. The strains from the application of 2% and 4% were similar to those expected from articular cartilage tissue. It is possible that the superficial and middle zone had stiffened as a result of the rate of strain application and the large strain applied, causing the deeper tissue to undergo a larger deformation than expected.

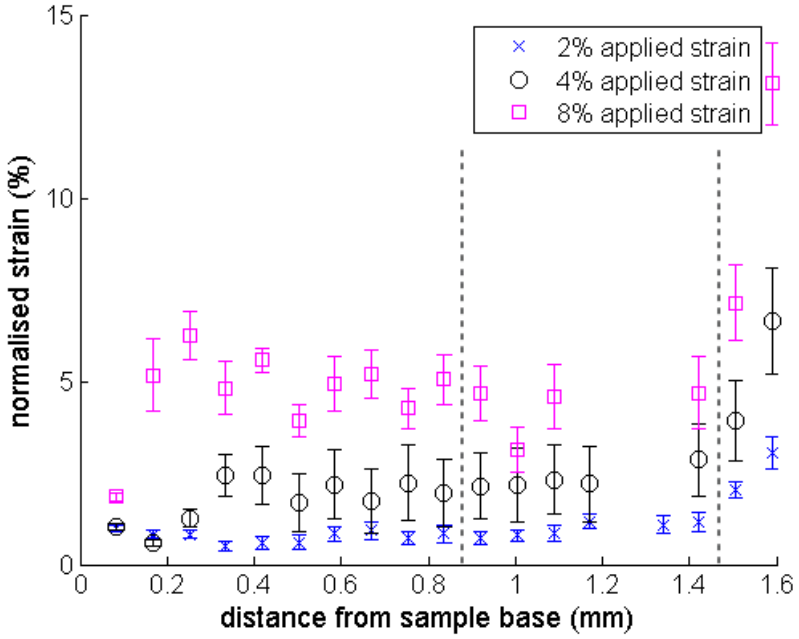

Figure 8-19: Comparison of the normalised elastography strain maps from articular cartilage (10 samples at each magnitude, error bars show standard deviation) resulting from application of the maximum strain in the first 1 Hz cycles. The dashed lines approximate the positions of the zones.

Figure 8-20 compares the depth-dependent strain distributions recorded from the final cycles during application of the maximum strain magnitude.

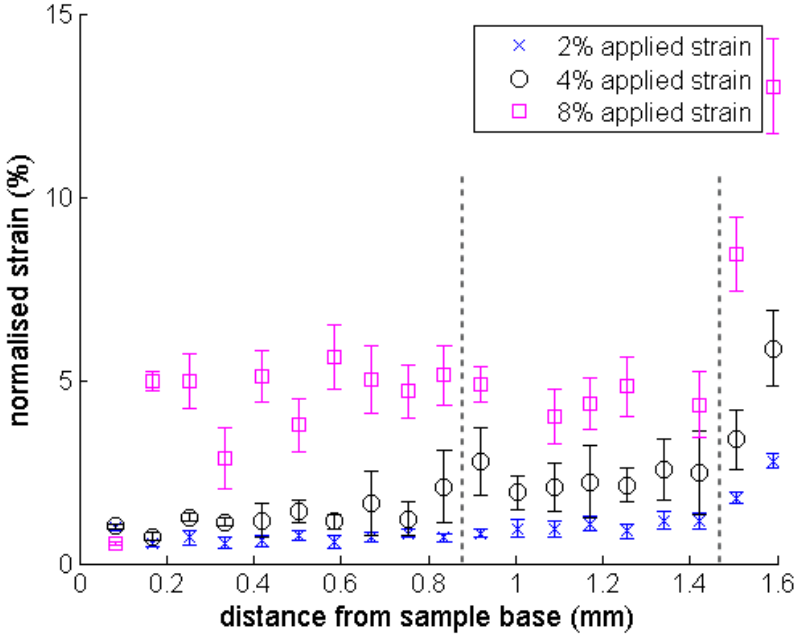

Figure 8-20: Normalised strain maps during application of maximum strain in the final 1 Hz cycle (10 articular cartilage specimens at each magnitude). Error bars show the standard deviation and dashed lines approximate zones.

The results were better correlated between pre- and post-compressional signals. The strains recorded, from 4% maximum global strain, had the largest error bars,

despite the scatter of the deep and middle zone strains under 8% global strain being greater. The results from both the first and final cycle maxima were similar enough to suggest that the magnitude of the tissue depth-dependent strain response, during both the initial part of the transient response and the approach to steady-state, was determined more by the frequency of the strain applied than the peak strain magnitude.

Figure 8-21 shows the residual strains measured during the minimum global strain application in the first 1 Hz cycles. The strain maps from 2% and 8% peak global strains were the most similar in magnitude, although the 8% results were consistently slightly larger. Due to the lower signal correlations measured at 4% peak strain (indicated by the high levels of scatter and large error bars) it is possible that these results were not particularly reliable for comparison, and that no significant difference in tissue behaviour actually occurred as a result of varying the peak global strain magnitude.

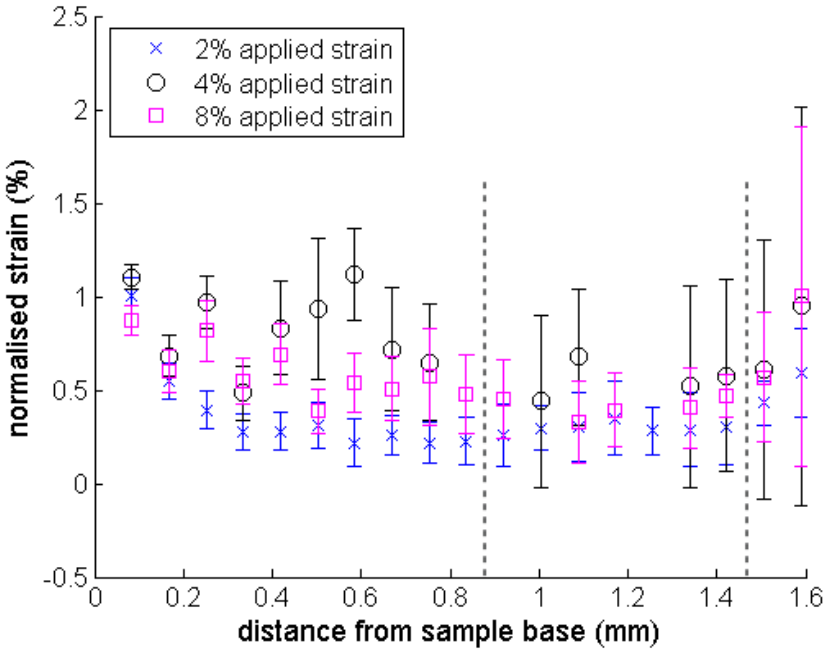

Figure 8-21: Comparison of the normalised depth-dependent strains during the minimum strain applications in the first cycle in 10 articular cartilage samples at each magnitude. Error bars show the standard deviation. Dashed lines approximate the zonal boundaries.

The results for the minimum strains applied in the final cycles after one minute, as the system approached steady-state, at 1 Hz are shown in Figure 8-22.

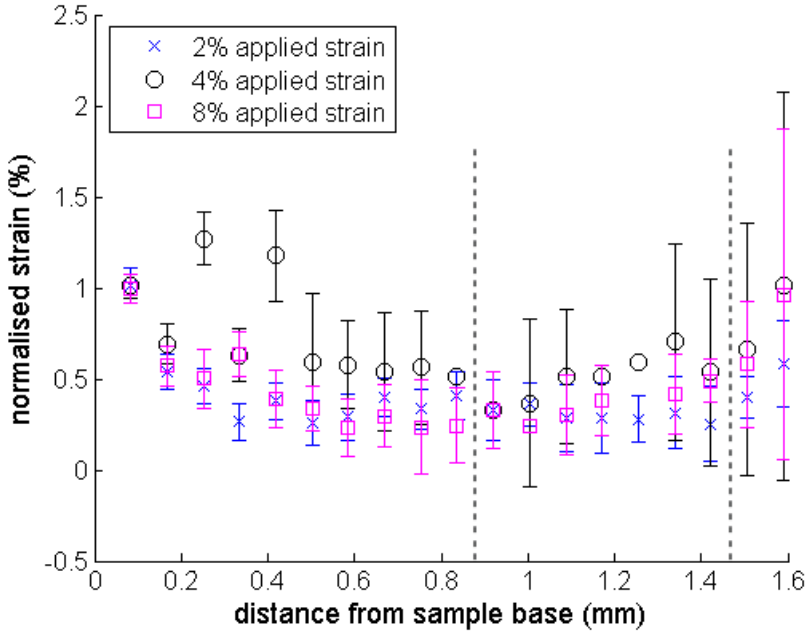

Figure 8-22: Comparison of the strain maps recorded for 10 articular cartilage samples, at each of the different strain magnitudes during minimum global strain application in the final 1 Hz cycles. Error bars show standard deviation. Dashed lines approximate the positions of zones.

The similarities between the maps from the 2% and 8% peak strain cycles and the large error bars in the 4% data suggest that it is likely that the depth-dependent distribution of residual strains are not dependent on the magnitude of the global strain applied, and are not significantly changed due to the system approaching steady-state conditions.

8.3.2.3Comparison between the two native cartilage structures

High levels of signal decorrelation occurred throughout the nasal cartilage structures and some, particularly in the middle zone, of articular samples. It was therefore difficult to draw as many conclusions from the depth-dependent results as compared with those for the quasi-static tests.

Despite the depth-varying articular cartilage structure, residual strains in recovery were evenly distributed. Nasal strains appear to accumulate in the tissue regions closest to the rigid surface, but in general not significantly. Neither nasal nor articular cartilage depth-dependent strain distributions appeared to be dependent on the magnitude of strain applied at 1 Hz. Similar to the results from varying the frequency, the strain gradients in articular cartilage were reduced from those obtained during quasi-static loading, suggesting that the response of hyaline

cartilage under cyclic loading is not as dependent on the tissue structure and depth-dependent matrix moduli distributions.

The recovery behaviours, both globally and depth-dependently, were very similar for both the hyaline cartilage structures. This result could be significant to tissue engineers, as cyclic strain applications are a likely mode of loading to occur *in vivo*.

8.3.2.4General elastography observations

The signal decorrelation in the middle zone of articular cartilage became more significant under the application of cyclic strains. This further supports the theory that the collagen fibril orientation is largely responsible for determining the pre- and post-compressional signal correlation (section 6.3.3). The random orientation of the fibrils throughout nasal cartilage specimens and in the middle zone of articular cartilage is unfavourable for elastography.

In order to allow further dynamic mechanical properties of the cartilages to be obtained the limitations of the oscilloscope sample rate would need to be addressed. A dedicated signal processing board (DSP) could provide the necessary increase to the rate of ultrasonic signal capture. An increased capture rate would allow for elastography to be performed at different times during the straining cycles, rather than just at the maxima and minima. The findings presented in this chapter merit these further investigations.

8.4 Summary

The maximum global composite moduli of both the cartilage structures were found to increase with respect to the frequency and magnitude of the cyclic strain applied. The moduli also increased over the course of one minute, as the system approached steady-state, suggesting a stiffening of the tissues compared to the initial transient response. The local strain distributions indicated that the depth profiles for the moduli did not change significantly with respect to the frequency of the strain or when the strains were applied for one minute. The global moduli in recovery conditions for both hyaline cartilages were found to be less dependent on the magnitude of the maximum applied strain than the global composite moduli under loading conditions. The depth-dependent strain distributions, in recovery, were found to be fairly consistent for both tissues with respect to the strain magnitudes.

The articular cartilage results suggested that the moduli gradients became less steep under cyclic loading. The nasal tissue local moduli remained fairly linear. Therefore the difference between the hyaline structures was found to be less than that observed for quasi-static loading conditions. This finding is likely to be of most interest to tissue engineers, as cyclic straining is a likely loading mode for cartilage tissue *in vivo*; if cyclic loading is less sensitive to the tissue structure, then the requirement for producing replacement tissues with structures identical to those of the surrounding tissue is reduced.

9 Conclusions

9.1 Overview

This thesis aimed to address the need for comprehensive characterisation of global and depth-dependent mechanical properties of hyaline cartilage tissue, in order to provide tissue engineers with the necessary information to design mechanically functional constructs. The contributions made in this thesis are presented. Further questions and problems arising from the work are then presented with suggestions of how they might be addressed in order to extend the existing work.

9.2 Summary of findings

A new non-destructive elastography test was developed, capable of determining the depth-dependent mechanical behaviour of cartilage tissue. The technique was successfully applied to collagen scaffold based engineered cartilage constructs, as well as native cartilage tissue. Differences between tissues cultured for periods up to 15 days were observed in both the global and depth-dependent properties.

The tests were performed under a range of strain protocols. These were used to determine new information regarding the importance of the specialised structure of articular cartilage, compared to the more homogeneous structure of nasal cartilage. From these novel results it was concluded that the most important similarities observed occurred during the cyclic strain applications. Both structures stiffened as the dynamic response approached steady-state, over the range of strain magnitudes and frequencies examined. Additionally, both tissue structures demonstrated an increase in the composite moduli with respect to the strain frequency and, to a lesser extent, the strain magnitude. The most important differences between the two tissue structures were observed during the quasi-static strain applications of single and multiple steps. Articular cartilage composite moduli were found to be dependent on the magnitude of the applied strain. However, during applications of multiple strain steps, articular cartilage demonstrated a lower dependency on the history of the applied strain than nasal tissue.

An innovative phenomenological model, capable of extracting matrix constants from the elastography data and literature inputs of permeability and void fraction, was constructed. The model was applied to data from the quasi-static single strain step application elastography experiments to determine the void fractions under the different strains and the elastic constants of the matrix.

The elastography method developed has the potential to be adapated for application to other tissues, such as skin. However, a study would need to be conducted to enable selection of the optimum ultrasonic frequencies for the new materials.

9.3 Original contributions

The specific original contributions in this thesis are outlined in the following section. References to the chapters containing the details are shown.

- Elastography tests were performed on cartilage tissue using a variety of strain protocols in an environment which was physiologically relevant. This allowed access to data from the tissue which was unavailable in the global mechanical cyclic strain tests of Park and Ateshian (2006), or the elastography experiments of Zheng et al. (2001), (2002a), (2002b), (2004), (2005), Qin et al. (2002) and Fortin et al. (2003). The design of the elastography system and the corresponding signal processing are shown in Chapter 4. The results from the various strain application protocols are presented in Chapters 6, 7 and 8.

- Elastography was applied to collagen scaffold based engineered cartilage tissue to extract depth-dependent and global mechanical behaviours. The elastography technique was able to distinguish changes in the tissues due to the length of culture period. These results are presented in Chapter 7.

- Two native hyaline cartilage structures were compared during each test protocol. No evidence of such a rigorous comparison approach of two hyaline cartilages was found in the literature. The results in Chapters 6, 7 and 8 demonstrate the important differences and similarities in the behaviour of the two native structures, providing tissue engineers with new information to guide the engineering of mechanically functional tissue.

- The phenomenological model (construction shown in Chapter 5) is novel in its ability to accept depth-dependent strain inputs provided by elastography. This provides access to the matrix constants through elastography experiments, without the need to wait for the system to reach equilibrium conditions. The results of the application of the model to elastography data are shown in Chapter 6.

This section has demonstrated the original contributions made by this thesis to the field of cartilage mechanics, tissue engineering and applied ultrasound.

9.4 Further work

Following the satisfactory achievements of the original objectives, subsequent questions and problems arose. These have been summarised and presented with suggestions for further work to improve the reliability of existing results and to extend the scope of the technique to a greater range of applications.

Identifying the greatest area of uncertainty in the results led to the need to improve the accuracy of strains found using the elastography results. Particularly with the native samples, the error bars and scatter were consistently large. Possible causes include, but are not limited to: sample conditions, such as the age of the animal, bone layer thickness, species or breed and the time between the death of the animal and performing the test; and test conditions such as temperature fluctuations and insufficient contact between the sample surfaces and the actuator. Improved equipment and methods could be used to extract the specimens and more sample collections could be performed to reduce the storage time of the samples and hence the variation in the condition of the specimens. It could be possible to reduce the temperature variations by improving the thermostatic temperature control of the environment.

The causes of decorrelation between pre- and post-compressional signals should also be investigated. The theory relating collagen alignment and ultrasonic reflections was presented in Chapter 6. This theory could be supported by eliminating other causes of signal decorrelation throughout the entire sample thicknesses, such as decreasing the system noise and increasing the gain of the useful signals. An oscilloscope where the gain can be digitally programmed to vary across the signal (digital variable gain amplifier (DVGA)) or a system with two oscilloscopes operating at different gains could allow improved signal capture from the sample-actuator interfaces at the top and bottom, as well as better defined signals from reflectors inside the samples. The DVGA would require programming to provide suitable gains for the application and would require synchronisation with the pulser. Collagen alignment requires quantification to enable signal loss at different orientations to be rigorously compared. This could be achieved by conducting more T_2 magnetic resonance experiments in conjunction with more detailed reflection tracking in the pre- and post-compressional signals.

With respect to the phenomenological model, it would be more satisfactory to be able to perform experiments to obtain values for permeability and initial void fractions. This would eliminate the necessity to rely on published values, which were shown to vary considerably. Access to these values for articular cartilage from different species, at different sample conditions, or from different sample structures such as nasal tissue, would allow the model to be applied in a wider range of situations.

The model could be further developed by addressing the current assumptions which currently limit the experimental input to quasi-static loading protocols. Similarly the assumptions preventing application of the model in indentation conditions should be reviewed and adapted to allow the extraction of matrix constants from conditions closer to *in vivo* test configurations. The global stress field and subsequent interstitial fluid pressures would require more rigorous and complex characterisation.

In order to extend the existing work it would be necessary to characterise human articular cartilage tissue instead of bovine. This would allow a range of absolute values to be provided to tissue engineers. However, as such tests require significant resources and are subsequently governed by strict regulations, it would not be appropriate to advance to this stage before the method reliability had been suitably improved. Bovine articular cartilage has been useful in proving the capabilities of the method so far, but the depth-dependent matrix values would not necessarily be suitable design criteria for engineered tissue for humans.

The ultimate goal of providing an elastography method suitable for the characterisation of depth-dependent elastic properties of healthy, damaged or repair tissue *in vivo* could be realised with the identification of a suitable strain application method and measurement technique. In terms of providing a direct strain *in vivo*, indentation compression is the most suitable method. This would be relatively easy to model, however, would require application under arthroscopy and would also create problems in aligning the ultrasonic beam to provide the reflector positions from the strained region. There is literature evidence of a similar ultrasonic arthroscopic technique having been trialled, but only for the determination of sound speed information from the tissue (Suh et al. 2001). An alternative ultrasonic

technique which could possibly be adapted for application to cartilage characterisation is vibro-acoustic modulation (VAM), where an oscillating strain field is provided directly within the tissue using the application of a high amplitude, low frequency ultrasonic pulse (Renaud et al. 2008). A transmitting-receiving pair of high frequency ultrasonic transducers is used to obtain signals from different depths within the tissue. These signals are used to indirectly extract the resulting tissue strains. The ultrasonic results relate to a combination the local nonlinear properties (which have been reported for articular cartilage as material density, variations in bulk and shear moduli, porosity and fluid viscosity (Donskoy et al. 1997), rather than directly to the elastic properties (available through elastography). This method has the potential for application through the skin, however, an extensive study is likely to be required to characterise actual elastic properties from the non-linear signal shapes obtained from the beam mixing. The elastography results presented in this thesis could provide a good foundation for the cross-characterisation study. Additional problems, such as system calibration and knee joint geometry would also need to be addressed.

References

Adams, M. A., Kerin, A. J., Bhatia, L. S., Chakrabarty, G., and Dolan, P. 1999. Experimental determination of stress distributions in articular cartilage before and after sustained loading. *Clinical Biomechanics* **14** [2], 88-96

Agemura, D. H., Obrien, W. D., Olerud, J. E., Chun, L. E., and Eyre, D. E. 1990. Ultrasonic Propagation Properties of Articular-Cartilage at 100 Mhz. *Journal of the Acoustical Society of America* **87** [4], 1786-1791

Akizuki, S., Mow, V. C., Muller, F., Pita, J. C., Howell, D. S., and Manicourt, D. H. 1986. Tensile Properties of Human Knee-Joint Cartilage .1. Influence of Ionic Conditions, Weight Bearing, and Fibrillation on the Tensile Modulus. *Journal of Orthopaedic Research* **4** [4], 379-392

Anderson, H. C. and Sajdera, S. W. 1971. Fine Structure of Bovine Nasal Cartilage - Extraction As A Technique to Study Proteoglycans and Collagen in Cartilage Matrix. *Journal of Cell Biology* **49** [3], 650-&

Ando, W., Tateishi, K., Hart, D. A., Katakai, D., Tanaka, Y., Nakata, K., Hashimoto, J., Fujie, H., Shino, K., Yoshikawa, H., and Nakamura, N. 2007. Cartilage repair using an in vitro generated scaffold-free tissue-engineered construct derived from porcine synovial mesenchymal stem cells. *Biomaterials* **28** [36], 5462-5470

Arokoski, J. P. A., Hyttinen, M. M., Helminen, H. J., and Jurvelin, J. S. 1999. Biomechanical and structural characteristics of canine femoral and tibial cartilage. *Journal of Biomedical Materials Research* **48** [2], 99-107

Arokoski, J. P. A., Hyttinen, M. M., Lapvetelainen, T., Takacs, P., Kosztbaczky, B., Modis, L., Kovanen, V., and Helminen, H. J. 1996. Decreased birefringence of the superficial zone collagen network in the canine knee (stifle) articular cartilage after long distance running training, detected by quantitative polarised light microscopy. *Annals of the Rheumatic Diseases* **55** [4], 253-264

Ashraf, F. 2010. Comparison of two strain estimators for use in the field of elastography. UCL.

Aspden, R. M. and Hukins, D. W. L. 1981. Collagen Organization in Articular-Cartilage, Determined by X-Ray-Diffraction, and Its Relationship to Tissue Function. *Proceedings of the Royal Society of London Series B-Biological Sciences* **212** [1188], 299-304

Ateshian, G. A., Chahine, N. O., Basalo, I. M., and Hung, C. T. 2004. The correspondence between equilibrium biphasic and triphasic material properties in mixture models of articular cartilage. *Journal of Biomechanics* **37** [3], 391-400

Ateshian, G. A. and Hung, C. T. 2004. Functional properties of native articular cartilage. Guilak, F., Butler, D. L., Goldstein, S. A., and Mooney, D. Functional Tissue Engineering. **1** [4], 46-68 New York, Springer-Verlag.

Ateshian, G. A., Warden, W. H., Kim, J. J., Grelsamer, R. P., and Mow, V. C. 1997. Finite deformation biphasic material properties of bovine articular cartilage from confined compression experiments. *Journal of Biomechanics* **30** [11-12], 1157-1164

Bachrach, N. M., Valhmu, W. B., Stazzone, E., Ratcliffe, A., Lai, W. M., and Mow, V. C. 1995. Changes in proteoglycan synthesis of chondrocytes in articular cartilage are associated with the time-dependent changes in their mechanical environment. *Journal of Biomechanics* **28** [12], 1561-1569

Barker, M. K. and Seedhom, B. B. 2001. The relationship of the compressive modulus of articular cartilage with its deformation response to cyclic loading: does cartilage optimize its modulus so as to minimize the strains arising in it due to the prevalent loading regime? *Rheumatology* **40** [3], 274-284

Basalo, I. P., Mauck, R. L., Kelly, T. A. N., Nicoll, S. B., Chen, F. H., Hung, C. T., and Ateshian, G. A. 2004. Cartilage interstitial fluid load support in unconfined compression following enzymatic digestion. *Journal of Biomechanical Engineering-Transactions of the Asme* **126** [6], 779-786

Benninghoff, A. 1925. Form und Bau der Gelenkknorpel in ihren Beziehungen zur Funktion. Erste Mitteilung: Die modellierenden und formerhltenden Faktoren des Knorpelreliefs. *Zeitschrift fur die gesamte Anatomie* **76**, 43-63

Bilgen, M. and Insana, M. F. 1997b. Error analysis in acoustic elastography .2. Strain estimation and SNR analysis. *Journal of the Acoustical Society of America* **101** [2], 1147-1154

Bilgen, M. and Insana, M. F. 1997a. Error analysis in acoustic elastography .1. Displacement estimation. *Journal of the Acoustical Society of America* **101** [2], 1139-1146

Brocklehurst, R., Bayliss, M. T., Maroudas, A., Coysh, H. L., Freeman, M. A. R., Revell, P. A., and Ali, S. Y. 1984. The composition of normal and osteoarthritic articular cartilage from human knee joints. *Journal of Bone and Joint Surgery-American Volume* **66A** [1], 95-106

Broom, N. D. and Oloyede, A. 1998. The importance of physicochemical swelling in cartilage illustrated with a model hydrogel system. *Biomaterials* **19** [13], 1179-1188

Brown, R. A., Wiseman, M., Chuo, C. B., Cheema, U., and Nazhat, S. N. 2005. Ultrarapid engineering of biomimetic materials and tissues: Fabrication of nano- and microstructures by plastic compression. *Advanced Functional Materials* **15** [11], 1762-1770

Buckwalter, J. A. and Mankin, H. J. 1997. Articular cartilage .2. Degeneration and osteoarthrosis, repair, regeneration, and transplantation. *Journal of Bone and Joint Surgery-American Volume* **79A** [4], 612-632

Buschmann, M. D., Soulhat, J., Shirazi-Adl, A., Jurvelin, J. S., and Hunziker, E. B. 1998. Confined compression of articular cartilage: Linearity in ramp and sinusoidal tests and the importance of interdigitation and incomplete confinement. *Journal of Biomechanics* **31** [2], 171-178

Charlebois, M., Mckee, M. D., and Buschmann, M. D. 2004. Nonlinear tensile properties of bovine articular cartilage and their variation with age and depth. *Journal of Biomechanical Engineering-Transactions of the Asme* **126** [2], 129-137

Chen, A. C., Bae, W. C., Schinagl, R. M., and Sah, R. L. 2001. Depth- and strain-dependent mechanical and electromechanical properties of full-thickness bovine articular cartilage in confined compression. *Journal of Biomechanics* **34** [1], 1-12

Chen, Y., Chen, X., and Hisada, T. 2006. Non-linear finite element analysis of mechanical electrochemical phenomena in hydrated soft tissues based on triphasic theory. *International Journal for Numerical Methods in Engineering* **65** [2], 147-173

Clark, J. M. 1985. The Organization of Collagen in Cryofractured Rabbit Articular-Cartilage - A Scanning Electron-Microscopic Study. *Journal of Orthopaedic Research* **3** [1], 17-29

Cohn, N. A., Emelianov, S. Y., Lubinski, M. A., and ODonnell, M. 1997a. An elasticity microscope .1. Methods. *Ieee Transactions on Ultrasonics Ferroelectrics and Frequency Control* **44** [6], 1304-1319

Cohn, N. A., Emelianov, S. Y., and ODonnell, M. 1997b. An elasticity microscope .2. Experimental results. *Ieee Transactions on Ultrasonics Ferroelectrics and Frequency Control* **44** [6], 1320-1331

Cohn, N. A., Kim, B. S., Erkamp, R. Q., Mooney, D. J., Emelianov, S. Y., Skovoroda, A. R., and O'Donnell, M. 2000. High-resolution elasticity imaging for

tissue engineering. *Ieee Transactions on Ultrasonics Ferroelectrics and Frequency Control* **47** [4], 956-966

Darcy, H. 1856. Les Fontaines publiques de la ville de Dijon (The public fountains of the city of Dijon). **English translation by Patricia Bobeck (2004)** , Kendall/Hunt Publishing Co.

de Korte, C. L., van der Steen, A. F. W., Dijkman, B. H. J., and Lancee, C. T. 1997. Performance of time delay estimation methods for small time shifts in ultrasonic signals. *Ultrasonics* **35**, 263-274 , Elsevier.

DiSilvestro, M. R. and Suh, J. K. F. 2002. Biphasic poroviscoelastic characteristics of proteoglycan-depleted articular cartilage: Simulation of degeneration. *Annals of Biomedical Engineering* **30** [6], 792-800

DiSilvestro, M. R., Zhu, Q. L., and Suh, J. K. F. 2001a. Biphasic poroviscoelastic simulation of the unconfined compression of articular cartilage: II - Effect of variable strain rates. *Journal of Biomechanical Engineering-Transactions of the Asme* **123** [2], 198-200

DiSilvestro, M. R., Zhu, Q. L., Wong, M., Jurvelin, J. S., and Suh, J. K. F. 2001b. Biphasic poroviscoelastic simulation of the unconfined compression of articular cartilage: I - Simultaneous prediction of reaction force and lateral displacement. *Journal of Biomechanical Engineering-Transactions of the Asme* **123** [2], 191-197

Donskoy, D. M., Khashanah, K., and McKee Jr., T. G. 1997. Nonlinear acoustic waves in porous media in the context of Biot's theory. *Journal of the Acoustical Society of America* **102** [5], 2521-2528

Donzelli, P. S., Spilker, R. L., Ateshian, G. A., and Mow, V. C. 1999. Contact analysis of biphasic transversely isotropic cartilage layers and correlations with tissue failure. *Journal of Biomechanics* **32** [10], 1037-1047

Duda, G. N., Haisch, A., Endres, M., Gebert, C., Schroeder, D., Hoffmann, J. E., and Sittinger, M. 2000. Mechanical quality of tissue engineered cartilage: Results after 6 and 12 weeks in vivo. *Journal of Biomedical Materials Research* **53** [6], 673-677

Dunn, Timothy C., Lu, Ying, Jin, Hua, Ries, Michael D., and Majumdar, Sharmila. 2004. T2 Relaxation Time of Cartilage at MR Imaging: Comparison with Severity of Knee Osteoarthritis1. *Radiology* **232** [2], 592-598

Eckstein, F., Tieschky, M., Faber, S., Englmeier, K. H., and Reiser, M. 1999. Functional analysis of articular cartilage deformation, recovery, and fluid flow following dynamic exercise in vivo. *Anatomy and Embryology* **200** [4], 419-424

Ehlers, W. and Markert, B. 2001. A linear viscoelastic biphasic model for soft tissues based on the theory of porous media. *Journal of Biomechanical Engineering-Transactions of the Asme* **123** [5], 418-424

Elliott, D. M., Narmoneva, D. A., and Setton, L. A. 2002. Direct measurement of the Poisson's ratio of human patella cartilage in tension. *Journal of Biomechanical Engineering-Transactions of the Asme* **124** [2], 223-228

Erne, O. K., Reid, J. B., Ehmke, L. W., Sommers, M. B., Madey, S. M., and Bottlang, M. 2005. Depth-dependent strain of patellofemoral articular cartilage in unconfined compression. *Journal of Biomechanics* **38** [4], 667-672

Fortin, M., Buschmann, M. D., Bertrand, M. J., Foster, F. S., and Ophir, J. 2003. Dynamic measurement of internal solid displacement in articular cartilage using ultrasound backscatter. *Journal of Biomechanics* **36** [3], 443-447

Fortin, M., Soulhat, J., Shirazi-Adl, A., Hunziker, E. B., and Buschmann, M. D. 2000. Unconfined compression of articular cartilage: Nonlinear behavior and comparison with a fibril-reinforced biphasic model. *Journal of Biomechanical Engineering-Transactions of the Asme* **122** [2], 189-195

Fung, Y. C. 1993. Biomechanics: Mechanical Properties of Living Tissue. **2** New York, Springer.

Garcia, J. J. and Cortes, D. H. 2006. A nonlinear biphasic viscohyperelastic model for articular cartilage. *Journal of Biomechanics* **39** [16], 2991-2998

Garcia, J. J. and Cortes, D. H. 2007. A biphasic viscohyperelastic fibril-reinforced model for articular cartilage: Formulation and comparison with experimental data. *Journal of Biomechanics* **40** [8], 1737-1744

Gratz, K. R., Wong, V. W., Chen, A. C., Fortier, L. A., Nixon, A. J., and Sah, R. L. 2006. Biomechanical assessment of tissue retrieved after in vivo cartilage defect repair: tensile modulus of repair tissue and integration with host cartilage. *Journal of Biomechanics* **39** [1], 138-146

Grellmann, W., Berghaus, A., Haberland, E.-J., Jamali, Y., Holweg, K., Reincke, K., and Bierogel, C. 2006. Determination of strength and deformation behavior of human cartilage for the definition of significant parameters. *Journal of Biomedical Materials Research Part A* **78A** [1], 168-174

Gu, W. Y., Lai, W. M., and Mow, V. C. 1993. Transport of Fluid and Ions Through A Porous-Permeable Charged-Hydrated Tissue, and Streaming Potential Data on Normal Bovine Articular-Cartilage. *Journal of Biomechanics* **26** [6], 709-723

Guilak, F., Butler, D. L., Goldstein, S. A., and Mooney, D. 2003. Functional Tissue Engineering. Guilak, F., Butler, D. L., Goldstein, S. A., and Mooney, D. New York, Springer-Verlag.

Hadjipanayi, E., Brown, R. A., and Mudera, V. 2009. Interface integration of layered cottagen scaffolds with defined matrix stiffness: implications for sheet-based tissue engineering. *Journal of Tissue Engineering and Regenerative Medicine* **3** [3], 230-241

Hadjipanayi, E., Mudera, V., and Brown, R. A. 2010. Guiding cell migration in 3D: A collagen matrix with graded directional stiffness. *Cell Motility and the Cytoskeleton* **66** [3], 121-128 , 2009 Wiley-Liss, Inc., A Wiley Company.

Haider, M. A. and Schugart, R. C. 2006. A numerical method for the continuous spectrum biphasic poroviscoelastic model of articular cartilage. *Journal of Biomechanics* **39** [1], 177-183

Hardingham, T. E., Muir, H., Kwan, M. K., Lai, W. M., and Mow, V. C. 1987. Viscoelastic Properties of Proteoglycan Solutions with Varying Proportions Present As Aggregates. *Journal of Orthopaedic Research* **5** [1], 36-46

Hattori, K., Mori, K., Habata, T., Takakura, Y., and Ikeuchi, K. 2003. Measurement of the mechanical condition of articular cartilage with an ultrasonic probe: quantitative evaluation using wavelet transformation. *Clinical Biomechanics* **18** [6], 553-557

Hattori, K., Takakura, Y., Ishimura, M., Habata, T., Uematsu, K., and Ikeuch, K. 2004. Quantitative arthroscopic ultrasound evaluation of living human cartilage. *Clinical Biomechanics* **19** [2], 213-216

Hayes, W. C., Herrmann, G., Mockros, L. F., and Keer, L. M. 1972. Mathematical-Analysis for Indentation Tests of Articular-Cartilage. *Journal of Biomechanics* **5** [5], 541-&

Herberhold, C., Faber, S., Stammberger, T., Steinlechner, M., Putz, R., Englmeier, K. H., Reiser, M., and Eckstein, F. 1999. In situ measurement of articular cartilage deformation in intact femoropatellar joints under static loading. *Journal of Biomechanics* **32** [12], 1287-1295

Hiroshi, M., Masakatsu, T., and Kozaburo, H. 1999. Tensile Tests of Collagen Fibrils of Approximately 1.MU.m Diameter. *Nihon Kikai Gakkai Nenji Taikai Koen Ronbunshu* **2**, 317-318

Hoyt, K., Forsberg, F., and Ophir, J. 2006. Comparison of shift estimation strategies in spectral elastography. *Ultrasonics* **44** [1], 99-108

Huang, C. Y., Mow, V. C., and Ateshian, G. A. 2001. The role of flow-independent viscoelasticity in the biphasic tensile and compressive responses of articular cartilage. *Journal of Biomechanical Engineering-Transactions of the Asme* **123** [5], 410-417

Huang, C. Y., Soltz, M. A., Kopacz, M., Mow, V. C., and Ateshian, G. A. 2003. Experimental verification of the roles of intrinsic matrix viscoelasticity and tension-compression nonlinearity in the biphasic response of cartilage. *Journal of Biomechanical Engineering-Transactions of the Asme* **125** [1], 84-93

Huckle, J., Dootson, G., Medcalf, N., McTaggart, S., Wright, E., Carter, A., Schreiber, R., Kirby, B., Dunkelman, N., Stevenson, S., Riley, S., Davisson, T., and Ratcliffe, A. 2003. Differentiated chondrocytes for cartilage tissue engineering. Tissue Engineering of Cartilage and Bone (Novartis Foundation Symposium 249). 103-117 Chichester, Wiley.

Hunziker, E. B. 1999. Biologic repair of articular cartilage - Defect models in experimental animals and matrix requirements. *Clinical Orthopaedics and Related Research* [367], S135-S146

Hunziker, E. B., Quinn, T. M., and Hauselmann, H. J. 2002. Quantitative structural organization of normal adult human articular cartilage. *Osteoarthritis and Cartilage* **10** [7], 564-572

Jones, W. R., Ting-Beall, H. P., Lee, G. M., Kelley, S. S., Hochmuth, R. M., and Guilak, F. 1999. Alterations in the Young's modulus and volumetric properties of chondrocytes isolated from normal and osteoarthritic human cartilage. *Journal of Biomechanics* **32** [2], 119-127

Julkunen, P., Kiviranta, P., Wilson, W., Jurvelin, J. S., and Korhonen, R. K. 2007. Characterization of articular cartilage by combining microscopic analysis with a fibril-reinforced finite-element model. *Journal of Biomechanics* **40** [8], 1862-1870

Julkunen, P., Korhonen, R. K., Nissi, M. J., and Jurvelin, J. S. 2008a. Mechanical characterization of articular cartilage by combining magnetic resonance imaging and finite-element analysis - a potential functional imaging technique. *Physics in Medicine and Biology* **53** [9], 2425-2438

Julkunen, P., Wilson, W., Jurvelin, J. S., Rieppo, J., Qu, C. J., Lammi, M. J., and Korhonen, R. K. 2008b. Stress-relaxation of human patellar articular cartilage in unconfined compression: Prediction of mechanical response by tissue composition and structure. *Journal of Biomechanics* **41** [9], 1978-1986

Jurvelin, J. S., Buschmann, M. D., and Hunziker, E. B. 2003. Mechanical anisotropy of the human knee articular cartilage in compression. *Proceedings of the*

Institution of Mechanical Engineers - H **217** [3], 215-219 , Professional Engineering Publishing Ltd.

Jurvelin, J. S., Rasanen, T., Kolmonen, P., and Lyyra, T. 1995. Comparison of Optical, Needle Probe and Ultrasonic Techniques for the Measurement of Articular-Cartilage Thickness. *Journal of Biomechanics* **28** [2], 231-235

Kaab, M. J., Gwynn, I. A., and Notzli, H. P. 1998. Collagen fibre arrangement in the tibial plateau articular cartilage of man and other mammalian species. *Journal of Anatomy* **193**, 23-34

Khaled, W., Reichling, S., Bruhns, O. T., and Ermert, H. 2006. Ultrasonic strain imaging and reconstructive elastography for biological tissue. *Ultrasonics* **44**, E199-E202

Kiviranta, P., Rieppo, J., Korhonen, R. K., Julkunen, P., Toyras, J., and Jurvelin, J. S. 2006. Collagen network primarily controls Poisson's ratio of bovine articular cartilage in compression. *Journal of Orthopaedic Research* **24** [4], 690-699

Klein, T. J., Chaudhry, M., Bae, W. C., and Sah, R. L. 2007. Depth-dependent biomechanical and biochemical properties of fetal, newborn, and tissue-engineered articular cartilage. *Journal of Biomechanics* **40** [1], 182-190

Konofagou, E. E. 2004. Quo vadis elasticity imaging? *Ultrasonics* **42** [1-9], 331-336

Konofagou, E. E., Varghese, T., and Ophir, J. 2000. Spectral estimators in elastography. *Ultrasonics* **38** [1-8], 412-416

Konofagou, E. E., Varghese, T., Ophir, J., and Alam, S. K. 1999. Power spectral strain estimators in elastography. *Ultrasound in Medicine and Biology* **25** [7], 1115-1129

Korhonen, R. K., Julkunen, P., Wilson, W., and Herzog, W. 2008. Importance of collagen orientation and depth-dependent fixed charge densities of cartilage on mechanical behavior of chondrocytes. *Journal of Biomechanical Engineering-Transactions of the Asme* **130** [2]

Laasanen, M. S., Saarakkala, S., Toyras, J., Rieppo, J., and Jurvelin, J. S. 2005. Site-specific ultrasound reflection properties and superficial collagen content of bovine knee articular cartilage. *Physics in Medicine and Biology* **50** [14], 3221-3233

Laasanen, M. S., Toyras, J., Vasara, A., Saarakkala, S., Hyttinen, M. M., Kiviranta, I., and Jurvelin, J. S. 2006. Quantitative ultrasound imaging of spontaneous repair of porcine cartilage. *Osteoarthritis and Cartilage* **14** [3], 258-263

Lai, W. M., Hou, J. S., and Mow, V. C. 1991. A Triphasic Theory for the Swelling and Deformation Behaviors of Articular-Cartilage. *Journal of Biomechanical Engineering-Transactions of the Asme* **113** [3], 245-258

Lai, W. M. and Mow, V. C. 1980. Drag induced compression of articular cartilage during a permeation experiment. *Biorheology* **17**, 111-123

Langeland, S., D'Hooge, J., Torp, H., Bijnens, B., and Suetens, P. 2003. Comparison of time-domain displacement estimators for two-dimensional rf tracking. *Ultrasound in Medicine and Biology* **29** [8], 1177-1186

Langelier, E. and Buschmann, M. D. 2003. Increasing strain and strain rate strengthen transient stiffness but weaken the response to subsequent compression for articular cartilage in unconfined compression. *Journal of Biomechanics* **36** [6], 853-859

Langsjo, T. K., Hyttinen, M., Pelttari, A., Kiraly, K., Arokoski, J., and Helminen, H. J. 1999. Electron microscopic stereological study of collagen fibrils in bovine articular cartilage: volume and surface densities are best obtained indirectly (from length densities and diameters) using isotropic uniform random sampling. *Journal of Anatomy* **195**, 281-293

Langsjo, T. K., Rieppo, J., Pelttari, A., Oksala, N., Kovanen, V., and Helminen, H. J. 2002. Collagenase-induced changes in articular cartilage as detected by electron-microscopic stereology, quantitative polarized light microscopy and biochemical assays. *Cells Tissues Organs* **172** [4], 265-275

Langworthy, M. J., Nelson, F. R. T, and Coutts, R. D. 2004. Basic Science. Cole, B. J. and Malek, M. M. Articular cartilage lesions: A practical guide to assessment and treatment. [1] New York, Springer-Verlag.

Lee, J. H., Kisiday, J., and Grodzinsky, A. J. 2003. Tissue-engineered versus native cartilage: linkage between cellular mechano-transduction and biomechanical properties. Tissue Engineering of Cartilage and Bone (Novartis Foundation Symposium 249). 52-69 Chichester, Wiley.

Li, L. P., Buschmann, M. D., and Shirazi-Adl, A. 2000. A fibril reinforced nonhomogeneous poroelastic model for articular cartilage: inhomogeneous response in unconfined compression. *Journal of Biomechanics* **33** [12], 1533-1541

Li, L. P., Buschmann, M. D., and Shirazi-Adl, A. 2002a. The role of fibril reinforcement in the mechanical behavior of cartilage. *Biorheology* **39** [1-2], 89-96

Li, L. P., Buschmann, M. D., and Shirazi-Adl, A. 2003a. Strain-rate dependent stiffness of articular cartilage in unconfined compression. *Journal of Biomechanical Engineering-Transactions of the Asme* **125** [2], 161-168

Li, L. P., Herzog, W., Korhonen, R. K., and Jurvelin, J. S. 2005. The role of viscoelasticity of collagen fibers in articular cartilage: axial tension versus compression. *Medical Engineering & Physics* **27** [1], 51-57

Li, L. P., Korhonen, R. K., Iivarinen, J., Jurvelin, J. S., and Herzog, W. 2008. Fluid pressure driven fibril reinforcement in creep and relaxation tests of articular cartilage. *Medical Engineering & Physics* **30** [2], 182-189

Li, L. P., Shirazi-Adl, A., and Buschman, M. D. 2002b. Alterations in mechanical behaviour of articular cartilage due to changes in depth varying material properties - A nonhomogeneous poroelastic model study. *Computer Methods in Biomehanics and Biomedical Engineering* **5** [1], 45-52 , Taylor & Francis.

Li, L. P., Shirazi-Adl, A., and Buschmann, M. D. 2003b. Investigation of mechanical behavior of articular cartilage by fibril reinforced poroelastic models. *Biorheology* **40** [1-3], 227-233

Lindahl, A., Brittberg, M., and Peterson, L. 2003. Cartilage repair with chondrocytes: clinical and cellular aspects. Tissue Engineering of Cartilage and Bone (Novartis Foundation Symposium 249). 175-189 Chichester, Wiley.

Ling, H. Y., Zheng, Y. P., and Patil, S. G. 2007. Strain dependence of ultrasound speed in bovine articular cartilage under compression in vitro. *Ultrasound in Medicine and Biology* **33** [10], 1599-1608

Lipshitz, H., Etheridge, R., and Glimcher, M. J. 1976. Changes in hexosamine content and swelling ratio of articular cartilage as a function of depth from the surface. *Journal of Bone and Joint Surgery-American Volume* **58A**, 1149-1153

Lohmander, L. S. 2003. Tissue engineering of cartilage: do we need it, can we do it, is it good and can we prove it? Tissue Engineering of Cartilage and Bone (Novartis Foundation Symposium 249). 2-16 Chichester, Wiley.

Lopez, O., Amrami, K. K., Manduca, A., and Ehman, R. L. 2008. Characterization of the dynamic shear properties of hyaline cartilage using high-frequency dynamic MR elastography. *Magnetic Resonance in Medicine* **59** [2], 356-364

Lu, X. L. and Mow, V. C. 2008. Biomechanics of articular cartilage and determination of material properties. *Medicine and Science in Sports and Exercise* **40** [2], 193-199

Ma, P. X., Schloo, B., Mooney, D., and Langer, R. 1995. Development of Biomechanical Properties and Morphogenesis of In-Vitro Tissue Engineered Cartilage. *Journal of Biomedical Materials Research* **29** [12], 1587-1595

Mansour, J. M. and Mow, V. C. 1976. Permeability of Articular-Cartilage Under Compressive Strain and at High-Pressures. *Journal of Bone and Joint Surgery-American Volume* **58** [4], 509-516

Maroudas, A. 1979. Adult Articular Cartilage. Freeman, M. A. R. Adult Articular Cartilage. **2**, 215-290 Tunbridge Wells, England, Pitman Medical.

Maroudas, A., Bullough, P., Swanson, S. A. V., and Freeman, M. A. R. 1968. The permeability of articular cartilage. *The Journal of Bone and Joint Surgery* **50B** [1], 166-177

Memarzadeh, K. 2009. Compressed collagen constructs for cartilage tissue engineering. Dept. Mechanical Engineering, University College London.

Miyata, S., Tateishi, T., Furukawa, K., and Ushida, T. 2005. Influence of structure and composition on dynamic viscoelastic property of cartilaginous tissue: Criteria for classification between hyaline cartilage and fibrocartilage based on mechanical function. *Jsme International Journal Series C-Mechanical Systems Machine Elements and Manufacturing* **48** [4], 547-554

Mlynarik, V., Szomolanyi, P., Toffanin, R., Vittur, F., and Trattnig, S. 2004. Transverse relaxation mechanisms in articular cartilage. *Journal of Magnetic Resonance* **169** [2], 300-307

Moretti, M., Wendt, D., Schaefer, D., Jakob, M., Hunziker, E. B., Heberer, M., and Martin, I. 2005. Structural characterization and reliable biomechanical assessment of integrative cartilage repair. *Journal of Biomechanics* **38** [9], 1846-1854

Morita, Y., Tomita, N., Aoki, H., Wakitani, S., Tamada, Y., Suguro, T., and Ikeuchi, K. 2003. Evaluation of dynamic visco-elastic properties during cartilage regenerating process in vitro. *Bio-Medical Materials and Engineering* **13** [4], 345-353

Mow, V. and Guo, X. E. 2002. Mechano-electrochemical properties of articular cartilage: Their inhomogeneities and anisotropies. *Annual Review of Biomedical Engineering* **4**, 175-209

Mow, V. C., Zhu, W., and Ratcliffe, A. 1991. Structure and function of articular cartilage and meniscus. Mow, V. C. and Hayes, W. C. Basic Orthopaedic Biomechanics. 143-198 New York, Raven Press.

Muir, I. H. M. 1979. Biochemistry. Freeman, M. A. R. Adult Articular Cartilage. 145-214 London, Pitman Medical.

Murakami, T., Sakai, N., Sawae, Y., Tanaka, K., and Ihara, M. 2004. Influence of proteoglycan on time-dependent mechanical behaviors of articular cartilage under

constant total compressive deformation. *Jsme International Journal Series C-Mechanical Systems Machine Elements and Manufacturing* **47** [4], 1049-1055

Neu, C. P. and Walton, J. H. 2008. Displacement encoding for the measurement of cartilage deformation. *Magnetic Resonance in Medicine* **59** [1], 149-155

Nguyen, T. and Oloyede, A. 2001. Predictive rheological models for the consolidation behaviour of articular cartilage under static loading. *Proceedings of the Institution of Mechanical Engineers Part H-Journal of Engineering in Medicine* **215** [H6], 565-577

Nieminen, H. J., Saarakkala, S., Laasanen, M. S., Hirvonen, J., Jurvelin, J. S., and Toyras, J. 2004. Ultrasound attenuation in normal and spontaneously degenerated articular cartilage. *Ultrasound in Medicine and Biology* **30** [4], 493-500

Nieminen, M. T., Rieppo, J., Toyras, J., Hakumaki, J. M., Silvennoinen, J., Hyttinen, M. M., Helminen, H. J., and Jurvelin, J. S. 2001. T-2 relaxation reveals spatial collagen architecture in articular cartilage: A comparative quantitative MRI and polarized light microscopic study. *Magnetic Resonance in Medicine* **46** [3], 487-493

Nissi, M. J., Rieppo, J., Toyras, J., Laasanen, M. S., Kiviranta, I., Jurvelin, J. S., and Nieminen, M. T. 2006. T-2 relaxation time mapping reveals age- and species-related diversity of collagen network architecture in articular cartilage. *Osteoarthritis and Cartilage* **14** [12], 1265-1271

O'Byrne, E., Pellas, T., and Laurent, D. 2003. Qualitative and quantitative in vivo assessment of articular cartilage using magnetic resonance imaging. Tissue Engineering of Cartilage and Bone (Novartis Foundation Symposium 249). 190-202 Chichester, Wiley.

Obradovic, B., Martin, I., Padera, R. F., Treppo, S., Freed, L. E., and Vunjak-Novakovic, G. 2001. Integration of engineered cartilage. *Journal of Orthopaedic Research* **19** [6], 1089-1097

Oloyede, A. and Broom, N. D. 1993. A Physical Model for the Time-Dependent Deformation of Articular-Cartilage. *Connective Tissue Research* **29** [4], 251-261

Olsen, S and Oloyede, A. 2002. A finite element analysis methodology for representing the articular cartilage functional structure. *Computer Methods in Biomehanics and Biomedical Engineering* **5** [6], 377-386

Olsen, S, Oloyede, A., and Adam, C. 2004. A finite element formulation and program to study transient swelling and load-carriage in healthy and degenerate articular cartilage. *Computer Methods in Biomehanics and Biomedical Engineering* **7** [2], 111-120

Olympus NDT. 2006. Ultrasonic transducers technical notes. Olympus NDT.

Ophir, J., Cespedes, I., Ponnekanti, H., Yazdi, Y., and Li, X. 1991. Elastography - A Quantitative Method for Imaging the Elasticity of Biological Tissues. *Ultrasonic Imaging* **13** [2], 111-134

Ostergaard, K., Petersen, J., Andersen, C. B., Bendtzen, K., and Salter, D. M. 1997. Histologic/histochemical grading system for osteoarthritic articular cartilage - Reproducibility and validity. *Arthritis and Rheumatism* **40** [10], 1766-1771

Outerbridge, R. E. 1961. The Etiology of Chondromalacia Patellae. *Journal of Bone and Joint Surgery - British Volume* **43-B** [4], 752-757

Park, S. and Ateshian, G. A. 2006. Dynamic response of immature bovine articular cartilage in tension and compression, and nonlinear viscoelastic modeling of the tensile response. *Journal of Biomechanical Engineering-Transactions of the Asme* **128** [4], 623-630

Park, S., Hung, C. T., and Ateshian, G. A. 2004. Mechanical response of bovine articular cartilage under dynamic unconfined compression loading at physiological stress levels. *Osteoarthritis and Cartilage* **12** [1], 65-73

Park, S., Nicoll, S. B., Mauck, R. L., and Ateshian, G. A. 2008. Cartilage mechanical response under dynamic compression at physiological stress levels following collagenase digestion. *Annals of Biomedical Engineering* **36** [3], 425-434

Patil, S. G. and Zheng, Y. P. 2004. Measurement of ultrasound speed of articular cartilage in variable conditions. *Proceedings of the 26Th Annual International Conference of the Ieee Engineering in Medicine and Biology Society, Vols 1-7* **26**, 1341-1344

Patil, S. G., Zheng, Y. P., Wu, J. Y., and Shi, J. 2004. Measurement of depth-dependence and anisotropy of ultrasound speed of bovine articular cartilage in vitro. *Ultrasound in Medicine and Biology* **30** [7], 953-963

Pavesio, A., Abatangelo, G., Borrione, A., Brocchetta, D., Hollander, A. P., Kon, E., Torasso, F., Zanasi, S., and Marcacci, M. 2003. Hyaluronan-based scaffolds (Hyalograft (R) C) in the treatment of knee cartilage defects: preliminary clinical findings. Tissue Engineering of Cartilage and Bone (Novartis Foundation Symposium 249). 203-217 Chichester, Wiley.

Pellaumail, B., Dewailly, V., Watrin, A., Loeuille, D., Netter, P., Berger, G., and Saied, A. 1999. Attenuation coefficient and speed of sound in immature and mature rat cartilage: a study in the 30-70 MHz frequency range. *1999 Ieee Ultrasonics Symposium Proceedings, Vols 1 and 2* , 1361-1364

Pellaumail, B., Loeuille, D., Watrin, A., Netter, P., Berger, G., and Saied, A. 1998. Correlation of high frequency ultrasound backscatter with cartilage matrix constituents. *1998 Ieee Ultrasonics Symposium - Proceedings, Vols 1 and 2* , 1463-1466

Qin, L., Zheng, Y. P., Leung, C. T., Mak, A., Choy, W. Y., and Chan, K. M. 2002. Ultrasound detection of trypsin-treated articular cartilage: its association with cartilaginous proteoglycans assessed by histological and biochemical methods. *Journal of Bone and Mineral Metabolism* **20** [5], 281-287

Rammohan, J and Eppell, S. J. 2002. The Effect of Pepsin Digestion on Type II Collagen Monomers. *Microscopic Microanalysis* **8** [Supplement 2], 1018CD-1019CD , Microscopy Society of America.

Renaud, G., Calle, S., Remenieras, J.-P., and Defontaine, M. 2008. Non-linear acoustic measurements to assess crack density in trabecular bone. *International Journal of Non-Linear Mechanics* **43**, 194-200

Riches, P. E., Dhillon, N., Lotz, J., Woods, A. W., and McNally, D. S. 2002. The internal mechanics of the invertebral disc under cyclic loading. *Journal of Biomechanics* **35**, 1263-1271 , Elsevier Science.

Rieppo, J., Toyras, J., Nieminen, M. T., Kovanen, V., Hyttinen, M. M., Korhonen, R. K., Jurvelin, J. S., and Helminen, H. J. 2003. Structure-function relationships in enzymatically modified articular cartilage. *Cells Tissues Organs* **175** [3], 121-132

Risbud, M. V. and Sittinger, M. 2002. Tissue engineering: advances in in vitro cartilage generation. *Trends in Biotechnology* **20** [8], 351-356

Rybicki, E. F., Glaeser, W. A., Strenkowski, J. S., and Tamm, M. A. 1979. Effects of cartilage stiffness and viscosity on a nonporous compliant bearing lubrication model for living joints. *Journal of Biomechanics* **12** [6], 403-409

Sasaki, N. and Odajima, S. 1996. Stress-strain curve and Young's modulus of a collagen molecule as determined by the X-ray diffraction techniques. *Journal of Biomechanics* **29** [5], 655-658

Satter, A., Iqbal, G. M., and Buchwalter, J. L. 2007. Practical enhanced reservoir engineering. Tulsa, Oklahoma, PennWell Corporation.

Schinagl, R. M., Gurskis, D., Chen, A. C., and Sah, R. L. 1997. Depth-dependent confined compression modulus of full-thickness bovine articular cartilage. *Journal of Orthopaedic Research* **15** [4], 499-506

Setton, L. A., Zhu, W. B., and Mow, V. C. 1993. The Biphasic Poroviscoelastic Behavior of Articular-Cartilage - Role of the Surface Zone in Governing the Compressive Behavior. *Journal of Biomechanics* **26** [4-5], 581-592

Silvast, T. S., Jurvelin, J. S., Lammi, M. J., and Toyras, J. 2009. pQCT study on diffusion and equilibrium distribution of iodinated anionic contrast agent in human articular cartilage - associations to matrix composition and integrity. *Osteoarthritis and Cartilage* **17** [1], 26-32

Simon, B. R., Coats, R. S., and Woo, S. L. Y. 1984. Relaxation and creep quasilinear viscoelastic models for normal articular cartilage. *Journal of Biomechanical Engineering* **106**, 159-169

Souchon, R., Hervieu, V., Gelet, A., Ophir, J., and Chapelon, J. Y. 2003. Human prostate elastography: in vitro study. *2003 Ieee Ultrasonics Symposium Proceedings, Vols 1 and 2* , 1251-1253

Soulhat, J., Buschmann, M. D., and Shirazi-Adl, A. 1999. A fibril-network-reinforced biphasic model of cartilage in unconfined compression. *Journal of Biomechanical Engineering-Transactions of the Asme* **121** [3], 340-347

Spirt, A. A., Mak, A. F., and Wassell, R. P. 1989. Nonlinear Viscoelastic Properties of Articular-Cartilage in Shear. *Journal of Orthopaedic Research* **7** [1], 43-49

Suan, J. C., Chhem, R. K., Gati, J. S., Norley, C. J., and Holdsworth, D. W. 2005. 4 T MRI of chondrocalcinosis in combination with three-dimensional CT, radiography, and arthroscopy: a report of three cases. *Skeletal Radiology* **34** [11], 714-721

Suh, J. K., Li, Z. F., and Woo, S. L. Y. 1995. Dynamic Behavior of A Biphasic Cartilage Model Under Cyclic Compressive Loading. *Journal of Biomechanics* **28** [4], 357-364

Suh, J. K. F., Youn, I., and Fu, F. H. 2001. An in situ calibration of an ultrasound transducer: a potential application for an ultrasonic indentation test of articular cartilage. *Journal of Biomechanics* **34** [10], 1347-1353

Sun, D. D., Guo, X. E., Likhitpanichkul, M., Lai, W. M., and Mow, V. C. 2004a. The influence of the fixed negative charges on mechanical and electrical behaviors of articular cartilage under unconfined compression. *Journal of Biomechanical Engineering-Transactions of the Asme* **126** [1], 6-16

Sun, Yu Long, Luo, Zong Ping, Fertala, Andrzej, and An, Kai Nan. 2004b. Stretching type II collagen with optical tweezers. *Journal of Biomechanics* **37** [11], 1665-1669

Tombs, M. P. and Peacocke, A. R. 1974. The Osmotic Pressure of Biological Macromolecules. Oxford, UK, Clarendon Press.

Toyras, J., Laasanen, M. S., Saarakkala, S., Lammi, M. J., Rieppo, J., Kurkijarvi, J., Lappalainen, R., and Jurvelin, J. S. 2003. Speed of sound in normal and degenerated bovine articular cartilage. *Ultrasound in Medicine and Biology* **29** [3], 447-454

Toyras, J., Rieppo, J., Nieminen, M. T., Helminen, H. J., and Jurvelin, J. S. 1999. Characterization of enzymatically induced degradation of articular cartilage using high frequency ultrasound. *Physics in Medicine and Biology* **44** [11], 2723-2733

Turgay, E., Salcudean, S., and Rohling, R. 2006. Identifying the mechanical properties of tissue by ultrasound strain imaging. *Ultrasound in Medicine and Biology* **32** [2], 221-235

Varghese, T., Konofagou, E. E., Ophir, J., Alam, S. K., and Bilgen, M. 2000. Direct strain estimation in elastography using spectral cross-correlation. *Ultrasound in Medicine and Biology* **26** [9], 1525-1537

Varghese, T. and Ophir, J. 1997b. A theoretical framework for performance characterization of elastography: The strain filter. *Ieee Transactions on Ultrasonics Ferroelectrics and Frequency Control* **44** [1], 164-172

Varghese, T. and Ophir, J. 1996. Estimating tissue strain from signal decorrelation using the correlation coefficient. *Ultrasound in Medicine and Biology* **22** [9], 1249-1254

Varghese, T. and Ophir, J. 1997a. Enhancement of echo-signal correlation in elastography using temporal stretching. *Ieee Transactions on Ultrasonics Ferroelectrics and Frequency Control* **44** [1], 173-180

Viola, F. and Walker, W. F. 2003. A comparison of the performance of time-delay estimators in medical ultrasound. *Ieee Transactions on Ultrasonics Ferroelectrics and Frequency Control* **50** [4], 392-401

Volpi, M. and Katz, E. P. 1991. On the Adaptive Structures of the Collagen Fibrils of Bone and Cartilage. *Journal of Biomechanics* **24**, 67-77

Vunjak-Novakovic, G. 2003. The fundamentals of tissue engineering: scaffolds and bioreactors. Tissue Engineering of Cartilage and Bone (Novartis Foundation Symposium 249). 34-51 Chichester, Wiley.

Wan, L. and Li, G. A. 2007. The effect of permeability of cartilage superficial zone on the behavior of stress relaxation and creep of human ankle joint. *Proceeding of the Amse Summer Bioengineering Conference - 2007* , 353-354

Wang, C. C. B., Deng, J. M., Ateshian, G. A., and Hung, C. T. 2002. An automated approach for direct measurement of two-dimensional strain distributions within articular cartilage under unconfined compression. *Journal of Biomechanical Engineering-Transactions of the Asme* **124** [5], 557-567

Wang, Q., Zheng, Y. P., Qin, L., Huang, Q. H., Lam, W. L., Leung, G., Guo, X., and Lu, H. B. 2008. Real-time ultrasonic assessment of progressive proteoglycan depletion in articular cartilage. *Ultrasound in Medicine and Biology* **34** [7], 1085-1092

Wells, P. N. T. 1977. Biomedical Ultrasonics. London, Academic Press.

White, D., Evans, J. A., Truscott, J. G., and Chivers, R. A. 2007. Can ultrasound propagate in the joint space of a human knee? *Ultrasound in Medicine and Biology* **33** [7], 1104-1111

Wilson, W., Huyghe, J. M., and van Donkelaar, C. C. 2007. Depth-dependent compressive equilibrium properties of articular cartilage explained by its composition. *Biomechanics and Modeling in Mechanobiology* **6** [1-2], 43-53

Wilson, W., Huyghe, J. M., and van Donkelaar, C. C. 2006. A composition-based cartilage model for the assessment of compositional changes during cartilage damage and adaptation. *Osteoarthritis and Cartilage* **14** [6], 554-560

Wilson, W., van Donkelaar, C. C., van Rietbergen, B., and Huiskes, R. 2005a. A fibril-reinforced poroviscoelastic swelling model for articular cartilage. *Journal of Biomechanics* **38** [6], 1195-1204

Wilson, W., van Donkelaar, C. C., van Rietbergen, B., Ito, K., and Huiskes, R. 2004. Stresses in the local collagen network of articular cartilage: a poroviscoelastic fibril-reinforced finite element study. *Journal of Biomechanics* **37** [3], 357-366

Wilson, W., van Donkelaar, C. C., van Rietbergen, B., Ito, K., and Huiskes, R. 2005b. Stresses in the local collagen network of articular cartilage: a poroviscoelastic fibril-reinforced finite element study (vol 37, pg 357, 2004). *Journal of Biomechanics* **38** [10], 2138-2140

Wong, M. and Carter, D. R. 2003. Articular cartilage functional histomorphology and mechanobiology: a research perspective. *Bone* **33** [1], 1-13

Wong, M., Wuethrich, P., Buschmann, M. D., Eggli, P., and Hunziker, E. 1997. Chondrocyte biosynthesis correlates with local tissue strain in statically compressed adult articular cartilage. *Journal of Orthopaedic Research* **15** [2], 189-196

Wu, J. Z. and Herzog, W. 2002. Elastic anisotropy of articular cartilage is associated with the microstructures of collagen fibers and chondrocytes. *Journal of Biomechanics* **35** [7], II

Xia, Y., Moody, J. B., and Alhadlaq, H. 2002. Orientational dependence of T-2 relaxation in articular cartilage: A microscopic MRI (mu MRI) study. *Magnetic Resonance in Medicine* **48** [3], 460-469

Zheng, Y. P., Bridal, S. L., Shi, J., Saied, A., Lu, M. H., Jaffre, B., Mak, A. F. T., and Laugier, P. 2004. High resolution ultrasound elastomicroscopy imaging of soft tissues: system development and feasibility. *Physics in Medicine and Biology* **49** [17], 3925-3938

Zheng, Y. P., Ding, C. X., Bai, J., Mak, A. F. T., and Qin, L. 2001. Measurement of the layered compressive properties of trypsin-treated articular cartilage: an ultrasound investigation. *Medical & Biological Engineering & Computing* **39** [5], 534-541

Zheng, Y. P. and Mak, A. F. T. 1996. An ultrasound indentation system for biomechanical properties assessment of soft tissues in-vivo. *Ieee Transactions on Biomedical Engineering* **43** [9], 912-918

Zheng, Y. P., Mak, A. F. T., and Lau, K. P. 2002a. Ultrasound measurement of depth-dependent strains of articular cartilage compression. Maev, R. Gr. Acoustical Imaging. [26], 111-119 , Kluwer Academic / Plenum Publishers.

Zheng, Y. P., Mak, A. F. T., Lau, K. P., and Qin, L. 2002b. An ultrasonic measurement for in vitro depth-dependent equilibrium strains of articular cartilage in compression. *Physics in Medicine and Biology* **47** [17], 3165-3180

Zheng, Y. P., Niu, H. J., Mak, F. T. A., and Huang, Y. P. 2005. Ultrasonic measurement of depth-dependent transient behaviors of articular cartilage under compression. *Journal of Biomechanics* **38** [9], 1830-1837

Zhu, W. B., Iatridis, J. C., Hlibczuk, V., Ratcliffe, A., and Mow, V. C. 1996. Determination of collagen-proteoglycan interactions in vitro. *Journal of Biomechanics* **29** [6], 773-783

A. Calibration of the test equipment

i. Actuator

The actual movement of the actuator was compared to the programmed movement using time of flight analysis of the actuator tip in distilled water. The Perspex delay-line was added and the tests repeated again to check this caused no difference.

Method

The distilled water was at room temperature 21 ± 0.05 °C.

The actuator was programmed to move in several increments of decreasing magnitude (1, 0.5, 0.1 and 0.01 mm).

Results

20 MHz water 1 mm

	Time (μs)	Time(s)	Double distance (m)	Distance (mm)
start	36.93	3.693E-5	0.0281	
1	35.62	3.562E-5	0.0271	**0.9939**
1	34.29	3.429E-5	0.0261	**1.0105**
1	32.96	3.296E-5	0.0251	**1.0112**
1	31.64	3.164E-5	0.0240	**1.0075**
			Average	**1.0058**
			Standard dev	**0.0081**
			% difference	**0.577**

20 MHz water plus Perspex 1 mm

	Time (μs)	Time(s)	Double distance (m)	Distance (mm)
start	32.38	3.238E-5	0.0246	
1	31.06	3.106E-5	0.0236	**1.0048**
1	29.73	2.973E-5	0.0226	**1.0078**
1	28.41	2.841E-5	0.0216	**1.0047**
1	27.10	2.710E-5	0.0206	**0.9941**
			Average	**1.0028**
			Standard dev	**0.0060**
			% difference	**0.282**

The percentage differences for both circumstances were calculated from the difference between the input and the output. For example, the programmed distance to move was 1 mm. In water it was found to move by 1.0058 mm, causing the percentage difference between input and output over 5 moves to be 0.577%.

20 MHz water 0.5 mm

	Time (μs)	Time(s)	Double distance (m)	Distance (mm)
start	36.93	3.693E-5	0.0281	
0.5	36.28	3.628E-5	0.0276	**0.4969**
0.5	35.65	3.565E-5	0.0271	**0.4777**
0.5	34.95	3.495E-5	0.0266	**0.5315**
0.5	34.29	3.429E-5	0.0261	**0.5059**
0.5	33.62	3.362E-5	0.0256	**0.5046**
0.5	32.96	3.296E-5	0.0250	**0.5039**
0.5	32.29	3.229E-5	0.0245	**0.5057**
0.5	31.63	3.163E-5	0.0240	**0.5040**
			Average	**0.5038**
			Standard dev	**0.0147**
			% difference	**0.7532**

20 MHz water plus Perspex 0.5 mm

	Time (μs)	Time(s)	Double distance (m)	Distance (mm)
start	32.38	3.238E-5	0.0246	
0.5	31.72	3.172E-5	0.0241	**0.4978**
0.5	31.06	3.106E-5	0.0236	**0.5039**
0.5	30.40	3.040E-5	0.0231	**0.5031**
0.5	29.74	2.974E-5	0.0226	**0.5031**
0.5	29.07	2.907E-5	0.0221	**0.5039**
0.5	28.41	2.841E-5	0.0216	**0.5024**
0.5	27.75	2.775E-5	0.0211	**0.5031**
0.5	27.10	2.710E-5	0.0206	**0.4955**
			Average	**0.5016**
			Standard dev	**0.0031**
			% difference	**0.3200**

A smaller percentage difference was found through the Perspex delay-line. This is likely to be due to the sound moving faster through this region, thus causing smaller changes between the flight times of the signals recorded before and after the moves. This could make it harder to detect an error.

20 MHz water 0.1 mm

	Time (μs)	Time(s)	Double distance (m)	Distance (mm)
start	36.93	3.693E-05	0.0281	
0.1	36.80	3.680E-05	0.0280	**0.0965**
0.1	36.67	3.667E-05	0.0279	**0.1018**
0.1	36.54	3.654E-05	0.0278	**0.1010**
0.1	36.40	3.640E-05	0.0277	**0.1028**
0.1	36.27	3.627E-05	0.0276	**0.1001**
0.1	36.14	3.614E-05	0.0275	**0.0982**
0.1	36.01	3.601E-05	0.0274	**0.1006**
0.1	35.87	3.587E-05	0.0273	**0.1028**
0.1	35.74	3.574E-05	0.0272	**0.1007**
0.1	35.61	3.561E-05	0.0271	**0.1009**
			Average	**0.1005**
			Standard dev	**0.0019**
			% difference	**0.5480**

20 MHz water plus Perspex 0.1 mm

	Time (μs)	Time(s)	Double distance (m)	Distance (mm)
start	32.39	3.239E-05	0.0246	
0.1	32.26	3.226E-05	0.0245	**0.0973**
0.1	32.12	3.212E-05	0.0244	**0.1018**
0.1	31.99	3.199E-05	0.0243	**0.1018**
0.1	31.86	3.186E-05	0.0242	**0.1018**
0.1	31.72	3.172E-05	0.0241	**0.1003**
0.1	31.59	3.159E-05	0.0240	**0.1011**
0.1	31.46	3.146E-05	0.0239	**0.1011**
0.1	31.33	3.133E-05	0.0238	**0.1003**
0.1	31.19	3.119E-05	0.0237	**0.1011**
0.1	31.06	3.106E-05	0.0236	**0.1003**
			Average	**0.1007**
			Standard dev	**0.0014**
			% difference	**0.7000**

	Time (μs)	Time(s)	Double distance (m)	Distance (mm)
start	36.926	3.693E-05	0.0281	
0.01	36.919	3.692E-05	0.0281	**0.0053**
0.01	36.907	3.691E-05	0.0280	**0.0091**
0.01	36.896	3.690E-05	0.0280	**0.0087**
0.01	36.882	3.688E-05	0.0280	**0.0108**
0.01	36.869	3.687E-05	0.0280	**0.0097**
0.01	36.854	3.685E-05	0.0280	**0.0114**
0.01	36.841	3.684E-05	0.0280	**0.0097**
0.01	36.826	3.683E-05	0.0280	**0.0116**
0.01	36.807	3.681E-05	0.0280	**0.0144**
			Average	**0.0101**
			Standard dev	**0.0025**
			% difference	**0.9111**

	Time (μs)	Time(s)	Double distance (m)	Distance (mm)
start	32.379	3.238E-05	0.0246	
0.01	32.372	3.237E-05	0.0246	**0.0053**
0.01	32.359	3.236E-05	0.0246	**0.0095**
0.01	32.346	3.235E-05	0.0246	**0.0099**
0.01	32.333	3.233E-05	0.0246	**0.0100**
0.01	32.320	3.232E-05	0.0246	**0.0101**
0.01	32.307	3.231E-05	0.0246	**0.0099**
0.01	32.294	3.229E-05	0.0245	**0.0099**
0.01	32.281	3.228E-05	0.0245	**0.0099**
0.01	32.267	3.227E-05	0.0245	**0.0103**
0.01	32.254	3.225E-05	0.0245	**0.0103**
			Average	**0.0100**
			Standard dev	**0.0002**
			% difference	**0.2250**

The difference between the input and output increased as the programmed distance changed between 0.1 mm to 0.01 mm for the water results. For the Perspex, the difference decreased.

The percentage differences in the water and Perspex were averaged. In water, which were the more precise measurements, the average difference was 0.697%. In the Perspex, which is how the experiments were performed, the average difference was 0.382%. The accuracy of the actuator was found to be 99.3%.

The actuator position with respect to time for cycles performed in the same manner as the dynamic cyclic tests was assessed.

Method

The actuator was programmed to move over distances approximately equivalent to applying 2% and 8% strain to the samples (0.05 and 0.2 mm, respectively). This was repeated at frequencies of 1, 0.5 and 0.25 Hz. The actuator position with respect to time was recorded in a series of ultrasonic A-lines for 10 seconds.

Results

The results in the tables are shown for the first 5 s. The results on the graphs (Figures A-1 and A-2) show the full 10 s.

0.05 mm	1 Hz		0.5 Hz			0.25 Hz		
time (s)	**flight time difference (us)**	**actuator move distance (mm)**	**time (s)**	**flight time difference (us)**	**actuator move distance (mm)**	**time (s)**	**flight time difference (us)**	**actuator move distance (mm)**
0.2503	4.447E-10	0.000327	0.2500	4.065E-10	0.000299	0.2505	-2.737E-10	-0.0002
0.5010	3.46E-08	0.025434	0.5007	1.111E-08	0.008164	0.5008	4.3227E-09	0.003177
0.7510	6.839E-08	0.050268	0.7501	3.362E-08	0.024708	0.7505	1.1011E-08	0.008093
1.0002	3.45E-08	0.025355	1.0006	5.996E-08	0.04407	1.0006	2.2269E-08	0.016367
1.2507	-6.72E-11	-4.9E-05	1.2510	6.772E-08	0.049773	1.2506	3.4215E-08	0.025148
1.5001	3.446E-08	0.025325	1.5005	5.919E-08	0.043506	1.5008	4.4375E-08	0.032615
1.7502	6.88E-08	0.050565	1.7505	3.463E-08	0.025454	1.7510	5.4907E-08	0.040357
2.0004	3.444E-08	0.025315	2.0003	1.175E-08	0.008639	2.0005	6.4038E-08	0.047068
2.2509	9.332E-10	0.000686	2.2508	3.491E-10	0.000257	2.2508	6.7705E-08	0.049763
2.5002	3.459E-08	0.025423	2.5006	1.127E-08	0.008284	2.5008	6.5125E-08	0.047867
2.7502	6.755E-08	0.049648	2.7504	3.384E-08	0.024872	2.7508	5.4986E-08	0.040415
3.0000	3.433E-08	0.025235	3.0001	5.890E-08	0.043293	3.0001	4.4757E-08	0.032897
3.2500	-4.88E-10	-0.00036	3.2501	6.805E-08	0.050015	3.2509	3.4529E-08	0.025379
3.5008	3.406E-08	0.025035	3.5007	5.953E-08	0.043756	3.5003	2.3020E-08	0.01692
3.7500	6.862E-08	0.050438	3.7505	3.463E-08	0.025451	3.7505	1.0923E-08	0.008029
4.0009	3.396E-08	0.024961	4.0005	1.082E-08	0.00795	4.0008	4.1901E-09	0.00308
4.2509	1.881E-10	0.000138	4.2509	6.592E-10	0.000484	4.2505	-2.669E-10	-0.0002
4.5010	3.479E-08	0.025572	4.5003	1.119E-08	0.008225	4.5010	4.0379E-09	0.002968
4.7504	6.816E-08	0.050101	4.7502	3.451E-08	0.025368	4.7501	1.1031E-08	0.008108
5.0002	3.416E-08	0.025107	5.0003	5.887E-08	0.043269	5.0000	2.273E-08	0.016705

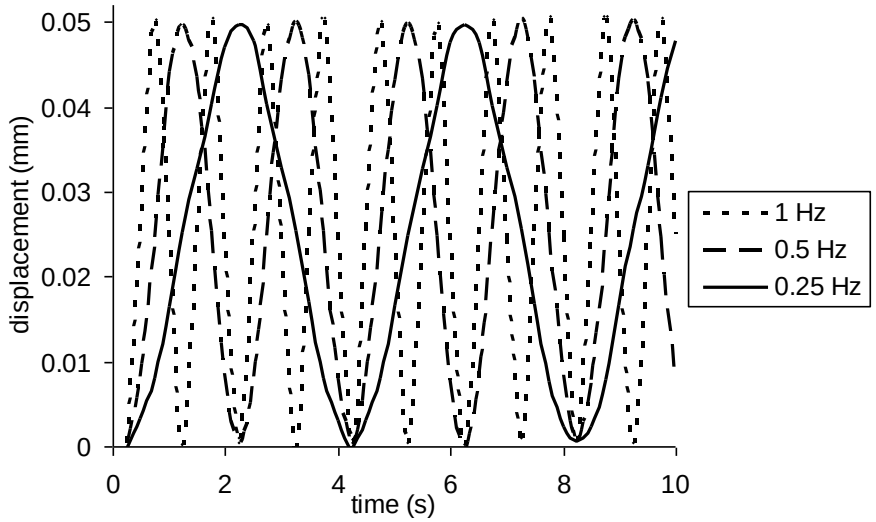

Figure A-1: Time dependent actuator position for 0.05 mm maximum cycle position.

0.2 mm	1 Hz		0.5 Hz			0.25 Hz		
time (s)	**flight time difference (us)**	**actuator move distance (mm)**	**time (s)**	**flight time difference (us)**	**actuator move distance (mm)**	**time (s)**	**flight time difference (us)**	**actuator move distance (mm)**
0.2501	5.202E-09	0.003824	0.2506	2.324E-09	0.001708	0.2504	1.532E-09	0.001126
0.5001	1.413E-07	0.103888	0.5004	4.665E-08	0.034291	0.5008	1.804E-08	0.013257
0.7508	2.778E-07	0.204169	0.7502	1.394E-07	0.102438	0.7509	4.765E-08	0.035022
1.0007	1.401E-07	0.102937	1.0007	2.378E-07	0.174801	1.0007	9.247E-08	0.067965
1.2508	2.302E-09	0.001692	1.2507	2.755E-07	0.202472	1.2503	1.387E-07	0.101962
1.5001	1.374E-07	0.100982	1.5005	2.421E-07	0.177916	1.5005	1.837E-07	0.135034
1.7502	2.770E-07	0.203607	1.7509	1.418E-07	0.104227	1.7506	2.227E-07	0.163696
2.0001	1.371E-07	0.100802	2.0000	4.804E-08	0.035311	2.0000	2.639E-07	0.19394
2.2500	5.138E-09	0.003776	2.2509	5.591E-09	0.00411	2.2501	2.780E-07	0.204294
2.5005	1.373E-07	0.100919	2.5008	4.840E-08	0.035576	2.5009	2.622E-07	0.192743
2.7500	2.743E-07	0.201639	2.7507	1.415E-07	0.103975	2.7506	2.216E-07	0.162903
3.0000	1.407E-07	0.103423	3.0005	2.418E-07	0.177698	3.0000	1.819E-07	0.13372
3.2501	5.881E-09	0.004322	3.2507	2.779E-07	0.20428	3.2501	1.411E-07	0.103697
3.5004	1.383E-07	0.10165	3.5000	2.417E-07	0.177625	3.5005	9.514E-08	0.069925
3.7502	2.761E-07	0.202921	3.7508	1.407E-07	0.103426	3.7509	4.604E-08	0.033841
4.0002	1.405E-07	0.103278	4.0009	4.527E-08	0.033271	4.0003	1.875E-08	0.013785
4.2501	2.355E-09	0.001731	4.2501	3.208E-09	0.002358	4.2500	5.848E-09	0.004299
4.5000	1.404E-07	0.103196	4.5003	4.952E-08	0.036395	4.5004	1.821E-08	0.013387
4.7503	2.758E-07	0.202735	4.7505	1.409E-07	0.10356	4.7508	4.824E-08	0.035456
5.0008	1.373E-07	0.100888	5.0001	2.420E-07	0.177863	5.0007	9.132E-08	0.067118

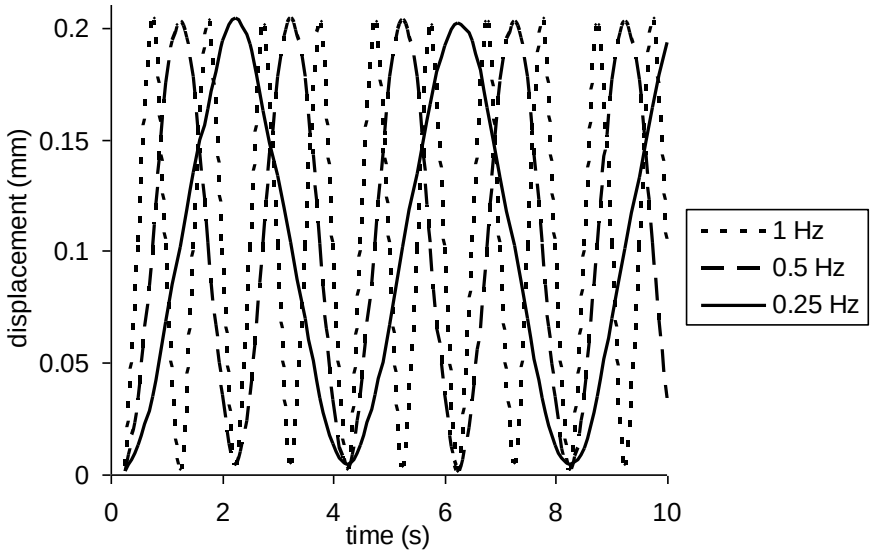

Figure A-2: Time-dependent actuator position for 0.2 mm maximum cycle position.

The results demonstrate that the cyclic actuator position is approximately the same during each cycle. There is no obvious backlash or increase or decrease in the average position with respect to time.

ii. Load cell

Method

Polymer material specimens were prepared and tested under 5% and 10% applied strain for 20 min. Three repeats were used for each strain level. The samples were also tested in a Zwicki Z5.0 TN material testing machine (BTI-FR5.0TN.D30, Zwick/Roell GmbH & Co. KG**,** Ulm, Germany), with a 250 N load cell (KAP-TC Zwick/Roell GmbH & Co. KG**,** Ulm, Germany) which had been calibrated at installation. The results are presented at the initial strain application and following 20 min of applied strain.

Results

5% applied strain (Δ denotes difference)

Applied strain %	Actual peak load	Measured peak load	ΔN/% strain	% Δ	(% Δ) / (% strain)	Actual load after 20 min	Measured load after 20 min	ΔN/% strain	% Δ	(% Δ) / (% strain)
5	4.76	5.02	0.05	5.18	1.04	4.45	4.66	0.04	4.51	0.90
5	4.93	5.26	0.07	6.27	1.25	4.76	5.02	0.05	5.18	1.04
5	4.92	5.21	0.06	5.57	1.11	4.83	5.11	0.06	5.48	1.10
		Average	**0.059**		**1.135**			**0.050**		**1.011**
		St. dev.	**0.007**		**0.111**			**0.007**		**0.100**

The average difference between the actual load and the measured load, at the instant of strain application, per percent of strain applied (at 5% strain), is 0.059 $N\%^{-1}$. After 20 min, the average difference in measured load is 0.05 $N\%^{-1}$.

10% applied strain

Applied strain %	Actual peak load	Measured peak load	ΔN/% strain	% Δ	(% Δ) / (% strain)	Actual load after 20 min	Measured load after 20 min	ΔN/% strain	% Δ	(% Δ) / (% strain)
10	8.28	8.83	0.06	6.23	0.62	8.17	8.69	0.05	5.98	0.60
10	8.15	9.02	0.09	9.65	0.96	7.98	8.76	0.08	8.90	0.89
10	7.96	8.37	0.04	4.90	0.49	7.88	8.35	0.05	5.63	0.56
		Average	**0.061**		**0.692**			**0.059**		**0.684**
		St. dev.	**0.024**		**0.245**			**0.017**		**0.180**

The average difference between the load cell reading and the actual load, at the instant of 10% strain application, was 0.061 $N\%^{-1}$. After 20 min, the average difference was 0.059 $N\%^{-1}$.

There was a slight increase between the differences at 10% compared to 5% applied strain. However, it appeared that the difference between the actual applied strain and the measured strain was a reasonably constant increase of approximately 0.057 $N\%^{-1}$. This means that at 8% applied strain in cartilage, the expected error in measured load would be approximately 0.46 N.

LVDT

The actuator was used to apply known displacement steps to the LVDT. The difference between the applied displacement and the measured displacement was found.

Method

The actuator was programmed to apply steps of 0.01 mm displacement to the LVDT. The LVDT was held in a rigid clamp attached to a rigid frame while the displacements were applied.

Results

Applied displacement (mm)	Measured displacement (mm)	Difference	% difference
0.01	0.0099	0.00005	0.52
0.02	0.0198	0.00016	0.78
0.03	0.0295	0.00052	1.73
0.04	0.0398	0.00015	0.38
0.05	0.0492	0.00080	1.60
0.06	0.0593	0.00074	1.23
0.07	0.0693	0.00070	1.00
0.08	0.0815	-0.00149	1.87
0.09	0.0915	-0.00149	1.65
0.10	0.1015	-0.00149	1.49
0.11	0.1089	0.00107	0.97
0.12	0.1193	0.00070	0.58
0.13	0.1316	-0.00156	1.20
0.14	0.1393	0.00075	0.54
0.15	0.1505	-0.00054	0.36
0.16	0.1609	-0.00092	0.58
0.17	0.1666	0.00339	1.99
0.18	0.1798	0.00025	0.14
0.19	0.1874	0.00261	1.37
0.20	0.1989	0.00110	0.55
0.21	0.2092	0.00076	0.36
0.22	0.2162	0.00381	1.73
0.23	0.2300	-0.00002	0.01
0.24	0.2426	-0.00256	1.07
0.25	0.2469	0.00312	1.25
0.26	0.2561	0.00392	1.51
0.27	0.2716	-0.00157	0.58
0.28	0.2839	-0.00391	1.40
0.29	0.2919	-0.00194	0.67
0.30	0.2978	0.00220	0.73
	Average	**0.0003**	**0.99**
	St. dev.	**0.0019**	**0.55**

The difference can be seen to change sign. It was not a consistent increase or decrease from the applied displacement. The error did not increase or decrease with respect to the applied displacement. It is important to consider the accuracy of the actuator position when assessing the true accuracy of the LVDT. If the actuator were 100% accurate, the LVDT would be 99.1% accurate. However, the true accuracy of the LVDT is likely to be slightly greater.

B. Statistical tests

i. Student's T-test (unpaired)

Use

The Student's T-test is used to compare the means of 2 unrelated data groups as a result of changing a single factor (for example, depth of tissue analysis or applied strain).

Method

The null hypothesis is that the group means are equal. The test is performed to determine whether the null hypothesis can be rejected at the required confidence level.

(1) Calculate the degrees of freedom (the total number of samples tested minus 1)
(2) Calculate the mean of each group.
(3) Subtract one mean from the other.
(4) Calculate the standard deviations of each group.
(5) Square the standard deviations to obtain the variances.
(6) Obtain $S_{X_1X_2}$ by subtracting the variances from one another, dividing that value by 2 and then square-rooting the result.
(7) Multiply $S_{X_1X_2}$ by the square rooted value of 2 divided by the number of repeat readings (*n*) (e.g. $\sqrt{(2/10)}$).
(8) Divide the result from step (2) by the result from (6) to obtain the $T_{student}$ test statistic:

$$T_{student} = \frac{\overline{X}_1 - \overline{X}_2}{S_{X_1X_2}\sqrt{\frac{2}{m}}}$$

(9) Compare the test statistic with the critical T-test tables to establish whether the means are significantly different at the required confidence level.

Critical tables

The tables are shown for the confidence levels of 90%, 95%, 99% and 99.9% (0.1, 0.05, 0.01, 0.001) respectively.

Degrees of Freedom	Probability, *p*			
	0.1	**0.05**	**0.01**	**0.001**
1	6.31	12.71	63.66	636.62
2	2.92	4.3	9.93	31.6
3	2.35	3.18	5.84	12.92
4	2.13	2.78	4.6	8.61
5	2.02	2.57	4.03	6.87
6	1.94	2.45	3.71	5.96
7	1.89	2.37	3.5	5.41
8	1.86	2.31	3.36	5.04
9	1.83	2.26	3.25	4.78
10	1.81	2.23	3.17	4.59
11	1.8	2.2	3.11	4.44
12	1.78	2.18	3.06	4.32
13	1.77	2.16	3.01	4.22
14	1.76	2.14	2.98	4.14
15	1.75	2.13	2.95	4.07
16	1.75	2.12	2.92	4.02
17	1.74	2.11	2.9	3.97
18	1.73	2.1	2.88	3.92
19	1.73	2.09	2.86	3.88
20	1.72	2.09	2.85	3.85

Limitations and assumptions

The groups are assumed to be completely independent and the distribution of the data following a normal distribution. Systematic differences may be reported as significant, although in these experiments the systematic differences should be minimal.

ii. Analysis of variance (ANOVA) 1-way

Use

The 1-way ANOVA is used to determine the effect of a single factor on the output data of several sample groups. Whereas the Student's T-test only compares pairs of means, the advantage of ANOVA is the ability to compare three or more groups directly and determine if the single changing factor affected the results.

Method

The null hypothesis is that the group means are equal. The test is performed to determine whether the null hypothesis can be rejected at the required confidence level.

(1) Calculate the degrees of freedom for each factor (column labels) and for the error (row labels). The factor degree of freedom is the number of changing factors (e.g. 4 different global applied strains) minus 1. The error degree of freedom is the total number of samples (e.g. 10 repeats at each of the 4 applied strains requires 40 samples) minus the number of changing factors (e.g. 4 strain levels).
(2) Calculate the overall mean (the mean for all the samples together).
(3) Calculate the means for each factor group.
(4) Calculate the sum of the sum of squares for each factor group (*SSA*) and all the samples overall (*SST*). Calculate the error sum of squares ($SSE = SST - SSA$).
(5) Calculate the sum of the mean square of the factor groups ($MSA = SSA$ / (degrees of freedom for each factor)) and of the error ($MSE = SSE$ / (degrees of freedom of the error)).
(6) Calculate the F_0 statistic for the factor ($F_0 = MSA / MSE$).
(7) Compare the F_0 statistic with the critical *F* tables at the required significance level.

Critical tables

The critical F value tables are shown at 99%, 95% and 90% significance of difference, respectively.

99%	1	2	3
1	4052.19	4999.52	5403.34
2	98.502	99	99.166
3	34.116	30.816	29.457
4	21.198	18	16.694
5	16.258	13.274	12.06
6	13.745	10.925	9.78
7	12.246	9.547	8.451
8	11.259	8.649	7.591
9	10.561	8.022	6.992
10	10.044	7.559	6.552
11	9.646	7.206	6.217
12	9.33	6.927	5.953
13	9.074	6.701	5.739
14	8.862	6.515	5.564
15	8.683	6.359	5.417
16	8.531	6.226	5.292
17	8.4	6.112	5.185
18	8.285	6.013	5.092
19	8.185	5.926	5.01
20	8.096	5.849	4.938
21	8.017	5.78	4.874
22	8.017	5.719	4.817
23	7.881	5.664	4.765
24	7.823	5.614	4.718
25	7.77	5.568	4.675
26	7.721	5.526	4.637
27	7.677	5.488	4.601
28	7.636	5.453	4.568
29	7.598	5.42	4.538
30	7.562	5.39	4.51
31	7.53	5.362	4.484
32	7.499	5.336	4.459
33	7.471	5.312	4.437
34	7.444	5.289	4.416
35	7.419	5.268	4.396
36	7.396	5.248	4.377

95%	1	2	3
1	161.45	199.5	215.71
2	18.513	19	19.164
3	10.128	9.552	9.227
4	7.709	6.944	6.591
5	6.608	5.786	5.409
6	5.987	5.143	4.757
7	5.591	4.737	4.347
8	5.318	4.459	4.066
9	5.117	4.256	3.863
10	4.965	4.103	3.708
11	4.844	3.982	3.587
12	4.747	3.885	3.49
13	4.667	3.806	3.411
14	4.6	3.739	3.344
15	4.543	3.682	3.287
16	4.494	3.634	3.239
17	4.451	3.592	3.197
18	4.414	3.555	3.16
19	4.381	3.522	3.127
20	4.351	3.493	3.098
21	4.325	3.467	3.072
22	4.301	3.443	3.049
23	4.279	3.422	3.028
24	4.26	3.403	3.009
25	4.242	3.385	2.991
26	4.225	3.369	2.975
27	4.21	3.354	2.96
28	4.196	3.34	2.947
29	4.183	3.328	2.934
30	4.171	3.316	2.922
31	4.16	3.305	2.911
32	4.149	3.295	2.901
33	4.139	3.285	2.892
34	4.13	3.276	2.883
35	4.121	3.267	2.874
36	4.113	3.259	2.866

90%	1	2	3
1	39.863	49.5	53.593
2	8.526	9	9.162
3	5.538	5.462	5.391
4	4.545	4.325	4.191
5	4.06	3.78	3.619
6	3.776	3.463	3.289
7	3.589	3.257	3.074
8	3.458	3.113	2.924
9	3.36	3.006	2.813
10	3.285	2.924	2.728
11	3.225	2.86	2.66
12	3.177	2.807	2.606
13	3.136	2.763	2.56
14	3.102	2.726	2.522
15	3.073	2.695	2.49
16	3.048	2.668	2.462
17	3.026	2.645	2.437
18	3.007	2.624	2.416
19	2.99	2.606	2.397
20	2.975	2.589	2.38
21	2.961	2.575	2.365
22	2.949	2.561	2.351
23	2.937	2.549	2.339
24	2.927	2.538	2.327
25	2.918	2.528	2.317
26	2.909	2.519	2.307
27	2.901	2.511	2.299
28	2.894	2.503	2.291
29	2.887	2.495	2.283
30	2.881	2.489	2.276
31	2.875	2.482	2.27
32	2.869	2.477	2.263
33	2.864	2.471	2.258
34	2.859	2.466	2.252
35	2.855	2.461	2.247
36	2.85	2.456	2.243

Limitations and assumptions

These are the same as for the student's T-test.

C. Temperature fluctuations with respect to time

The function of the thermostatic control and water heater caused there to be some fluctuation with respect to time of the temperature of the PBS during the experiments. Results are shown of a typical fluctuation. The results were recorded from an independent thermocouple for every experiment.

A selection of these data are plotted for a 30 min period (Figure C-1) and for 2 different whole days, where experiments were conducted (Figure C-2 and C-3). They are representative of the results across all the days.

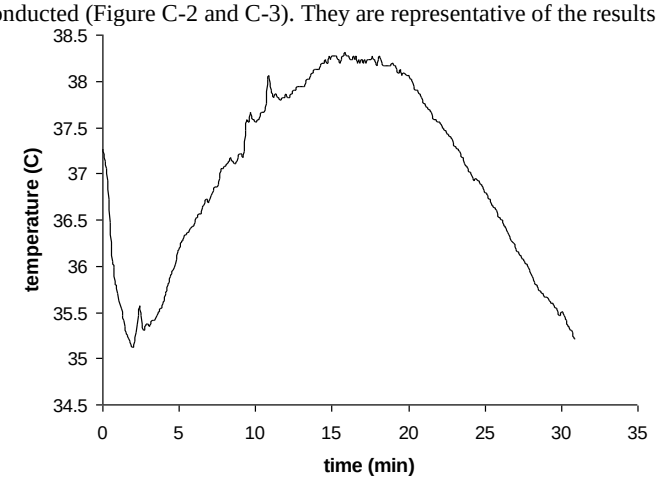

Figure C-1: Graph of temperature fluctuations over 30 min.

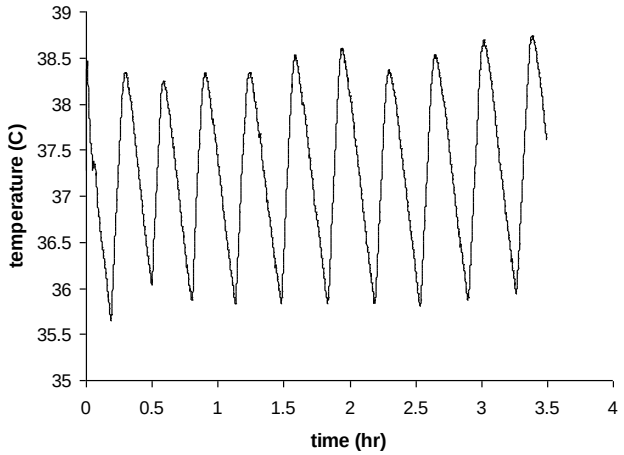

Figure C-9-1: Temperature fluctuations recorded over 3.5 hr during a day's experiments.

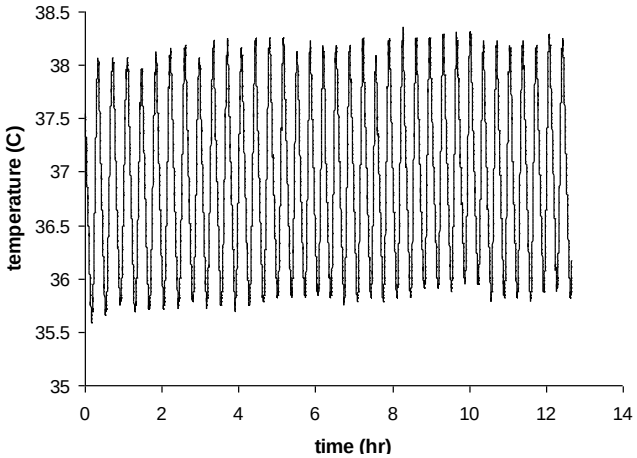

Figure C-1: Temperature fluctuations in the PBS water bath recorded over 13 hr of a whole day.

D. Matlab® code

i. Mechanical test data processing

Process

(1) Load the mechanical test data of sample thickness, time-dependent load and displacement and time stamps
(2) Calculate the displacement nominally applied to the sample
(3) Transfer the test time into minutes
(4) Find the start of the test as the time the maximum load voltage occurs
(5) Average the data over 10 adjacent time points
(6) Correct the value of applied displacement and strain with LVDT displacement values
(7) Calculate moduli
(8) Smooth the data between the time points
(9) Average the moduli values between the repeats for each applied global strain
(10) Plot moduli with respect to time

Input and output variables

Thickness of the samples	thickness_matrix_N_QS_' (strain)'
Load cell data (V)	loadv
LVDT displacement data (V)	disp
Time stamp data	time
Time points to be plotted	new_time
Average modulus to be plotted at each time point	N_' (strain) '_mod
Standard deviation of modulus at each time point	N_' (strain) '_mod_std

(The code is shown for nasal specimens, but can be transferred for articular data by changing 'N's into 'A's.)

Code

%%this subroutine calculates the composite moduli from the load, applied displacement and load cell data

```
clear
load thicknesses
repeats=10;
for st = 1:4
   strn = 2*st;
   eval(['thickness = thickness_matrix_N_QS_' num2str(strn) ';'])
   strain = 0.01*strn;
   eval(['save QS_N_' num2str(strn) ' repeats '])
   eval(['save QS_N_' num2str(strn) ' thickness -append strain -append'])
%%specify file names to load
for yt=1:repeats
   eval(['load N_QS_' num2str(strn) '_' num2str(yt) 'load'])
   ee=whos;
   eval(['load N_QS_' num2str(strn) '_' num2str(yt) 'stamp'])
   eval(['load N_QS_' num2str(strn) '_' num2str(yt) 'disp'])
   samp_thick = thickness(yt);
   app_disp = samp_thick*strain;
   app_disp_matrix(yt)=app_disp;
   %%find the number of variables in the file
   numb=size(ee,1);
   num=(numb-(25*yt*strn))/4;
   %%load the variable in  order. change the variable names
   for nn=1:num
      eval(['loadv = load' num2str(num) ';']);
      eval(['time = stamp' num2str(num) ';']);
      eval(['disp = displacement' num2str(num) ';']);
   end
   %%transfer the time into min
   for uu=1:num
      t_min(uu)=(time(uu)/60)+((uu)/1000000);
   end
   %%find the start of the curve
   [Y I] = max(loadv(1:floor(num/2))); p1=I;
   I = find(t_min>20);
   p10 = min(I);
   new_reps = floor((p10-p1)/10);
   %%smooth the displacement and load voltage values
   for new_val = 1:new_reps
      high_l(new_val) = max(loadv((p1+(10*(new_val-1))):(p1+(10*new_val))));
      high_d(new_val) = max(disp((p1+(10*(new_val-1))):(p1+(10*new_val))));
      low_l(new_val) = min(loadv((p1+(10*(new_val-1))):(p1+(10*new_val))));
      low_d(new_val) = min(disp((p1+(10*(new_val-1))):(p1+(10*new_val))));
      mid_l(new_val) = (high_l(new_val) + low_l(new_val))/2;
      mid_d(new_val) = (high_d(new_val) + low_d(new_val))/2;
     %%take away the measured displacement from the applied value. the displacement is converted from a
    %%voltage into a distance
      corrected_disp(new_val) = app_disp - mid_d(new_val)*(1.121E-4);
      %%calculate the strain from the correct displacement
      corrected_strain(new_val) = (corrected_disp(new_val) / samp_thick);
      %%calculate the composite moduli. the load is converted from a voltage into Newtons
      apparant_mod(new_val) = ((mid_l(new_val))*(5.026548E-5))/corrected_strain(new_val);
      t_space(new_val) = ((t_min(p10)-t_min(p1))/new_reps)*(new_val)+0.05;
   end
end
   eval(['t_space' num2str(yt) '=t_space;']);
   eval(['apparant_mod' num2str(yt) '=apparant_mod;']);
   eval(['save QS_N_' num2str(strn) ' t_space' num2str(yt) ' -append apparant_mod' num2str(yt) ' -append'])
   %%clear unecessary values before applying the loop again
   clear load* t_* time* stamp* disp* high* low* mid* corrected* app* p* I num* ee samp* new* uu TT…
  …MM Y nn
%%smooth the data further between the points
for rpt=1:10
eval(['smoothed_mod' num2str(rpt) ' = (interp(apparant_mod' num2str(rpt) ' , 100))*100;'])
   for vc=1:81
      new_time(vc) = ((vc)*0.25)-0.25;
      eval(['len_sm(rpt) = length(smoothed_mod' num2str(rpt) ');'])
      I(vc) = round((len_sm(rpt)/81)*(vc)); Iv = I(vc);
```

```
        eval(['load_point' num2str(rpt) '(vc) = smoothed_mod' num2str(rpt) '(Iv);'])
    end
end
%%average the load across the 10 repeats
for vc=1:81
    X = [load_point1(vc) load_point2(vc) load_point3(vc) load_point4(vc) load_point5(vc) load_point6(vc)…
    …load_point7(vc) load_point8(vc) load_point9(vc) load_point10(vc)];
    mod_ave(vc) = mean(X);
    mod_std(vc) = std(X);
end
%%save the new values
eval(['save QS_N_' num2str(strn) '_ave_mech new_time'])
eval(['save QS_N_' num2str(strn) '_ave_mech mod_ave -append mod_std -append'])
    %%clear unecessary values before applying the loop again
    clear load* t_* time* stamp* disp* high* low* mid* corrected* app* p* I num* ee samp* new* uu …
    … TT MM m* Y nn s* Q* X l*
end
%%plot all the modulus curves for the different applied strains 1st change variable names to be unique to each
%%global strain
load QS_N_2_ave_mech1
N_2_mod = mod_ave; N_2_mod_std = mod_std;
clear mod_ave mod_std
load QS1_N_4_ave_mech1
N_4_mod = mod_ave; N_4_mod_std = mod_std;
clear mod_ave mod_std
load QS1_N_6_ave_mech1
N_6_mod = mod_ave; N_6_mod_std = mod_std;
clear mod_ave mod_std
load QS1_N_8_ave_mech1
N_8_mod = mod_ave; N_8_mod_std = mod_std;
clear mod_ave mod_std
%%plot values together
figure
set(gcf,'color','w')
plot(new_time, N_2_mod)
xlabel('Time (min)')
ylabel('Composite modulus (MPa)')
hold on
plot(new_time, N_4_mod,'k')
plot(new_time, N_6_mod,'c')
plot(new_time, N_8_mod,'m')
hold off
```

ii. Elastography routine

Process

(1) Enter the global strain value for the data
(2) Determine the number of points in the signal
(3) Define the number of repeat readings requiring the loop
(4) Low-pass filter the signals
(5) Determine the pre-compressional signal
(6) Determine the post-compressional signals at the times required (T0, T10, T20, etc)
(7) Remove accidental offsets between the signals caused by temperature shifts (align signal starts)
(8) Define the windows
(9) Apply the windows and loop the SSD routine in each one in turn
(10) Determine the time shift associated with the minimum signal difference and calculate the strain from the duration of the full window
(11) Average the strains found for each window
(12) Apply the 55% correlation filter and average the suitably correlated strains in each window
(13) Save the strain values
(14) Normalise the strain values
(15) Plot non-normalised and normalised strains with respect to distance through the tissue

Input variable names

Global strain	g_strain
RF signals for experiment duration	N_QS_' (strain) '_' (time) '
Number of windows (without overlap) to divide signal by	g_split
Number of points in the signal	pz

Number of readings in 20 min	reps
Oscilloscope acquisition rate	acq
Cut-off frequency of low-pass filter	cut
Pre-compressed signal	x_pre
Post-compressed signal	x_comp
How far to move the window position	wind_shift
Window shape	window_exp
Non-normalised time- and depth-dependent strain data	N_' (strain) '_T' (time) '_strain55

The code shown is for nasal cartilage specimens, but can be run for articular by changing the input (RF) and output (strain) name.

Code

```
%% this routine windows first finds where the dynamic cycles starts and then finds the signals pre and post
%%compressional signals. within the signals it then shifts a matrix along point-wise and then computes the
%%SSD
clear %clear trailing variables
g_strain = 8; %enter the strain value for this comparison
g55(1:30, 1:10) = 0;
for gr = 1:5 %index used for determining time (T0…T20)
for gg = 1:10%for each repeat reading in turn
eval(['load N_QS_' num2str(g_strain) '_' num2str(gg) ';']); %load the signals
%% g_split is the number of portions to divide the signal into. It should be 10 for nasal and 8 for articular
g_split = 10;
%% find the beginning and end of the signal of interest
pzp = length(x_T1); %complete signal length
first_third = floor(pzp/3);
second_third = floor(2*pzp/3);
[Y I] = min(x_T1(1:first_third)); %find the minimum point in the first third of the signal
start_z = I + 16;
clear I
[Y I] = max(x_T1(first_third:pzp)); %find the maximum point in the last 2/3rds of the signal
second_third_z = I + first_third;
last_half_z = second_third_z + 10; %add some extra points
   if last_half_z > pzp
      last_half_z = pzp;
   end
pz = last_half_z - start_z + 1;
 %%make dt and t uniform variables in the code
dt = dt_T1; t0 = t0_T1 + (dt*start_z);
%% define the number of repetitions to be looped
ee = whos; numb = size(ee, 1); reps = (numb - 60 - gg*10 - gr*2)/4;
acq = 2500000000; %acquisition rate of oscilloscope
cut = 25000000; %cut off frequency for low pass filter
%%read the numbers in the variable names
for ss = 1:reps
   eval(['xS(ss, :) = x_T' num2str(ss) ';']);
end
%%find the filter coefficients
Fnorm = (cut/(acq/2));
[b, a] = butter(10, Fnorm, 'low'); %butterworth filter
%%loop the filter
for aa = 1:reps
   xS_low(aa, :) = filtfilt(b, a, xS(aa,:));
end
%% insert the first file name (a pre compression file)
dt_pre = dt_T1; t0_pre = t0_T1; x_pre = xS_low(1, start_z:pz);
%%instert the second file name (to use the first signal from the compression series)
dt_comp = dt_T1; t0_comp = t0_T1;
if gr == 1
   t_val = 7;  g_time = 0;
elseif gr == 2
   t_val = floor((reps - 70) / 4); g_time = 5;
elseif gr == 3
   t_val = floor((reps - 70) / 2); g_time = 10;
elseif gr == 4;
   t_val = floor((3*(reps - 70)) / 4); g_time = 15;
```

```
elseif gr == 5;
   t_val = floor(reps - 70); g_time = 20;
end
%% find correlation coefficients for each signal to be compared
for vf = 2:12
   sim_mat = abs(corrcoef(x_pre, xS_low(vf, start_z:pz)));
   sig_coef(vf, gg) = sim_mat(1, 2);
end
x_comp = xS_low(t_val, start_z:pz);
%% line up the two first peaks of the signals to remove changes caused by temperature changes or
%%experimental error
[Y I] = max(x_pre(1:first_third/2)); pre_start_peak = I;
clear I
[Y I] = max(x_comp(1:first_third/2)); comp_start_peak = I;
clear I
compensation = pre_start_peak - comp_start_peak;
if compensation <= 0
   compensation = 0;
elseif compensation >= start_z
   compensation = start_z - 1;
end
x_comp_new = xS_low(7, (start_z - compensation):(pz - compensation));
for rr = 1:(pz-start_z) + 1
   tt_pre(rr) = (t0_pre + (rr(:)*dt_pre)).*10^6;
end
for rr = 1:(pz - start_z) + 1
   tt_comp(rr) = (t0_comp + (rr(:)*dt_comp)).*10^6;
end
%% split signals into windows
windbase = floor((pz)/g_split); windedge = hann(2); windpad = ones((windbase-size(windedge)),1);
window_exp = [windedge(1:size(windedge, 1)/2); windpad; windedge(size(windedge, 1)/2+1:size(windedge,…
…1))];
%%the rest of the window then needs to be made equal to zero
window_exp = [window_exp]'; window_length = length(window_exp);
wind_shift = floor(0.3*window_length); num_win = floor(((pz) - window_length)/wind_shift);
pz = 1 + (pz - start_z);
%%loop SSD elastography routine
for yu = 0:1:(window_length - 1)
   x_pre2 = x_pre(1, (1 + yu):pz);
   x_comp2 = x_comp_new(1, 1:length(x_pre2));
   x_diff = x_pre2 - x_comp2;
   glob_SSD(yu + 1) = (x_diff*x_diff');
   time_shift(yu + 1) = dt*yu*10^6;
   %%change window
   for position = 1:(floor(num_win) - 4)
      if position == 1
         whole_win = zeros(1, pz);
         whole_win(1:window_length) = [window_exp];
      else
         whole_win = zeros(1, pz);
            whole_win = [zeros((position - 1)*wind_shift, 1);(window_exp)';zeros(pz - window_length-…
            …(wind_shift*(position - 1)), 1)];
      end
      win_strt = (position)*wind_shift - (wind_shift - 1);
      win_end = win_strt + window_length;
      if length(x_diff) < win_end
         win_end = length(x_diff);
      end
      x_win = x_diff(win_strt:win_end);
      SSD(yu + 1, position) = (x_win*(x_win)')';
   end
end
%%determine the position in time in the sample
for yy = 1:num_win - 4
   tissue_time(yy) = ((window_length/2) + (wind_shift*(yy-1)))*dt_comp*10^6;
end
%%find the minimum SSD values for each window
```

```
for uh = 1:floor(num_win) - 4
   if length(time_shift) <= find(SSD(:,uh) == min(SSD(:,uh)))
      SSD_shift(uh) = time_shift(1);
   else
   SSD_shift(uh) = time_shift((find(SSD(:, uh) == min(SSD(:, uh)))));
   end
   gg_w_strain(uh, gg) = (SSD_shift(uh)/(window_length*dt*10^6))*100;
   x_pre3 = x_pre(1, (1 + SSD_shift(uh)):pz);
   x_comp3 = x_comp(1, 1:length(x_pre2));
      if uh == 1
         whole_win = zeros(1, pz);
         whole_win(1:window_length) = [window_exp];
      else
         whole_win = zeros(1, pz);
         whole_win = [zeros((uh-1)*wind_shift, 1);(window_exp)';zeros(pz - window_length - (wind_shift…
            …*(uh-1)), 1)];
      end
      win_strt = (uh)*wind_shift - (wind_shift - 1);
      win_end = win_strt + window_length;
      if win_end > length(x_pre3)
         win_end = length(x_pre3);
      elseif win_end > length(x_comp3);
         win_end = length(x_comp3);
      end
      se = abs(corrcoef(x_pre3(win_strt:win_end), x_comp3(win_strt:win_end)));
      win_coef(uh, gg) = se(1, 2);
      %%calculate the average strain for each window(no correlation filter)
      if gg == 1
         if uh == 1 %the first point
            gt(1, 1) = 1; %to ensure that the first point can actually be zero
         elseif gg_w_strain(uh, gg) > 0
            gt(uh, 1) = 1; %this means zeroes will be excluded from the average
         end
      else
         if uh == 1
            gt(1, gg) = gg; %to ensure that the first point can actually be zero
         elseif gg_w_strain(uh, gg) > 0
            gt(uh, gg) = gt(uh, gg - 1) + 1; %this means zeroes will be excluded from the average
         else
            gt(uh, gg) = gt(uh, gg - 1);
         end
      end
   ave_strain1(uh, gg) = mean(gg_w_strain(uh, 1:gg));
   std_strain1(uh, gg) = std(gg_w_strain(uh, 1:gg));
   %% 55% correlation
   gg_w_strain55(uh, gg) = gg_w_strain(uh, gg);
      if win_coef(uh, gg) < 0.55;
         gg_w_strain55(uh, gg) = 0;
      end
      %%calculate the average strain for each window
      if gg == 1
         if uh == 1
            g55(1, 1) = 1; %to ensure that the first point can actually be zero
         elseif gg_w_strain55(uh, gg) > 0
            g55(uh, 1) = 1; %this means zeroes will be excluded from the average
         end
      else
         if uh == 1
            g55(1, gg) = gg; %to ensure that the first point can actually be zero
         elseif gg_w_strain55(uh, gg) > 0
            g55(uh, gg) = g55(uh, gg - 1) + 1; %this means zeroes will be excluded from the average
         else
            g55(uh, gg) = g55(uh, gg - 1);
         end
      end
    ave_strain55(uh, gg) = (sum(gg_w_strain55(uh, 1:gg))/g55(uh, gg));
    std_strain55(uh, gg) = std(gg_w_strain55(uh, 1:gg));
```

```
    end
%%rename values after final repeat loop
if gg == 10
   g_tissue_time = tissue_time;
   eval(['N_' num2str(g_strain) '_T' num2str(g_time) '_strain60 = ave_strain60(:, 10);']);
   eval(['N_' num2str(g_strain) '_T' num2str(g_time) '_strain60std = std_strain60(:, 10);']);
   eval(['N_' num2str(g_strain) '_T' num2str(g_time) '_strain55 = ave_strain55(:, 10);']);
   eval(['N_' num2str(g_strain) '_T' num2str(g_time) '_strain55std = std_strain55(:, 10);']);
   eval(['N_' num2str(g_strain) '_T' num2str(g_time) '_strain50 = ave_strain50(:, 10);']);
   eval(['N_' num2str(g_strain) '_T' num2str(g_time) '_strain50std = std_strain50(:, 10);']);
   eval(['N_' num2str(g_strain) '_T' num2str(g_time) '_strain1 = ave_strain1(:, 10);']);
   eval(['N_' num2str(g_strain) '_T' num2str(g_time) '_strain1std = std_strain1(:, 10);']);
end
%%clear variables for the next loop
clear y* x* w* u* t* s* p* n* l* f* F* ee d* c*
end
end
%%save values
eval(['save N_' num2str(g_strain) '_strain1 N*'])
eval(['save N_' num2str(g_strain) '_strain1 g_tissue_time -append'])
clear
%%plot normalised and non-normalised strains
for ts = 1:4;
st = 2*ts;
%%reload the strain info
eval(['load N_' num2str(st) '_strain1;'])
num_w = length(g_tissue_time);
h_n_w = round(num_w / 2);
%%loop for each required time value
   for time = 1:5
         ytol = 55;
      if time == 1
         ytime = 0;
      elseif time == 2
         ytime = 5;
      elseif time == 3
         ytime = 10;
      elseif time == 4
         ytime = 15;
      elseif time == 5;
         ytime = 20;
      end
      eval(['y(:, ts) = A_' num2str(st) '_T' num2str(ytime) '_strain' num2str(ytol) ';'])
      eval(['ydev(:, ts) = A_' num2str(st) '_T' num2str(ytime) '_strain' num2str(ytol) 'std;'])
      figure
      set(gcf, 'Color', 'w')
      elast_graph = errorbar(g_tissue_time, y(:, ts), ydev(:, ts), 'LineStyle','none', 'Marker', 'x', 'MarkerSize',8);
      title('strains')
      xlabel('tissue time (us)')
      ylabel('strain in the window (us)')
      %% normalise the windowed data
      for win = 1:num_w
         y_norm(win, ts) = y(win, ts)*(h_n_w / win);
      end
      figure
      set(gcf, 'Color', 'w')
      norm_graph = errorbar(g_tissue_time, y_norm(ts, :), ydev(ts, :), 'LineStyle','none', 'Marker', …
            …'x', 'MarkerSize',8);
      title('normalised strains')
      xlabel('tissue time (us)')
      ylabel('normalised strain in the window (us)')
   end
end
end
      figure %plot non-normalised data
      set(gcf, 'Color', 'w')
      elast_graph = errorbar(g_tissue_time, y(1, :), ydev(1, :), 'LineStyle','none', 'Marker', 'x', 'MarkerSize',8);
```

```
title('strains')
xlabel('tissue time (us)')
ylabel('strain in the window (us)')
hold on
errorbar(g_tissue_time, y(2, :), ydev(2, :), 'LineStyle','none', 'Marker', 'o', 'MarkerSize',8);
errorbar(g_tissue_time, y(3, :), ydev(3, :), 'LineStyle','none', 'Marker', 'v', 'MarkerSize',8);
errorbar(g_tissue_time, y(4, :), ydev(4, :), 'LineStyle','none', 'Marker', '^', 'MarkerSize',8);
hold off
figure %plot normalised data
set(gcf, 'Color', 'w')
norm_graph = errorbar(g_tissue_time, y_norm(1, :), ydev(1, :), 'LineStyle','none', 'Marker',…
    … 'x', 'MarkerSize',8);
title('normalised strains')
xlabel('tissue time (us)')
ylabel('normalised strain in the window (us)')
hold on
errorbar(g_tissue_time, y_norm(2, :), ydev(2, :), 'LineStyle','none', 'Marker', 'o', 'MarkerSize',8);
errorbar(g_tissue_time, y_norm(3, :), ydev(3, :), 'LineStyle','none', 'Marker', 'v', 'MarkerSize',8);
errorbar(g_tissue_time, y_norm(4, :), ydev(4, :), 'LineStyle','none', 'Marker', '^', 'MarkerSize',8);
hold off
```

iii. Phenomenological model

Process

(1) load the initial test variables from the results and literature
(2) change the names of some of the test data to those easier to use in the iteration
(3) calculate the initial depth-dependent permeability
(4) iterate the model to find time- and depth-dependent moduli
(5) average time-dependent moduli and find the standard deviation of the results
(6) normalise the moduli
(7) calculate the total fluid movement for each time step at each depth (sum all of the previous discrete fluid movements at each depth
(8) calculate the void fraction
(9) plot normalised moduli and void fractions

Input and output variable names

global applied strain (%)	strain
nominal sample height (m)	samp_thick
dynamic fluid viscosity ($kgs^{-1}m^{-1}$)	visc
sample disc radius (m)	R
level of correlation of results (%)	lev
depth-dependent fluid fraction height	b_0
time-dependent stress data	Sg
number of discrete windows	num_win
number of time steps	time_steps
strain data at each time step in each window	dd_strain(time_steps, num_win)
time- and depth-dependent fluid out	A_' (strain) '_complete_f
total fluid out	fluid_o_' (strain)'
normalised depth-dependent moduli	E_' (strain) '_norm
time- and depth-dependent void fraction	e' (strain)'

Code

```
% %this programme calculates time dependent fluid movement to obtain the depth-dependent matrix moduli
%% and void fractions.
clear %clear any trailing variables
%% loop the value for the applied strain in %
for ss = 1:4
strain = 2*ss; % global strain in %
samp_thick = 0.0157; % sample thickness in metres
visc = 0.02; % dynamic viscosity of fluid
R = 0.004; % disc radius in metres
lev = 55; % level of correlation between the results
%% load time dependent stress data
eval(['load QS1_A_' num2str(strain) '_ave_mech1'])
%% load depth dependent strain data and calculate initial layer thickness
eval(['load A_' num2str(strain) '_strain1']) % depth-dependent strains
load b_0 % depth-dependent fluid fraction
load E_ideal % ideal strains for comparison
load exp_strains % strains from experimental data
eval(['num_win = length(A_' num2str(strain) '_T0_strain' num2str(lev) ');']) %find number of windows
```

```
h_0_i = samp_thick / num_win; % initial slice height
%% allocate the number of time points
time_steps = 20;
eval(['ideal_strain = ideal_strain_' num2str(strain) '_rw(:) / 100;']) %set-up ideal strain for comparison
%% change all the time step strains to a more convenient name and normalise the strain values
h_n_w = round(num_win / 2); % half the number of windows (for normalising)
for w = 1:num_win
   for tm = 1:time_steps
      eval(['dd_strain(tm, w) = (a_' num2str(strain) '_T' num2str(tm) '_strain' num2str(lev) '(w) / 100);'])
      tissue_depth(w) = w*(1.57 / 19); % thickness plottting points
   end
end
%% calculate equlibrium stress from the average of the last 4 points
stress_ave_eqm = (glob_stress(81) + glob_stress(80) + glob_stress(79) + glob_stress(78)) / 4;
%% separate out the time dependent stress at each time step
for ty = 1:time_steps
   Sg(ty) = glob_stress(ty*4 - 3);
end
%% calculate initial permeability from literature equation
for win = 1:num_win
            k(20-win) = 1*(2*10^-15)*abs(1 + (4.3*(win / num_win)) - (7.8*(win / num_win)^2) + (3.1*…
            …(win / num_win)^3)); % initial permeability
end
%% run the iteration model
for time = 1:19
   for win = 1:num_win
      A = 0.00000001;
      B = 0.000000009;
      C = (Sg(time) - ((A*(R^2))/(8*k(win)*h_0_i*(1 - dd_strain(time, win)))) / dd_strain(time, win));
      D = (Sg(time+1) - ((B*(R^2))/(8*k(win)*h_0_i*(1 - dd_strain(time+1, win)))) / dd_strain(time+1, win));
      while C > D
         B = B - 0.00000000001
         C = (Sg(time) - ((A*(R^2))/(8*k(win)*h_0_i*(1 - dd_strain(time, win)))) / dd_strain(time, win));
         D = (Sg(time+1) - ((B*(R^2))/(8*k(win)*h_0_i*(1 - dd_strain(time+1, win)))) / dd_strain(time+1, win))
      end
      while D > C
         A = A - 0.0000000000001
         C = (Sg(time) - ((A*(R^2))/(8*k(win)*h_0_i*(1 - dd_strain(time, win)))) / dd_strain(time, win));
         D = (Sg(time+1) - ((B*(R^2))/(8*k(win)*h_0_i*(1 - dd_strain(time+1, win)))) / dd_strain(time+1, win))
      end
      while C > D
         B = B - 0.00000000000001
         C = (Sg(time) - ((A*(R^2))/(8*k(win)*h_0_i*(1 - dd_strain(time, win)))) / dd_strain(time, win));
         D = (Sg(time+1) - ((B*(R^2))/(8*k(win)*h_0_i*(1 - dd_strain(time+1, win)))) / dd_strain(time+1, win))
      end
      while D > C
         A = A - 0.000000000000001
         C = (Sg(time) - ((A*(R^2))/(8*k(win)*h_0_i*(1 - dd_strain(time, win)))) / dd_strain(time, win));
         D = (Sg(time+1) - ((B*(R^2))/(8*k(win)*h_0_i*(1 - dd_strain(time+1, win)))) / dd_strain(time+1, win))
      end
      while C > D
         B = B - 0.0000000000000001
         C = (Sg(time) - ((A*(R^2))/(8*k(win)*h_0_i*(1 - dd_strain(time, win)))) / dd_strain(time, win));
         D = (Sg(time+1) - ((B*(R^2))/(8*k(win)*h_0_i*(1 - dd_strain(time+1, win)))) / dd_strain(time+1, win))
      end
      while D > C
         A = A - 0.00000000000000001
         C = (Sg(time) - ((A*(R^2))/(8*k(win)*h_0_i*(1 - dd_strain(time, win)))) / dd_strain(time, win));
         D = (Sg(time+1) - ((B*(R^2))/(8*k(win)*h_0_i*(1 - dd_strain(time+1, win)))) / dd_strain(time+1, win))
      end
      while C > D
         B = B - 0.00000000000000001
         C = (Sg(time) - ((A*(R^2))/(8*k(win)*h_0_i*(1 - dd_strain(time, win)))) / dd_strain(time, win));
         D = (Sg(time+1) - ((B*(R^2))/(8*k(win)*h_0_i*(1 - dd_strain(time+1, win)))) / dd_strain(time+1, win))
      end
      while D > C
         A = A - 0.000000000000000001
```

```
        C = (Sg(time) - ((A*(R^2))/(8*k(win)*h_0_i*(1 - dd_strain(time, win))))) / dd_strain(time, win));
        D = (Sg(time+1) - ((B*(R^2))/(8*k(win)*h_0_i*(1 - dd_strain(time+1, win))))) / dd_strain(time+1, win))
      end
      E_mo_A(time, win) = C; % moduli values
      E_mo_B(time, win) = D; % moduli values
      A_mo(time, win) = A; % flow rate values
      B_mo(time, win) = B; % flow rate values
    end
end
%% evaluate the outcomes of the iteration
eval(['E_A_' num2str(strain) '_complete = abs(E_mo_A(:,:));'])
eval(['A_' num2str(strain) '_complete_f = abs(A_mo(:,:));'])
%% save the values so far
save E_values tissue_depth -append E_* -append A_* -append B_* -append
%% average and normalise the depth-dependent moduli across the time-steps
eval(['E_' num2str(strain) '_average = mean(E_A_' num2str(strain) '_complete(:,1:win));'])
eval(['E_' num2str(strain) '_std = std(E_A_' num2str(strain) '_complete(:,1:win));'])
for ii = 1:19
   eval(['E_' num2str(strain) '_norm(ii) = 9.5*(E_' num2str(strain) '_average(ii)*(ii/19));'])
end
%% save values so far
save E_norm E*
b_0 = b_0';
%% calculate the summed fluid outflow from the discrete time flow steps
for tt = 1:19
   for layer = 1:19
      eval(['fluid_o_' num2str(strain) '(tt, layer) = sum(A_' num2str(strain) '_complete_f(1:tt, layer));'])
   end
   eval(['b_' num2str(strain) '(tt, :) = b_0 - fluid_o_' num2str(strain) '(tt, :);'])
end
%% e = b/h where h is known from h_0(1 - strain)
eval(['ideal_strain' num2str(strain) ' = ideal_strain_' num2str(strain) '_rw(:) / 100;'])
%% change all the time step strains to a more convenient name
for tm = 1:19
   for w = 1:19
      eval(['dd_strain' num2str(strain) '(tm, w) = a_' num2str(strain) '_T' num2str(tm) '_strain55(w) / 100;'])
   end
end
%% calculate the depth and time dependent layer thicknesses from the strains and the initial layer thickness
%% h_0_i
for w = 1:19
   for t = 1:19
      eval(['h' num2str(strain) '(t, w) = h_0_i*((dd_strain' num2str(strain) '(t, w) / (h_n_w / w)) + 1);'])
      tissue_depth(w) = (19 - w)*(1.57 / 19);
      %% find the void fraction
      eval(['e' num2str(strain) '(t, w) = b_' num2str(strain) '(t, w) / h' num2str(strain) '(t, w);'])
   end
end
%% save new values
save void_fractions_dd e* -append b* -append
clear %clear current variables before next strain
end
%% load information required to plot values
load E_values E_norm void_fractions
tissue_depth = (20 - (1:19))*(1.57 / 19);
%% plot normalised moduli
figure
set(gcf, 'color', 'w')
plot(tissue_depth, E_2_norm)
hold on
plot(tissue_depth, E_4_norm, 'k'), plot(tissue_depth, E_6_norm, 'g'), plot(tissue_depth, E_8_norm, 'm')
hold off
%% plot void fractions
figure
set(gcf, 'color', 'w')
plot(tissue_depth, e2(1,:))
hold on
```

```
plot(tissue_depth, e2(10,:), '--'), plot(tissue_depth, e2(19,:), ':'), plot(tissue_depth, e4(1,:), 'k')
plot(tissue_depth, e4(10,:), 'k--'), plot(tissue_depth, e4(19,:), 'k:'), plot(tissue_depth, e6(1,:), 'm')
plot(tissue_depth, e6(10,:), 'm--'), plot(tissue_depth, e6(19,:), 'm:'), plot(tissue_depth, e8(1,:), 'g')
plot(tissue_depth, e8(10,:), 'g--'), plot(tissue_depth, e8(19,:), 'g:'), plot(tissue_depth, e_0(19,:), 'c*')
hold off
xlabel('distance from tissue base (mm)')
ylabel('void fraction')
legend('2% T1', '2% T10', '2% T20', '4% T1', '4% T10', '4% T20', '6% T1', '6% T10', '6% T20', '8% T1', …
…'8% T10', '8% T20', 'b0')
```

E. Partial derivatives used for model error analysis

Equation 5.30, from Chapter 5, shows the root-sum-squared error of the model.

$$dE_{Mi} = \sqrt{\left(\frac{\partial E_{Mi}}{\partial \sigma_G} d\sigma_G\right)^2 + \left(\frac{\partial E_{Mi}}{\partial R} dR\right)^2 + \left(\frac{\partial E_{Mi}}{\partial \dot{b}_i} d\dot{b}_i\right)^2 + \left(\frac{\partial E_{Mi}}{\partial \mu} d\mu\right)^2 + \left(\frac{\partial E_{Mi}}{\partial k_i} dk_i\right)^2 + \left(\frac{\partial E_{Mi}}{\partial h_0} dh_0\right)^2 + \left(\frac{\partial E_{Mi}}{\partial \varepsilon_i} d\varepsilon_i\right)^2} \quad \textbf{[5.30]}$$

The partial derivatives used in the equation are presented below:

$$\frac{\partial E_{Mi}}{\partial \sigma_G} = \frac{1}{\varepsilon_i} \qquad \frac{\partial E_{Mi}}{\partial R} = -\frac{2R\dot{b}_i\mu}{8k_i h_0 \varepsilon_i (1-\varepsilon_i)} \qquad \frac{\partial E_{Mi}}{\partial \dot{b}_i} = -\frac{R^2\mu}{8k_i h_0 \varepsilon_i (1-\varepsilon_i)} \qquad \frac{\partial E_{Mi}}{\partial \mu} = -\frac{R^2\dot{b}_i}{8k_i h_0 \varepsilon_i (1-\varepsilon_i)}$$

$$\frac{\partial E_{Mi}}{\partial k_i} = -\frac{R^2\dot{b}_i\mu}{8k_i^2 h_0 \varepsilon_i (1-\varepsilon_i)} \qquad \frac{\partial E_{Mi}}{\partial h_0} = -\frac{R^2\dot{b}_i\mu}{8k_i h_0^2 \varepsilon_i (1-\varepsilon_i)}$$

$$\frac{\partial E_{Mi}}{\partial \varepsilon_i} = -\frac{\sigma_G}{\varepsilon_i^2} \frac{R^2\dot{b}_i\mu}{8k_i h_0 \varepsilon_i^2 (1-2\varepsilon_i)}$$